64-13

STUDIES IN THE PHYSICS OF ROUGHLY DISPERSED AEROSOLS

TRANSLATION NO.

815

JUNE 1963

U.S. ARMY BIOLOGICAL LABORATORIES
FORT DETRICK, FREDERICK, MARYLAND

CCBL: FD2-3742 (T-38-1)
JPRS: R-3006-D

11 June 1963

STUDIES IN THE PHYSICS OF ROUGHLY DISPERSED AEROSOLS *

Translated for:

U. S. CHEMICAL CORPS BIOLOGICAL LABORATORIES
Ft. Detrick, Maryland

By:

U. S. DEPARTMENT OF COMMERCE
OFFICE OF TECHNICAL SERVICES
JOINT PUBLICATIONS RESEARCH SERVICE
BUILDING T-30
Ohio Drive & Independence Ave., S.W.
Washington 25, D. C.

*From material furnished through the Foreign Science and Technology Center, U. S. Army Materiel Command and the Foreign Intelligence Officer, Fort Detrick, Frederick, Maryland.

The monograph is devoted to the physics of clouds and precipitation, which is a new branch in the physics of the atmosphere. Research is described concerning the processes of inertial and electrostatic precipitation of coarsely-dispersed aerosol particles from a stream on various obstacles. The theory is developed as applied to microphysical processes in clouds, but the results obtained can be used in the investigation of processes in arbitrary coarsely-dispersed aerosols.

The book is designed for scientific workers in the field of the physics of the atmosphere, and also in the field of the mechanics of liquids and gases.

TABLE OF CONTENTS

Foreword..... v
Principal Symbols and Definitions..... xii

Chapter I

EFFECT OF INERTIA OF AEROSOL PARTICLES ON THE PRECIPITATION AND ASPIRATION

1. Formation of Problem. Capture and Aspiration Coefficients..... 1
2. Equations of Motion and Continuity for Aerosol Particles..... 8
3. Certain General Consequences of the Equations of Motion and Continuity for Aerosol Particles..... 14
4. Exact Solutions of Simplest Equations of Motion of Aerosol Particles..... 19
5. Critical Conditions for the Settling of Aerosol Particles from a Stream on an Obstacle..... 34
6. Critical Value of the Stokes Number k_{cr} for Potential and Viscous Streams. Estimate of the Influence of the Boundary Layer on k_{cr} of a Potential..... 45
7. Theory of Aerosol Traps. Procedure for Calculating the Capture Coefficient..... 62
8. Calculation of the Capture Coefficient for Surface and Airborne Aerosol Traps..... 72
9. Gathering Aerosol Samples. The Aspiration Coefficient when Aerosol is Drawn into a Tube or a Slot..... 81

Chapter II

ELECTROSTATIC COAGULATION AND SETTLING OF AEROSOL PARTICLES

10. Formulation of the Problem..... 101
11. Coagulation of Two Aerosol Particles of Unlike Charge..... 105
12. Coagulation of Aerosol Particles with Like Charges..... 128
13. Influence of External Electric Field on the Coagulation of Aerosol Particles..... 137
14. Role of Electrostatic Coagulation of Cloud Drops in the Process of Cloud Development..... 148
15. Random Electrification of Cloud and Rain Drops... 159
16. Electrostatic Precipitation of Aerosol Particles from a Stream on Large Bodies..... 165

Chapter III

SOME RESULTS OF EXPERIMENTAL INVESTIGATIONS

17. Aerosol Traps Used in the Operations of the Elbruss Expedition..... 171
18. On the Distribution Function of Cloud Drops by Dimensions..... 189
19. Calculation of the Optical Density of Clouds..... 207
20. Fluctuation of Microstructural Characteristics of Clouds..... 217

APPENDICES

I. Field of Air Velocities Near the Symmetry Line and the Critical Point of the Stream..... 225
II. Calculation of the Field of the Air Velocities Near a Symmetry Line and the Critical Point for Various Obstacles..... 230
III. Qualitative Analysis of the Trajectories for the Case of Two Drops of Like Charges..... 239
IV. Interaction Between Two Charged Conducting Spheres..... 246
V. Trajectories of Particles in the Presence of an External Electric Field..... 252
VI. Example of Construction of the Gamma Distribution from Experimental Data..... 265

Bibliography..... 267

FOREWORD

During the last 15--20 years research in the field of aerodispersed systems has developed vigorously, owing to the great practical value of the study of aerosols for the investigation of numerous and natural and technical processes, particularly to the study of processes that occur in clouds during their natural development or after artificial action.

In almost all of the phenomena connected with aerosols we deal with visible motion of aerosol particles and their motion relative to bodies and surfaces located inside the aerosol or containing the aerosol. Particles then either settle on various surfaces, or are aspired through various devices. Therefore, the investigation of precipitation and aspiration of aerosol particles plays an important role in the study of many phenomena in which aerosols participate. Thus, for example, a study of such processes as gravitational coagulation of cloud drops (which in final analysis is the main mechanism of precipitation-formation in clouds), the icing of airplanes and wires in supercooled clouds and fogs, certain phenomena which occur during artificial action on clouds, etc., are very closely related with the theory of precipitation of aerosol particles from the stream on obstacles. Also connected with it are such practical important problems as the purification of air by eliminating aerosol contamination, the struggle against agricultural pests, various methods of investigating the microstructure of aerosols, etc. Many of the foregoing problems are related also with the theory of aspiration (drawing-in) of aerosols.

The present book summarizes to a certain degree the result of investigations made on the physics of coarsely-

dispersed aerosols (the microstructure of clouds), carried out by the El'bruss Expedition of the Institute of Applied Geophysics of the Academy of Sciences USSR during the last few years. It is devoted essentially to the investigation of processes of inertial and electrostatic precipitation of coarsely-dispersed aerosol particles from the stream on various obstacles (and in particular the processes of coagulation of such particles) and also to processes of aspiration of aerosol. We consider in great detail in this extensive field problems connected with the investigation of microphysical processes in clouds and a study of microstructural characteristics of the cloud. However, the results obtained have a general character and are directly applicable also to the investigation of processes in all coarsely-dispersed aerosols.*

In Chapter I of the book, which is devoted to an investigation of the influence of the inertia of the aerosol particles on their precipitation and aspiration, we consider three problems of practical importance:

(a) Investigation of the critical conditions for the precipitation of particles of aerosol from the stream on the obstacle.

(b) Determination of the coefficient of aspiration upon drawing of the aerosol into a tube.

(c) Methods for calculating the capture coefficient of the aerosol particles.

The existence of critical precipitation conditions, which determine the minimum dimension (d_{min}) of the aerosol particles that are precipitated from the stream on obstacles is of principal significance for several phenomena which occur in coarsely-dispersed aerosols, and therefore calls for careful investigation. The critical precipitation conditions determine the limit of the cloud-drop dimensions ($D \approx 30$

---

*Aerosols are called coarsely-dispersed if their particle dimensions exceed one micron [66, Sec 2]. In coarsely-dispersed aerosols such processes as precipitation (coagulation) and aspiration do not depend on the Brownian (thermal) motion of the particles and are determined by the inertia of the particles and the external forces acting on them (for example, electrostatic).

microns), below which so important a process for the development of a cloud as is gravitational coagulation of the drops which causes in turn the formation of the precipitation [76], [103], goes unobserved. The critical conditions for the precipitation determine also the dimension limits of the aerosol particles that settle on different devices used to purify gases (cyclones, filters of various types, etc.). Consequently, the proof of existence of critical precipitation conditions and an investigation of this phenomena is an essential element of the mechanics of coarsely-dispersed aerosols.

The proof of the existence of critical precipitation condition is given for an extensive class of symmetrical streams, both potential and viscous. For potential streams we obtain here simple calculation formulas, which make it possible to determine the minimum dimensions of the precipitated particles for many obstacles (for example, for a three-axis ellipsoid and all its particular cases such as elliptical cylinders, plates, round discs, or sphere; for plates located in streams with detachment of jets, etc.). For viscous streams, a simple procedure was obtained for calculating the minimum dimensions of the aerosol particles, and an extrapolation formula is found relating the volume of d_{min} with the behavior of the stream near its forward critical point. This formula is applicable, in particular, for the determination of the minimum dimension of the aerosol particle and the case of settling flow around a sphere. In addition, an estimate is made of the influence of the boundary layer of the potential stream on the value of d_{min}.

The question of the change of concentration of aerosol particles during the drawing of aerosols in various types of instruments was discussed in the literature many times. However, this problem received no quantitative solution, and sometimes even the qualitative picture of the phenomenon was treated in contradictory fashion (see, for example, the discussion of Davis and Walton [126]). At the same time, for many practical problems and primarily for the investigation of the microstructure of the aerosol, it is necessary to know the coefficient of aspiration which characterizes the change in the concentration and the spectrocomposition of the aerosol particles upon aspiration into various devices or instruments. The solution of this problem given in the book is the first theoretical investigation of the aspiration of aerosol, in which account is taken of the inertia of the particles. This solution

establishes the connection between the coefficient of aspiration of the aerosol particles with their dimensions and density, with the volume flow Q of the air through the aspiration unit, and with the velocity of the aerosol particles away from the unit.*

An analysis of the solution obtained enables us to establish a simple relation for the volume flow Q and other parameters of the phenomena at which no essential changes of the particle concentration and their spectrocomposition still does not arise.

Calculations of the capture coefficient, which characterizes the rate of inertial precipitation of the aerosol particles from the stream on obstacles, was carried out earlier for a limited number of body forms. The point is that such calculations are connected with many difficulties, owing to the non-linearity of the equations of motion of the aerosol particles and the complexity of calculating the field of the air velocities around bodies of even relatively simple forms. In this connection, it is possible to find in the literature calculations for the capture coefficients of bodies in which the velocity field of the air stream flowing around them can be readily easily calculated (a cylinder or sphere).

In the present book we develop a procedure for calculating the local capture coefficient near the forward critical point of symmetrical bodies. In this case we succeeded in greatly simplifying the calculations and finding the capture coefficients for many shapes of bodies and many types of streams, calculations which are suitable for practical use. In particular, we calculated the local capture coefficients for a stream flowing around a plate, with detachment of the jets (Kirchhoff flow). These calculations and the results of the remaining theoretical investigations developed in Chapter I of the present book made it possible to point towards ways of improving the procedure for investigating the microstructure of clouds (and other coarsely-dispersed aerosols).

In Chapter II we investigate coagulation and settling of aerosol particles as a result of electrostatic forces.

---

*The velocity of the aerosol particles away from the unit is equal to the geometrical sum of the wind velocity and the particle-sedimentation velocity.

The investigation of this phenomenon and many natural and commercial processes, connected with coarsely-dispersed aerosols, is of particular interest in the study of microphysical processes in clouds. The point is that in the earlier stage of development of the cloud, when the diameters of the cloud drops did not reach even 25--30 microns, gravitational coagulation is impossible. According to the existing theories of precipitation formation, the particles grow during this stage of development of the cloud as a result of condensation processes. On the other hand, the condensation growth of cloud drops occurs sufficiently rapidly only for very small drops ($D < 1$--2 microns), and slows down greatly even for drops 10--30 microns in diameter. The time of development of real clouds prior to formation of the precipitated drops is usually much smaller than that predicted by the theories which attribute the growth of drops to a diameter $D = 30$ microns to condensation. Therefore the author has advanced the hypothesis that in the interval $d = 1$--30 microns the growth of cloud drops can occur to a considerable degree as a result of electrostatic coagulation.

To investigate this problem it is necessary to know the capture coefficients which determine the rate of such a coagulation.

The calculation of the coefficient of the capture of small particles of aerosol by large particles, due to the electrostatic forces of interaction between particles, is made for several combinations of particle charges and external electric field. For this purpose a calculation procedure is developed, based on a qualitative analysis of the differential equations of motion of the aerosol particles. On the basis of this procedure, cases are considered in which one of the particles is charged and the other is neutral, when the particles are charged differently and when the particle charges are of the same sign. The case is also considered when both particles are neutral in the electric field (for example, the atmospheric-electricity field), or when one of them is charged. In all the cases account is taken of the influence of the force of gravity. A comparison of the obtained solutions with the experimental data on individual charges of cloud particles shows that electrostatic coagulation can play a noticeable role in the process of cloud development, when the diameters of its drops are less than 30 microns, and consequently, gravitational coagulation is forbidden. On the other hand, in processes involving the coagulation of large cloud drops

($d > 50$ microns) the electrostatic forces cannot play an appreciable role. This circumstance has made it possible to solve the problem of random electrification of large cloud and rain drops. Finally, in Chapter II, a formula is obtained for the coefficient of capture of charged aerosol particles by a large collector, the sign of the charge of which is opposite to the sign of the particle charge. The result obtained is applicable to a collector of arbitrary form and to any incompressible stream of the gas phase of the aerosol.

In Chapter III are considered some general results of experimental investigations of the microstructure of clouds and fogs.

The most widely used method of studying the microstructure characteristics of clouds and fogs is presently the method of inertial precipitation of drops from the stream on obstacles covered with special oil to prevent the trapped particles from evaporating. However, the use of this method for surface and aerostatic measurements was associated in the case of the majority of investigators with the use of such trapping devices (drop trap), which in principal did not make it possible to correct the resultant distribution functions by introducing the capture coefficient. It is obvious that as a result of such experiments the data obtained on the distribution functions of cloud drops by dimensions (drop spectra) were distorted.

On the basis of the theoretical investigations developed in Chapter I of the book, general requirements for drops of cloud particles (particles of coarsely-dispersed aerosols) were formulated and the principal scheme and the principal parameters of the traps were chosen. At the beginning of Chapter III is presented a description of the construction of such traps. The described surface and aerostatic traps of cloud drops differ appreciably from those previously employed. In gathering samples a stationary air stream is established in the trap and this stream is incident on the receiving part of the trap. The velocity of the stream can be readily measured with the aid of a simple device. The stationarity of the velocity and knowledge of its magnitude make it possible to correct the distribution function of the trapped particles by taking into account the capture coefficient. By introducing a shutter which opens the receiving part of the drop for a definite adjustable time it becomes possible to determine not only the distribution function of the drops but also

the count concentration, the water content, and the specific cross section of the drops in the cloud.

The large statistical material on the microstructure of clouds and artificial fogs, gathered with the aid of the traps, obeys well a logarithmically-normal drop distribution by dimensions and is well approximated by gamma-distributions. A simple procedure is described for very fine agreement between the experimental material and the gamma-distributions. The use of gamma-distributions simplifies the solution of many theoretical problems connected with the functions of the distribution of aerosol particles by dimensions. In particular, it made it possible to obtain an analytic expression for the optical density of a cloud and to analyze the influence of various parameters of the phenomenon on the attenuation of the electromagnetic radiation in the clouds. Finally, in Chapter III are described the space-time fluctuations of the microstructural characteristics of the clouds, observed with the aid of these traps and reflecting the turbulence of the average scale.

In order not to clutter up the main text of the book, many mathematical discussions have been transferred to appendices.

In conclusion, I consider it my pleasant duty to express sincere gratitude to Academician Ye. K. Fedorov for much valuable advice and for continuous interest in the present work.

L. M. Levin

PRINCIPAL SYMBOLS AND DEFINITIONS

We present below the principal symbols used in the book. For the most important symbols we indicate in parentheses the page on which they are introduced.

A -- Aspiration coefficient (7)
A_l -- Local aspiration coefficient (7)

$a = \frac{\partial v_r}{\partial r}$;
$b = \frac{1}{r} \cdot \frac{\partial v_r}{\partial \theta}$;
$c = \frac{\partial v_\theta}{\partial r}$;
$d = \frac{1}{r} \cdot \frac{\partial v_\theta}{\partial \theta}$
-- Functions defining the type of singular point of the differential equation (241)

c -- Flow concentration (5)
c_{ik} -- Capacitive coefficients (246)
D, d -- Diameters of particles
D_μ, d_μ -- Diameters of particles in microns
d_2 -- Mean square diameter of distribution
d_3 -- Mean cube diameter of distribution
E -- Capture coefficient (3)
E_l -- Local capture coefficient (4)
E_0 -- External electric field (137)
e -- Elementary charge, eccentricity of ellipse

$f(r, \varkappa, g_1)$ -- Ratio of the force of electrostatic interaction between two spheres and the Coulomb component of this force (104, 117)

G_1 -- Unit vector of force of gravity (10)

g -- Acceleration due to force of gravity

$g_1 = \left(\frac{d_1^2}{D^2}\right)$ -- Ratio of sedimentation velocities of two particles (106)

$N(d)$ -- Distribution function of sampling -- "accumulated frequency" (192)

I -- Flux of aerosol particles through the collector surface (166); Poincare index of the singular point of a differential equation

$j = nv$ -- Particle flux density (5)

$K(\rho)$ -- Function of scattering of electromagnetic radiation on a sphere (207)

$K = \frac{\rho_0 d^2 v_\infty}{18 \eta l}$ -- Stokes number (11)

$\ldots \quad \varkappa \frac{ds_{12}}{\ldots} - 1;$

$l = \frac{r^2}{2} \cdot \frac{ds_{22}}{dr};$

$l_2 = \frac{r^2}{2} \frac{ds_{11}}{dr};$

$L = f(r, \varkappa, g_1) \cdot l$

-- Functions determining the electrostatic indirection of two charge bodies (117, 249)

l -- Characteristic length (9)

M -- Calculated concentration of the particles of a polydispersed aerosol (94, 188)

n -- Counted concentration of particles of monodispersed aerosol (3)

$n(d)$ -- Distribution function of aerosol particles by dimensions, normalized to unity (94)

$p = -(a + b)$; $q = \begin{vmatrix} a & b \\ c & d \end{vmatrix}$ -- Functions determining the type of the singular point of the differential equation (241, 133)

q_1 -- Electric charge of larger particle (104)

q_2 -- Electric charge of smaller particle (104)

$\bar{q}$ -- Average charge of aerosol particle

$\bar{q}_a = |q - \bar{q}|$ -- Average absolute charge of aerosol particles (164)

Q -- Bulk flow of air through the instrument, sink (5, 82); electric charge of collector (163)

Q_1 -- Bulk flow of air through a unit length of linear source or sink (92); electric charge of cylindrical collector per unit length (168)

$q = N\frac{\pi d_s^3}{6}$ -- Water content of cloud (188)

$R = \frac{\pi d_s}{\lambda}$ -- Similarity criterion for the phenomenon of scattering of light by a disperse aerosol (210)

$Re_u = \frac{lu_\infty}{\nu}$ -- Reynolds number of stream (9)

$Re_p = \frac{du_\infty}{\nu}$ -- Reynolds number of particle (11)

$Re_M = \frac{dv_R}{\nu}$ -- Local Reynolds number of particle (9)

r -- Radius vector of center of gravity of aerosol particle

S_M -- Midsection of the collector (167)

$S_g = N\frac{\pi d^2}{4}$ -- Specific geometric cross section of aerosol particles (188, 209)

$S_{opt} = N\int_0^\infty \frac{\pi d^2}{4} K(\rho) n(d)\, Dd$ -- Specific optical cross section of aerosol particles (208)

$S_\alpha = \frac{S_{opt}}{S_g}$ -- Dimensional optical cross section (201)

s_{ik} -- Potential coefficients (114)

t -- Time

$t_c = \frac{l}{u_\infty}$ -- Characteristic time (10)

u(r) -- Velocity of air stream (8)

u_∞ -- Unperturbed velocity of air away from obstacle (9)

v(r) -- Velocity of center of gravity of aerosol particle (8)

$v_R = v - u$ -- Velocity of center of gravity of aerosol particle relative to the air (8)

$w(z)$ -- Complex potential of two-dimensional air stream

$\alpha = -\frac{4q_1q_2}{3\pi\eta dD^2u_\infty}$ -- Coagulation parameter of two oppositely-charged aerosol particles (106)

$\alpha_1 = -\alpha$ -- Coagulation parameter of two like-charged aerosol particles (130)

$\beta = \alpha x = \frac{4q_2^2}{3\pi\eta dD^2u_\infty}$ -- Coagulation parameter of neutral larger particle with charged smaller one (121)

$\beta_1 = \frac{ag_1^{3/2}}{\pi} = \frac{4q_1^2d^2}{3\pi\eta D^3u_\infty}$ -- Coagulation parameter of charged large particle with neutral smaller one (121)

$\gamma = \frac{E_0^2d^2}{4\pi\eta Du_\infty}$ -- Coagulation parameter of two neutral particles in external electric field (139)

$\gamma_\alpha(z) = \frac{1}{\Gamma(\alpha+1)}\int_0^z t^\alpha e^{-t}dt$ -- Incomplete gamma function of index α (196)

$\delta_1 = \frac{E_0q_2}{3\pi\eta u_\infty d}$ -- Coagulation parameter of large neutral drop with charged small drop in an external electric field (139)

$\delta_2 = \frac{E_0q_1d^2}{3\pi\eta u_\infty D^2}$ -- Coagulation parameter of charged large drop with neutral small drop in external electric field (139)

$\zeta = u_x - iu_y$ -- Complex velocity of two-dimensional air stream

η -- Coefficient of viscosity of air (11)

$\varkappa = -q_2/q_1 = -\lambda$ -- Ratio of electric charges of aerosol particles (104, 130)

$\varkappa_f$ -- Dynamic form coefficient (9)

$\nu = \frac{\eta}{\rho_u}$ -- Kinematic coefficient of viscosity of air (9)

ρ_u -- Density of air (8)

ρ_p -- Density of aerosol particle (10)

$\sigma_1 = \frac{\alpha}{k}$, $\sigma_2 = \frac{\beta}{k}$

$\sigma_3 = \frac{\beta_1}{k}$, $\sigma_4 = \frac{\gamma}{k}$

$\sigma_5 = \frac{\delta_1}{k}$, $\sigma_6 = \frac{\delta_2}{k}$

-- Dimensionless criteria characterizing the ratio of various types of electrostatic forces, acting on a small particle, to the inertial forces (106, 121, 140, 144)

τ --Relaxation time of aerosol particle (20)

Ψ -- Stream function of air current (107)

$\psi_1 = \psi - \frac{g_1 r^2 \sin^2 \theta}{2}$ -- Special stream function (107)

ω -- Velocity on the jet boundary in streams where the jets are detached (233)

CHAPTER I

EFFECT OF INERTIA OF AEROSOL PARTICLES ON THE PRECIPITATION AND ASPIRATION

1. FORMATION OF PROBLEM. CAPTURE AND ASPIRATION COEFFICIENTS.

To investigate aerosols, it is necessary to measure their counted concentration and dispersion, i.e., to determine the distribution function of the aerosol particles by dimensions (the microstructure of the aerosol). With exception of a few methods (which for the time being are still weakly developed), in which the aerosol particles are directly photographed in their natural state [131], the microstructure of the aerosol is usually either drawn in (aspirated) in some instrument or else the aerosol particles are precipitated on some surface. Very frequently both operations are carried out simultaneously; the aerosol is drawn into some instrument, in which subsequently the aerosol particles are precipitated on various types of surfaces. This operation will be henceforth called the taking (gathering) of the aerosol sample.

In taking a sample of a coarsely-dispersed aerosol, the inertia of its particles may cause more or less appreciable changes in the counted concentration and in the particle distribution function by dimensions, compared with these characteristics of a free aerosol (not disturbed by the instrument). These changes are connected with the fact that the aerosol particles generally speaking do not follow the current lines of the air. Let us illustrate this by means of very simple schemes of the phenomenon. Let, for

example, a stationary potential stream of mono-dispersed aerosol, which is homogeneous far away from the obstacle, flow around some body A. Then, the air current lines will have the form shown by the dashed lines in Figure 1. With exception of one current line OO', which terminates on the obstacle at the so-called forward critical point of the stream O (where the stream velocity is equal to zero), all the remaining current lines will flow around the body. The trajectories of the aerosol particles are shown in the same figure by solid lines. By virtue of the inertia, some aerosol particles arrive at the body with a velocity whose component normal to the surface of the body is finite.

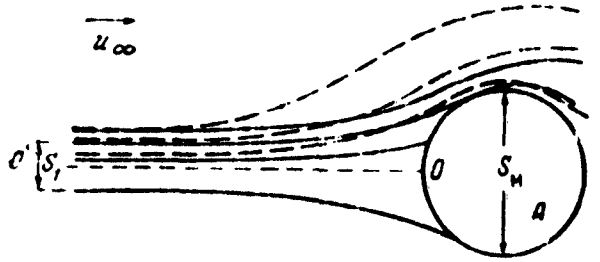

Fig. 1. Diagram showing the flow of an aerosol around an obstacle.

Such particles will strike the surface of the body and will settle on this surface under certain conditions.* Were the mass of the aerosol particles very large, then their trajectory would differ little from straight lines parallel to the stream velocity at infinity u_∞, and their velocities would everywhere be close to u_∞. In this case, there would settle on the body A during the time T all the particles contained in a volume $u_\infty TS_M$, where S_M is the mid-section of the body A. In fact, however, the two particle trajectories of the aerosol particles, which have a finite mass, are curved as shown in Figure 1. Therefore, the particles that can settle on the body A during the time T come only from the volume $u_\infty TS_1$, where S_1 is the cross section (away from the obstacle) of the current tube formed

*We shall not consider the impact of the particles against the surface and will assume that all the particles whose trajectories cross the surface of the body settle on the surface.

by the extreme (limiting) trajectories of the center of gravity of the particles which still strike the obstacle. If the aerosol-particle dimensions are comparable with the dimensions of the obstacle A, then we take into account the so-called "coupling effect" and understand by "limiting trajectories" the trajectories of the center of gravity of the particle such that a particle moving along such a trajectory does not strike the body A, but is merely tangent to it (Fig. 2).

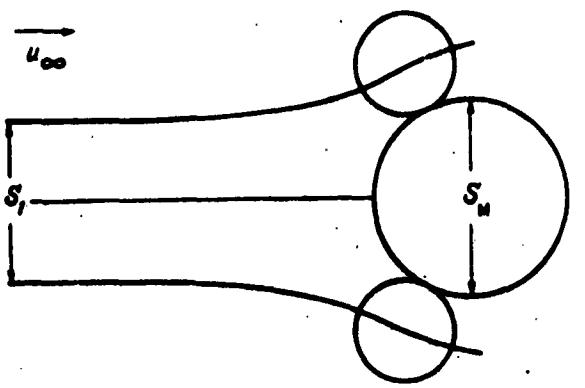

Fig. 2. "Coupling effect."

By capture coefficient of the obstacle as a whole, E, is meant the quantity

$$E = \frac{S_1}{S_M}. \qquad (I.1)$$

Knowing the number N_t of particles that strike the obstacle A during the time T, is is possible to calculate the counted concentration of the particles in the free aerosol, N, which is equal to the number of particles per unit volume:

$$n = \frac{N_t}{u_\infty T S_1} = \frac{N_t}{wE}, \qquad (I.2)$$

where $w = S_M T u_\infty$ is the volume of the aerosol "flowing onto" the body during the time T.* The value of w can be readily determined from the experimental conditions.

*In the foreign literature, this volume is frequently called the volume "swept" by the obstacle.

It is possible to define quite analogously the local capture coefficient E_l, as the ratio of the cross section σ_1 (away from the obstacle) of the current tube formed by the extreme trajectories of the particles that still strike the area σ of a specified part of the obstacle (Fig. 3):

$$E_l = \frac{\sigma_1}{\sigma}. \qquad (I.3)$$

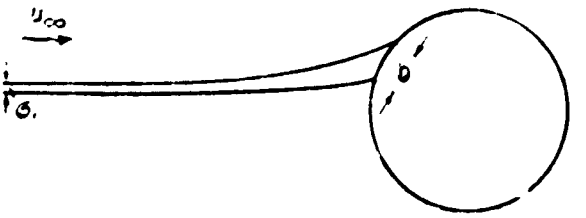

Fig. 3. Local capture coefficient.

It is easy to see that in the case when there are no forces to attract the aerosol particles to the obstacle, the capture coefficients E and E_l will be the larger (other conditions being equal), the larger the mass of the particles, since the trajectories of the heavier particles will bend less than the trajectories of the light particles. It is obvious that in the case under consideration, if the dimensions of the captured particles are negligibly small compared with the dimensions of the obstacle, the expression $0 \leqslant E \leqslant 1$ will hold true. If the dimensions of the captured particles are of the same order as the dimensions of the obstacle, then the upper limit of the capture coefficients is increased, owing to the coupling effect, to a value of the order of 4 for an obstacle whose form is close to spherical, and to a value of the order of 2 for a cylindrical obstacle.

Processes connected with the aspiration of aerosol are frequently conveniently characterized by the number of aerosol particles per unit volume of air passing through the instrument. In this connection, we introduce the concept of the flow concentration of the aerosol particles.

The number of particles passing per unit time through any elementary area $d\sigma$ located on the flow of a monodispersed aerosol is expressed by the formula

$$j_n d\sigma = n v_n d\sigma,$$

where n is the counted concentration of the aerosol particles; $j = nv$ is the flux density vector of the aerosol particles*; j_n and v_n are the components of the vectors j and v normal to $d\sigma$.

Let the volume flow of air through the same area be

$$dQ = u_n d\sigma,$$

where u_n is the component of the air velocity u normal to $d\sigma$. We shall define the flow concentration of the aerosol particles, c, as the number of aerosol particles flowing per unit time through an area normal to the air velocity and calculated per unit volume flow of air through the same area. It is obvious that

$$c = \frac{nv_n d\sigma}{dQ} = \frac{nv_n}{u}. \qquad \text{(I.4)}$$

Analogously, we introduce the concept of average flow concentration of the aerosol particles passing through the finite area σ:

$$\bar{c} = \frac{\int_\sigma nv_n d\sigma}{Q} = \frac{\int_\sigma j_n d\sigma}{Q}, \qquad \text{(I.4a)}$$

where Q is the volume flow of air through the area σ.

It is obvious that for an area element located in that place of the aerosol stream where the aerosol particle velocity concides with the velocity of the air stream (for example, at an infinite distance from the instrument), we have

$$c = c_\infty = n_\infty.$$

---

*We note that the local capture coefficient is $E_l = j_n/j_\infty$, where j_n is the component of j normal to the surface of the body, and j_∞ is the modulus of the vector j at infinity. Analogously, the capture coefficient of the obstacle as a whole is

$$E = \frac{1}{S_M j_\infty}\int_S j_n d\sigma = \bar{j}_n / j_\infty,$$

where $\bar{j}_n$ is the average value (referred to the mid-area) of the flux of the vector j through the surface of the body.

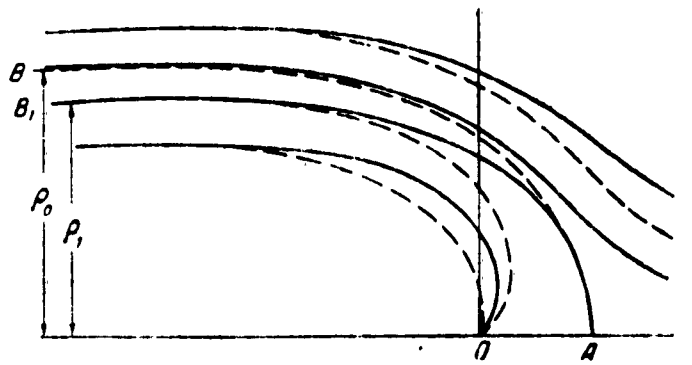

Fig. 4. Diagram of trajectories of the intake of aerosols in the tube.

Let us consider now the intake of aerosol in a narrow tube. For this purpose we consider the motion of the particles of a monodispersed aerosol in the field of a uniform wind in the presence of a point sink located at the origin 0 (Fig. 4). We shall assume that away from the sink (tube) the particles move together with the wind at velocity u_∞. The current lines of the air which are produced thereby are shown in Figure 4 by the dashed lines. The dashed line AB corresponds to the critical current line, which separates the volumes of the air that enter into the sink from the volumes of the air that go past it. The trajectories of the aerosol particles are shown in Figure 4 by continuous lines. In this case, the line B_1A corresponds to the limiting particle trajectory. It is easy to see that the ratio of the average flow concentration of the aerosol particles entering inside the sink (tube), $\bar{c}_0$, to the concentration of the particles away from the sink, c_∞, is equal to the ratio of the transverse cross sections of the current tubes formed by the limiting trajectory of the particles and the critical current line

$$\frac{\bar{c}_0}{c_\infty} = \frac{\rho_1^2}{\rho_0^2},$$

where ρ_1 is the distance between the limiting trajectory of the particles and the abscissa axis away from the sink, and

ρ_0 is the corresponding distance for the critical current line.

It is obvious that $\bar{c}_0/c_\infty < 1$.

In analogy with the capture coefficient for the settling of aerosol particles on an obstacle, we introduce the aspiration coefficient for the case of drawing in of an aerosol into some instrument. By aspiration coefficient A of the aerosol as a whole we define the ratio of the full concentration of the particles, averaged over the inlet cross section of the instrument, c_0, to the concentration of the particles in the unperturbed aerosol, $c_\infty = n_\infty$:

$$A = \frac{\bar{c}_0}{c_\infty}. \qquad (I.5)$$

In analogy, we can introduce the concept of local aspiration coefficient, defining it as the ratio of the flow concentration of the particles in some place in the instrument, c_l, to c_∞ *:

$$A_l = \frac{c_l}{c_\infty}. \qquad (I.5a)$$

It becomes clear in this connection that the definition of the capture and aspiration coefficients is one of the central problems of the mechanics of inertial settling and aspiration of aerosol particles, phenomena which play an essential role in many processes which occur in aerosols, and also in the study of the structure of the aerosol. These coefficients can be determined experimentally or calculated theoretically.

A theoretical determination of the capture and aspiration coefficients involves the calculation of the trajectories of the aerosol particles relative to the obstacle or to the intake instrument. These trajectories can be determined by solving the equations of motion of the aerosol particles which move in the inhomogeneous air stream. To determine the particle concentrations it is necessary also to consider the equation for the conservation of the number of aerosol particles (the continuity equation). A derivation of these equations will be considered in the next section.

---

*We recall that the capture and aspiration coefficients, introduced with the aid of formulas (I.1), (I.3), (I.5), are defined for a monodispersed aerosol (the isodispersed fraction of a polydispersed aerosol).

2. EQUATIONS OF MOTION AND CONTINUITY FOR AEROSOL PARTICLES

We shall consider the equations of motion of aerosol particles in the inhomogeneous stream of its air component under the following assumptions.

a) The air stream is stationary (relative to the obstacle or the aspiration instrument).

b) The presence of aerosol particles does not influence the motion of the air or the motion of each of the particles. Usually the volume concentration of aerosol particles is small. Thus, the water content in a cloud is on the order of 1 g/m^3, i.e., the volume of drops in a cloud is approximately one millionth of the volume of the air in which they are situated. This circumstance justifies the present assumption. However, in the case when the aerosol-particle dimension is comparable with the dimension of the obstacle, appreciable hydrodynamic-interaction forces can arise, where one can no longer regard the motion of the air stream as determined only by the obstacle. Such a circumstance can arise when the distance from particle to the obstacle is on the order of the dimension of the particle.

c) The aerosol particle is acted upon by an aerodynamic force F_a, the force due to gravity F_g, and other forces F_1, F_2, ..., (for example, different electrostatic forces).

d) The shape of the particle is spherical. In this case

$$F_a = c_x \frac{\pi d^2}{4} \frac{\rho_a v_{R_1}}{2} [u_1(r_1) - v_1(r_1)]. \qquad (I.6)$$

where r_1 is the radius of the vector of the particle center of gravity;
v_1 its velocity vector;
d the diameter of the particle;
$u_1(r_1)$ the velocity field of the air stream;
ρ_a the air density;
$v_{R_1} = |u_1 - v_1|$ the modulus of the velocity v_{R_1} of the particle relative to the air; and
c_x a dimensionless resistance coefficient.

The velocity field $u(r_1)$ is a function of the Reynolds number of the stream

$$Re_u = \frac{lu_\infty}{\nu},$$

where l is the characteristic dimension of the obstacle (instrument), for example the radius for a sphere or a tube, the half-width for a plate, etc.;
u_∞ is the velocity of the air stream incident on the obstacle (instrument), and
ν is the kinematic viscosity coeffifient.

On the other hand, the coefficient c is a function of the local Reynolds number for the particle, $Re_{pl} = \frac{dv_{R1}}{\nu}$.

When $Re_{pl} < 1$ or $Re_{pl} \approx 1$, we go over to the so-called Stokes case of flow around a sphere, when*

$$F_a = 3\pi\nu\rho_a d v_{R_1}; \quad c_x = \frac{24}{Re_{pl}}. \tag{I.6a}$$

If the particle is not spherical, we shall average the aerodynamic force over different orientations of the particle relative to the velocity v_{R1} and different Reynolds numbers, and assume that F_a can be expressed by formula (I.6), where c_x differs from the resistance coefficient of the sphere by a certain factor χ_f, which is called the dynamic form coefficient, and by d is meant the diameter of the sphere, the volume of which is equal to the volume of the particle.**

On the assumptions made, the differential equation of motion of the particle in a coordinate system connected with the obstacle in the flow (or the aspiration instrument) can be written in the following fashion:

---

*Similar information concerning the applicability of the Stokes formula to spherical particles of coarsely-dispersed aerosol are given in [66, Sections 7, 10, 17].

**Information on the value of χ_f is found, for example, in the book by M. A. Fuks [66, Section 12].

$$\frac{\pi}{6}\rho_p d^3 \frac{dv_1(r_1)}{dt_1} = c_x(\mathrm{Re}_{pl})\frac{\pi d^2}{4}\cdot\frac{\rho_e v_{R_1}}{2}|u_1(r_1)-v_1(r_1)| + \\ + \frac{\pi}{6}\rho_p d^3 g G_1 + F_1(r_1), \tag{I.7}$$

where ρ_p is the density of the particle;
g is the acceleration due to the force of gravity;
G_1 is its unit vector;
F_1 is the sum of all the remaining forces; and
t_1 is the time.

In equation (I.7) we go over to dimensionless quantities, choosing u_∞ as the unit of velocity and l as the unit of length. Then, the unit time must be chosen to be $t_e = \frac{l}{u}$, which is the time that the path all is traversed at a velocity u_∞. Then, the dimensionless velocities are $v = \frac{v_1}{u_\infty}$, $u = \frac{u_1}{u_\infty}$, $v_R = \frac{v_{R_1}}{u_\infty}$, the dimensionless radius vector is $r = \frac{r_1}{l}$, and the dimensionless time is $t = \frac{t_1}{t_e} = \frac{t_1 u_\infty}{l}$.

The differential equation (I.7) for these quantities assumes the form

$$\chi\frac{dv}{dt} = v_R(u-v) + \frac{4}{3}\frac{\rho_p d g}{\rho_e c_x u_\infty^2} G_1 + \frac{8}{\pi c_x \rho_e d^2 u_\infty^2} F_1(r), \tag{I.8}$$

where

$$\chi = \frac{4}{3}\cdot\frac{d}{l}\cdot\frac{\rho_p}{\rho_e}\cdot\frac{1}{c_x};$$

$F_1(r)$ is a quantity that has the dimension of a force. Its form depends on the specific expression for the force F_1; for the particular cases of electrostatic forces this expression will be considered below (see Chapter II).

In this form, the equation is convenient for use at large values of $Re_{p\ell}$, when the coefficient c_x becomes almost constant and has an approximate 0.4. For small and medium values of $Re_{p\ell}$, it is convenient to use a different form of equation (I.8).

We introduce for the ratio of the coefficient c_x to the Stokes value $c_x = 24/Re_{p\ell}$ the notation

$$c(Re_{p\ell}) = \frac{c_x(Re_{p\ell})Re_{p\ell}}{24}. \qquad (I.9)$$

We can then rewrite (I.8) in the form

$$\frac{k}{c}\frac{dw}{dt} + w = u(r, Re_u) + \frac{k}{c}Fr \cdot G_1 + \frac{k}{c}\frac{q\ell}{\nu\rho_p d^2 u_\infty^2}F_1(r), \qquad (I.10)$$

where

$$k = \frac{\rho_p d^2 u_\infty}{18\eta\ell} \qquad (I.11)$$

is a dimensionless parameter, called the Stoke number*; $\eta = \nu\rho_0$ is the coefficient of viscosity of air; and

$Fr = \frac{g\ell}{u_\infty^2}$ is the Froude number.

From equations (I.8) and (I.10) we see that the phenomenon of the settling of an aerosol on an obstacle (or aspiration of an aerosol through an instrument) is determined by the dimensionless parameters k (or χ), Re_u, $Re_{p\ell}$, Fr, and also by parameters connected with the form of the forces F_1 (see Chapter II). In place of the parameter $Re_{p\ell}$, which has a variable value on the trajectory, it is convenient to introduce the Reynolds number of the particle $Re_p = \frac{du_\infty}{\nu} =$

---

*For non-spherical particles $k = \frac{\rho_p d^2 u_\infty}{18\eta\ell\chi_f}$, where χ_f is the dynamic form coefficient (see page 9).

$= \mathrm{Re}_{pl} \cdot \frac{1}{v_R}$, which is constant on all trajectories.

Inasmuch as $\mathrm{Re}_p/\mathrm{Re}_u = d/l$, then if geometrical similarity is maintained $\left(\frac{d}{l} = \text{const}\right)$ for the precipitation (aspiration) phenomena, the similarity of these phenomena is guaranteed by the equality of the similarity criteria k, Re_p, Fr and a few other parameters connected with form of the forces F_1. We note that whereas the Reynolds numbers characterize the ratio of the inertial forces acting on the elementary volumes of the air to the viscosity forces, the Stokes number k characterizes in perfect analogy the ratio of the inertial forces acting on a particle to the aerodynamic forces.

Very frequently, over large intervals of the Reynolds numbers, the velocity field and the coefficient c (or c_x) are self-similar with respect to the Reynolds number, i.e., they are independent of the latter. In particular, when $\mathrm{Re}_p < 1$ or $\mathrm{Re}_p \approx 1$ the value of c is equal to unity with great accuracy. On the other hand, at large values $\mathrm{Re}_{pl} \approx$ $\approx 10^3 \div 3 \cdot 10^5$ the coefficient $c_x \approx 0.4$ and consequently the coefficient c_x is self-similar with respect to Re_{pl}.

In most practical cases (with the exception of problems connected with icing of an airplane and precipitation on very small obstacles) the velocity field u(r) is self-similar relative to Re_u, and the coefficient c can be assumed equal to unity. Then equation (I.10) assumes the form

$$k\frac{dv}{dt} + v = u(r) + k\,\mathrm{Fr}\,G_1 + k\frac{6l}{\pi\rho_p d^3 u_\infty^2}F_1(r). \qquad \text{(I.12)}$$

In the investigation of particle trajectories with respect to an airplane, it is necessary to take into account the fact that the velocity field u(r) is usually self-similar relative to Re_u, but the value of Re_{pl} greatly exceeds unity. It is no longer possible to assume here that c = 1. Within the limits $\mathrm{Re}_{pl} < 10^3$, the quantity c_x can be well approximated by the expression [41]

$$c_x = \frac{24}{\mathrm{Re}_{pl}}(1 + 0{,}17\,\mathrm{Re}_{pl}^{2/3}). \qquad \text{(I.13)}$$

Taking this expression into account, equation (I.10), neglecting the force of gravity and the forces F_1, assumes the form usually employed in the investigation of the icing of an airplane or the settling of aerosol particles on large obstacles at large stream velocities:

$$k\frac{dv}{dt} = [u(r) - v(r)][1 + 0{,}17\mathrm{Re}_p^{3/4}|u - v|^{3/4}]. \qquad (I.14)$$

In settling of aerosol particles on small obstacles, when $\mathrm{Re}_u \sim 1 + 100$, it is necessary to take into account the dependence of the field u(r) of Re_u. In this case, the equation (I.12) is used, in which ($u = u(r)$, Re_u).

Each of the equations (I.8), (I.10), (I.12), and (I.14) represents a system of three second-order ordinary differential equations for the coordinates x, y, and z (or for some curvilinear coordinates q_1, q_2, q_3), regarded as functions of the time t. Their solution corresponds to definite trajectories for certain specified initial conditions, i.e., values of x, y, z, $\dot{x}$, $\dot{y}$, $\dot{z}$ at a certain definite instant of time. Usually one assumes as the initial condition the equality of the aerosol particle velocity to the velocity of the air stream away from the obstacle of the aspiration instrument.

One can, however, interpret the foregoing equations in a different fashion, convenient for many theoretical considerations [116]. Assume that for a monodispersed aerosol there are specified at the instant of time t_0 values of the velocity $v_0(r)$ on a certain surface. Then, the continuum of these initial conditions will correspond to a continuum of trajectories, which will usually fill densely a certain region of space [we shall assume that in this region the solutions of equations (I.8) -- (I.14) are continuous with respect to the initial conditions]. In this region we can then consider the motion of an ensemble of particles, obeying the equations of motion (I.8) -- (I.14) with initial conditions $v(r, t_0) = v_0(r)$, as the motion of a certain aerosol pseudo-liquid, the velocity field of which v(r) satisfies the above-mentioned equations. In this case, the derivative dv/dt in equations (I.8) -- (I.14) must be understood as the total derivative of the stationary field v(r) in the moving pseudo-liquid, and it must be replaced

by the expression $\frac{D\mathbf{v}}{Dt} = (\mathbf{v}\nabla)\mathbf{v}$ *.

Under this interpretation of the aerosol-particle motion, the counted particle concentration of the aerosol corresponds to a density of the pseudoliquid, and the condition of conservation of the number of aerosol particles can be written in the form of a continuity equation for the pseudoliquid. We can therefore write for the counted concentration of the aerosol particles, and, in the regions where there are no surfaces on which the aerosol particles can settle and where there is no coagulation of the aerosol particles, the following equation

$$\operatorname{div}(n\mathbf{v}) = 0, \tag{I.15}$$

which for nonstationary streams has the form

$$\frac{\partial n}{\partial t} + \operatorname{div}(n\mathbf{v}) = 0. \tag{I.15a}$$

The aggregate of one of the equations (I.8), (I.10), (I.12), or (I.14) with equation (I.15) simultaneously with the boundary conditions (which are usually specified at infinity) yield the solution of the problem concerning the velocity field (trajectories) and the particle concentration of an aerosol flowing around the obstacle or drawn into an instrument.

3. CERTAIN GENERAL CONSEQUENCES OF THE EQUATIONS OF MOTION AND CONTINUITY FOR AEROSOL PARTICLES

Let us consider the case of stationary motion of relatively small aerosol particles, when the velocities of the air stream are small, i.e., when the local Reynolds number is $\mathrm{Re}_{\gamma} \leqslant 1$. In this case the motion is described by equation (12), which we rewrite for brevity as

$$k\frac{D\mathbf{v}}{Dt} + \mathbf{v} = \mathbf{u} + \mathbf{F}, \tag{I.16}$$

*It must be noted here that for a nonstationary air stream all the equations (I.8), (I.10), (I.12), and (I.14), retain their form, but the velocities in them will depend on the time, and

$$\frac{d\mathbf{v}}{dt} = \frac{D\mathbf{v}(r,t)}{Dt} = \frac{\partial \mathbf{v}}{\partial t} + (\mathbf{v}\nabla)\mathbf{v}.$$

taking the vector F to mean the sum of the forces of gravity and the remaining forces [together with the constant coefficients which are contained in equation (I.12)]. We shall assume that sufficiently far from the obstacles or the instruments (at infinity), where the gradient of the air velocity is infinitely small, the aerosol particles move together with the air. We assume further that at infinity the counted concentration of the aerosol particles is uniform and equal to n_∞. Let us dwell first on two extreme cases, corresponding to very large and very small particles. In the former case, the Stokes number k is very large and according to formula (I.16) the derivative Dv/Dt is very small, while the velocity v changes very little along the particle trajectory. Consequently, in this case div $v \approx 0$. In the second case $k \approx 0$ and it follows from (I.16) that div $v \approx$ div $(u + F)$. If at the same time the velocity field u(r) and the force field F(r) are solenoidal, i.e., div $u = 0$ and div $F = 0$ (this is the case with the velocity fields of an incompressible liquid and with the field of the force of gravity, of a Coulomb electrostatic field, etc.), then div $v \approx 0$.

The continuity equation (I.16) can be rewritten as

$$\frac{1}{n} \cdot \frac{Dn}{Dt} = -\operatorname{div} v. \qquad \text{(I.17)}$$

In both asymptotic cases considered div $v \approx 0$ and by virtue of formula (I.17)the derivative is

$$\frac{Dn}{Dt} \approx 0.$$

Consequently, the counted particle concentration of the aerosol along the particle trajectories remains constant. But at infinity, in accordance with our condition, the concentration is homogeneous and is the same on all trajectories. Consequently, for very large aerosol particles ($k \to \infty$) and for very small particles ($k \to 0$; div $(u+F)=0$), the counted concentration n is homogeneous for the entire volume filled with trajectories, starting at infinity, where $n = n_\infty$ [29].

For intermediate values of the Stokes number k, the counted concentration varies in the stream. Let us demonstrate this for a potential stream u(r) and for force

fields F(r) possessing a potential. We assume that

$$u(r) = \operatorname{grad} \varphi(r), \quad F(r) = -\operatorname{grad} U(r), \tag{I.18}$$

where $\varphi(r)$ is the potential of the air field and
$U(r)$ is the potential of the forces F.

A. M. Yaglom and A. Robinson have shown that in this the velocity field of the aerosol particle v(r) will also be potential [116]*. To prove this, let us consider the circulation Γ of the velocity v over a certain closed contour connected with the particles. Then, in accordance with the well known field-theorem, the derivative $d\Gamma/dt$ is equal to the circulation of the acceleration dv/dt over the same contour [16, Section 21].

On the basis of equation (16) we get

$$\frac{d\Gamma}{dt} = \frac{1}{k}\oint (u + F - v)\, dl = -\frac{1}{k}\oint v\, dl = -\frac{1}{k}\Gamma,$$

from which it follows that $\Gamma = \Gamma_0 e^{-t/k}$. Thus, if the circulation of the velocity v over the contour connected with the particles is equal to zero at some instant of time, it will be equal to zero on this contour (which moves in space) at any other instant of time. But at $t = -\infty$ (i.e., far away from the obstacles and the instruments), the velocity v of the aerosol particles coincides with the velocity u(r) of the air, and in view of the fact that the field u is potential, the circulation is

$$\oint v\, dl = \oint u\, dl = 0.$$

It follows therefore that $\Gamma_0 = 0$ and consequently $\Gamma = 0$. This means that

$$\operatorname{rot} v = 0 \tag{I.19}$$

and

$$v(r) = \operatorname{grad} \Phi(r). \tag{I.20}$$

---

*A. M. Yaglom reported the results of his investigations in 1951 at a seminar of the Geophysics Institute of the Academy of Sciences USSR, but they were never printed.

Since as a result of (I.19) we have

$$(\mathbf{v}\nabla)\mathbf{v} = \frac{1}{2}\operatorname{grad} v^2 + [\mathbf{v}, \operatorname{rot}\mathbf{v}] = \frac{1}{2}\operatorname{grad} v^2,$$

equation (I.16) with account of formula (I.18) and (I.19) can be written in the form

$$\frac{k}{2}\operatorname{grad} v^2 + \operatorname{grad}\Phi = \operatorname{grad}(\varphi - U). \tag{I.21}$$

Equation (I.21) has a first integral analogous to the Bernoulli-Euler integral [15, page 115]

$$\frac{kv^2}{2} = \frac{k}{2}\left[\left(\frac{\partial\Phi}{\partial x}\right)^2 + \left(\frac{\partial\Phi}{\partial y}\right)^2 + \left(\frac{\partial\Phi}{\partial z}\right)^2\right] = \varphi - U - \Phi. \tag{I.22}$$

Let us assume now that the velocity field u(r) and the force field F are solenoidal and let us apply the divergence operator to the right and left halves of equation (I.16). Then, by virtue of the fact that fields u and F are solenoidal we get

$$k\operatorname{div}\left(\frac{D\mathbf{v}}{Dt}\right) + \operatorname{div}\mathbf{v} = 0. \tag{I.23}$$

Taking (I.19) into account we can readily show that

$$\operatorname{div}\left(\frac{D\mathbf{v}}{Dt}\right) = \frac{D}{Dt}(\operatorname{div}\mathbf{v}) + H, \tag{I.24}$$

where

$$H = (\operatorname{grad} v_x)^2 + (\operatorname{grad} v_y)^2 + (\operatorname{grad} v_z)^2. \tag{I.25}$$

Equation (I.23) with account of formula (I.24) assumes the form

$$k\frac{D}{Dt}(\operatorname{div}\mathbf{v}) + \operatorname{div}\mathbf{v} = -kH. \tag{I.26}$$

This equation can be regarded as an ordinary differential equation for the unknown variable div v, if we recognize that the operator D/Dt denotes differentiation with respect to time while following along the vector line of the field v(r), i.e., while following along the particle trajectory.

Equation (I.26) has a solution

$$\operatorname{div} v = Ce^{-t/k} - e^{-t/k}\int_{t_0}^{t} H(\xi)\, e^{\xi/k}\, d\xi.$$

If we choose as the initial instant of time t_0 the time when the particle is located sufficiently far away from the obstacle or the aspiration instrument, then $(\operatorname{div} v)_{t = t_0} = (\operatorname{div} u)_{t = t_0} = 0$ and consequently the sought-for solution of equation (I.26) under our assumptions will be the expression*

$$\operatorname{div} v = -e^{-t/k}\int_{t_0}^{t} H(\xi)\, e^{\xi/k}\, d\xi. \qquad (I.27)$$

Inasmuch as the function H is always non-negative, it follows from (I. 27) that

$$\operatorname{div} v \leqslant 0, \qquad (I.28)$$

and the equality sign in (I.28) is obtained only when H = 0, i.e., when the stream v(r) is homogeneous. On the other hand, the homogeneity of the stream v(r), in accordance with equation (I.16), will occur only when the field u + F is homogeneous, i.e., practically in the absence of forces and when the field u is homogeneous, if at the same time v = u everywhere.

Comparing equations (I.28) and (I.17) we arrive at a conclusion, deduced by A. Robinson, that the counted concentration of the aerosol particles is an increasing function of the time along the particle trajectories [116], with exception of the trivial case when v = u = const. In the latter case, the concentration remains constant along the trajectory. This means that for any flow of aerosol around obstacles or for aspiration of aerosol by instruments, the counted concentration of the particles of the aerosol is inhomogeneous near the obstacles [29].

Furthermore, inasmuch as when k = 0 and $k \to \infty$ the particle concentration is inhomogeneous, and when $k \neq 0$ it

---

*Equation (I.21) will also have a solution when div v = 0 on some arbitrary point of the trajectory.

is inhomogeneous, it follows therefore (as a result of the continuity) that as the Stokes number k increases, the inhomogeneity of the counted concentration first increases and then decreases. This means that when an aerosol flows around an obstacle or is aspirated its distribution functions by dimensions always change relative to the unperturbed aerosol [29].

We note finally that from the condition div v = 0 (when $k \neq 0$) it follows from (I.26) that the field v(r) is homogeneous (since H = 0). Thus, if the velocity field is inhomogeneous, then when $k \neq 0$ it is not solenoidal (div v = 0) [29].

4. EXACT SOLUTIONS OF SIMPLEST EQUATIONS OF MOTION OF AEROSOL PARTICLES

The equations of motion of aerosol particles are usually nonlinear (owing to the nonlinear dependence of the velocity field u and of the forces F on the coordinates). By virtue of this circumstance, their solution entails great mathematical difficulties and has been carried out in most investigated cases by numerical methods. However, there exist several schemes of motion (to be sure, very simple ones), when it is possible to obtain analytic solutions of the equations of motion. Since it is possible to trace on these very simple schemes, in explicit form, certain general laws of the motion, it is of interest to consider these schemes.

A. Let us consider with the very simple case, first considered by Albrecht, of the motion of small aerosol particles in a homogeneous airstream in the absence of forces F [79]. In view of the absence of a characteristic stream dimension in this case, it is more convenient to consider the equation of motion in dimensional form

$$m\frac{dv_1}{dt_1} = 3\pi\nu_1 d(u_1 - v_1) + mgG_1.$$

Dividing this equation by $3\pi\nu_1 d$, we rewrite it in the form

$$\tau\frac{dv_1}{dt_1} + v_1 = u_1 + \tau gG_1 = u_0. \qquad (I.29)$$

where

$$\tau = \frac{\rho_p d^2}{18\nu_1} \qquad (I.30)$$

is a quantity having the dimensionality of time and called the "relaxation time"; u_0 is the sum of the constant vectors u and $\tau g G_1$ (the latter vector is equal to the velocity of sedimentation of the particles).

Taking a plane Cartesian system of coordinates such that at the initial instant of time ($t_1 = 0$) the origin coincides with the position of the particle, the Ox axis is parallel to the vector u_0, and the particle initial-velocity vector lies in the coordinate plane Oxy, we obtain after elementary integration the following expressions for the velocities v_{1x}, v_{1y}, and the coordinates x, y of the particle:

$$v_{1x} = u_0 + (\dot{x}_0 - u_0)e^{-t_1/\tau};\ v_{1y} = \dot{y}_0 e^{-t_1/\tau}, \qquad (I.31.1)$$

$$x = u_0 t_1 + \tau(\dot{x}_0 - u_0)(1 - e^{-t_1/\tau});\ y = \dot{y}_0 \tau(1 - e^{-t_1/\tau}), \qquad (I.31.2)$$

where $\dot{x}_0$, $\dot{y}_0$ are the initial values ($t_1 = 0$) of the velocity components.

From (I.31) we can draw the following conclusions.

1. The initial difference between the particle and the stream velocities ($\dot{x}_0 - u_0$ and $\dot{y}_0$) decreases by a factor e within a time $t_1 = \tau$. Hence the designation "relaxation time" for the expression (I.30).

2. If the particle begins to move in the stationary air in the absence of forces of gravity with initial velocity v_0, then it will cover during the entire (infinite) time of motion a segment called the range (inertial):

$$\lambda_1 = v_0\tau. \qquad (I.32)$$

3. If the particle moves in stationary air, then it

acquires under the influence of the force of gravity (after an infinite time) a stationary settling speed (sedimentation speed)

$$v_s = g\tau = \frac{\rho_p d^2 g}{18\eta}. \qquad (I.33)$$

4. If the initial velocity of the particle is zero, then its velocity will reach a value au_0 (where $a < 1$) within a time $-\tau \ln(1 - a)$. In this case, it will cover a path

$$x_a = -\tau u_0 [a + \ln(1 - a)].$$

Table 1

d [μ]	τ [sec]	v_s [cm/sec]	λ_1 [cm]	x_a [cm]
1	$3{,}1 \cdot 10^{-6}$	0,003	0,022	$3{,}4 \cdot 10^{-8}$
2	$1{,}2 \cdot 10^{-5}$	0,012	0,084	$5{,}2 \cdot 10^{-7}$
5	$7{,}8 \cdot 10^{-5}$	0,076	0,55	$2{,}1 \cdot 10^{-5}$
10	$3{,}1 \cdot 10^{-4}$	0,3	2,17	$3{,}4 \cdot 10^{-4}$
20	$1{,}2 \cdot 10^{-3}$	1,2	8,4	$5{,}2 \cdot 10^{-3}$
50	$7{,}8 \cdot 10^{-3}$	7,6	54,6	0,21
100	$3{,}1 \cdot 10^{-2}$	30	217	3,4

Table 1 lists the values of τ, v_s, λ_1 ($v_0 = 70$ m/sec is the speed of a passenger airplane), and x_a for $a = 0.99$ (with $u_0 = v_s$) for water drops ($\rho_p = 1$ g/cm^3) at an air temperature 20°C and pressure 760 mm mercury ($\eta = 1.8 \cdot 10^{-4}$ poise). The last two lines of the table give tentative values of the foregoing quantities, for at such drop dimensions usually noticeable deviations from Stokes law set in.

It is seen from Table 1 that the relaxation time for cloud drops ($d < 50$ microns) is very small). Therefore, very frequently (when the gradients of the velocity $u_1(r_1)$ are small) it is possible to assume for them a velocity v_1 equal to the stream velocity u_1, or the smallness of τ causes a very rapid equalization of the velocities v_1 and u_1. This means that in these cases it is possible to neglect the inertial term of equation (I.12).

We note, finally, that equations (I.31) frequently serve as the basis for calculating the motion of aerosol particles in an inhomogeneous velocity field (see, for example, [79] and [41]). For this purpose the particle trajectory is broken up into several parts, in each of which one assumes the velocity field to be inhomogeneous with velocity u_{av} equal to the arithmetic mean value of the quantity u at the beginning and the start of the segment. This method of calculation makes it possible to break up the trajectory into a small number of portions than would be necessary, for example, in the usual Euler method (for equal computation accuracy).

B. Let us consider the motion of small aerosol particles in a so-called hyperbolic stream, corresponding to the flow of air over an infinite wall [141]. The velocity components of this stream have the form

$$u_{1x} = -a_1 x;\ u_{1y} = b y_1 \qquad (a_1 > 0;\ b_1 > 0) \tag{I.34}$$

and for a planar stream we have $b_1 = a_1$, while for an axially symmetrical one $b_1 = \frac{1}{2}a_1$. The current lines for such a stream are hyperbolas ($x_1 y_1 = \text{const}$ for a planar stream and $x_1 y_1^2 = \text{const}$ for an axially-symmetrical one). They are shown in Figure 5.

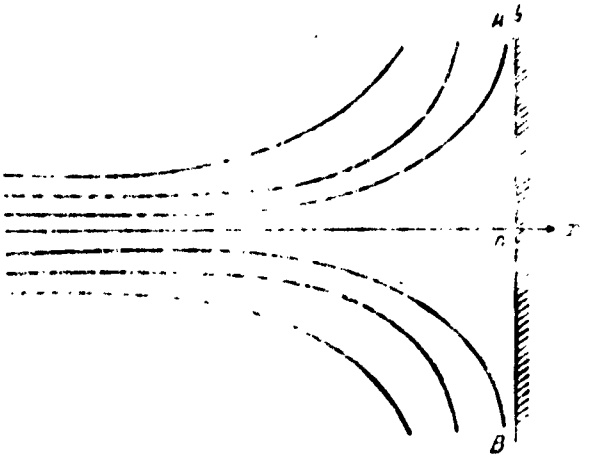

Fig. 5. Diagram of "hyperbolic stream."

The equations of motion of aerosol particles in this stream have the following (dimensionless) form:

$$k\frac{d^2x}{dt^2}+\frac{dx}{dt}+ax=0 \qquad \text{(I.35.1)}$$

and

$$k\frac{d^2y}{dt^2}+\frac{dy}{dt}-by=0, \qquad \text{(I.35.2)}$$

where $k=\tau\frac{u_\infty}{l}$, $a=\frac{a_1 l}{u_\infty}$, $b=\frac{b_1 l}{u_\infty}$ are dimensionless parameters.

The unit velocity u_∞ and the unit length l are chosen to be arbitrary but fixed quantities (the stream has no characteristic velocity or length).

These equations are homogeneous linear second-order equations, so we can write down their solutions immediately:

$$x=C_1e^{\lambda_1 t}+C_2e^{\lambda_2 t}, \qquad \text{(I.36.1)}$$

$$y=C_3e^{\mu_1 t}+C_4e^{\mu_2 t}, \qquad \text{(I.36.2)}$$

where $\lambda_{1,2}$ and $\mu_{1,2}$ are the roots of the corresponding characteristic equations

$$\lambda_{1,2}=\frac{-1\pm\sqrt{1-4ak}}{2k}, \quad \mu_{1,2}=\frac{-1\pm\sqrt{1+4bk}}{2k}. \qquad \text{(I.37)}$$

and the arbitrary integration constants C_1, C_2, C_3, and C_4 are determined from the initial conditions:

$$\text{for} \quad t=0:\ x=x_0;\ y=y_0;\ \dot{x}=\dot{x}_0;\ \dot{y}=\dot{y}_0. \qquad \text{(I.36.3)}$$

The system (I.35) was broken up into two individual equations (I.35.1) and (I.35.2). An analysis of the behavior of the trajectories of this system is best carried out by plotting the phase trajectories in the phase planes (x, v_x) and (y, v_y). For this purpose we rewrite (I.35) in the form

$$\frac{dv_x}{dx}=\frac{-ax-v_x}{kv_x}, \qquad \text{(I.38.1)}$$

$$\frac{dv_y}{dy} = \frac{by - v_y}{kv_y} \qquad \text{(I.38.2)}$$

We consider first equation (I.38.2). We can readily visualize the phase-trajectory pattern by noting that the origin on the phase plane (y, v_y) is a singularity of the saddle type. Recognizing that $\mu_2 = \frac{-1-\sqrt{1+4bk}}{2k} < 0$ and $0 < \mu_1 < b$, it is possible to plot the phase trajectories (Fig. 6). It is seen from Figure 6 that for all initial conditions (with exception of the initial conditions corresponding to the asymptote $v_y = \mu_2 y$) the phase trajectory will approach after a finite time interval to the asymptote $v_y = \mu_1 y$. This means that the trajectory will have in final analysis values of y of ever increasing absolute magnitude.

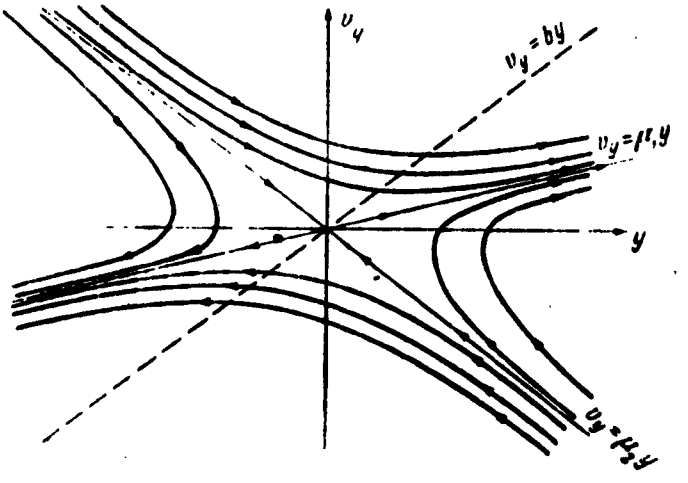

Fig. 6. Phase trajectories of equation (I.38.2). Singularity of the saddle type.

Let us procede now to an examination of equation (I.38.1). In this case, the phase-trajectory pattern depends on the parameter k. If $k > 1/4a$, then the origin of the phase plane (x, v_x) is a singular point of the stable-focus type and the phase-trajectory pattern has the form shown in Figure 7. It is seen from Figure 7 that for

arbitrary initial conditions corresponding to the points on the left half of the figure (the second and third quadrants; we recall that in Figure 5 the coordinate is $x \leqslant 0$), the trajectory will cross after a finite time interval the axis $x = 0$ (the wall AB in Fig. 5), and will have then a finite component v_x. This means that when $k > 1/4a$ the aerosol particles must sooner or later settle on the wall AB.

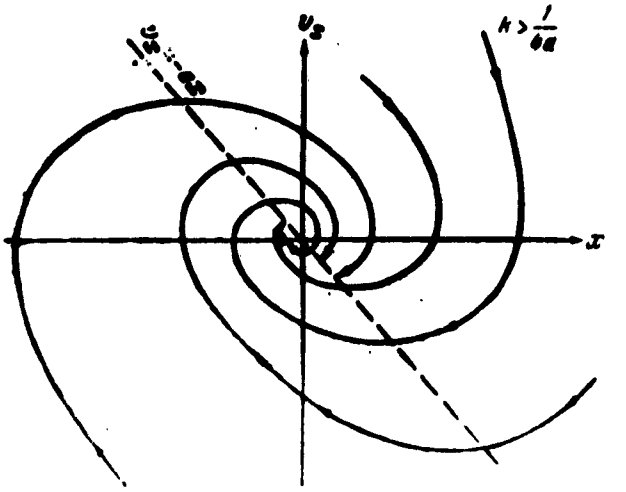

Fig. 7. Phase trajectories of equation (I.38.1) when $4ak > 1$. Singularity of the focus type.

The situation is different when $k \leqslant 1/4a$. In this case, the origin of the phase plane (x, v_x) is a singular point of the node type. Recognizing that according to (I.37) λ_1 and λ_2 are negative, and when $k \leqslant 1/4a$ the inequalities $\lambda_2 \leqslant \lambda_1 \leqslant$ - a hold true, we can plot the phase trajectories (Fig. 8). It is seen from this figure that for all the initial conditions corresponding to points lying on the left half of the figure below the line $v_x = \lambda_2 x$ ($v_x \leqslant \lambda_2 x$), the trajectories terminate at the origin. This means that under the initial condition $\dot{x}_0 \leqslant \lambda_2 x$ the particle reaches the wall AB ($x = 0$) after an infinite time. During that time, the particle, in accordance with equation (38.2) (see Fig. 7), will be moved away an infinite distance along the y axis. This means that the aerosol particles having a parameter $k \leqslant 1/4a$ will not settle on the wall AB if $\dot{x}_0 \leqslant \lambda_2 x$.

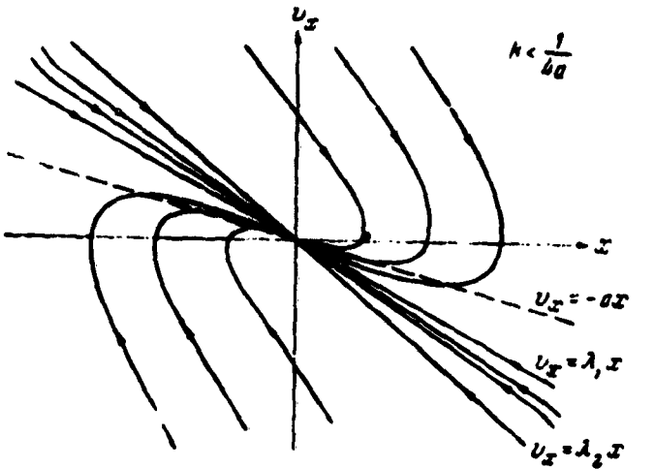

Fig. 8a. Phase trajectories of equation (I.38.1) when $4ak < 1$. Singularity of the node type.

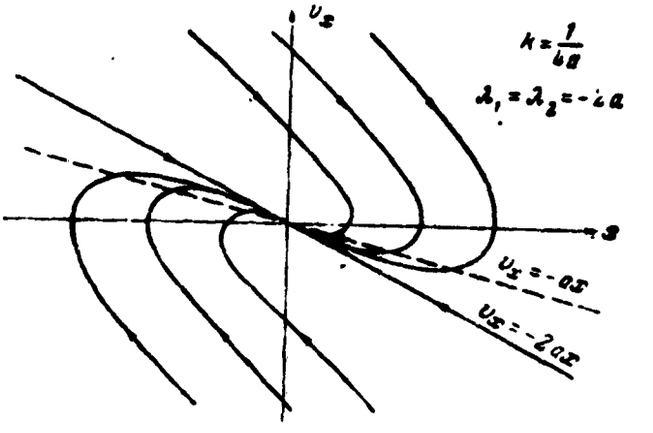

Fig. 8b. Phase trajectories of equations (I.38.1) when $4ak = 1$. Singularity of the degenerate node type.

If $\dot{x}_0 > \lambda_2 x$, then as can be seen from Figure 8, the trajectory crosses the axis $x = 0$ after a finite time interval, and has a finite value of the velocity component v_x. This means that when $\dot{x}_0 > \lambda_2 x$ the aerosol particle will settle on the wall AB.

The absence of settling of the aerosol particles of finite mass from the stream (I.34) for a broad class of initial conditions is a particular case of a phenomenon which is of principal significance for the process of inertial settling of aerosol particles from a stream on obstacles. In the next section we shall consider this phenomenon in detail.

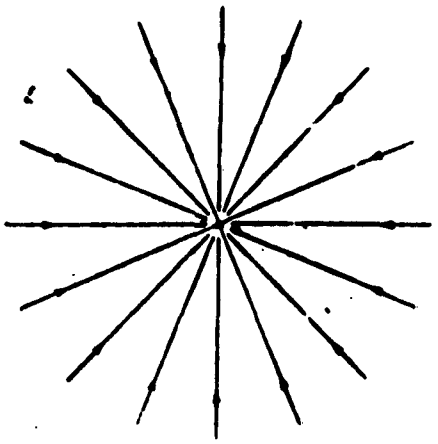

Fig. 9. Current lines of a sink.

C. Let us consider the motion of small aerosol particles in the field of air velocities brought about by a linear sink or source. We note that the case of a linear sink is a scheme that stylizes the drawing of an aerosol which is stationary at infinity into a narrow slot. The field $u_1(r_1)$ has in this case actual symmetry and has in cylindrical coordinates the following components:

$$u_{1r} = \mp \frac{Q_1}{2\pi r_1}; \; u_{1\varphi} = 0; \; u_{1z} = 0. \qquad (I.39)$$

where Q_1 is the volume strength per unit length of the sink or source, the sign "-" pertains to a sink, and the sign "+" to a source. Figure 9 shows the current lines of such fields.

If the initial velocities of the aerosol particles are radial, then the velocity $v_1(r_1)$ will have only one non-vanishing component v_{1r}, satisfying the equation

$$\tau \frac{dv_{1r}}{dt_1} + v_{1r} = \mp \frac{Q_1}{2\pi r_1}. \qquad \text{(I.40)}$$

Obviously, in this case the particle trajectories will coincide with the current lines of the air.

The problem formulated here contains only two characteristic physical quantities, Q_1 and τ. By choosing expressions containing Q_1 and τ and having the dimensions of length and velocity:

$$l = \sqrt{\frac{Q_1 \tau}{2\pi}}, \quad u_0 = \sqrt{\frac{Q_1}{2\pi\tau}}$$

(here $t_0 = l/u_0 = \tau$), we assume them to be the units length and velocity and reduce equation (I.40) to dimensionless quantities, writing this equation in the form:

$$\frac{dv_r}{dt} + v_r = \mp \frac{1}{r},$$

or

$$v_r \frac{dv_r}{dr} + v_r = \mp \frac{1}{r}. \qquad \text{(I.41)}$$

This equation of motion must be supplemented, in order to present a complete description of the problem, by the continuity equation, which in our case has the form

$$nv_r r = \text{const.} \qquad \text{(I.42)}$$

To solve (I.41) we make the change of variables

$$v_r = w - r, \quad \rho = \frac{1}{r}. \qquad \text{(I.43)}$$

We then obtain for the new variables ρ and w the linear equation:

$$\frac{d\rho}{dw} \mp (\rho w - 1) = 0. \qquad \text{(I.44)}$$

Equation (I.44) has the following solutions: for the case of a sink

$$\frac{1}{r} = \rho = \rho_0 \exp\left[\frac{w^2 - w_0^2}{2}\right] +$$

$$+ \sqrt{\frac{\pi}{2}} \exp\left[\frac{w^2}{2}\right]\left[\operatorname{erf}\frac{w_0}{\sqrt{2}} - \operatorname{erf}\frac{w}{\sqrt{2}}\right], \; v_r = w - r, \qquad \text{(I.45)}$$

for the case of a source

$$\frac{1}{r} = \rho = \sqrt{2}F\left(\frac{w}{\sqrt{2}}\right) + \exp\left[-\frac{w^2 - w_0^2}{2}\right]\left[\rho_0 - \sqrt{2}F\left(\frac{w_0}{\sqrt{2}}\right)\right],$$

$$v_r = w - r, \qquad \text{(I.46)}$$

where the initial condition $v_r = v_0$ when $r = r_0$ corresponds to the values

$$\rho_0 = \frac{1}{r_0} \text{ and } w_0 = v_0 + r_0,$$

and

$$\operatorname{erf} x = \frac{2}{\sqrt{\pi}}\int_0^x e^{-t^2}\,dt, \quad F(x) = e^{-x^2}\int_0^x e^{t^2}\,dt$$

are known calculated functions (see, for example, [20, Chapter II]).

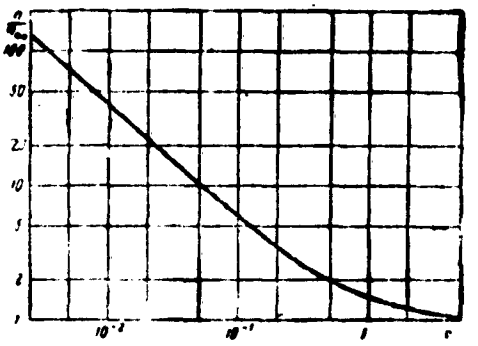

Fig. 10. Variation of the counted concentration of the aerosol particles in the velocity field of a sink.

Let us examine solution (I.45) under initial conditions corresponding to the motion of the aerosol particles together with the air at large distances from the source ($v_r \approx u_r$ when $r \to \infty$). In this case we have $w_0 = +\infty$, $\rho_0 = 0$ and consequently

$$\rho = \sqrt{\frac{\pi}{2}}\, e^{\frac{w^2}{2}}\left[1 - \operatorname{erf}\left(\frac{w}{\sqrt{2}}\right)\right]. \qquad \text{(I.47)}$$

Since at infinity we have in this case $v_r = u_r = -1/r$,

it follows from the continuity equation (I.42) that*

$$\frac{n_\infty}{n(r)} = -rv_r = \frac{v_r}{u_r}. \qquad \text{(I.48)}$$

Figure 10 shows a plot of the dependence of the quantities $\frac{n}{n_\infty} = \frac{u_r}{v_r}$ on r, constructed on the basis of equations (I.47) and (I.48). As can be seen from Figure 10, the velocities of the aerosol particles are always smaller than the stream velocity u_r, and consequently, the concentration of the aerosol particles is everywhere larger than the concentration n_∞ of the unperturbed aerosol (see Section 3). It is seen from Figure 10 that noticeable changes in the concentration (larger than 10 percent) arise when $r < 2.4$. When $r = 0.1$, the ratio $n/n_\infty = 5$. When $r \to 0$, the ratio $\frac{n}{n_\infty} = \frac{u_r}{v_r}$ tends to infinity. Indeed, according to equation (I.47, $r \to 0$ when $w \to -\infty$. At the same time, $\rho = \frac{1}{r} \to \sqrt{2\pi}\, e^{\frac{w^2}{2}}$, and $v_r = w - r \to w$. Consequently

$$\frac{n}{n_\infty} = \frac{u_r}{v_r} \to -\frac{\sqrt{2\pi}}{w} e^{-\frac{w^2}{2}} = \frac{1}{r\sqrt{-\ln(2\pi r^2)}}.$$

We note, however, that in spite of the fact that n(r) tends to infinity near the sink, in a finite vicinity near the sink ($0 \leqslant r \leqslant R$) there is contained a finite number of aerosol particles

$$N_R = \int_0^R 2\pi r n(r)\, dr = n_\infty \pi \left(1 - \operatorname{erf}\sqrt{-\tfrac{1}{2}\ln(2\pi R^2)}\right).$$

At large distances from the sink, one can readily obtain the following series for r, v_r, and n/n_∞:

$$r = w + \frac{1}{w} - \frac{2}{w^3} + \frac{10}{w^5} - \frac{74}{w^7} \cdots$$

---

*It follows from (I.48) that in the cases of the sinks and sources considered here the flow concentration of the aerosol particles remains constant.

$$-v_r = \frac{1}{r^2} - \frac{2}{r^3} + \frac{10}{r^5} - \frac{74}{r^7} \cdots$$

$$\frac{n}{n_\infty} = 1 + \frac{1}{r^3} - \frac{5}{r^4} + \frac{39}{r^6} \cdots$$

A complete qualitative picture of the behavior of the aerosol particles on the trajectories for arbitrary initial conditions is shown in Figure 11, which represents the phase trajectories of equation (I.41) for a sink on the phase plane (r, v_r). In this figure the curve AB corresponds to motion of aerosol particles, described by equation (I.47), i.e., to motion such that at infinity they move together with the air. The velocity $u_r(r) = -1/r$ is represented by the curve CD. (This is the curve of the maxima for the phase trajectories). The curves EF and E_1F_1, described by the equation $r = v_r - 1/v_r$, represent the geometric locus of the points of inflexion of the phase trajectories. The phase trajectories (with the exception of the trajectory AB) are represented by dashed lines. The arrows on them characterize the direction of motion of the aerosol particles in time. As shown by Figure 11, the phase trajectory AB represents an asymptotic curve for all other phase trajectories as $t \to \infty$.

From the methodological point of view, it is interesting to trace the variation of the aerosol-particle concentrations as they move along a trajectory with arbitrary initial conditions. To employ in this case the concept of concentration we can visualize that at the instant time $t = t_0$ there are contained inside the annular region bounded by the surfaces $r = r_0$; $r = r_0 + dr$, aerosol particles with concentration n_0 and velocity $v_r = v_0$. Inasmuch as we have along the trajectory

$$\frac{1}{n} \cdot \frac{Dn}{Dt} = -\operatorname{div} v, \qquad (I.28)$$

then the change in the concentration is connected with the sign of div v. But in our case [see equation (I.41)]

$$\operatorname{div} v = \frac{v_r}{r} + \frac{dv_r}{dr} = \frac{v_r}{r} + \left(-1 - \frac{1}{rv_r}\right) = \frac{1}{r}\left(v_r - \frac{1}{v_r} - r\right).$$

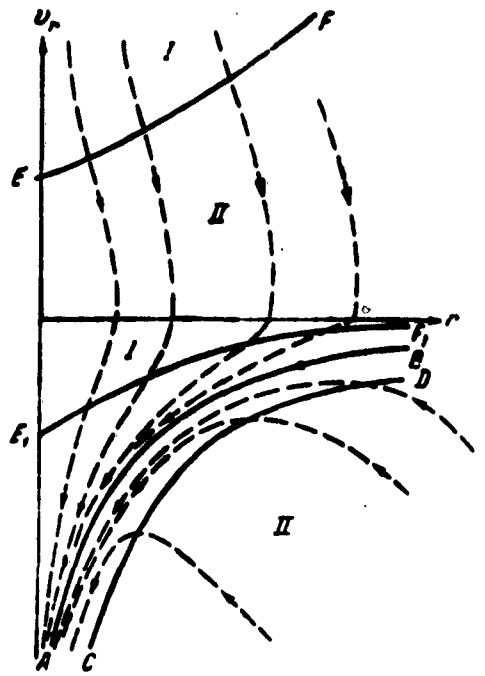

Fig. 11. Phase trajectories of equation (I.41) in the case of a sink.

The expression in the parentheses reverses sign on the curves EF and E_1F_1. In the regions below the curve EF and between the curve E_1F_1 and the axis $v_r = 0$ this expression is positive, and below the curve E_1F_1 and in the region between the curve EF and the axis $v_r = 0$ it is negative. Consequently, in the regions designated by I in Figure 11, the concentration n decreases (while in the regions designated by II the concentration n increases). The reduction in the concentration along the trajectory in certain regions of the phase plane (r, v_r) does not contradict the conclusion that n increases along the trajectory, a conclusion given in Section 3, since this conclusion was based on the assumption that at the initial instant of time div $v \leqslant 0$.

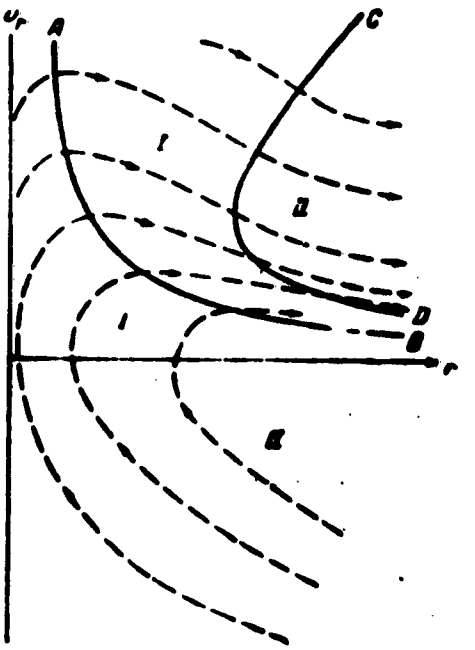

Fig. 12. Phase trajectories of equation (I.41) in the case of a source.

Let us consider now briefly the case of a source, a case of lesser physical interest on the case of a sink. Figure 12 shows the phase trajectories for equation (I.41) (case of source). In Figure 12, the curve AB, which corresponds to a velocity $u_r = 1/r$, represents the geometric locus of the maxima of the phase trajectories. The curve CD, the equation of which is $r = v^r + 1/v_r$, is the geometric locus of the points of inflection of the phase trajectories and is simultaneously the geometric locus of the points where div v = 0. In the regions denoted by the number I, we have

$$\operatorname{div} v = \frac{1}{r}\left(v_r + \frac{1}{v_r} - r\right) > 0$$

and the concentration n decreases along the trajectory. In the regions denoted by II we have

$$\operatorname{div} v < 0 \text{ and } \frac{Dn}{Dt} > 0.$$

For the case of a point-like sink or source, the equation of motion has a form analogous to that of equation (I.41):

$$v_r \frac{dv_r}{dr} + v_r = \mp \frac{1}{r^2}. \qquad (I.49)$$

By means of a system of substitutions

$$v_r = w - r, \quad \rho = \frac{1}{r}, \quad \rho = v \pm \frac{w^2}{2}$$

equation (I.41) is reduced to a Riccati equation [126]:

$$\frac{dw}{dv} \pm v + \frac{w^2}{2} = 0,$$

which by the substitution

$$w = \frac{2}{u} \cdot \frac{du}{dv}$$

can be reduced to the linear equation

$$\frac{d^2u}{dv^2} \pm \frac{vu}{2} = 0.$$

The last equation has a solution that can be expressed in terms of Bessel functions of order 1/3. The results of the analysis of equations (I.49) are analogous to the arguments made with respect to equations (I.41). The phase trajectories of equations (I.49) coincide qualitatively with the phase trajectories shown in Figs. 11 and 12.

5. CRITICAL CONDITIONS FOR THE SETTLING OF AEROSOL PARTICLES FROM A STREAM ON AN OBSTACLE

We have already seen in the preceding section, with the inertial settling of aerosol particles on a wall from a hyperbolic stream as an example, that there exists a critical Stokes number

$$k_{cr} = \frac{1}{4\pi}.$$

It was shown there that when $k < k_{cr}$ the aerosol particles do not settle on the wall, and consequently their capture coefficient is $E = 0$. This means that in the indicated case there exists a minimum dimension d_{min} for the aerosol particles that settle from the stream.

Such a phenomenon is observed not only for a hyper-

bolic stream.* In the present section we shall prove the existence of critical conditions of settling for a large class of symmetrical aerosol streams and will show the connection between the value of the critical Stokes number and the behavior of the stream near its symmetry line and near its critical point [21, 32]. We shall consider the flow around symmetrical bodies by streams in which the current lines which terminate in the forward critical point are straight lines. Such streams are formed when a body is placed in a stream whose velocity at infinity is parallel to the axis of the symmetrical body. These bodies should have either axial symmetry (longitudinal flow around bodies of revolution), or an n-fold rotation axis ($n \geqslant 2$). Such bodies include also those having two mutually-perpendicular symmetry planes, and, in particular, bodies of revolution which have a symmetry plane perpendicular to the axis of revolution, in the case when the flow around them is transverse. Finally, such bodies include also cylinders with a plane of symmetry (two-dimensional flows around symmetrical cylinders).

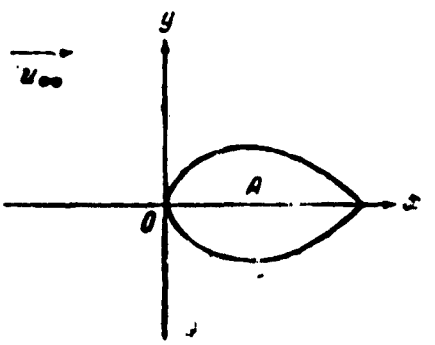

Fig. 13. Coordinate system.

For the sake of being specific, we shall prove the existence of critical settling conditions for plane symmetrical streams, since all the main features of this proof remain in force also for all the other streams. Let us

*Even in the first paper where the capture coefficient was calculated [79], it was found by calculation for the case of inertial settling of aerosol particles on a cylinder from a potential stream, that the critical Stokes number is $k = k_{cr} \approx 0.18$, which is the upper limit of the value of k for which E = 0.

consider a two-dimensional symmetrical incompressible flow of aerosol around a symmetrical cylindrical body A. To investigate the motion of the aerosol particles in a plane perpendicular to the cylinder axis, we choose the origin of the Cartisian system of coordinates in the forward critical point of the stream flowing around obstacle A (Fig. 13). The Ox axis is the symmetry line of the stream. Then, the velocity vector of the air stream u will have on the Ox axis components $u_y = 0$; $u_x = \varphi(x)$. In the vicinity of the symmetry line (the coordinate y is small) it is possible, taking into account the symmetry of the stream, to expand the components $u_x(x, y)$, $u_y(x, y)$ in powers of y

$$u_x(x, y) = \varphi(x) + y^2\varphi_2(x) + y^4\varphi_4(x) + \dots$$
$$u_y(x, y) = yf_1(x) + y^3f_3(x) + y^5f_5(x) + \dots$$

Using the continuity equation for the air stream

$$\operatorname{div} u = \frac{\partial u_x}{\partial x} + \frac{\partial u_y}{\partial y} = 0,$$

we obtain

$$f_1(x) = -\varphi'(x),\ f_3(x) = -\frac{1}{3}\varphi_2'(x) \text{ etc.}$$

Consequently, accurate to terms of order of smallness in y, we have near the symmetry line

$$u_x = \varphi(x);\ u_y = -y\varphi'(x). \tag{I.50}$$

Let us consider now the type of the function $\varphi(x)$. Recognizing that the dimensionless velocity u(r) is obtained by dividing the velocity $u_1(r_1)$ by the stream velocity at intensity u_∞, we obtain that $\varphi(x) = 1$ when $x = -\infty$. At a large distance from the body, the velocity gradients are very small. Consequently, when $x = -\infty$ the derivative is $\varphi'(x) = 0$. In the interval $x[-\infty, -\varepsilon]$, where $\varepsilon > 0$ and is as small as desired, the function $\varphi(x)$ is positive everywhere and decreases monotonically with increasing x, i.e., when $-\infty < x < -\varepsilon$ we have

$$\varphi(x) > 0,\ \varphi'(x) < 0. \tag{I.51}$$

At the origin (critical point) we have $\varphi(x) = 0$. As regards the value of the derivative $\varphi'(x)$ at the origin, it can differ, since it depends on the character of the stream.

For potential streams it usually will have a finite negative value $\varphi'(0) = -a$. It can be shown (see Appendix I) that for bodies that have a convex wall at the critical point, a potential stream will have at the origin finite negative values of the first and second derivatives $\varphi'(x)$ and $\varphi''(x)$. In these cases near the critical point, the stream velocity can be approximated in the following fashion

$$u_x = -ax, \quad u_y = +ay. \tag{I.52}$$

This means that near the critical point in this case a potential air stream is approximated by a hyperbolic stream (the current lines are the hyperbolas $xy = \text{const}$). In the case of a viscous air stream, the stream velocity on the wall is equal to zero (adhesion condition) and consequently on the entire surface of the body the tangential component of the velocity is equal to zero, and in particular, we have at the critical point

$$\frac{\partial u_y}{\partial y} = 0.$$

We then have by virtue of the continuity equation

$$\varphi'(0) = \left(\frac{\partial u_x}{\partial x}\right)_0 = -\left(\frac{\partial u_y}{\partial y}\right)_0 = 0.$$

Consequently, near the origin, the following approximate expressions will be valid for the velocity of a viscous stream:*

$$u_x = \alpha |x|^n, \quad u_y = n\alpha y |x|^{n-1}. \tag{I.53}$$

The motion of the aerosol particles near the symmetry line will be described by the equations

$$k\frac{dv_x}{dt} + v_x = \varphi(x), \tag{I.54}$$

$$k\frac{dv_y}{dt} + v_y = -y\frac{d\varphi(x)}{dx} \tag{I.55}$$

with the following initial conditions:

$$\text{for} \quad t = -\infty: \; x = -\infty, \; v_x = \dot{x} = 1, \; y = y_0, \; v_y = \dot{y} = 0. \tag{I.56}$$

---

*We note that the same relations (I.53) can hold true also for a potential stream if the origin is a point on the counter of the body (see Appendix I).

The first equation of this system is independent.

Let us investigate first the solution of this equation (I.54), which we rewrite in the form

$$kv_x \frac{dv_x}{dx} + v_x = \varphi(x). \qquad (I.57)$$

We are interested in solutions of equation (I.57), $v_1(x, k)$, satisfying the condition (I.56), i.e., the condition $v_x = 1$ when $x = -\infty$. Let us consider the set of such solutions $v_1(x\ k)$, corresponding to values of k from 0 to $+\infty$. We shall prove that this is an ordered set. For this purpose we apply to equation (I.57), rewritten in the form

$$\Phi(v_x, x) = \frac{dv_x}{dx} - \frac{\varphi(x) - v_x}{kv_x} = 0, \qquad (I.58)$$

the theorem of S. A. Chaplygin concerning differential inequalities [72]. According to this theorem, if we succeed in choosing such a function $z(x)$ which coincides with v_x when $x = -\infty$, and which satisfies in the entire remaining interval the relation

$$\Phi(z, x) \gtrless 0, \text{ then } z(x) \gtrless v_x(x).$$

By way of such a function we choose $z(x) = \varphi(x)$. Then,

$$\Phi(z, x) = \frac{d\varphi}{dx} < 0$$

on the interval $x[-\infty, -\varepsilon]$, and consequently on the same interval we have

$$z(x) = \varphi(x) < v_x(x).$$

It follows therefore that on the same interval

$$\frac{dv_x}{dx} < 0.$$

Employing the Chaplygin theorem in the same way, we can readily show that on the interval $x[-\infty, -\varepsilon]$, we have

$$\varphi(x) < v_1(x, k_2) < v_1(x, k_1) < 1, \qquad (I.59)$$

if

$$0 < k_2 < k_1.$$

It is obvious that $v_1(0, k) \geqslant 0$. When $k = +\infty$ the solution of equation (I.57) will be $v_1(x, +\infty) = 1$, and when $k = 0$ we have $v_1(x, 0) = \varphi(x)$ (Fig. 14). The set of continuous functions $v_1(x, k)$ which are ordered in accordance with expression (I.59) tends as $k \to 0$ to a limiting function $\inf v_1(x)$ which cannot differ from $\varphi(x)$, for otherwise at very small values of k the function $v_1(x, k)$ would have a derivative which would be as large in absolute magnitude value as desired:

$$\frac{dv_1(x, k)}{dx} = \frac{1}{k^2}\,|\varphi(x) - v_1(x, k)|$$

at each point where $\inf v_1(x)$ differs from $\varphi(x)$. Therefore the sequence $v_1(x, k)$ converges continuously to $\varphi(x)$ as $k \to 0$ over the entire interval $[-\infty, -\varepsilon]$ of x.

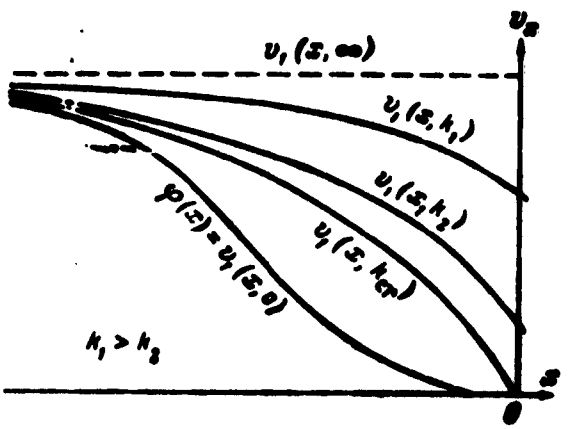

Fig. 14. Velocity plots.

The curves $v_1(x, k)$ on the phase plane (x, v_x) can cross the $0v_x$ axis with $v_x \neq 0$ or pass through the origin: $v_1(0, k) \geqslant 0$.

In the first case the derivative is $v_1'(0, k) = \frac{dv_1(x, k)}{dx}\Big|_{x=0} = -\frac{1}{k}$. In the second case the value of $v_1(0, k)$ is in-

determinate, since the origin is a singular point for equation (I.57). For the case described by equations (I.57) and (I.52) (a potential stream, for which $a \neq 0$), qualitative pictures of the integral curve near the origin were already considered by us in the preceding section. They were shown in Figs. 7 and 8. When $k > \frac{1}{4a}$ the origin will be a singular point of the stable focus type and therefore when $k > \frac{1}{4a}$ there will exist no integral curve passing through the origin (see Fig. 7). When $k \leqslant \frac{1}{4a}$ the origin will be a singular point of the stable node type. When $k < \frac{1}{4a}$ we have in this singular point two exclusing directions,* determined by the equation $v_x = \lambda_1 x$ (this direction corresponds to a bundle of integral curves which have at a common tangent $v_x = \lambda_1 x$) and $v_x = \lambda_2 x$ (corresponding to this direction is an isolated integral curve), where the

---

*By exclusive directions are meant such directions along which the integral curves can enter into the singular point [45]. Two cases are possible: either the singular point has a finite number of exclusive directions, or else the integral curves enter into the singular point along arbitrary directions. For the equation

$$\frac{dy}{dx} = \frac{P_m + \eta_1}{Q_n + \eta_2},$$

where P_m and Q_n are homogeneous polynomial of degrees m and n, while η_1 and η_2 include the terms of higher order relative to x and y, the exclusive directions are determined from the characteristic equation

$$F(\varphi) = 0,$$

where

$$F(\varphi) = P_m(\cos\varphi, \sin\varphi)\cos\varphi - Q_n(\cos\varphi, \sin\varphi)\sin\varphi,$$

and the direction $\varphi = \varphi_0$, where $F(\varphi_0) = 0$, is certainly an exclusive direction, if

$$G(\varphi_0) = Q_n(\cos\varphi_0, \sin\varphi_0)\cos\varphi_0 + P_m(\cos\varphi_0, \sin\varphi_0)\sin\varphi_0 \neq 0.$$

coefficients $-a \geqslant \lambda_1 > \lambda_2$ are determined by equation (I.37) (see Fig. 8a). When $k = \frac{1}{4a}$ there is one exclusive direction $v_x = -2ax$ (Fig. 8b).

Let us consider now the pattern of the interval curves near the origin for the case described by equations (I.57) and (I.53) (a viscous stream and several singular cases of a potential stream, when $a = 0$). In this case, the exclusive directions are determined by an equation that yields two solutions:

$$v_x = -\frac{x}{k} \text{ and } v_x = 0.$$

The affine transformation

$$v_x = a^{-\frac{1}{n-1}} k^{-\frac{n}{n-1}} w, \quad x = (ak)^{-\frac{1}{n-1}} \xi$$

converts equations (I.57) and (I.53) into the Emden equation

$$w \frac{dw}{d\xi} + w = |\xi|^n.$$

Thus, in this case the pattern of the integral curves near the singular point is the same as near the singular point of the Emden equation. Moreover, in exactly the same manner as is done for the Emden equation [52], it can be shown that the integral curves for equation (I.57), for which when $x \to 0$ we have $\varphi(x) \to x|x|^n$, have the following properties:

1. For a given k there exists one and only one integral curve G(x), which enters into the origin along the direction $v_x = -x/k$. This curve G divides all the integral curves into two classes: the class of curves F, which pass through the second quadrant above the curve G and cross the Ov_x axis with slope $v'_x = -1/k$, and the class of curves M, which pass through the origin and which lie in the second quadrant above the curve G.

2. For the curves of class M we have

$$\lim_{x \to -0} \frac{v_x(x)}{\varphi(x)} = 1.$$

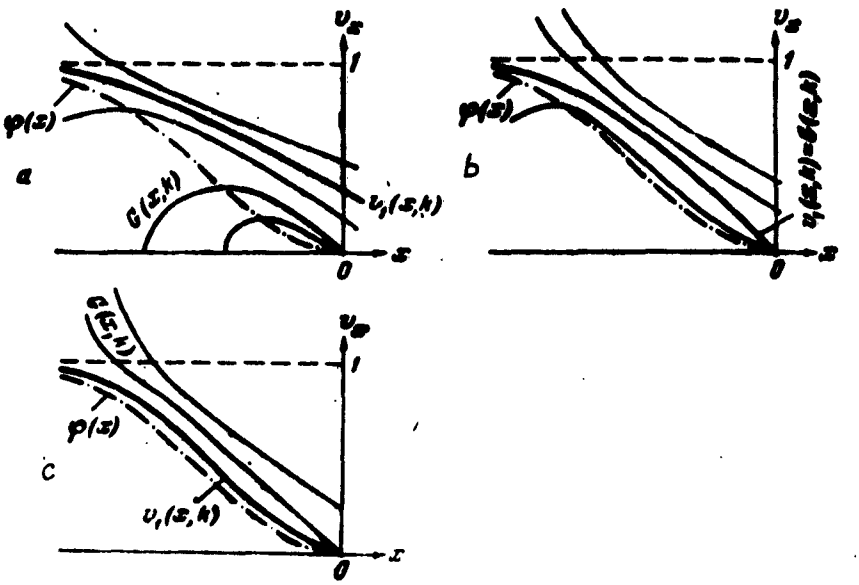

Fig. 15. Form of the integral curves of equation (I.57) for different values of the Stokes number:

$$a - k > k_{cr},\ v_1(x, k) = F(x, k);$$
$$b - k = k_{cr},\ v_1(x, k) = G(x, k);$$
$$c - k < k_{cr},\ v_1(x, k) = M(x, k).$$

In Figures 15a, b, and c are shown qualitative pictures of the integral curves for three cases, when $v_1(x, k)$ represents a curve of the path F, G, and M respectively. It is easy to see [taking formula (I.59) into account] that in Figure 15 cases a, b, and c correspond to decreasing values of k.

We shall now define as the critical value $k = k_{cr}$ the upper limit of the set X of the parameters k, at which the curve $v_1(x, k)$ pass through the origin ($k_{cr} = \sup X$).*

*We note that the set X is not empty, since it contains at least one element $k = 0$. This set is bounded from above, since for large values of k the curve $v_1(x, k)$ crosses the ordinate axis above the origin.

We shall show that k_{cr} defined in this manner is greater than zero and when k is less than or equal to k_{cr} the coefficient for the capture of the aerosol particles by the body under consideration is equal to zero. We shall prove this first for the case of a potential stream ($a \neq 0$). Were we to have $k_{cr} = 0$, then for all values $k > 0$ the curve $v_1(x, k)$ would cross the Ov_x axis above the origin. Then, for a very small value of k the curve $v_1(x, k)$ would pass above the exclusive direction $v_x = \lambda_2 x$ and since $\lambda_2 \to -\infty$ when $k \to 0$, then the curve $v_1(x, k)$ would lie near the origin very close to the ordinate axis. But when $k = 0$ the curve $v_1(x, k)$ coincides with the curve $\varphi(x)$ and consequently it is located close to the origin near the line $v_x = -ax$. If therefore $k_{cr} = 0$, then for small but finite values of $|x|$ the continuity of the function $v_1(x, k)$ with respect to k, which was proved above, would be violated. From this follows the relation $k_{cr} > 0$. In the case under consideration it can be stated that $k_{cr} \leqslant 1/4a$, since when $k > 1/4a$ the origin is a singular point of the type of a focus and there exist no integral curves passing through the origin, i.e., when $k > 1/4a$ the curve $v_1(x, k)$ always crosses the Ov_x axis above the origin. Thus, for a potential stream ($a \neq 0$) we have

$$0 < k_{cr} \leqslant \frac{1}{4a}. \tag{I.60}$$

We shall now show that when $k \leqslant k_{cr}$ the capture coefficient is $E = 0$. For this purpose we consider equation (I.55), which we rewrite in the form

$$kv_x \frac{dv_y}{dx} + v_y = -\varphi\varphi'(x). \tag{I.61}$$

According to equation (I.61) with initial conditions (I.56), the coordinate y(x) should satisfy the equation

$$y(x) - y_0 = \int_{-\infty}^{x} v_y\,dt = \int_{-\infty}^{x} \frac{v_y}{v_x}\,dx = -kv_y(x) - \\ - \int_{-\infty}^{x} \frac{y(x)\varphi'(x)}{v_x(x)}\,dx. \tag{I.62}$$

But when $k \leqslant k_{cr}$, the velocity is $v_x(x) \approx \lambda_1 x$ when $x \to 0$. Therefore, y(x) cannot remain constant when $x \to 0$, owing to the divergence of the integral in the right half

of equation (I.62). This means that no matter how small the value of y_0, the quantity y/y_0 becomes as large as desired as the particle approaches the obstacle. Consequently, the local capture coefficient near the critical point of the stream under consideration is equal to zero when $k \leqslant k_{cr}$. The result obtained can be generalized to include also the capture coefficient of the entire coefficient as a whole. Indeed, when the aerosol particle moving near the symmetry plane, on leaving the vicinity of the critical point, will have a finite velocity v_y and a very low velocity v_x. Since on the boundary of the obstacle the normal component of the air velocity $v_n = 0$, v_n will be small everywhere near the obstacle. Therefore such a particle is carried out by the air stream and does not strike the obstacle. We note further that the trajectories of particles of identical size moving to infinity with the air stream should not cross one another, for in the opposite case the particle velocities of concentrations would be as large as desired near these points of intersection [on the basis of the continuity equation (I.15)]. Therefore when $k \leqslant k_{cr}$, the trajectories of the particles which have large values of y_0 when $x = -\infty$ (they are located away from the symmetry line) cannot terminate on the obstacle. Consequently, when $k \leqslant k_{cr}$ the capture coefficient of the obstacle as a whole is equal to zero [21].

We now proceed to consider a viscous stream. In this case, too, k_{cr} cannot equal zero, for then the curve $v_1(x, k)$ for the very small values of k would belong to class F and would cross the Ov_x axis along the direction $v'_x = -1/k$, close to the direction of the Ov_x axis. This would mean that small but finite values of x the continuity of the function $v_1(x, k)$ with respect to k would be violated, since when $k = 0$ we have $v_1(x, k) = \varphi(x)$ and $v'_1(0, 0) = 0$. It follows therefore that for viscous flow we have

$$k_{cr} > 0. \qquad (I.63)$$

It is obvious that when $k = k_{cr}$ the curve $v_1(x, k_{cr})$ represents a G-curve corresponding to the value $k = k_{cr}$. This is seen from the fact that in the opposite case $v_1(x, k_{cr})$ would represent a curve of the type M, and $v_1(x, k_{cr} + \delta)$, where δ is a small positive number as small as desired, would represent a type F curve. Since this would violate

the continuity of $v_1(x, k)$ with respect to k, the curve $v_1(x, k_{cr})$ is a curve of the type G. Since when $k < k_{cr}$ the curve $v_1(x, k)$ is a curve of class M, we have from the property of these curves $v_1(x, k) \to \varphi(x)$ when $x \to -0$. Therefore y(x) in equation (I.62) cannot remain finite, and consequently when $k < k_{cr}$ the local capture coefficient is equal to 0. By virtue of the continuity of the function E(k), the local capture coefficient should equal 0 also when $k = k_{cr}$. Using the same arguments as for a potential stream, it can be shown that for a viscous stream the capture coefficient of the obstacle as a whole is equal to zero when $k < k_{cr}$ [32].

6. CRITICAL VALUE OF THE STOKES NUMBER k_{cr} FOR POTENTIAL AND VISCOUS STREAMS.

ESTIMATE OF THE INFLUENCE OF THE BOUNDARY LAYER ON k_{cr} OF A POTENTIAL

In the preceding section it was shown that for a wide class of incompressible potential and viscous streams, flowing around symmetrical bodies, there exists a critical value of the Stokes number, $k = k_{cr}$, such that when $k \leqslant k_{cr}$ the capture coefficient of the obstacle is equal to zero. However, this proof did not enable us to determine the value of k_{cr}. In the present section we shall determine the value of k_{cr} for a potential stream (when $a \neq 0$), and we shall consider a calculation method and an interpolation formula for k_{cr} of a viscous stream.

We consider first a certain relation between the values of k_{cr} of different values, a relation which will be useful for an estimate of the value of k_{cr}. If we have two different symmetrical streams, in one of which the function $\varphi^{I}(x)$ is larger everywhere on the interval $x[-\infty, 0]$ than the function $\varphi^{II}(x)$ of the second stream, then for a specified value of the parameter k we can establish the following relation:

$$v_1^{I}(x, k) > v_1^{II}(x, k). \qquad (I.64)$$

Inequality (I.64) can be readily obtained by using the Chaplygin theorem on differential inequalities [72] as applied to the equation (I.58). From the inequality (I.64)

it follows that

$$k_{cr}^{I} \leqslant k_{cr}^{II}, \tag{I.65}$$

for in the opposite case when $k = k_{cr}^{I}$ the function $v_1^{I}(x, k_{cr}^{I})$ passes through the origin, while the function $v_1^{II}(x, k_{cr}^{I})$ crosses the Ov_x axis above the origin. In this case, there would exist on a finite segment to the left of the origin the inequality $v_1^{II}(x, k_{cr}^{I}) > v_1^{I}(x, k_{cr}^{I})$, which would contradict relation (I.64).

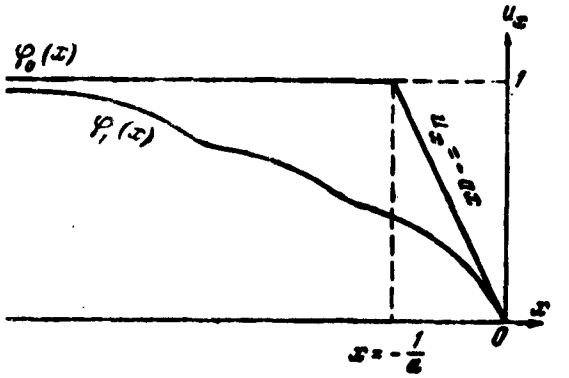

Fig. 16. Illustrating the proof of formula (I.68).

From equation (I.65) it follows that for a stream having the function $\varphi_2(x)$ which is contained on the interval $x[-\infty, 0]$ between the functions $\varphi_1(x)$ and $\varphi_3(x)$, namely

$$\varphi_1(x) < \varphi_2(x) < \varphi_3(x) \tag{I.66}$$

the value of the critical Stokes parameter k_{cr}^{II} lies between the values of k_{cr}^{I} and K_{cr}^{III}:

$$k_{cr}^{I} \geqslant k_{cr}^{II} \geqslant k_{cr}^{III}. \tag{I.67}$$

It is now easy to establish the value of k_{cr} for a

large class of potential streams. For this purpose we consider an artificial stream which has on the Ox axis a velocity $u_x(x) = \varphi_0(x)$, and a plot which is shown in Figure 16 [$\varphi_0(x) = 1$ when $x \leqslant -1/a$; $\varphi_0(x) = -ax$ when $x > -1/a$]. For a stream whose velocity on the Ox axis is equal to $\varphi_0(x)$, we get $k^0_{cr} = 1/4a$, for to the right of the point $x = -1/a$ it coincides with the hyperbolic stream considered in Section 4, and the velocity of the particle at the point $x = -1/a$ is equal to unity. This velocity corresponds on a phase plane (x, v_x) to a point line below the line $v_x = \lambda_2 x$, therefore, as was shown in Section 4, the particle will not settle on the obstacle when $k \leqslant 1/4a$. If we now consider any flux which has on the interval $x[-\infty, 0]$ a function $\varphi(x) < \varphi_0(x)$, a derivative $\varphi'(x) < 0$ and $\varphi'(0) = -a$ (Fig. 16), then for such a stream, in accordance with (I.65), the following inequality holds true

$$k_{cr} \geqslant k^0_{cr} = \frac{1}{4a}.$$

On the other hand, for such a stream we have established in Section 5 the limits

$$0 < k_{cr} \leqslant \frac{1}{4a}. \qquad (I.60)$$

From a comparison of the last two inequalities we can conclude that for a stream with a function $\varphi(x)$ as shown in Figure 16 (i.e., for the majority of the potential streams), the critical Stokes number is*:

$$k_{cr} = \frac{1}{4a}. \qquad (I.68)$$

Formula (I.68) shows that in the case of potential flow around bodies, the critical Stokes number is connected with the behavior of the stream near the critical point and is completely determined essentially by the value of the dimensionless gradient of the normal component of the velocity at critical point a. The value of k_{cr} determines for a given configuration of the body the minimum dimension of the particles, d_{min}, which settle on the body. According

---

*It was previously established [21] that $k_{cr} = 1/4a$ for potential streams which have negative derivatives $\varphi'(x)$ and $\varphi''(x)$ on the interval $x[-\infty, 0]$.

to equation (I.11) we have*

$$d_{min} = \sqrt{\frac{18\nu_1 k_{cr}}{\rho_p u_\infty}}. \qquad (I.69)$$

Consequently, the critical Stokes number k_{cr} may turn out to be the criterion for the trapping of small particles by the obstacle: larger k_{cr} the worse, other conditions being equal, the trapping of the small particles by the given obstacle.

Table 2 lists the values of k_{cr} for symmetrical obstacles of various forms. The table shows also for certain forms the values of d_{min} at the stream parameters encountered in practice. Table 3 lists the values of k_{cr} for ellipsoids of revolution.

An examination of Tables 2 and 3 show that better stream line obstacles are characterized by smaller values of k_{cr} (compare, for example, the potential and detached flow around a plate, flow around elliptical cylinders of various elongations, etc.). In particular, a two-dimensional obstacle gathers minute particles more poorly than a corresponding axially-symmetrical obstacle, having the same meridional cross section, as the transverse cross section of the two-dimensional obstacle (round disc -- plate, round cylinder -- sphere, etc.).

For an obstacle of given form (and consequently for a given value of k_{cr}), the larger the stream velocity and the higher the particle density, and the smaller the linear dimensions of the obstacle, the better are the particles trapped. The minimum dimension of the trapped particles (d_{min}) is proportional in this case to the square root of the linear dimensions of the body and is inversely proportional to the square root of the velocity of the incoming stream and the density of the particles.

---

*For non-spherical particles we have

$$d_{min} = \sqrt{\frac{18\nu_1 \chi_f k_{cr}}{\rho_p u_\infty}},$$

where χ_f is the dynamic form coefficient and d is the diameter of the sphere of equivalent volume (see page 9).

Table 2

Value of Critical Stokes Number k_{cr} and Minimum Particle Dimension d_{min} for Symmetrical Bodies and Streams

Serial No.	Type of obstacle (beam)	k_{cr}	k_{cr}	d_{min} [μ]
1	Ellipsoid $\frac{x^2}{a^2}+\frac{y^2}{b^2}+\frac{z^2}{c^2}=1$; $a \neq b \neq c$; $l=a$	$\frac{(2-A_0)\,b^2c^2}{8\,(b^2+c^2)}$	—	—
2	Axial flow around ellipsoid of revolution			
	a) prolate.....	$\frac{\sqrt{1-e^2}}{16e^3}\left[2e-(1-e^2)\ln\frac{1+e}{1-e}\right]$	—	—
	b) oblate.....	$\frac{1}{8e^3}\left[\arcsin e - e\sqrt{1-e^2}\right]$	—	—
3	Transverse flow around ellipsoid of revolution			
	a) prolate.....	$\frac{1}{16e^3(2-e^2)}\left[4e^3-2e+(1-e^2)\ln\frac{1+e}{1-e}\right]$	—	—
	b) oblate	$\frac{1-e^2}{8e^3(2-e^2)}\left[e^3+e-\sqrt{1-e^2}\arcsin e\right]$		
4	Elliptical cylinder	$\frac{1}{4(1+A)}$	—	—
5	Round cylinder.....	1/8	0,125	2,6
6	Sphere.....	1/12	0,083	2,1
7	Round disc.....	π/16	0,196	3,2
8	Plate.....			
	a) potential stream	1/4	0,250	3,6
	b) the same with detachment of jet	$4/(\pi+4)$	0,560	5,4
9	Plate in a tube			
	a) potential stream	$\frac{L}{2\pi}\sin\frac{\pi}{2L}$	0,248	3,6
	b) the same with detachment of jet			
	b) the same with detachment of jet	$\frac{2L}{\pi}\left(\frac{\operatorname{tg}\mu}{\operatorname{tg}2\mu}\right)^2$	0,382	4,5
10	Impact of jet against a plane	$\frac{1}{2\pi}\cos^{-4}\left(\frac{\nu}{2}\right)$	—	—

Table 2 (continued)

Serial No.	Type of obstacle (beam)	k_{cr}	k_{cr}	d_{min} [μ]
11	The same (h = ∞)	2/π	0,637	4,5
12	Half-body (source plus homogeneous stream)			
	a) two-dimensional	1/4π	0,080	2,0
	b) axially symmetrical	1/16	0,062	1,8

Remarks:

1. The characteristic dimensions were chosen to be as follows: 1 -- axis of ellipsoid parallel to the stream u_∞; Nos. 2, 3 -- transverse axis of ellipsoid revolution; No. 4 -- cylinder axis transverse to the stream; Nos. 5, 6, 7 -- radius of cylinder, sphere, and disc; Nos. 8, 9 -- half width of plate; Nos. 10, 11 -- half width of jet; 12 -- half width (radius) of half-body at large distance from the nose.

2. In calculating d_{min} the following was used: u_∞ = 15 m/sec, l = 2.5 mm; width of tube, 40 mm (No. 9).

3. $A_0 = abc\int_0^\infty \frac{du}{(u+a^2)\sqrt{(u+a^2)(u+b^2)(u+c^2)}}$; e -- eccentricity of meridional section of ellipsoid of revolution; A -- ratio of the axis of the elliptical cylinder which is longitudinal relative to the stream to the transverse axis; L -- ratio of width of tube to the width of the plate, No. 10 corresponds to a flat jet, emerging from a fitting of width 2l, located at an arbitrary distance h from the plane, No. 11, h = ∞. The parameters μ and ν (Nos. 9 and 10) are determined by equations (A. 31) and (A. 37) of Appendix II, where analytic expressions are also given for A_0.

Table 3

Values of Critical Stokes Number k_{cr} for Longitudinal and Transverse Flow Around Ellipsoids of Revolution

ε	I	II	III	IV	ε	I	II	III	IV
0	0	1,125	0,196	0	0,6	0,059	0,111	0,109	0,049
0,1	0,012	0,125	0,174	0,0023	0,7	0,066	0,104	0,101	0,059
0,2	0,020	0,125	0,156	0,0064	0,8	0,073	0,098	0,095	0,068
0,3	0,034	0,124	0,141	0,017	0,9	0,078	0,090	0,089	0,076
0,4	0,043	0,122	0,128	0,027	0,95	0,081	0,086	0,086	0,080
0,5	0,052	0,117	0,118	0,038	1,0	0,083	0,083	0,083	0,083

Remark: ε -- ratio of minor axis of meridional section of the ellipsoid of revolution to the major axis. Columns I and II -- for prolate ellipsoid of revolution; III and IV -- for oblate ellipsoid of revolution; I and III -- for axial flow around ellipsoid; II and IV -- for transverse flow around ellipsoid.

Let us proceed now to consider the value of the critical Stokes number k_{cr} for a viscous stream. The proof of the existence of a value $k_{cr} > 0$ for a viscous stream (presented in Section 5), while not yielding the value of k_{cr}, does lead, however, to a relatively simple and exact method of determining k_{cr}. This method is based on taking account of the circumstance that when $k = k_{cr}$ the curve $v_1(x, k_{cr})$ is a curve of type G (see Section 5). The curve $G(x, k)$ for a chosen value $k = k_1$ can be readily plotted on the relatively large interval $x[-b, 0]$, if we expand in (I.54) or (I.57) the right half in a Maclaurin series and then seek the solution of this equation in the form of a series with undetermined coefficients (recalling that the inclination of $G(x, k_1)$ to the abscissa axis at the origin is equal to $-1/k_1$). Then determining the integral curve $v_1(x, k_1)$ on the interval $x[-\infty, -b]$ [for example, by numerical integration of equation (I.54) or (I.57) subject to the condition (I.56)], we readily establish that $k_{cr} \lessgtr k_1$ if $v_1(-b, k_1) \gtrless G(-b, k_1)$. The advantage of such a method of determining the quantity k_{cr} lies in the

fact that in this case the calculation of $v_1(x, k)$ can be terminated sufficiently far away from the surface of the body (the critical point). On the other hand, exact calculations of the curve $v_1(x, k)$ near the body are always cumbersome, whereas calculations of $G(x, k)$ are elementary in this case.

On the basis of formula (I.68) for a potential stream and on the basis of the method of proving the existence of $k_{cr} > 0$ for a viscous stream, we can advance the hypothesis that k_{cr} of a viscous stream is determined by the behavior of the integral curve near the singular (critical point of the stream). Then, taking (I.53) into account, we can assume that k_{cr} is the function of the parameter α only:

$$k_{cr} = f(\alpha). \tag{I.70}$$

Applying to equations (I.57) and (I.58) the transformation $x = \beta x_1$, we obtain the equation

$$\frac{k}{\beta} v_x \frac{dv_x}{dx_1} + v_x = \varphi(\beta x_1) = \alpha\beta^n |x_1|^n,$$

from which on the basis of (I.70) we can conclude that

$$\frac{k_{cr}}{\beta} = f(\alpha\beta^n). \tag{I.71}$$

If we seek a solution of the equation (I.70) in the form

$$k_{cr} = C\alpha^m,$$

then it will follow from (I.70) and (I.71) that

$$k_{cr} = C\alpha^m = \beta \cdot f(\alpha\beta^n) = \beta \cdot C(\alpha\beta^n)^m.$$

The last relation should hold true for any value of the transformation coefficient β. Consequently, $mn + 1 = 0$ and

$$k_{cr} = C\alpha^{-\frac{1}{n}}. \tag{I.72}$$

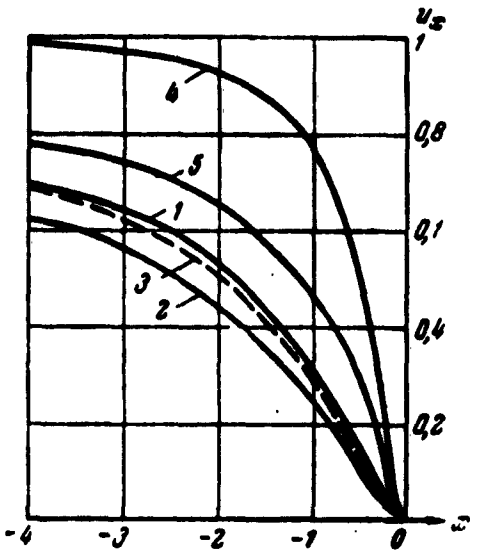

Fig. 17. Velocities of artificial streams. Numbers on the curves correspond to the numbering of Table 4.

For a potential stream, n = 1 and equation (I.72) leads to the relation $k_{cr} = C/a$. Actually, under certain limitations we have in this case $k_{cr} = 1/4a$ [see (I.68)]. For a viscous stream usually n = 2 and one should expect $k_{cr} = C/\sqrt{\alpha}$. For the case of a Stokes flow around a sphere ($\alpha = 1.5$), Langmuir found by numerical means a value $k_{cr} = 1.214$ [103]. Therefore, under the assumption (I.70) which we introduce we can expect

$$C = k_{cr}\sqrt{a} = \\ = 1{,}214\sqrt{1{,}5} = 1{,}49$$

and

$$k_{cr} = \frac{1{,}49}{\sqrt{a}}. \qquad (I.73)$$

In order to check on the estimated value of k_{cr} for a viscous stream, determined by means of assumption (I.70) and consequently by means of equation (I.73), we calculated (by the method described above) value of k_{cr} in equation

(I.57) for different forms of the function $\varphi(x)$, corresponding to artificially constructed streams. Table 4 gives the functions $\varphi(x)$ and the first terms of the Maclaurin expansion of $\varphi(x)$ near the origin, and also the values of k_{cr}, calculated by numerical integration and by means of formula (I.73). Figure 17 shows plots of some of these functions.

Table 4

Serial No.	$\varphi(x)$	α	k_{cr} Calculated by numerical integration	k_{cr} Calculated by formula (I.73)
1	$1-1{,}5(1-x)^{-1}+0{,}5(1-x)^{-2}=$ $=1{,}5x^2+3{,}5x^3+6x^4+\ldots$ (STOKES)	1,5	1,22	1,214
2	$[1-(1-x)^{-1}]^2=x^2+2x^3+3x^4+\ldots$	1	1,53	1,49
3	$1-1{,}5(1-x)^{-1}+1-x)^{-4}-$ $-0{,}5(1-x)^{-5}=x^2+x^3-1{,}5x^4+\ldots$	1	1,32	1,49
4	$[1-(1-x)^{-3}]^2=9x^2+36x^3+96x^4+\ldots$	9	0,40	0,50
5	$1-\frac{18}{17}(1-x)^{-1}+\frac{1}{17}(1-x)^{-16}=$ $=9x^2+66x^3+351x^4+\ldots$	9	0,57	0,50
6	$\varphi(x)=x^2$ FOR $-1<x<0$; $\varphi(x)=1$ FOR $x\leqslant -1\ldots$	1	0,60	1,49
7	$\varphi(x)=9x^2$ FOR $-\frac{1}{3}<x<0$; $\varphi(x)=1$ FOR $x\leqslant -\frac{1}{3}\ldots$	9	0,20	0,50
8	$1-1{,}475(1-x)^{-1}+0{,}930(1-x)^{-4}-$ $-0{,}455(1-x)^{-5}=-0{,}03x+$ $+x^2+1{,}2x^3-0{,}775x^4+\ldots$		1,24	

From an examination of the first five streams of Table 4 and Figure 17 we can see that not too considerable a change in the general form of the curve $\varphi(x)$, formula (I.73) yields the tentative value of k_{cr} over the entire interval $x[-\infty, 0]$.

However, this formula is not exact. In addition to depending on the coefficient α, k_{cr} is also influenced

apparently by the general character of $\varphi(x)$ curve. The latter circumstance is particularly clearly seen in streams Nos. 6 and 7, for which the values of k_{cr} are quite remote from those calculated by formula (I.73).*

Starting from the foregoing, we can expect formula (I.72) to be an interpolation (extrapolation) formula for problems where it is necessary to find the value of k_{cr} for a family of streams, in which the general form of the curves $\varphi(x)$ on the interval $x[-\infty, 0]$ does not change very strongly. For example, if we consider axial flow around a sphere (with diameter D) we can apply to it equation (I.72) in the form (I.73), for in the limit

$$\left(\mathrm{Re}_u = \frac{Du_\infty}{\nu} \to 0\right)$$

axial flow goes over into the Stokes flow. For axial flow around the sphere we have

$$\varphi(x) = \alpha x^3 + O(x^5),$$

where

$$\alpha = \frac{24 + 12\mathrm{Re}_u}{16 - 3\mathrm{Re}_u}$$

(see, for example, [55]). Consequently,

$$k_{cr} = 1{,}49\sqrt{\frac{16 - 3\mathrm{Re}_u}{24 + 12\mathrm{Re}_u}}. \qquad (I.74)$$

---

*At the same time, for streams of this type, determined by the functions $\varphi(x) = \alpha |x|^n$ when $0 \geqslant x > -(\alpha)^{-1/n}$ and $\varphi(x) = 1$ when $x \leqslant -(\alpha)^{-1/n}$, the relation (I.72) $k_{cr} = C\alpha^{-1/n}$ is satisfied perfectly accurately, since by means of the transformation $x_1 = x\sqrt[n]{\alpha}$ equation (I.57) is reduced to the form $k\sqrt[n]{\alpha}\, v_x \frac{dv_x}{dx_1} + v_x = |x_1|^n$ (under the initial condition $v_x = 1$ when $x_1 = -1$), which has the same value of $k_{cr}\sqrt[n]{\alpha}$ for all values of α.

For $Re_u = 0.1$ formula (I.74) yields $k_{cr} = 1.17$, while for $Re_u = 0.5$ we get $k_{cr} = 1.03$. The value $k_{cr} = 1.17$ coincides satisfactorily with the value $k_{cr} = 1.15 \pm 0.01$ calculated by G. L. Natanson for $Re_u = 0.1$ [44]. As shown by formula (74), when Re_u increases, k_{cr} decreases. At very large values of Re_u, when the axial approximation for flow around a sphere no longer holds and when the stream can be regarded as potential ($a = 3$), we have

$$k_{cr} = \frac{1}{4a} = \frac{1}{12}.$$

Analogously, for axial flow around a cylinder, with accuracy to terms of order Re_u, the coefficient is

$$\alpha(Re_u) = \frac{2 + Re_u [K_0(0{,}25Re_u) - 0{,}25]}{1 + 2K_0(0{,}25Re_u)},$$

where K_0 is the Macdonald function. (This expression for α can be obtained, for example, from formulas (5) of reference [44]).

In the work of G. L. Natanson [44], a value $k_{cr} = 4.3$ was calculated for $Re_u = 0.1$. At the same time, according to the formula given above, $\alpha(0.1) = 0.272$. Therefore, according to (I.72) we can assume for the cylinder a value

$$C = k_{cr}\sqrt{\alpha} = 4{,}3\sqrt{0{,}272} = 2{,}24$$

and we can consider that for Reynolds numbers that do not differ greatly from 0.1, the critical Stokes number for a cylinder in a viscous stream is expressed by the formula

$$k_{cr} = 2{,}24\sqrt{\frac{1 + 2K_0(0{,}25Re_u)}{2 + Re_u[K_0(0{,}25Re_u) - 0{,}25]}}. \qquad \text{(I.74a)}$$

It follows from (I.74a), for example, that when $Re_u = 0.2$ we can expect a value $k_{cr} = 3.75$. The value $k_{cr} = 0.90$ obtained in [85] (for $Re_u = 0.2$) is obviously in error, since it was determined by the authors by means of formula (I.68), in spite of the fact that for a viscous stream the equation $a = 0$ should be observed [44]. Analogously, the same authors, approximating the Thomas solution for $Re_u = 10$, obtained in error $a = 0.6$, and consequently

$k_{cr} = 0.417$.

Let us turn attention, finally, to stream No. 8 of Table 4. For it there exists a finite value a = 0.03, so that according to formula (I.68) the value of k_{cr} for this stream should be 8.33. However, in view of the violations of the conditions for which formula (I.68) was derived, for this stream we have $k_{cr} = 1.24$. This value is close to the value $k_{cr} = 1.32$ for stream No. 3 of Table 4, which has almost everywhere a function $\varphi(x)$ which is close to $\varphi(x)$ of stream No. 8 and for which $\alpha = 1$.

Let us estimate now the influence of the boundary layer on the value of k_{cr} of a potential stream. As is known from boundary-layer theory [77], near the critical point away from the obstacle the velocity components of a potential stream will differ appreciably within the limits of the thickness of the boundary layer $\delta \approx 2.4(a\mathrm{Re}_l)^{-1/2}$* [for an axially symmetrical stream $\delta \approx 2.8(a\mathrm{Re}_l)^{-1/2}$] from the approximation expressions (I.52) near the critical point of a purely potential stream. Inside the boundary layer they are determined by the relations

$$u_x = \sqrt{\frac{a}{\mathrm{Re}_u}}\varphi(\sqrt{a\,\mathrm{Re}_u}\,x);\quad u_y = -y\sqrt{\frac{a}{\mathrm{Re}_u}}\frac{d}{dx}[\varphi(\sqrt{a\,\mathrm{Re}_u}x), \qquad (I.75)$$

where the function φ has a form as shown in Figure 18. In this case we have near the origin

$$u_x = ax^2 + O(x^3).$$

It is clear from general considerations that because of the small thickness of the boundary layer the value of k_{cr} for a potential stream with boundary layer cannot differ appreciably from the value 1/4a in a purely potential stream. To estimate the change in the value of k_{cr}, brought about by the presence of a boundary layer, one can use

---

*Here the thickness of the boundary layer is referred to the characteristic length l of the obstacle. The Reynolds number is $\mathrm{Re}_u = \frac{lu_\infty}{\nu}$; a is the dimensionless gradient of the normal velocity component at the critical point.

relation (I.65). Inasmuch as the real stream coincides far away from the origin with the purely potential stream, while near the origin the function corresponding to it is $\varphi_p(x) < -ax$ (Fig. 18), the critical Stokes number for the real stream will be in accord with (I.65):

$$\bar{k}_{cr} > \frac{1}{4a}. \qquad (I.76)$$

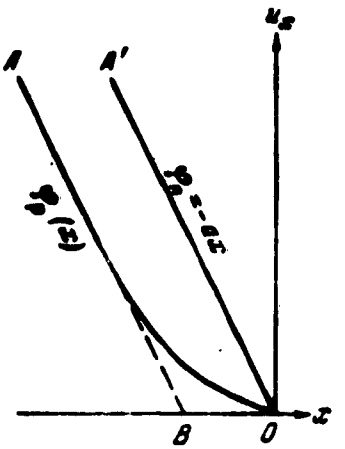

Fig. 18. Curve AO -- velocity u_x for boundary layer. Curve A'O -- purely potential stream.

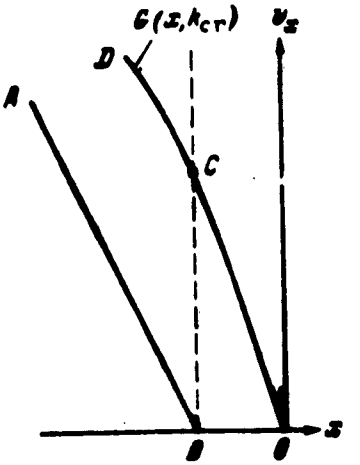

Fig. 19. Type G curve (DCO) for the stream ABO.

Furthermore, inasmuch as $\varphi_p(x)$ near the origin exceeds everywhere the functions of $\varphi^I(x)$, which is made up of segments AB and BO (Fig. 18), we get

$$\bar{k}_{cr} \leqslant k^I_{cr}, \qquad (I.77)$$

where k_{cr}^I is the critical Stokes number for a stream that coincides away from the origin with the real stream, and which is described near the origin by the broken line ABO. This stream will coincide in practice with the purely potential stream of the problem, to which the stagnation region BO is added, where the stream velocity is equal to zero. From the boundary-layer theory it follows that for a plane

stream the segment OB = $f\delta \approx 0.27\delta$ (for an axially symmetrical stream OB $\approx 0.5\delta$). To calculate k_{cr}^{I} it is possible to make use of the fact that the curve $G(x, k_{cr}^{I})$ for the stream under consideration consists (Fig. 19) of a segment DC, which represents the curve $v_1(x, k_{cr}^{I})$ of a purely potential stream, and a segment CO corresponding to motion in a resting medium on the segment OB = $f\delta$. On this segment $\varphi = 0$ and equation (I.57) has here a solution $v_x = -x/k$.

From simple geometric considerations (Fig. 19) we obtain for the determination of k_{cr}^{I} the equation

$$BC = \frac{BO}{k_{cr}^{I}} = \frac{f\delta}{k_{cr}^{I}} = v_1(0, k_{cr}^{I}), \qquad (I.78)$$

where $v_1(0, k_{cr}^{I})$ is the value of the velocity v_1 for a purely potential stream. Equations (I.76), (I.77), and (I.78) establish the limits of k_{cr} for a potential stream with boundary-layer [32].

Numerical calculations of $v_1(0, k)$, carried out for potential streams near a cylinder and a plate, have shown that for them

$$v_1(0, k) \approx A\left(k - \frac{1}{4a}\right)^2,$$

where $A \approx 1.8$ for a plate and $A \approx 3.8$ for a cylinder. Equation (I.78) then assumes the form

$$k_{cr}^{I} = \frac{1}{4a} + \sqrt{\frac{0{,}85}{A\sqrt{a\,Re_u}}}\frac{1}{\sqrt{k_{cr}^{I}}}. \qquad (I.79)$$

Solving equation (I.79) by iteration, we find, for example, that for a cylinder $0.125 < k_{cr} < 0.172$ and for a plate $0.25 < k_{cr} < 0.31$. The upper limit for k_{cr} correspond to an increase in d_{min} compared with d_{min} for a purely potential stream by 17 percent for a cylinder and by 12 percent for a plate. The actual increase in d_{min} due to the boundary layer will in this case be, of course, smaller.

An investigation of the critical conditions for the

precipitation was carred out for equation (I.57) for small Reynolds numbers Re_p. At large values of Re_p, it is necessary to consider equation (I.14), which we rewrite in the form

$$\Phi(v_x, x) = \frac{dv_x}{dx} - \frac{1}{kv_x}|\varphi(x) - v_x|(1 + 0{,}17\,Re_p^{2/3}|\varphi - v_x|^{1/3}) = 0. \tag{I.80}$$

Confining ourselves to the case of a potential stream, when $a \neq 0$ (the case of a viscous stream does not have any significance for large Re_p), we can prove that equation (I.68) holds true also for equation (I.80).

Applying to equation (I.80) the Chaplygin theorem concerning differential inequalities, we shall prove for the set of its solutions $v_1(x, k)$ relation (I.59) [and consequently the continuity of $v_1(x, k)$ with respect to k], and also the inequality

$$v_x^0 > v_x, \tag{I.81}$$

where v_x^0 is the velocity that satisfies equation (I.57) for specified $\varphi(x)$. Comparing formulas (I.64), (I.65), and (I.81), we conclude that for equation (I.80) we have

$$k_{cr} \geqslant k_{cr}^0 = \frac{1}{4a}. \tag{I.82}$$

where k_{cr}^0 is the critical Stokes number of equation (I.87).

On the other hand, near the origin of the phase plane (x, v_x), the qualitative patterns of the trajectories of equations (I.80) and (I.57) are the same. The latter circumstance together with the continuity of the function $v_1(x, k)$ of equation (I.80) with respect to k leads (as in the case of Section 5) to the relation

$$0 < k_{cr} \leqslant \frac{1}{4a}. \tag{I.60}$$

Comparing (I.60) with (I.82) we obtain for (I.80) we obtain for (I.80) the sought-for equality

$$k_{cr} = \frac{1}{4\alpha}. \qquad (I.83)$$

In conclusion we note that the capture coefficient is $E = 0$ for $k \leqslant k_{cr}$ only for inertial precipitation of aerosol particles and also if we neglect the dimensions of the precipitating particles compared with the dimensions of the obstacle. Other mechanisms for the precipitation of aerosol particles on an obstacle, besides the inertial mechanism, are also possible. V. G. Levich has carried out an interesting investigation of turbulent and Brownian diffusion of aerosol particles to an obstacle around which an aerosol stream flows [37, 38]. However, owing to the lack of experimental data on the main characteristics of the turbulence in such streams, it is difficult to estimate at present the magnitude of the capture coefficient for the turbulent diffusion process. On the other hand, Brownian diffusion is negligible for particles with $d > 1$ microns (for them the diffusion coefficient is $D < 10^{-7}$ cm^2/sec). There are grounds for stating that when $k < k_{cr}$ the capture coefficient will usually be very small. This is evidenced by the fact that usually the samples of cloud drops do not contain particles whose diameter is smaller than the values of d_{min} calculated by formula (I.69). Ranz and Wong, in laboratory experiments with impactors, likewise did not observe a noticeable precipitation of particles in which the Stokes parameter is less than critical [114].

If the dimensions of the aerosol particles are comparable with the dimensions of the obstacle ($\frac{d}{l} \approx 1$), it is impossible to employ the methods developed for the determination, nor can the equations of motions (I.54) and (I.55) themselves by employed. At these parameters of the precipitation process an appreciable hydrodynamic interaction sets in between the particles and the obstacle, connected with the interaction of their aerodynamic fields. Neglecting this interaction, we can take into account the finite value of d/l (the "coupling effect"). When $d/l \ll 1$ an account of the coupling effect, developed by N. A. Fuks [65, 66, Section 34] leads at $k < k_{cr}$ to nonzero values of the capture coefficient. However, the values of E obtained in this case are very small ($E \approx \beta \frac{d}{l}$ for a plane stream and $E \approx \beta \frac{d^2}{l^2}$ for an axially symmetrical stream; the value of $\beta \approx 2 \div 3$).

7. THEORY OF AEROSOL TRAPS. PROCEDURE FOR CALCULATING THE CAPTURE COEFFICIENT.

Various physical properties of aerosol are determined to a considerable degree by its dispersion. Therefore, measurement of the aerosol particle distribution function by dimensions is one of the main problems in the investigation of aerosols. In particular, those who investigate the physical processes which give rise to the development and formation of clouds have encountered this problem long ago. Many methods have been proposed for such measurements, and a review of these can be found in the book by N. A. Fuks [66] or in the article by A. M. Borovikov [3]. In the present section we shall dwell in greater detail only on impactor methods of investigating the structure of coarsely-dispersed aerosols, and particularly clouds. By impactor methods of investigating the structure of clouds we mean methods connected with inertial settling of aerosol particles from the stream on obstacles and the subsequent investigation of the gathered sample. This investigation, in a most thorough study of the structure, was carried out by microphotography of the settling aerosol particles with subsequent determination of their dimensions. Sometimes the investigation is limited to a weight or chemical analysis of the gathered aerosol samples. For microphotography of samples of cloud drops, the latter frequently trapped on transparent obstacles, covered with a thin layer of special oil, which prevents the evaporation of the water drops striking it. Sometimes the drops are trapped on obstacles covered with a thin layer of magnesium oxide or lampblack.

Impactor methods of measuring microstructural characteristics of a coarsely dispersed aerosol are widely used at the present both in the USSR and abroad. An essential element of this procedure is the transition from a spectrum of particles (function of distribution by dimensions), settling on the gathering part of the employed traps, to the spectrum of particles of the unperturbed aerosol. For such a transition one uses the capture coefficient of the gathering part of the trap as given by equation (2). Therefore the theory of aerosol traps is connected to a considerable extent with a calculation of the capture coefficient of the simplest forms, used as gathering parts of traps. As was indicated in Sections 1--2, the determination of the capture coefficient of an obstacle involves the solution of equations of motion of the aerosol particles.

For aerosol traps, it is possible to neglect in these equations all the forces except the aerodynamic forces, and to consider motion of particles as described by equation (I.14). This equation is a system of nonlinear differential second-order equations, since the vector of air velocity u, which is contained in the right half of equation (I.14), is a nonlinear function of the coordinates.

Even without the fact that the analytic solution of such equations are not known at the present time, it must be noted that a numerical solution of this system over a wide range of initial conditions entails in most cases appreciable computational difficulties owing to the cumbersomeness of the calculation of the velocity field (r). There are well known calculations for the capture coefficient of a cylinder and a sphere (in the case of potential streams), carried out by Albrecht [79], Sell [121], Glauert [89], Langmuir and Blodgett [102], Mazin [41], Davies and Pietz [85], and others. These examples are perhaps the only cases when the field u(r) is relatively easy to calculate. However, the geometrical forms of these bodies are not convenient for use in a procedure where the aerosol particles are trapped and then microphotographed, since the latter, naturally, calls for the use of bodies with flat portions of the surface as trapping obstacles.* It is therefore desirable to consider the settling of aerosol particles from a stream onto a plate (strip) [22, 35].**

For the case of a potential non-detached flow around a plate (Fig. 20), the air velocity field u(x, y) is described by the following equations [15, page 271]:

*Of course, it is possible to use curvilinear surfaces with large radii of curvature. In this case the dimensions of the obstacle turn out to be large (ℓ is large), and at a given velocity u_∞ and a given value of k_{cr} of the surface this increases the minimum dimension d_{min} of the trapped particles (see Section 6).

**Calculations of the capture coefficient for a strip around which a potential stream flows were carried out by Langmuir and Blodgett [102]. In view of the inaccessibility of these results, these calculations were repeated by us in 1951 and independently of us also by Khrgian and Mazin [40]. It seems to us, however, that it is essential to investigate the settling of aerosol particles on a plate around which a stream flows with jet detachment (see Section 8).

$$\left.\begin{aligned} u_x &= -x\sqrt{\frac{\sqrt{(x^2-y^2+1)^2+4x^2y^2}+x^2-y^2+1}{2(x^2-y^2+1)^2+8x^2y^2}}+\\ &+y\sqrt{\frac{\sqrt{(x^2-y^2+1)^2+4x^2y^2}-x^2+y^2-1}{2(x^2-y^2+1)^2+8x^2y^2}}\\ u_y &= x\sqrt{\frac{\sqrt{(x^2-y^2+1)^2+4x^2y^2}-x^2+y^2-1}{2(x^2-y^2+1)^2+8x^2y^2}}+\\ &+y\sqrt{\frac{\sqrt{(x^2-y^2+1)^2+4x^2y^2}+x^2-y^2+1}{2(x^2-y^2+1)^2+8x^2y^2}} \end{aligned}\right\} \quad (I.84)$$

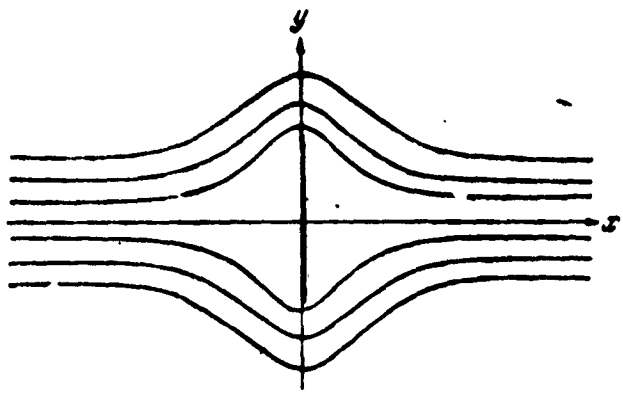

Fig. 20. Diagram of potential non-detached flow around a plate.

It is obvious that the cumbersomeness of these formulas makes it very difficult to carry out the calculations even in this relatively simple case. In the case of potential flow around a plate with detachment of the stream on the edges (the so-called Kirchhoff flow, Fig. 21), the velocity field is given by the following equation [15, page 312]:

$$z = \frac{4}{\pi+4}\left\{\frac{1}{2}\ln\frac{1-\zeta}{1+\zeta}+\frac{\zeta(\zeta^2-3)}{(1-\zeta^2)^2}\right\} = F(\zeta), \quad (I.85)$$

where $\zeta = u_x - iu_y;\ z = x + iy.$

This is a transcendental equation and cannot be solved in explicit form with respect to the complex velocity ζ. Since in the solution of the equation (I.14) it

is necessary to obtain from equation (I.85) the velocity field u(x, y), it is necessary for this purpose to solve a series of transcendental equations in the real domain with subsequent double interpolation.* Analogous transcendental equations of the type $z = F(\zeta)$ are obtained for a broad class of flow of practical interest with separation surfaces (for example, for a jet leaving a nozzle, striking a plane or a corner, in the case of detached flow around a plate in a tube, the escape of the liquid through an aperture from a vessel, etc.).

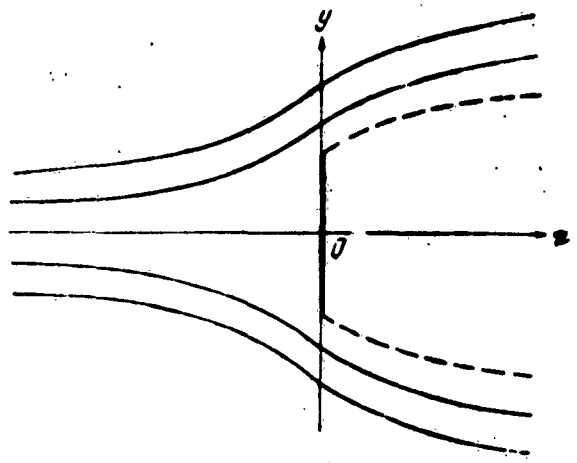

Fig. 21. Diagram of detached (Kirchhoff) flow around a plate.

It follows from the foregoing that calculation of the capture coefficient for a series of practically interesting obstacles entails considerable difficulties. Yet, the calculation of the capture coefficient for the entire obstacle as a whole (and consequently, the calculation of the drop trajectories over a wide range of inertial conditions) is organically not required by the drop-trapping procedure. To investigate the structure of the aerosol it is sufficient to calculate the capture coefficient not of the entire obstacle as a whole, but only of a certain part of it. Such a formulation of the problem makes it possible to simplify greatly the calculations and also the experimental procedures, for in this case there is no need for

*Expansion in series does not lead here to results that are of practical use.

microphotography to be carried out over the entire obstacle, it is sufficient to photograph the drops that settle only on a definite part of the obstacle. It is possible to simplify the calculations appreciably by seeking for the obstacle with the symmetry plane (for a two-dimensional stream) or with symmetry axis (for a three-dimensional stream) the local capture coefficient for the central part (for the vicinity of the critical point of the stream flowing around the obstacle).

Let us trace, using Kirchhoff flow around a plate as an example, the simplification in the calculation that is obtained thereby. The current lines of the air are shown in this case in Figure 21, and the velocity field is given by equation (I.85). On the symmetry plane $y = 0$, $x < 0$ the component $u_y = 0$ (because of the symmetry of the flow) and consequently $\zeta = u_x$. Near the symmetry plane, the velocity field can be readily obtained by expanding in a Taylor series the right half of equation (I.85). Near the symmetry plane, u_y and y are small. Consequently,

$$z = x + iy = F(u_x - iu_y) = F(u_x) + (-iu_y)\frac{dF}{d\zeta}\Big|_{\zeta=u_x} +$$

$$+\frac{1}{2!}(-iu)^2\frac{d^2F}{d\zeta^2}\Big|_{\zeta=u_x} + \frac{1}{3!}(-iu_y)^3\frac{d^3F}{d\zeta^3}\Big|_{\zeta=u_x} + \ldots$$

Separating in this equation the real and imaginary parts we obtain* the formulas

$$x = F(u_x) + O(u_y^2) \qquad \text{(I.86)}$$

and

$$y = -u_y\left\{\frac{dF}{d\zeta}\Big|_{\zeta=u_x} + O(u_y^2)\right\}. \qquad \text{(I.87)}$$

Accurate to infinitesimals of second order we have

$$x = F(u_x) = \frac{4}{\pi+4}\left\{\frac{1}{2}\ln\frac{1-u_x}{1+u_x} + \frac{u_x(u_x^2-3)}{(1-u_x^2)^2}\right\}, \qquad \text{(I.88)}$$

$$y = -u_y\frac{dF(u_x)}{du_x} \qquad \text{(I.89)}$$

---

*It is obvious that formulas (I.86) and (I.87) are obtained in any case when $F(\zeta)$ is a real function of ζ, i.e., for any flow which is symmetrical about the Ox axis.

or

$$u_y = y\frac{\pi+4}{4}\cdot\frac{(1-x_x^2)^2}{1+u_x^2} = yf(u_x). \qquad \text{(I.90)}$$

The tables of the functions

$$f(u_x) \text{ and } F(u_x) = -\int_0^{u_x}\frac{du_x}{f(u_x)}$$

make it possible to calculate readily the velocity field near the symmetry plane using the scheme

$$x \to u_x \to f(u_x) \to u_y.$$

Thus, to find the local capture coefficient of a symmetrical body at its forward critical point it is necessary to solve the system of equations (I.14), which for the case of a plane stream is written in the form:

$$k\ddot{x} = [\varphi(x) - \dot{x}]\{1 + 0{,}17\mathrm{Re}_\beta^{2/3}|\varphi(x) - \dot{x}|^{2/3}\}, \qquad \text{(I.91)}$$

$$k\dot{y} = [-y\varphi'(x) - \dot{y}]\{1 + 0{,}17\mathrm{Re}_\beta^{2/3}|\varphi(x) - \dot{x}|^{2/3}\}. \qquad \text{(I.92)}$$

The first of these equations does not contain the coordinate y and is independent. Equation (I.92) is linear in y. Therefore, without loss of generality, we can assume the following initial conditions.

When $t = -\infty$:

$$x = -\infty,\ v_x = \dot{x} = 1;\ y = 1;\ v_y = \dot{y} = 0. \qquad \text{(I.93)}$$

By finding the point where the trajectory of the particle crosses the body x = 0, $y = y_1$, we determine the local capture coefficient E_l from the equation

$$E_l = \frac{1}{y_1}. \qquad \text{(I.94)}$$

The determination of the coefficient E_l can be simplified in many cases by taking into account the continuity equation, which for a region close to the symmetry line can be written in the form:

$$n(x)v_x(x)y = n_\infty. \qquad \text{(I.95)}$$

Then

$$\psi_1 = \frac{n_\infty}{n(0)\, v_1(0, k)}$$

and formula (I.94) assumes the form:

$$E_l = \frac{n(0)}{n_\infty} v_1(0, k), \qquad \text{(I.96)}$$

where, as was found in Section 5, $v_1(0, k)$ is the solution of equation (I.91) subject to initial condition (I.93) at the point $x = 0$.

Let us consider cases when the variation of the aerosol particle concentration n can be neglected. Then

$$\frac{n(0)}{n_\infty} \approx 1$$

and

$$E_l = v_1(0, k). \qquad \text{(I.97)}$$

This means that in cases when the concentration of the aerosol particles changes level on flowing over an obstacle, the capture coefficient E_l can be calculated by formula (I.97), solving for this purpose only the first of the equations of motion, namely equation (I.91) [46]. The concentration n is almost constant over the entire aerosol stream flowing around the obstacle, when the value of k is small (when $k = 0$ the concentration n is constant; see Section 3). However, this case is of no practical interest for the calculation of E_l, since at small values of $k < k_{cr}$ the coefficient $E_l = 0$. The small variability of the concentration n appears also in a different extreme case, that of very large values of k, when the inertia of the aerosol particles is very large and when the air stream influences their motion little (see Section 3).

Ye. A. Novikov established certain conditions under which the variability of the concentration n is small [46]. Let us examine for the sake of being definite the case of small Reynolds numbers Re_p, when in equations (I.91) and (I.92) the factor $|1 + 0{,}17\,\mathrm{Re}_p^{2/3}|\varphi - \dot{x}|^{2/3}|$ can be set equal to unity. We shall consider here the quantities v_x and y as being functions of x. Then

$$\ddot{x} = v_x v_x'; \ \dot{y} = v_x y'; \ \ddot{y} = v_x v_x' y' + v_x^2 y''$$

and equations (I.91) and (I.92) as well as the initial conditions (I.93) assume the form

$$k v_x v_x' + v_x = \varphi(x), \tag{I.98}$$

$$k v_x^2 y'' + (y\varphi)' = 0. \tag{I.99}$$

When $x = -\infty$, we have

$$v_x = 1, \quad y = 1, \quad y' = 0. \tag{I.100}$$

Noting that the first term of equation (I.99) is

$$k v_x^2 y'' = k (v_x^2 y')' - k y' (v_x^2)',$$

we stipulate that the following inequality be satisfied

$$k |y' (v_x^2)'| < |(y\varphi)'|. \tag{I.101}$$

Then, replacing in (I.99) the term $kv_x^2 y''$ by $k(v_x^2 y')'$, we readily obtain the first integral of this equation. Taking (I.100) and the equation $\varphi(-\infty) = 1$ into account, this integral assumes the form

$$k v_x^2 y' + y\varphi = 1.$$

Substituting here the expression for $\varphi(x)$ from (I.98), we obtain the equation

$$k v_x (v_x y)' + v_x y = 1,$$

the solution of which subject to initial condition (I.100) will be

$$v_x y = 1. \tag{I.102}$$

From this we conclude on the basis of the continuity equation (I.95) that $n(x) = n_\infty$. Thus, if the inequality (I.101) is observed in the aerosol stream, then it is possible to neglect in it the variation of the aerosol particle concentration.

Let us interpret now the meaning of the inequality

(I.101). For this purpose we first derive a few auxiliary relations. We note first that the equation for the current lines of the airstream will have the form

$$y_u\varphi(x) = \text{const} = y_{u\infty}, \qquad \text{(I.103)}$$

where y_u is the coordinate y of the current line of the air.

From this we conclude that

$$y'_u = -\frac{y_{u\infty}\varphi'}{\varphi^2} > 0$$

(since $\varphi'(x) < 0$, see Section 5). For the sake of being specific, we consider the upper half of the stream, for which $y > 0$, and consequently $y_{u\infty} > 0$ and

$$y''_u = y_{u\infty}\frac{2(\varphi')^2 - \varphi\varphi''}{\varphi^3} > 0,$$

if*

$$\varphi\varphi'' - 2(\varphi')^2 < 0. \qquad \text{(I.104)}$$

Writing (I.99) in the form

$$\Phi(z, x) = z' + z^2 + \frac{\varphi}{kv_x^2}z + \frac{\varphi'}{kv_x^2} = 0,$$

where $z = y'/y$, we obtain on the basis of (I.104) the formula

$$\Phi\left(\frac{y'_u}{y_u}, x\right) = \Phi\left(-\frac{\varphi'}{\varphi}, x\right) = -\left(\frac{\varphi'}{\varphi}\right)' + \left(\frac{\varphi'}{\varphi}\right)^2 =$$
$$= -\frac{\varphi\varphi'' - 2(\varphi')^2}{\varphi^2} > 0,$$

from which, according to Chaplygin's theorem on differential inequalities [72] we conclude that

$$z = \frac{y'}{y} < \frac{y'_u}{y_u} = -\frac{\varphi'}{\varphi}$$

---

*The condition (I.104) is satisfied for a broad class of air streams.

or

$$(\varphi y)' < 0. \tag{I.105}$$

Using this relation and equation (I.99) we obtain*

$$y'' = \frac{dy'}{dx} = -\frac{(\varphi y)'}{kv_x^2} > 0. \tag{I.106}$$

Since the derivative $y' = 0$ when $x = -\infty$ [see conditions (I.100)], the last inequality enables us to state that everywhere on the interval $x[-\infty, 0]$

$$y' > 0. \tag{I.107}$$

On the basis of the inequalities (I.105) and (I.107), and also the inequality

$$v_x' < 0, \tag{I.107a}$$

which is the consequence of equations (I.59) and (I.98), we can rewrite the condition (I.101) in the following form:

$$-2ky'v_xv_x' < -(y\varphi)'.$$

Substituting here the values of y, y', and v_x', expressed on the basis of (I.98) and (I.102) in terms of $\varphi(x)$ and v_x, we obtain the formula

$$k + \frac{\varphi(v_x - \varphi)}{\varphi' v_x^2} > -2\frac{(v_x - \varphi)^2}{\varphi' v_x^2}. \tag{I.108}$$

Inasmuch as the concentration of the aerosol particles increases with increasing x (see Section 3), the

---

*We note that by using (I.105) and (I.59) we can readily obtain on the basis of Chaplygin's theorem from equation (I.99) a relation that is convenient for the analysis of the motion of the aerosol particles:

$$y_2 > y_1 > y_1 > 1,$$

where y_1 and y_2 are the solutions of equations (I.99) and (I.100) at values of the parameters k, equal to k_1 and k_2 respectively, with $k_1 > k_2$.

greatest change in n(x) is observed at the critical point of the obstacle. Therefore the satisfaction of the condition $\frac{n(x)}{n_\infty} \approx 1$ at the critical point guarantees the fulfillment of this condition at any other point of the investigated region of the stream. But at the critical point the condition (I.108) assumes the following form (inasmuch as $\varphi(x) = 0$ at this point) [46]*:

$$k > \frac{2}{\varphi'(0)} = 8k_{cr}. \tag{I.109}$$

The criterion (I.109) that the particle concentration change in the aerosol be small can be used in practice in the following manner. The calculations of the capture coefficient E_ℓ begin at small values of k, by solving equations (I.91) and (I.92) and determining E_ℓ from formula (I.94). Simultaneously one determines at the critical point the value of n(0) from formula (I.95). If for a certain value $k = k_1$ the concentration n(0) becomes equal to n_∞ with sufficient degree of accuracy, then it is possible to determine for $k > k_1$ the value of E_ℓ by formula (I.97), solving thereby only the one equation (I.91).

8. CALCULATION OF THE CAPTURE COEFFICIENT FOR SURFACE AND AIRBORNE AEROSOL TRAPS

The selected scheme for a surface trap for cloud drops (coarsely-dispersed aerosol) is shown in Figure 22. A stationary and homogeneous stream of aerosol is produced in tube A with the aid of fan B which is connected to electric motor C. A glass plate D, covered with a shutter, is installed in the stream. After the stationary stream has been established in the tube, the shutter is opened

---

*In the axially symmetrical case analogous derivations lead to the condition

$$k \gg 6k_{cr}. \tag{I.109a}$$

When Re_p are not small and one cannot neglect in (I.91) and (I.92) the deviation of the force acting on the particle from the Stokes law, we can obtain a condition analogous to (I.109).

for a definite time. Then the aerosol particles settle on the glass. The velocity of the stream is calculated from the readings of a manometer which measures the static pressure on the wall of the tube. Such a scheme for a surface trap, unlike the one previously used, makes it possible, as a result of the stationarity of the stream from which the aerosol particles are precipitated, to take into account the capture coefficient of the aerosol particles by the plate and thus determine the true concentration and the aerosol-particle distribution function.

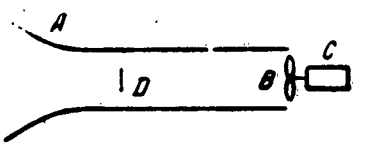

Fig. 22. Scheme of surface trap for aerosol particles.

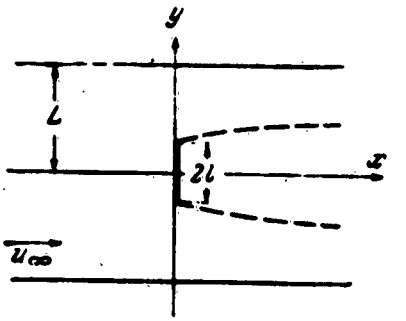

Fig. 23. Scheme of air-stream in the trap for aerosol particles.

The capture coefficient for the surface trap were calculated in accordance with a two-dimensional scheme (Fig. 23). It seems to us that in connection with the relatively small width of the plate in the trap (the ratio of the width of the plate 2l to the tube diameter 2L is 13 percent) and the location of the shutter in the central part of the tube the choice of a two-dimensional scheme for calculating the stream in the trap cannot lead to any appreciable errors.

Assuming that the air stream in the tube flows around the plate in accordance with a Kirchhoff flow, the air-velocity field around the plate can be determined by the method of N. Ye. Zhukovskiy [10] (see Appendix II). It is given by the equation*

*We recall that the unit of length is chosen to be the half-width of the plate.

$$z = \frac{2L \operatorname{tg}\mu}{\pi}\left\{\ln\frac{1+\zeta\operatorname{tg}\mu}{1-\zeta\operatorname{tg}\mu} - \operatorname{ctg}\mu\ln\frac{1+\zeta}{1-\zeta} - \right.$$

$$\left. - \frac{\operatorname{tg}\mu}{2}\ln\frac{1+\zeta\operatorname{tg}^2\mu}{1-\zeta\operatorname{tg}^2\mu}\right\}. \qquad \text{(I.110)}$$

where

$$\frac{1}{L} = 1 - \operatorname{tg}\mu\left(1 + \frac{2}{\pi}\frac{2\mu}{\operatorname{tg}2\mu}\right) \quad . \qquad \text{(I.111)}$$

From equation (I.110), by determining $dz/d\zeta$ at the critical point of the plate, we can readily obtain the value of the critical Stokes parameter for the plate in the tube:

$$k_{cr} = \frac{2L\operatorname{tg}^2\mu}{\pi\operatorname{tg}^2 2\mu}. \qquad \text{(I.112)}$$

As L varies from 1 to infinity, the value of μ changes from 0 to $\frac{\pi}{4}$, while k_{cr} changes from $\frac{1}{2\pi}$ to $\frac{4}{\pi+4}$. The last value of $k_{cr} = \frac{4}{\pi+4}$ corresponds to Kirchhoff flow around a plate by an unbounded stream (see Section 6). Figure 24 shows the connection between the quantities L and k_{cr} and the parameter μ.

In accordance with the procedure used to calculate the capture coefficient and developed in the preceding section, we tabulated the functions

$$\frac{1}{f(u_x)} = \frac{2L}{\pi}\left[\frac{1}{1-u_x^2} + \frac{1}{\operatorname{ctg}^2\mu - u_x^2} - \frac{2}{\operatorname{ctg}^2\mu - u_x^2}\right]$$

and

$$F(u_x) = -\int_0^{u_x}\frac{du_x}{f(u_x)}$$

at a value of $\mu = 0.575$, corresponding to the structural parameter of the manufactured trap ($\frac{1}{L} = 0.13$). The calculation of the aerosol particle trajectories at different values of the Stokes number k was carried by numerical integration of the differential equations (I.91), and (I.92)

by the Bless method [12], which is very convenient for these equations.

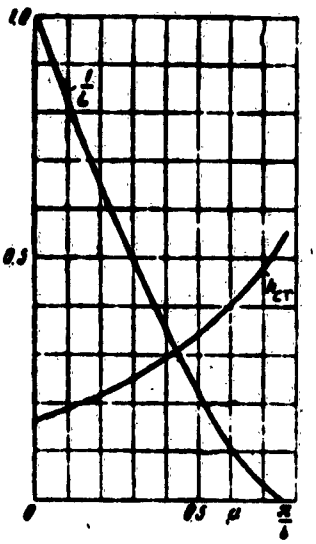

Fig. 24. Dependence of the dimensionless width of the tube L and the critical Stokes number k_{cr} on the parameter μ.

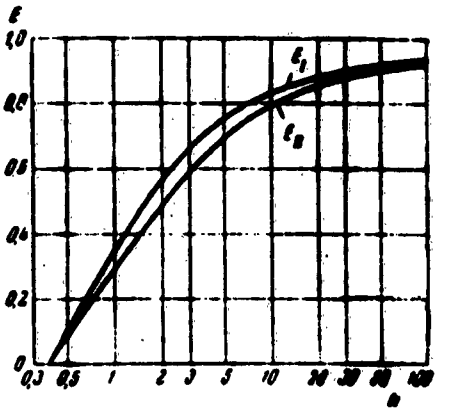

Fig. 25. Dependence of the capture coefficient E for the plate in the tube on the Stokes number k at $l/L = 0.13$.

Figure 25 and Table 5 show the values of the dependence E(k). The E_I curve corresponds to calculations without account of the deviation of the aerodynamic force, acting on the particle, from the Stokes value [this corresponds to assuming $Re_p = 0$ in equations (I.91) and (I.92)]. The curve E_{II} is calculated with account of this deviation at a stream velocity in the tube $u_\infty = 20$ m/sec ($Re_u = \frac{2 \cdot 10^3 \cdot 0.35}{0.145} = 4800$). As can be seen from Figure 25, both plots are quite close to each other all over the entire interval of the calculated values of k.

For airborne traps for cloud drops, a very simple scheme of an unbounded stream was chosen, flowing around a long plate with Kirchhoff flow. It seems to us that such a scheme should reflect more accurately the flow around the

plate than the scheme employed by several authors of using non-detached potential flow. This can be verified, for example, from an examination of Figure 26, which shows the distribution of the dimensionless pressure coefficient

$$c_p = \frac{p - p_\infty}{0{,}5\rho_f u_\infty^2}$$

on the frontal side of the plate for the place of Kirchhoff and non-detached potential flow around a plate. The circles in Figure 26 show the experimentally measured values of the coefficient c_p [109]. The functions $F(u_x)$ and $f(u_x)$ corresponding to equations (I.88) and (I.90) were tabulated. The capture coefficient was calculated by the same method as for a surface trap.

Table 5

Values of the Capture Coefficient E for a Plate in a Tube

h	E_I	E_{II}	$Re_p = \frac{du_\infty}{\nu}$
$h_{cr} = 0{,}384$	0	0	5
0,667	0,203	—	—
1,0	0,349	0,285	8
1,6	0,500	—	—
2,5	0,619	0,543	12
5	0,750	—	—
10	0,829	0,793	25
20	0,873	0,855	35
100	0,932	0,918	80

Figure 27 and Table 6 show the value of the capture coefficient for two cases. The curve E_I corresponds to calculations without inclusion of the deviation of the aerodynamic force F_a from the Stokes value, while curve E_{II} is calculated with account of this deviation and corresponds to $Re_u = 50{,}000$ ($l = 0.9$ cm; $u_\infty = 80$ m/sec).

As can be seen from Figure 27, at such large Reynolds numbers the calculation of the capture coefficient must be carried out with account of the deviation of the force acting on the particle from the Stokes force ($Re_{pl} \neq 0$).

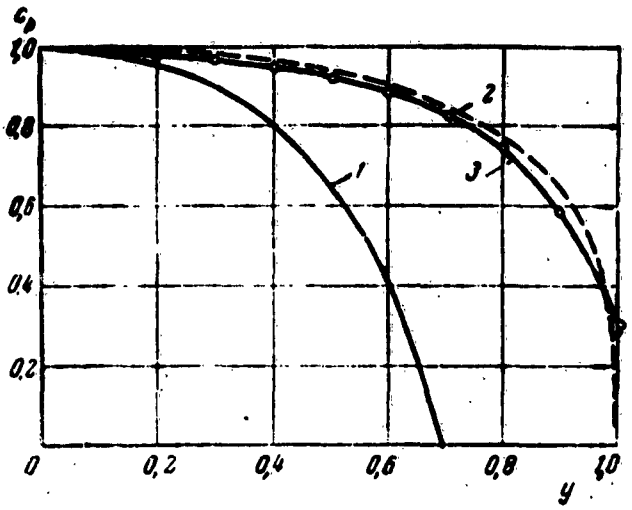

Fig. 26. Distribution of the dimensionless pressure coefficient c_p on the front side of the plate:

1--potential stream; 2--Kirchoff flow; 3--experimental values.

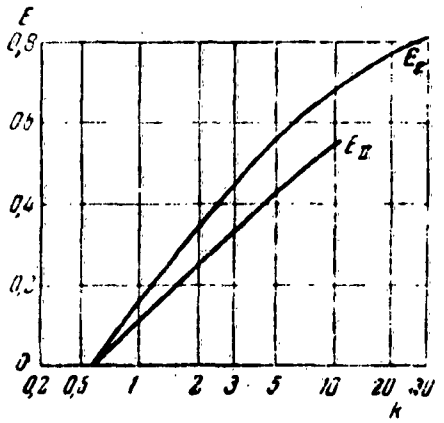

Fig. 27. Dependence of the capture coefficient E for a plate in an unbounded stream on the Stokes number k.

Table 6

Capture Coefficient E for a Plate in an Unbounded Stream (Kirchhoff Flow)

h	E_I	E_{II}	$Re_\rho = \frac{du_\infty}{\nu}$
$h_{cr} = 0{,}560$	0	0	25
1	0,150	0,095	34
2	0,347	0,235	48
3	0,443	0,317	58
4	0,492	0,362	67
5	0,562	0,415	75
7,5	0,627	0,490	92
10	0,669	0,540	106
15	0,724	—	130
20	0,768	—	150
30	0,813	—	184

After taking the sample of the aerosol particles on the plate, the regions near the symmetry line of the plate are photographed. In this type of photography, certain of the picture frames may deviate from the central line of the plate, and the width of the frame can in some cases be comparable with the width of the plate (it may amount to 10--15 percent of the width of the plate). It is therefore of interest, in order to make more precise the pattern of the settling of the aerosol on the plate from the stream, to consider the variation of the local capture coefficient transversely to the plate [11]. Inasmuch as it is impossible to carry out this operation on schemes using Kirchhoff flow (see Section 7), we shall consider this problem for a non-detached potential flow around a plate, assuming that the main results obtained here are qualitatively duplicated also in streams with detachment, by virtue of the identical geometry of the obstacle.

As was already indicated in Section 7, calculation of the potential field of the air speeds around the plate by means of formulas (I.84) is too cumbersome. This calculation can be simplified if it is taken into account that we are interested in trajectories lying in a band corresponding to values of the ordinate y lying between $\pm$ 1.

In this region it is possible to effectively expand the velocity components $u_x(x, y)$ and $u_y(x, y)$ in powers of y. This expansion is best carried out by noting that

$$\zeta = u_x - iu_y = F(x + iy) = F(x) + iy\frac{dF}{dz}_{|z=x} - y^2\frac{d^2F}{dz^2}_{|z=x} + \ldots$$

Separating the real and imaginary parts in this equation and recognizing that for potential flow around a plate we have

$$F(x) = \frac{x \operatorname{sign} x}{\sqrt{1+x^2}},$$

we obtain

$$u_x = \frac{x \operatorname{sign} x}{\sqrt{1+x^2}}\left\{1 + \frac{3y^2}{2(1+x^2)^2} + \frac{5y^4(3-4x^2)}{8(1+x^2)^4} + \right.$$
$$\left. + \frac{7y^6(5-28x^2+8x^4)}{16(1+x^2)^6} + 0(y^8)\right\},$$
$$u_y = -\frac{y \operatorname{sign} x}{\sqrt{(1+x^2)^3}}\left\{1 - \frac{y^2(4x^2-1)}{2(1+x^2)^2} + \frac{3y^4(1-12x^2+8x^4)}{8(1+x^2)^4} - \right. \quad \text{(I.113)}$$
$$\left. - \frac{y^6(5-144x^2-320x^4-64x^6)}{16(1+x^2)^6} + 0(y^8)\right\}.$$

For the velocity field (I.113), equations (I.91) and (I.92) were solved for the following initial conditions:

when $x = -\infty$: $\dot{x} = 1$, $\dot{y} = 0$, $y = y_0$.

The ordinate y_1 where the calculated trajectory crosses the plate determined the averaged capture coefficient E_{y_1} on the plate inside the band $\pm y_1$ from the formula $E_{y_1} = y_0/y_1$. The results of the calculations are shown in Figure 28 and in Table 7.

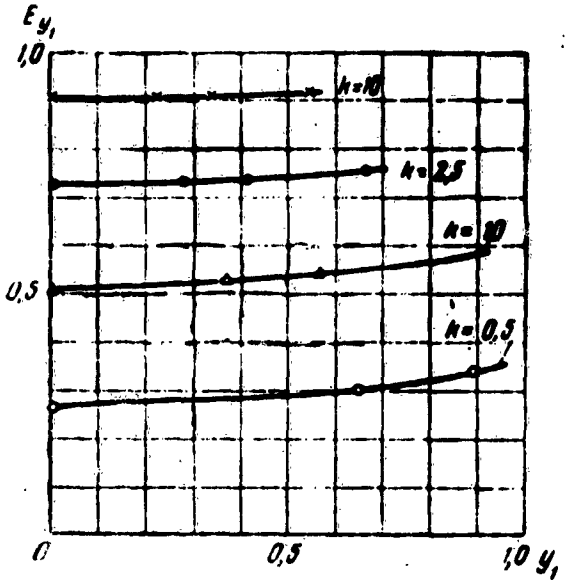

Fig. 28. Variation of the average capture coefficient transversely to the plate.

Table 7

Average Capture Coefficient E_{y_1} for a Plate in an Unbounded Stream (Potential Non-Detached Flow)

k	$y_0 = 5 \cdot 10^{-4}$	$y_0 = 0,2$		$y_0 = 0,3$		$y_0 = 0,5$	
	E_{y_1}	y_1	E_{y_1}	y_1	E_{y_1}	y_1	E_{y_1}
0,5	0,27	0,65	0,31	0,88	0,34	—	—
1,0	0,51	0,37	0,54	0,56	0,55	0,86	0,58
2,5	0,73	0,27	0,74	0,41	0,74	0,66	0,76
10	0,91	0,22	0,91	0,33	0,91	0,54	0,92

It is seen from Figure 28 and Table 7 that the average capture coefficient of the region $(-y_1, +y_1)$ changes insignificantly with the variation of y_1, increasing slightly with increase of y_1. When $k \geqslant 2.5$

inside a band amounting to 50 percent of the entire plate ($y_1 = 0.5$), the capture coefficient Ey_1 changes by less than 2 percent, and only when $k \sim 0.5$ does this change reach 10 percent. Thus, it can be assumed, with perfectly satisfactory practical accuracy, that in the central half of the plate ($y_1 < 0.5$) the capture coefficient is constant. In this respect the plate differs considerably from the curvilinear surfaces (in particular, from a circular cylinder), where the local capture coefficient has a maximum near the symmetry plane of the surface, by virtue of the geometry of the surface, and decreases rather sharply with increasing distance from the symmetry plane.

9. GATHERING AEROSOL SAMPLES. THE ASPIRATION COEFFICIENT WHEN AEROSOL IS DRAWN INTO A TUBE OR A SLOT

Usually in investigations of aerosol, it is necessary to draw a sample of the aerosol in some instrument. By virtue of the inertia of the aerosol particles, as was already indicated in Sections 1 and 3, changes will occur in the concentration and in the aerosol particle distribution function in the sample as compared with the concentration and the particles spectrum in the unperturbed aerosol. In the present section we shall consider the variation of the average flow concentration of the aerosol particles as the aerosol is drawn into a small tube or a narrow slot, disregarding for the time being the settling of the particles on the walls of the tube or the slot. We shall take account here of the influence of the wind velocity and the sedimentation velocity. This problem was solved by Davies [84] and by Walton [128], who neglected the inertia of the particles. However, in such a formulation, the solution they obtained for the problem is somewhat trivial. As was already indicated in Section 3, if the inertia of the particles is negligible ($k = 0$) the aerosol particle concentration in a field of solenoidal forces (div $F = 0$; the force of gravity is also solenoidal) should not change on being drawn into an instrument.

To investigate the variation of the average flow concentration of the aerosol particles as the aerosol is drawn into a small tube, let us consider the motion of the particles of monodispersed aerosol in the field of a homogeneous wind in the presence of a point sink. We assume here that away from the sink the particles move with the wind velocity. Such a formulation of the problem, subject to a certain limitation which will be referred to below,

imitates the motion of the particles outside the tube but of course does not take into account the sedimentation of the particles on the wall tube [29].

Let the wind velocity be u_w and the volume rate at which the air enters the sink Q. The rate of settling of the particles (the sedimentation velocity) is denoted by v_s. Then the equation of motion of the aerosol particles will be written in the form:

$$m\frac{dv_1}{dt_1} = 3\pi\eta d(u_1 - v_1) + mg = 3\pi\eta d(u_1 - v_1 - v_s). \quad \text{(I.114)}$$

If we place the sink at the origin, and the axis of a spherical (or cylindrical) coordinate system is directed along the vector $u_0 = u_w + v_s$*, then in dimensionless quantities equation (I.114) assumes the form:

$$k\frac{dv}{dt} + v = u, \quad \text{(I.115)}$$

where u is the dimensionless vector sum of the velocity of the air stream u_1 and the sedimentation velocity v_s. To obtain a simple form for writing down u it is necessary to choose as the characteristic length $l = \sqrt{\frac{Q}{4\pi u_0}}$, and as the characteristic velocity u_0. Then the dimensionless velocity will have in the spherical coordinate system components

$$u_r = \cos\theta - \frac{1}{r^2}, \quad u_\theta = -\sin\theta. \quad \text{(I.116)}$$

The Stokes number k will be expressed as

$$k = \frac{\rho_0 d^2}{18\eta}\sqrt{\frac{4\pi u_0^3}{Q}} =$$

$$= \tau\sqrt{\frac{4\pi u_0^3}{Q}}\left|1 + \left(\frac{v_s}{u_w}\right)^2 + 2\frac{v_s}{u_w}\cos(v_s, u_w)\right|^{3/4}, \quad \text{(I.117)}$$

---

*Such a choice of the coordinate axis direction leads to an axially symmetrical pattern of the aerosol-particle trajectories.

where $\tau = \frac{\rho_p d^2}{18\eta}$ is the relaxation time of the aerosol particles.

Let us consider first the solution of the problem in the case when the inertia of the aerosol particles can be neglected (τ and consequently k are very small). Then equation (I.115) assumes the form:

$$v_r = \frac{dr}{dt} = \cos\theta - \frac{1}{r^2}, \quad v_\theta = r\frac{d\theta}{dt} = -\sin\theta. \tag{I.118}$$

The solution of (I.118) must be sought under the following initial conditions:

$$\text{when} \quad t = -\infty: \; z = -\infty, \; \dot{z} = 1, \; \rho = \rho_0, \; \dot{\rho} = 0. \tag{I.119}$$

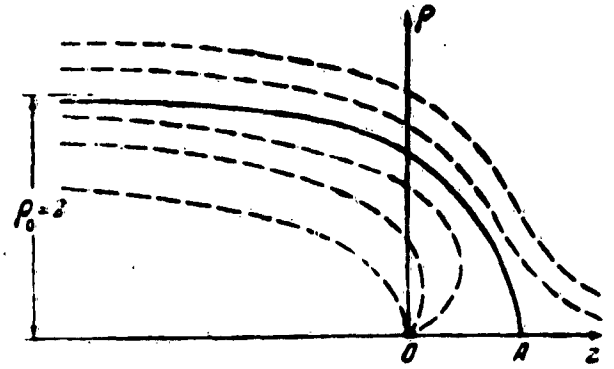

Fig. 29. Qualitative picture of the trajectories of inertialess aerosol particles (current lines of the air) when a moving aerosol is drawn into a tube.

The particle trajectory will be described in this case by the equation

$$\frac{r^2\sin^2\theta}{2} + \cos\theta = \text{const}. \tag{I.120}$$

The system of equations (I.118) has two singular points: a stable node at the origin and a saddle at the point A(1, 0) on the motion axis. The qualitative picture of the trajectories (in the meridional plane) which satisfy

the relations (I.118) and (I.119) is shown in Figure 29. As can be seen from Figure 29, the separatrix AB which passes through the saddle A is the limiting trajectory and separates two classes of the trajectories under consideration: those terminating at the origin (i.e., those entering into the drawing tube) and those going to infinity ($z = +\infty$). Its equation is obtained from formula (I.120), after determining the integration constant from the condition that $r = 1$ when $\theta = 0$. After simple transformations we find that the equation of the separatrix AB has the form:

$$r = \cos^{-1}\left(\frac{\theta}{2}\right), \qquad \text{(I.121)}$$

and its distance from the symmetry axis at $z = -\infty$ ($\theta = \pi$) is $\rho_0 = 2$. The number of particles entering per unit time inside the sink

$$N = \pi(\rho_0 l)^2 u_0 n_\infty,$$

where n_∞ is the counted particle concentration away from the sink.

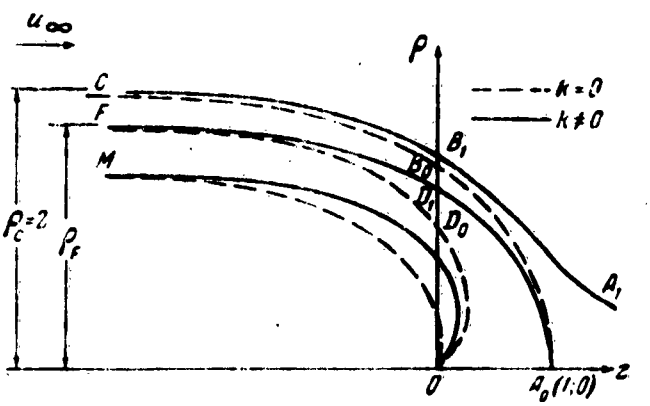

Fig. 30. Qualitative picture of the aerosol-particle trajectories when a moving aerosol is drawn into a tube.

The average flow concentration of the particles of the drawn-in aerosol (in the tube) is therefore

$$c_0 = \frac{N}{Q} = \frac{4\pi l^2 u_0 n_\infty}{Q_i} = n_\infty.$$

Thus (as was generally proved in Section 3), if we neglect the inertia of the aerosol particles, their concentration does not change on being drawn into the tube.

It is obvious that the trajectories of the inertial particles ($k \neq 0$) will differ from the trajectories shown in Figure 29. In this case, the qualitative picture of the trajectories will have the form shown in Figure 30. In constructing this pattern of transformed trajectories, account was taken of the fact that the geometric locus of the singular points of the system (I.115) in the plane (z, ρ) coincides with the geometric locus of the singular points of the system (I.118). Consequently, the singular (1.0) of the system (I.118) should be a singular point also of the system (I.115). The separatrix A_0D_1F passing through it should, in view of the physical continuity of the problem at small values of k, be a limiting trajectory.* Our task is to trace quantitatively the transformation of the separatrix A_0B_0C into A_0D_1F on going from the system of equations (I.118) through the system (I.115).

To find the trajectories of equation (I.115) for small values of k, we employ the method of small parameter. We seek a solution of (I.115) in the form of a series in powers of k:

$$v = v_0 + kv_1 + k^2v_2 + \ldots + k^nv_n + \ldots \qquad (I.122)$$

We substitute the series (I.122) into equation (I.115) written in the form

---

*We did not succeed in proving mathematically that the singular point A_0 for $k \neq 0$ under conditions (I.119) is a singular point of the saddle type in the plane (z, ρ). An analogous problem of the transformation of the trajectory pattern near the separatrix when k varies, for the case when the separatrix is a straight line, was considered by us in Sections 5 and 6. We have shown there with mathematical rigor that when k varies in the interval $0 \leqslant k \leqslant 1/4a$ (where a is a dimensionless gradient of the velocity at the singular point) the singular point remains a saddle. For the problem considered in the present section, $a = 1$ and when $k \leqslant 0.25$ the point should be a singular point of the singular type. We justify assumption not only by the physical continuity of the problem but also by the results of the calculations given below.

$$k(v\nabla)v + v = u, \qquad \text{(I.123)}$$

and equate the expressions containing equal powers of k.* We then obtain for the sought functions v_0, v_1, ... v_n the recurrence formulas

$$v_0 = u; \quad v_1 = -(v_0\nabla)v_0, \quad v_2 = -(v_0\nabla)v_1 - (v_1\nabla)v_0 \ldots$$

$$v_n = -(v_0\nabla)v_{n-1} - (v_1\nabla)v_{n-2} - \ldots - (v_{n-1}\nabla)v_0. \qquad \text{(I.124)}$$

If we recognize that for arbitrary vector fields a and b the following relation holds true

$$(a\nabla)b + (b\nabla)a = \operatorname{grad}(ab) - [a, \operatorname{rot} b] - [b, \operatorname{rot} a],$$

then relations (I.124) can be simplified. Indeed, inasmuch as rot u = 0 we have

$$\operatorname{rot} v_1 = 0 \text{ and } v_1 = -\frac{1}{2}\operatorname{grad} v_0^2.$$

Consequently,

$$\operatorname{rot} v_1 = 0 \text{ and } v_2 = -\operatorname{grad}(v_0 v_1) \text{ etc.}**$$

We ultimately obtain

$$v_0 = u; \quad v_1 = -\frac{1}{2}\operatorname{grad} v_0^2; \quad v_2 = -\operatorname{grad}(v_0 v_1) \ldots$$

$$v_n = -\operatorname{grad}(v_0 v_{n-1} + v_1 v_{n-2} + \ldots) \qquad \text{(I.125)}$$

---

*The method of small parameter was used by Ya. M. Yaglom for equation (I.123) in solving the problem of the flow of an aerosol stream around a cylinder (see the footnote on page 16).

**Thus, in the case when the solution (I.122) exists, we obtain still another proof that the field v is potential, since

$$\operatorname{rot} v = \sum_{n=0}^{\infty} k^n \operatorname{rot} v_n = 0.$$

Applying the general expression (I.125) to the problem which we are considering, we obtain

$$v_{0r} = \cos\theta - \frac{1}{r^3}, \quad v_{0\theta} = -\sin\theta \quad v_{1r} = \frac{2(1 - r^3\cos\theta)}{r^6},$$

$$v_{1\theta} = -\frac{\sin\theta}{r^6}, \quad v_{2r} = \frac{3(1 - 3\cos^2\theta)}{r^4} + \frac{20\cos\theta}{r^6} - \frac{14}{r^9}, \qquad \text{(I.126)}$$

$$v_{2\theta} = -\frac{6\sin\theta\cos\theta}{r^4} + \frac{4\sin\theta}{r^6} \ldots$$

It is easy to see that all the v_n for $n \geqslant 1$ vanish when $z = -\infty$ (i.e., when $r = \infty$, $\theta = \pi$) and consequently the solution $v = \sum_{n=0}^{\infty} k^n v_n$ satisfies the initial conditions (I.119). To the trajectories it is necessary to solve the equation $r^2 v_r \sin\theta \, d\theta - r\, v_\theta \sin\theta \, dr = 0$, in which we substitute the values of v_r and v_θ from (I.126). Accurate to second-order terms inclusive, we obtain after simple transformations

$$d\left[\frac{r^3\sin^2\theta}{2} + \cos\theta - \frac{k\sin^2\theta}{r} - \frac{3k^2\cos\theta\sin^2\theta}{r^2} + \frac{k^2\sin^2\theta}{r^4}\right] =$$

$$= -\frac{2k\sin\theta\, d\theta}{r^6} + \frac{14k^2\sin\theta\, d\theta}{r^9} - \frac{18k^2\sin\theta\cos\theta\, d\theta}{r^4}. \qquad \text{(I.127)}$$

To find the separatrix A_0D_1F we put in the right half of (I.127) in first approximation $r = \cos^{-1}\left(\frac{\theta}{2}\right)$, which is equivalent to assuming that the separatrix A_0D_1F differs little from separatrix A_0B_0C. After such a substitution equation (I.127) can be readily integrated. The integration constant is obtained from the condition that the separatrix must pass through the point A_0 (1.0). After finding thus in first approximation the equation of the separatrix A_0D_1F, we substitute the value $r = r(\theta)$ obtained from it into equation (I.127) and again integrate the latter. From the equation obtained in the second approximation for the curve A_0D_1F we obtain for its distance ρ_F from the axis when $z = -\infty$ the expression

$$\rho_p^2 = 4 - \frac{16k}{5} + 0{,}32k^2 \ldots,$$

from which we readily determine the average flow concentration c_0 of the particles in the tube and the aspiration coefficient in the inlet section of the tube

$$A = \frac{c_0}{c_\infty} = \frac{\pi (\rho_p l)^2 u_0}{Q} = 1 - 0{,}8k + 0{,}08k^2 \ldots \qquad \text{(I.128)}$$

To check at which values formula (I.128) still yields satisfactory results and to check on the character of the pattern of the trajectories, equations (I.115) and (I.116) were integrated numerically for k = 0.25 and 0.5. Figure 31 shows the results of these calculations for k = = 0.25. As assumed, the point A_0 (1,0) in Figure 31 is a singular point of the saddle type. When k = 0.25 the ratio c_0/c_∞ lies in the interval 0.810 -- 0.795, differing from the value c_0/c_∞ = 0.805 obtained from equation (I.128) by not more than one percent. When k = 0.5 the ratio c_0/c_∞ lies in the interval 0.625 -- 0.635 and differs from (I.128) by not more than 2.5 percent.

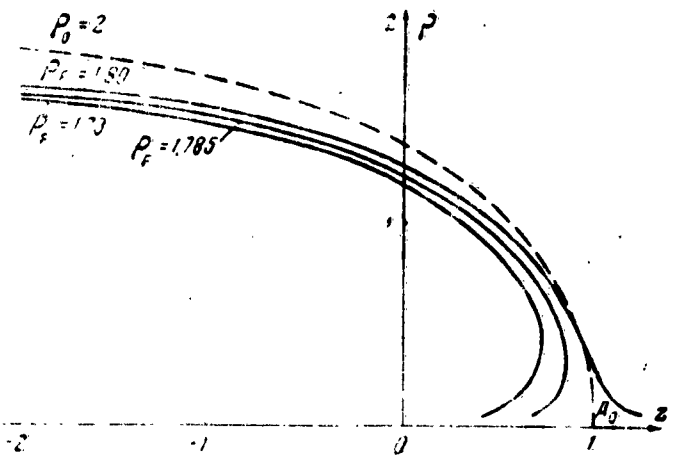

Fig. 31. Results of calculations delimiting trajectory for the Stokes number k = 0.25.

Let us proceed now to a specific analysis of the results obtained. In Table 8 are listed the values of k for different values of the volume flow Q, the velocity u_0

for a water-aerosol (ρ_p = 1 g/cm3; η = 1.8 x 10^{-4} poise).

Table 8

Dependence of the Stokes Number on the Particle Diameter of the Aerosol D, the Velocity u_0, and the Volume Flow Q

u_0 [cm/sec]	d [μ]					Q [cm³/sec]
	1	10	20	30	100	
100	$1,1 \cdot 10^{-4}$	0,011	0,044	0,10	1,1	10^4
200	$3,1 \cdot 10^{-4}$	0,031	0,12	0,28	3,1	10^4
500	$1,2 \cdot 10^{-3}$	0,12	0,48	1,10	12	10^4
30	$1,8 \cdot 10^{-4}$	0,018	0,072	0,16	1,8	10^3
100	$1,1 \cdot 10^{-3}$	0,11	0,44	1,0	11,0	10^3
200	$3,1 \cdot 10^{-3}$	0,31	1,2	2,8	31	10^3
10	$3,5 \cdot 10^{-4}$	0,035	0,14	0,31	3,5	1
30	$1,8 \cdot 10^{-3}$	0,18	0,72	1,6	18	1
100	0,011	1,1	4,4	10	110	1
200	0,031	3,1	12	28	310	1
v_s [cm/sec]	$3,1 \cdot 10^{-3}$	0,31	1,2	2,8	31	
τ [sec]	$3,1 \cdot 10^{-6}$	$3,1 \cdot 10^{-4}$	$1,2 \cdot 10^{-3}$	$2,8 \cdot 10^{-3}$	$3,1 \cdot 10^{-3}$	

Table 9

Dependence of Q Satisfying the Condition (I.130) on d_μ and u_0

d_μ	u_0 [m/sec]				$u_w = 0$, $u_{wn} = v_s$
	1	2	5	10	
1	$1,9 \cdot 10^{-3}$	0,015	0,24	1,9	
2	$8 \cdot 10^{-3}$	0,25	3,8	30	
5	1,2	9,5	150	1200	$5 \cdot 10^{-10}$
10	10	150	2400	$1,9 \cdot 10^4$	$8 \cdot 10^{-7}$
20	300	2400	$3,8 \cdot 10^4$	$3,0 \cdot 10^5$	$5 \cdot 10^{-4}$
30	1500	$1,2 \cdot 10^4$	$1,9 \cdot 10^5$	$1,5 \cdot 10^6$	$3 \cdot 10^{-2}$

In order for the reduction in the concentration in the tube not to be excessive, it is necessary that the criterion k not be large. If we confine ourselves to the requirement that $c_0/c_\infty > 0.8$, then this will lead, in accordance with equation (I.128), to the condition $k \quad 0.25$. It is seen from Table 8 that $k < 0.25$ for drops with diameter $d = 30$ microns at a wind velocity 2 m/sec only when $Q > 10^4$ cm^3/sec, while for drops with diameter $d = 10$ microns this holds for $Q > 10^2$ cm^3/sec. At very small flows ($Q \approx 1$ cm^3/sec) we can expect small changes in the spectrum of particles in the range $d < 10$ microns when the aerosol is drawn in only when the wind velocity does not exceed 0.5 m/sec. In the range $d < 100$ microns considerable variations of the spectrum can occur when $Q < 10^2$ cm^3/sec given in the absence of one since for drops of 100 microns in diameter the sedimentation velocity is $v_s = 31$ cm/sec.

On the basis of equation (I.117) we can find the relationship between the parameters of the phenomenon at which the condition $\frac{c_0}{c_\infty} > 0{,}8$ $(k < 0{,}25)$ is satisfied:

$$Q > \frac{16\pi\rho_\rho^2 d^4 u_0^2}{81\eta^2}. \qquad \text{(I.129)}$$

For water aerosol the relation (I.129) has the form

$$Q > 1{,}9 \cdot 10^{-3} d_\mu^4 u_{0m}^2. \qquad \text{(I.130)}$$

where d_μ is the diameter of the drop in microns;
u_{0m} is the velocity in meters per second;
Q is the volume flow in cm^3/sec.

Table 9 shows values of Q [cm^3/sec] satisfying conditions (I.130) for different values of u_{0m} and d_μ.* It

---

*If we consider the drawing in of aerosol from quiet air ($u_w = 0$, $u_{0m} = v_s = 0.3 \times 10^{-4} d_\mu^2$), then conditions (I.130) will usually be satisfied for cloud drops at very small flows Q. Thus, for example, when $d = 50$ microns, the flow Q should be larger than 6 cm^3/sec. But even when $d = 100$ microns the condition (I.130) calls for $Q > 5700$ cm^3/sec. Thus, when drawing in drops from quiet air a drop with diameter $d < 50$ microns will hardly change its

follows from Table 9, for example, that in order to take in a sample of quality drops in surface aerosol traps it is necessary to use flows $Q > 12{,}000$ cm^3/sec in order to ensure a weakly distorted spectrum down to diameters of 30 microns and at a wind velocity not larger than two meters per second. In this case, for drops with diameter $d<20$ microns the concentration ratio is $\frac{c_0}{c_\infty} > 0.9$. On the other hand, in drawing in finely dispersed aerosol ($d < 1$--2 microns) in various instruments (for example in a thermorespirator), one can use flows $Q \approx 0.1$ cm^3/sec if the wind velocity does not exceed two meters per second.

At large wind velocities ($u_0 \approx 5$--10 m/sec), in order to draw in particles 20--30 microns in diameter, it is necessary according to Table 9 to employ devices with very large values of Q (100--1,000 litres per second). An analogous deduction is obtained also for airplane aerosol gathering devices. In these cases, however, it is not advisable to attempt to effect nearly isokinetic ingathering of the samples, taking into account the orientation of the wind relative to the tube axis [66, sec. 32]. At the same time, at wind velocities less than 2 or 3 meters per second (which usually change rapidly in magnitude and direction) it is convenient to gather the aerosol samples without regard for the wind direction. It is then necessary to satisfy condition (I.130).

We have considered the process of drawing in aerosol into a tube under the assumption that the tube diameter is very small. One can expect the theory developed to retain its principal features if the radius of the tube R is smaller than the distance from the saddle A_0 to the origin, i.e., when $R < l$. If we denote by $\bar{u}$ the average velocity of air in the tube, then $Q = \pi R^2 \bar{u}$ and consequently the ratio $R < l$ will be equivalent to the inequality $\bar{u} > 4u_0$.

Finally, it is easy to see from general considerations that an increase in the tube dimaeter for a given flow

---

average concentration in the inlet opening even at very small flows Q (see [84], where it is indicated that experiments show no noticeable distortion of the concentration when particles with $d < 100$ microns are drawn in from quiet air at $Q > 100$ cm^3/sec).

should lead to a reduction in the flow concentration of the aerosol particles in the tube, for the radial component of the air velocity near the tube is decreased then.

To investigate the change in the aerosol particle concentration when the aerosol is drawn into a narrow slot, let us consider the motion of the aerosol particle in the field of a homogeneous wind in the presence of a straight-line sink and the force of gravity. It is obvious that in this case we can confine ourselves to the case when the vector $u_0 = u_w + v_s$ is perpendicular to the sink line, for in the opposite case we can resolve the vector u_0 into two components, one parallel and one perpendicular to the sink line, and we need to take into consideration then only the perpendicular component. The vector component of u_0 parallel to the sink line causes the aerosol particles to move along the sink line and cannot exert any influence on the drawing in of the particles into the sink.

Thus, the problem under consideration is two-dimensional, and to answer the posed questions it is necessary to find the trajectories of motion in a plane perpendicular to the sink line. As before, by locating the point of intersection of the sink line with the plane of motion under consideration at the origin, and by choosing as the characteristic velocity u_0 and as the characteristic line $l = Q_1/2\pi u_0$ (where Q_1 is the volume inflow of air per unit length of the sink line), we can write down the equation of motion of the aerosol particles in the form of the equation (I.115)*

$$u_r = \cos\varphi - \frac{1}{r}; \quad u_\varphi = -\sin\varphi, \tag{I.131}$$

$$k = \frac{2\pi u_0^2 \tau}{Q_1} = \frac{2\pi u_w^2 \tau}{Q_1}\left[1 + \left(\frac{v_s}{u_w}\right)^2 + 2\frac{v_s}{u_w}\cos(v_s, u_w)\right]. \tag{I.132}$$

The qualitative picture of the trajectories will in this case be the same as in the case of a tube. The singular point of the saddle type A_0 has coordinates (1, 0). When k = 0 the equation of the trajectories has the form

$$r\sin\varphi - \varphi = \text{const}, \tag{I.133}$$

*Here r and φ are the polar coordinates, the axis of which is directed along the vector u_0.

and the separatrix A_0B_0C (see Fig. 30; it is necessary here to replace only the coordinate z by x and ρ by y) is described by the equation

$$y = r\sin\varphi = \varphi. \tag{I.134}$$

It is seen from formula (I.134) that the distance from the separatrix A_0B_0C to the Ox axis when $x = -\infty$ is $y_0 = \pi$. Since the dimensionless velocity gradient near the singular point A_0 is equal to unity, we can expect that when $k \leq 0.25$ the singular A_0 will remain of the same type (saddle). Employing, as before, the method of small parameter, we obtain

$$v_{0r} = \cos\varphi - \frac{1}{r};\quad v_{0\varphi} = -\sin\varphi;\quad v_{1r} = -\frac{\cos\varphi}{r^2} + \frac{1}{r^2};$$
$$v_{1\varphi} = -\frac{\sin\varphi}{r^2};\quad v_{2r} = -\frac{2\cos 2\varphi}{r^3} + \frac{6\cos\varphi}{r^4} - \frac{4}{r^5}; \tag{I.135}$$
$$v_{2\varphi} = -\frac{2\sin 2\varphi}{r^3} + \frac{2\sin\varphi}{r^4}, \ldots.$$

Substituting the obtained values of v_r and v_φ into the equation $rv_r d\varphi - v_\varphi dr = 0$, we obtain the trajectory equation

$$d\left[r\sin\varphi - \varphi - \frac{k\sin\varphi}{r} - \frac{k^2\sin 2\varphi}{r^3} + \frac{2k^3\sin\varphi}{3r^3}\right] =$$
$$= -\frac{k\,d\varphi}{r^2} - \frac{16k^3\cos\varphi\,d\varphi}{3r^3} + \frac{4k^2\,d\varphi}{r^4}. \tag{I.136}$$

Substituting in the right half of (I.136) in the first approximation $r = \varphi/\sin\varphi$, i.e., assuming that the separatrix A_0B_0C and A_0D_1F differ little from each other, we can integrate the equation. Carrying out then the iteration, the same as in the preceding case when aerosol was drawn into a tube, we determine the distance y_F of the separatrix A_0D_1F from the axis when $x = -\infty$:

$$y_F = \pi - kSi(2\pi) - 0{,}465k^2\ldots \tag{I.137}$$

From equation (I.137) we can already determine readily the average flow of concentration of the particles in the slot and the aspiration coefficient in the inlet section of the slot:

$$A = \frac{c_0}{c_\infty} = \frac{2y_p\, lu_0}{Q_1} = \frac{y_p}{a} = 1 - 0{,}451k - 0{,}148k^2 \ldots \quad \text{(I.138)}$$

Using equations (I.138) and (I.132), we can obtain the relation between the parameters of the phenomenon, at which the condition $\frac{c_0}{c_\infty} > 0{,}8$ $(k < 0{,}45)$ is satisfied:

$$Q_1 > \frac{\pi u_0^2 \rho_p d^2}{4\eta}. \quad \text{(I.139)}$$

For a water aerosol the relation (I.138) assumes the form

$$Q_1 > 0{,}44\, d_p^2\, u_{0m}^2. \quad \text{(I.140)}$$

The relations obtained are applicable if the half-width of the slot is smaller than l, i.e., when the average velocity of air in the slot is $\bar{u} > \pi u_0$.

On the basis of formulas (I.118) and (I.138) we can determine the variation of the spectrum and the main spectral characteristics of the aerosol (the number of particles per unit volume N, the water content q, the specific cross section of the particles S_g, the mean-cube, mean-square, and mean diameters d_3, d_2, and d_1), when the aerosol is drawn into a tube or into a slot. If we designate by n(d) the normalized distribution density of the number of particles by diameters $\left(\int_0^\infty n(d)\, Dd = 1\right)$, then the number of particles in the range of diameters from d to d + Dd will be Nn(d)Dd. When aerosol is drawn into a tube or a slot, this number becomes equal to $Nn(d)(1 - \gamma d^2)Dd$, where $\gamma = 0{,}8\frac{\rho_p}{18\eta}\sqrt{\frac{4\pi u_0^2}{Q}}$ for a tube and $\gamma = 0{,}45\frac{\pi \rho_p u_0^2}{g\eta Q_1}$ for a slot [we confine ourselves to the first two terms of the series in (I.128) and (I.138)]. We denote the i-th moment of the distribution n(d) by $M_i = \int_0^\infty d^i n(d)\, Dd$ (it is obvious that $d_1 = M_1$; $d_2^2 = M_2$; $d_3^3 = M_3$).

Then the number of particles per unit volume inside the tube or slot is*

$$N' = N(1 - \gamma d_3^3), \tag{I.141}$$

and the normalized density of the distribution n' in the tube or in the slot has the form

$$n'(d) = \frac{n(d)(1 - \gamma d^3)}{1 - \gamma d_3^3}. \tag{I.142}$$

From this we readily find that the water content q', the specific cross section S'_g, and the diameters d'_3, d'_2, and d'_1 in the aerosol that is drawn into the tube or the slot will be related with the corresponding quantities in the free aerosol by the following equation:

$$q' = q\left(1 - \gamma \frac{M_3}{M_3}\right), \quad S'_r = S_r\left(1 - \gamma \frac{M_3}{M_3}\right),$$

$$\left(\frac{d'_3}{d_3}\right)^3 = \frac{M_3 - \gamma M_3}{M_3(1 - \gamma M_3)}, \quad \left(\frac{d'_2}{d_2}\right)^2 = \frac{M_2 - \gamma M_3}{M_2(1 - \gamma M_3)},$$

$$\frac{d'_1}{d_1} = \frac{M_1 - \gamma M_3}{M_1(1 - \gamma M_3)}. \tag{I.143}$$

Let us consider in conclusion the process of drawing in aerosol into a tube of finite width. Not being able to investigate at present this question to its full extent, we confine ourselves to qualitative considerations of the phenomenon of the gathering of the aerosol samples through a thin-walled tube, oriented parallel to the stream at infinity. Three different cases arise in this case and are shown schematically in Figure 32. The first case (Fig. 32a) corresponds to the so-called isokinetic conditions of sample gathering, when the velocity of the air stream inside the tube is equal to the velocity of the incoming stream.

---

*Usually the overwhelming number of particles lie in the diameter range 0 -- 2.5 d_2. Therefore, in spite of the use of formulas (I.128) and (I.138) is restricted to small values of k(d), integration with respect to d for the calculation of N' and then q' and S'_g can be extended to $d = \infty$.

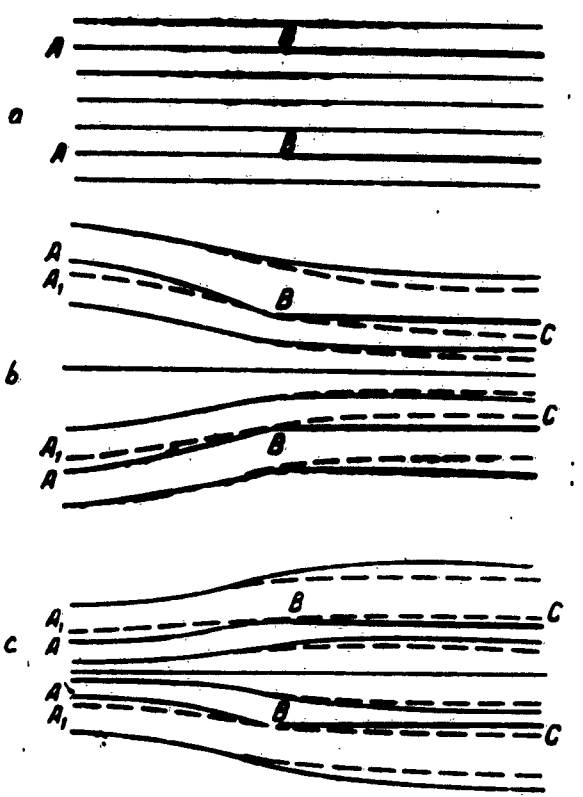

Fig. 32. Different cases of gathering of aerosol samples:

$$a - \frac{u_\infty}{u_0} = 1;\quad b - \frac{u_\infty}{u_0} < 1;\quad c - \frac{u_\infty}{u_0} > 1.$$

In this case (neglecting the thickness of the walls) the tubes introduce no distortions whatever in the aerosol stream. The stream remains inhomogeneous everywhere, and therefore (see Section 3) the counted concentration n_0 (and also the flow concentration $c_0 = \frac{n_0 v_{x0}}{u_{x0}} = n_0$) inside the tube is equal to the concentration n_∞ of the unperturbed aerosol. In the second case (Fig. 32b) the velocity of the air inside the tube, u_0, exceeds the velocity of the incoming stream in u_∞, while the third (Fig. 32c) $u_\infty/u_0 > 1$. In all these figures the solid lines represent the current

lines of the air, while the dashed lines show the trajectories of the aerosol particles. The lines AB correspond to the boundary lines of the air current, which separate the region of the air stream entering into the tube from the region which flows past the tube. The lines A_1BC show the limiting particle trajectories. It is easy to see from Figure 32 that the flow concentration of the aerosol particles inside the tube, c_0, exceeds the concentration of the particles at infinity ($c_\infty = n_\infty$) if $u_0/u_\infty < 1$, and that $c_0 < c_\infty$, if $u_0 > u_\infty$. This follows from the fact that in the former case the limiting trajectories of the aerosol particles lie outside the limiting current lines of the air, and in this latter case they lie inside the limiting lines of the air current.

For very small particles (the Stokes parameter k is small) we have $v \approx u$ and $n \approx$ const. Consequently, in small particles the counted and the flow concentrations inside the tube are close to n_∞. For very large particles ($k \to \infty$) the velocity is $v(r) \approx v_\infty = u_\infty$ and $n(r) \approx n_\infty$ (see Section 7). Therefore it is sufficiently large distances from the entry into the tube, inside of which the air stream speed becomes uniform and equal to u_0, the flow concentration is

$$\frac{c}{c_\infty} = \frac{nv_{x0}}{n_\infty u_{x0}} = \frac{u_\infty}{u_0}.$$

For intermediate values of k, the ratio $n/n_\infty > 1$ (see Sec. 3) and the ratio c/c_∞ lies between 1 and v_∞/u_0 (Fig. 33). Of course, all these relations are qualitative in nature. They can be greatly distorted by settling of particles of the wall, which is connected to a considerable degree with the form of the air stream near the inlet to the tube, etc. For a more or less rigorous solution of the problem under discussion it is necessary to carry out calculations of the aerosol particle trajectories for specifically chosen schemes of air streams aspired through the tube. However, an analytic expression for the velocity field u(r) is in these cases (for example, for the Borda fitting [19]) very complicated, and it is likewise inefficient to carry out such calculations without electronic computers.

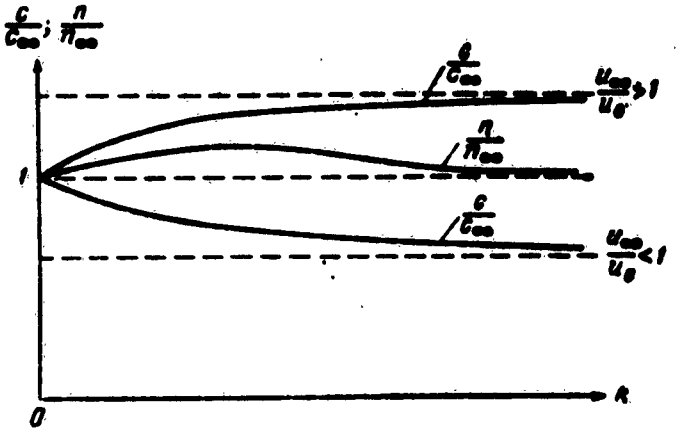

Fig. 33. Variation of flow and counted concentrations of aerosol particles with Stokes number k when drawing-in aerosol into a tube parallel to the air stream.

The variation of the aerosol particle concentration during the gathering of samples was investigated experimentally by many workers (see, for example, [90, 108, 129]). We shall dwell here only on some of the results obtained in the semi-empirical work of Watson [129]. In this investigation we consider the ratio of the diameters of the current tubes, formed by the boundary current lines of the air D_a and the limiting trajectories of the aerosol particles D_p (see Fig. 32). From similarity theory it is clear that this ratio is a function of the Stokes number, Re_u, Re_p, the relative thickness of the wall, and the velocity ratio u_0/u_∞. Watson proposes that the ratio D_p/D_a is a function of the Stokes number only,

$$k = \frac{\rho_p \delta^2 u_\infty}{18 \eta D},$$

where D is the tube diameter.

Introducing the notation

$$\frac{D_p - D}{D_a - D} = f(k), \qquad \text{(I.144)}$$

he obtains for the ratio c_0/c_∞ the formula*

$$\frac{c_0}{c_\infty} = \frac{D_0^3}{D_\infty^3} = \frac{1}{D_\infty^3}[D + (D_\infty - D) f(k)]^3 =$$

$$= \frac{u_\infty}{u_0}\left[1 + f(k)\left(\sqrt{\frac{u_0}{u_\infty}} - 1\right)\right]^3, \qquad \text{(I.145)}$$

since

$$\left(\frac{D}{D_\infty}\right)^3 = \frac{u_\infty}{u_0}.$$

On the basis of the two experiments performed, characterized by quantities

1) $\frac{u_\infty}{u_0} = 2{,}25$; $k = 1{,}39$; $D = 1{,}05$ см; $\frac{\sqrt{c_0}}{c_\infty} = 1{,}57$;

2) $\frac{u_\infty}{u_0} = 0{,}43$; $k = 3{,}19$; $D = 0{,}46$ см; $\frac{c_0}{c_\infty} = 0{,}49$,

Weston calculates, starting from formula (I.145), the corresponding values of f(k) and plots the curve of f(k) as shown in Figure 34 (it is obvious that when $k \to \infty$ the function $f(k) \to 0$).

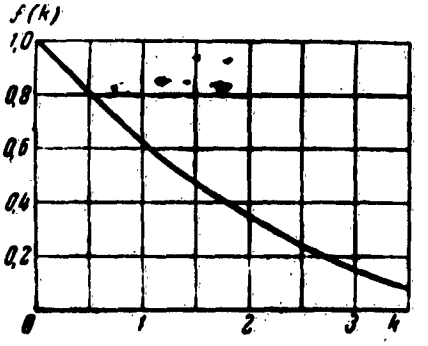

Fig. 34. Plot showing the dependence of the function f(k), determined by equation (I.144).

*It must be noted that Watson, like others, did not distinguish between the flow and the counted concentration, designating c as merely the concentration.

We note that the plot of Figure 34 has been plotted essentially only from two experimental points, corresponding to appreciably different ratios $u_{\infty 0}/u_0$. It seems to us that additional experimental material is necessary to clarify the dependence of c_0/c_∞ on the parameters listed above and to check the correctness of Watson's assumption (I.144).

CHAPTER II

ELECTROSTATIC COAGULATION AND SETTLING OF AEROSOL PARTICLES

10. FORMULATION OF THE PROBLEM

In the present chapter it is our task to examine the rule of electrostatic forces in processes involving the coagulation of the particles of a coarsely-dispersed aerosol, and also in processes of settling of such particles from the stream on different obstacles. The first problem is of certain physical and geophysical interest, since coagulation processes play an appreciable role in the aging of coarsely-dispersed aerosol, occupying a large volume, and in particular in the growth of cloud droplets leading to precipitation. An examination of the second problem can have various technical applications, connected with elimination of aerosol particles from air, the precipitation of aerosol particles on electric wires, etc.

As regards the role of electric forces in coagulation processes of cloud drops, the information and opinions expressed in the literature are contradictory. Thus, for example, Shushkin [76] believes that electric forces do not play an appreciable role in processes of coagulation in clouds.

In many other works [23, 83, 117, 125] an opposing point of view is expressed. It seems to us that such contradictory notions are connected with the inadequacy of the theoretical research on this question, and also with the fact that the magnitudes and signs of the electric charges of the individual cloud drops have still been poorly

investigated up to now.

Whereas the final solution of the problem is left until thorough experiments are performed on the measurement of the charges of individual cloud drops in clouds of various types and experiments on the direct investigation of the influence of electric forces on the coagulation of cloud drops, it is advantageous to consider theoretically the effect expected from the action of the electric charges of the drops and of atmospheric electric fields on the growth of cloud droplets. Naturally, such an investigation should be carried out, wherever possible, under broad assumptions concerning the sizes of the charges and electric fields, so as to be able to extend the investigation to the phenomenon of coagulation and sedimentation of particles of any coarsely-dispersed aerosol.

Anticipating the results of such an investigation, it should be noted here that even relatively small charges of cloud drops may turn out to be essential for the growth of drops with diameter d = 1 -- 30 microns. The point is that according to modern theory of formation of precipitation [103, 76] the growth of cloud drops in the indicated range of diameters cannot occur as a result of gravitational coagulation, and is determined only by the condensation of the water vapor. This is connected with the existence of a critical Stokes number $k_{cr} = 1.21$ for the presses of inertial sedimentation of drops on the sphere around which a viscous stream flows (see Section 6), leading to the elimination of gravitational coagulation in the case of drops with a diameter less than 30 microns [76].* On the other hand, the condensation growth of cloud droplets occurs sufficiently rapidly only for small drops ($d < 1$ micron). Therefore the condensation growth of drops up to diameter $d \approx 30$ microns, when the gravitational coagulation goes into effect, occurs too slowly. For example [76], when the rising air stream has a velocity 10 centimeters per second, the diameter of the drop increases as a result of condensation from 11 to 30 microns within 7.5 hours, and then

---

*As was already noted (Section 6), an account of the finite dimensions of the small drops, and also an account of the Brownian and turbulent diffusion of the drops lifts the absolute character of the exclusion of coagulation in the range under consideration [37, 38, 86]. However, the coagulation which is brought about by these effects has apparently low intensity.

increases to 1,300 microns as a result of gravitational coagulation (the latter is the dimension of the rain drop) after 15 -- 20 minutes. Such a length of formation of rain drops in a cloud exceeds greatly the axially observed times of formation of precipitation from the cloud. It is mainly by virtue of the circumstances that coagulation of cloud drops, brought about by electric forces, can play an appreciable role in the development of a cloud during its initial stage, when the gravitational coagulation is still missing [23, 26, 28].

The speed of coagulation of the aerosol particles is determined by the value of the capture coefficient E of the small particles (with diameter d), moving relative to the large particle (with diameter D). We shall seek the values of the capture coefficient E, determined by the difference in the rates of drops of the particles and the electrostatic interaction between them. To find the capture coefficient E, as was indicated in Section 1, it is necessary to find the limiting trajectories of the small particles relative to the large ones.

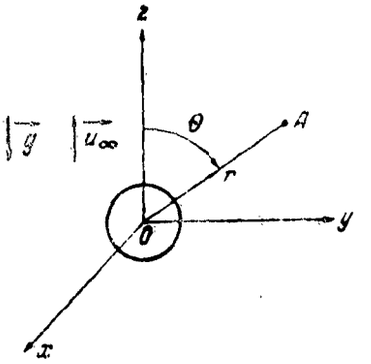

Fig. 35. Coordinate system.

The trajectories of motion of the small particles of aerosol will be sought in a coordinate system connected with the center of gravity of the large particles. In this system the Oz axis will be directed vertically upward (Fig. 35). In this system of coordinates there is incoming on the large particle a stream of air with velocity u_∞ at $z = -\infty$ (u_∞ is the rate of fall of the large particles). The small particle is acted upon by the force of gravity, by the aerodynamic force F_a, and by the electrostatic force F_e.

It should be noted that Langmuir [103] and Shushkin [76] assume without consistency the theory of sedimentation of aerosol particles on obstacles and applied to the theory of growth of cloud drops. The capture coefficient in the sedimentation of an aerosol on a sphere was calculated by Langmuir [103], who assumed that this sphere is much larger than the aerosol particles. Therefore the results of these calculations can be applied to the falling of drops of rain dimensions in a cloud, and not when both drops are of comparable dimensions. Yet in the calculation of the velocity of growth of the cloud drops, Langmuir actually assumes all the cloud drops to be fixed in space, except for one (sometimes having the same dimensions as the remainder, and sometimes even smaller), the latter moving under the influence of gravity and of the rising streams [103]. Shushkin, on the other hand, assumes that the coagulation of the drops depends only on their relative velocity [76], although it is easy to see that in the case of drops of comparable dimensions, the air velocity fields near the drops depend on the drop velocity relative to the air, and not on the relative velocity of the drops.

Not being able to account for the interaction of the aerodynamic fields of both drops,* we consider it rational to carry out the calculations for cases when one drop is much smaller than the other, and assume at the same time that the aerodynamic field of the small drop does not influence the field of the large drop. Then because of the smallness of the Reynolds number corresponding to the rates of fall of cloud drops and the smallness of the ratio d/D we can assume for the aerodynamic force the expression which is determined by the Stokes law.

In the chosen system of coordinates, the equation of motion of the small particle will then be equation (I.12), where the electrostatic force is

$$F_e = \frac{q_1 q_2}{r^2} f\left(r,\ \varkappa,\ \frac{d}{D}\right) r + q_2 E_e(r) + F_{ep}. \qquad \text{(II.1)}$$

where q_1 and q_2 are the electric charges of the large and the small particle, respectively,
$\varkappa = -\ q_2/q_1$;

---

*Several recent papers [49, 50, 51, 111, 117, 118, 119, 125] indicate the important effect that the hydrodynamic interaction between drops exerts on their coagulation.

E_0 -- external electric field;

F_{ep} is the electrostatic interaction force of the particles, due to polarization of the particles in the external field E_0.

The influence of the remaining aerosol particles, whether large or small, is neglected, since usually the aerosol particle concentration is small and the distances between them exceed by tens of times the diameter of the larger particle. The function $f(r, \varkappa, d/D)$ in equation (II.1) represents a dimensionless correction factor to the Coulomb force q_1q_2/r^2, due to the induced (mirror) forces which become significant when the distance between particles is comparable with their dimensions. The expression for $f(r)$ will be determined below. We merely note at present that when $r \to \infty$ the function $f(r) \to 1$.

We shall henceforth consider various particular cases of the general expression (II.1), since it is very difficult to determine analytically the trajectories of the particles from the general expression (II.1) for the electrostatic force acting on the particle. We shall consider here cases when both particles are charged by like or unlike charges, when one of the particles is not charged, and when the particles move in a homogeneous electric field. Although we shall consider electrostatic coagulation and sedimentation of spherical particles of aerosol (drops), the principal results can be transferred to a certain degree also to particles of irregular shape (including the dynamic form coefficient).

11. COAGULATION OF TWO AEROSOL PARTICLES OF UNLIKE CHARGE

In equation (I.12) for the motion of the aerosol particles, we confine ourselves for F_e to the first term of expression (II.1). Taking as the characteristic length ℓ the radius of the larger particle and as the characteristic velocity the rate of fall of the large particle

we write down equation (I.12) in dimensionless form [23]:

$$k\frac{dv(r)}{dt} + v(r) = u(r) - \frac{kc_1}{\ell}f(r, \varkappa, g_1)\frac{r}{r^3} + g_1G_1, \qquad (II.2)$$

where

$$\sigma_1 = -\frac{12q_1q_2}{\pi\rho_p d^3 D u_\infty^2}; \quad g_1 = \frac{\rho_p d^2 g}{18\eta u_\infty} = \frac{d^2}{D^2}. \qquad \text{(II.3)}$$

The dimensionless criterion σ_1 characterizes the ratio of the electrostatic force of attraction of the two particles to the inertial forces acting on the small particles. It is obvious that when $\sigma_1 \gg 1$ we can neglect in the equation of motion (II.1) the inertia term $k\frac{dV}{dt}$, and when $\sigma_1 \ll 1$ we can neglect the electrostatic interaction. In particular, for large values of D (and consequently also for large values of $u_\infty = \frac{\rho_p D^2 g}{18\eta}$) the quantity σ_1 will be small. This means that one can expect the electrostatic forces to influence the coagulation of charged particles of the aerosol only in the case when these particles are relatively small (see Section 15). It is obvious that equations (II.2) and (II.3) are applicable also for the investigation of the sedimentation of charged particles from the stream on a charged spherical collector, if u_∞ is taken to mean the velocity of the stream in coming on the collector at infinity, and if g_1 is set equal to zero (the force of gravity is neglected).

To investigate the dependence of the capture coefficient E on the parameters of the phenomenon, let us consider first the case when $\sigma_1 \gg 1$. In this case we can neglect the equation of motion of the particles (II.2) the inertial term, which assumes the form

$$v = u - k\sigma_1 f(r, \varkappa, g_1)\frac{r}{r^3} + g_1 G_1. \qquad \text{(II.4)}$$

In spherical coordinates r, θ (see Fig. 35), equation (II.4) can be rewritten as

$$v_r = u_r - \frac{\alpha}{r^2} f(r) - g_1 \cos\theta, \quad v_\theta = u_\theta + g_1 \sin\theta, \qquad \text{(II.5)}$$

where

$$\alpha = k\sigma_1 = -\frac{4q_1q_2}{3\pi\eta d D^2 u_\infty}.$$

The coefficient $\alpha > 0$ if the particles have opposite

charges, and $\alpha < 0$ if the charges are of the same sign.

By virtue of the incompressibility of the air at the velocities of motion and counted in our problem, we have div u = 0. The last equation together with the axial symmetry of the problem causes the existence of a current function $\psi(r, \theta)$ for the velocity field u such that

$$u_r = \frac{1}{r^2 \sin\theta} \cdot \frac{\partial \psi}{\partial \theta}; \quad u_\theta = -\frac{1}{r \sin\theta} \cdot \frac{\partial \psi}{\partial r}. \qquad \text{(II.6)}$$

Equations (II.5) and (II.6) yield an equation for the trajectories of the aerosol particles in the form [23]

$$\frac{dr}{r d\theta} = \frac{v_r}{v_\theta} = \frac{\frac{1}{r^2 \sin\theta} \frac{\partial \psi}{\partial \theta} - \frac{\alpha}{r^2} f(r) - g_1 \cos\theta}{-\frac{1}{r \sin\theta} \frac{\partial \psi}{\partial r} + g_1 \sin\theta} \qquad \text{(II.7)}$$

or
$$d\psi_1 = \alpha f(r) \sin\theta \, d\theta; \qquad \text{(II.8)}$$

where
$$\psi_1 = \psi - \frac{g_1 r^2 \sin^2\theta}{2}. \qquad \text{(II.9)}$$

Inasmuch as the run of number is small also for the large particles, we can assume that the velocity field u(r) is described by a Stokes flow around a sphere. This means that

$$\psi = \frac{\sin^2\theta}{2}\left(r^2 - \frac{3}{2}r + \frac{1}{2r}\right) = \frac{\sin^2\theta}{2} F(r). \qquad \text{(II.10)}$$

In this case equation (9) assumes the form

$$\psi_1 = \frac{\sin^2\theta}{2} F_1(r), \quad F_1(r) = (1 - g_1) r^2 - \frac{3}{2} r + \frac{1}{2r}. \qquad \text{(II.11)}$$

For the case when the induction forces can be neglected [f(r) = 1],* equation (II.8) can be integrated in final form and the particle trajectories are described by the following equation (we consider trajectories in the

---

*This case corresponds to sufficiently large values of α, when the limiting trajectory is located far away from the large particle and in its calculation one can neglect the mirror forces.

meridional section yoz)*

$$F_1(r) = \frac{y_\pi^2(1-g_1) - 4\alpha\cos^2\frac{\theta}{2}}{\sin^2\theta}, \qquad \text{(II.12)}$$

where y_π is the value of the coordinate y of the trajectory when $\theta = \pi$ (i.e., when $z = -\infty$).

We note that equation (II.4) has a solution in explicit form

$$\psi - \frac{g_1 r^2 \sin^2\theta}{2} - \alpha\omega(r, \theta) = \text{const} \qquad \text{(II.13)}$$

for any velocity field u(r) having a stream function ψ and for any interruption force $\alpha F(r, \theta)$ for which div F = 0. This follows from the fact that equation (II.4) leads in this case to the equality div v = 0. From the solenoidal nature of the field v it follows that there exists for it a current function which represents the sum of the current functions of the components of equation (II.4) (by virtue of the linearity of the operation (II.6)). The existence of a stream function for the field v leads in turn to equation (II.13). To separate from the family of trajectories (II.12) the limiting trajectory, a qualitative investigation was made of the system of differential equation (II.5) (see Appendix III). Figure 36 shows qualitative patterns of the trajectories of equations (II.5). At small values of α (Fig. 36a) there are seven singular points (the four saddles A_1, A_2, A_3, and A_4 on the Oz axis, the dipole at the origin, and two points A_5 of the center type away from the axis). At large values of α (Fig. 36b) only three axial singular points are left, A_1, A_2, and O. These figures show that the separatrices passing through the saddle A_1 are limiting trajectories which separate the trajectories into two classes: trajectories which terminate inside the sphere r = 1, and trajectories bypassing the sphere r = 1 and go into infinity ($r = +\infty$). A proof of this statement is contained in Appendix III.

---

*Equation (II.12) is valid for any form of the current function $\psi(r, \theta)$ for an air stream flowing around a sphere, since we always have at infinity ($r \to \infty$, $\theta \to \pi$; $z \to -\infty$) that the function

$$\psi - \frac{r^2\sin^2\theta}{2} = \frac{y_\pi^2}{2}.$$

The value of the coordinate y when $z = -\infty$ ($y = y_\pi$) for this separatrix BA_1 determines the cross section of the current tube of the trajectories that terminate on the sphere. The sought-for coefficients for the capture of small particles by the large particles is $E = y_\pi^2$.

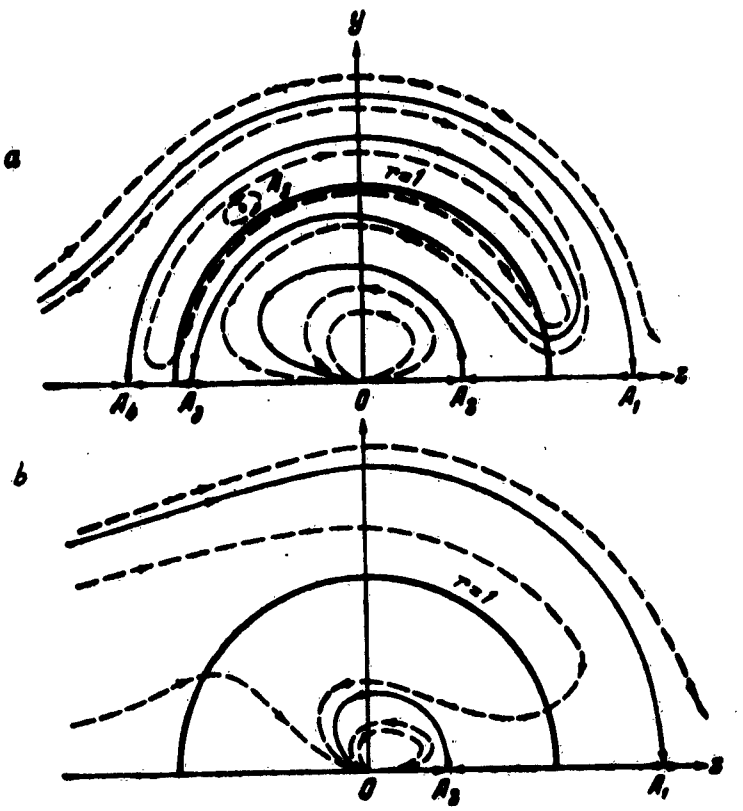

Fig. 36. Qualitative pattern of trajectories of equations of motion (I.5), which determine the electrostatic coagulation of oppositely charged aerosol particles:

a--when $\varepsilon < \frac{3}{4}\cdot\frac{r_c^2-1}{r_c}$; b--when $\varepsilon > \frac{3}{4}\cdot\frac{r_c^2-1}{r_c}$.

The value of y_π for the separatrix BA_1 can be readily obtained from equation (II.12), it it is recognized

that on this separatrix the radius vector r will have a finite value $r = OA_1 = r_0$ when $\theta = 0$. According to equation (II.12), the last circumstance is valid only when the numerator of the right half of equation (II.12) is equal to zero for $\theta = 0$; consequently,*

$$E = y_*^2 = \frac{4\kappa}{1-\varepsilon_1}. \qquad \text{(II.14)}$$

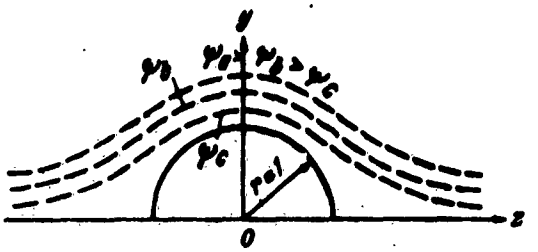

Fig. 37. Current lines of air flowing around a sphere.

Formula (II.14) is valid not only for the case of Stokes flow around a large particle, but also for almost any flow around a sphere by a stream of incompressible liquid, if at the same time there are no backward flows ($u_\theta \leq 0$) and the velocity along the Oz axis behind the sphere increases monotonically ($\frac{\partial u_r}{\partial r} > 0$ when $r > 1$ and $\theta = 0$) [26, 28, 36]. Indeed, as a result of the incompressibility of the liquid (div u = 0) there exists a current function $\psi(r, \theta)$ which vanishes on the axis of motion and on the sphere. Outside the sphere ($r > 1$) the character of the current lines and the variation of the function $\psi(r, \theta)$

---

*This formula was first obtained by us in 1953 [23]. Formula (II.14) can be obtained also by a simpler method (see Section 16). However, the procedure for finding the capture coefficient with the aid of a qualitative investigation of the differential equations of motion and using equation (II.8) turned out to be fruitful for many cases when the method of Section 16 cannot be employed (account of the induction forces, case of drops with like charges, coagulation of drops in an external electric field, account of the coupling coefficient, etc...). We therefore leave here the proof of formula (II.14) obtained above.

are shown in Figure 37.

If one moves along a certain radius (θ = const), then current lines will be crossed, corresponding to monotonically increasing values of the stream function ψ, for in this case $d\psi = -r \sin\theta\, u_\theta\, dr > 0$ (II.6). When $r \to \infty$ the function ψ will tend to a value $\frac{r^2 \sin^2\theta}{2}$. It follows therefore that the current lines corresponding to the stream function

$$\psi_1 = \psi - \frac{g_1 r^2 \sin^2\theta}{2},$$

will have the same structure as the lines ψ = const but only not outside the sphere r = 1, but outside some closed surface on which $\psi = \frac{1}{2} g_1 r^2 \sin^2\theta$, i.e., on which $\psi_1 = 0$. The latter circumstance follows from the fact that the two monotonically increasing functions of the radius vector $\psi(r)$ and $\frac{1}{2} g_1 r^2 \sin^2\theta$ (for θ = const) will be equal at one and only one point, which has $r > 1$, for when $r = 1$ the function $\psi = 0$, $\frac{1}{2} g_1 r^2 \sin^2\theta \geqslant 0$, and when $r \to \infty$ the function $\psi \to \frac{1}{2} r^2 \sin^2\theta > \frac{1}{2} g_1 r^2 \sin^2\theta$.

Let us consider now for this case the aggregate of singular points on the Oz axis. By virtue of the axial symmetry of the problem, the function $\psi(r, \theta)$ near the axis of motion ($\theta \to 0$) can be represented in the form

$$\psi(r, \theta) = \frac{\theta^2}{2!} p(r) + \frac{\theta^4}{4!} s(r) + \ldots \qquad \text{(II.15)}$$

Therefore

$$u_r = \frac{1}{r^2 \sin\theta} \frac{\partial \psi}{\partial \theta} = \frac{p(r)}{r^2} + O(\theta^2),$$

$$u_\theta = -\frac{1}{r \sin\theta} \frac{\partial \psi}{\partial r} = -\frac{\theta p'(r)}{2r} + O(\theta^3) \qquad \text{(II.16)}$$

and consequently

$$v_r = \frac{p_1(r) - 2}{r^2} + O(\theta^2),$$

$$v_\theta = -\frac{\theta p_1'(r)}{2r} + O(\theta^3), \qquad \text{(II.17)}$$

where

$$p_1(r) = p(r) - g_1 r^2. \qquad \text{(II.18)}$$

The stream line $\psi_1 = 0$, as was already determined above, consists of the Oz axis and a closed surface crossing the Oz axis at the point $z = r_2$, where r_2 is given by the root of the equation $p_1(r) = 0$; $r_2 > 1$. Since u_r is a monotonically increasing positive function of r when $\theta = 0$, the function $p/r^2 - g_1$ when $r > r_2$ is likewise of the same kind, by virtue of equation (II.16), and consequently also the function $p_1 = p - g_1 r^2$ (being the product of two positive monotonically increasing functions). Therefore the equation $p_1(r) = \alpha$ has one and only one solution $r = r_0 > r_2$. Consequently, on the Oz axis there is one and only one singular point A_1 outside the surface $\psi_1 = 0$ (when $\theta = 0$).

Let us determine the character of this singular point (see Appendix III). Elementary calculations with the aid of formula (II.17) show that at this point we have

$$\frac{\partial v_r}{\partial r} = a = \frac{1}{r^3}\frac{dp_1(r)}{dr} = -2d = -2\frac{1}{r}\frac{\partial v_\theta}{\partial \theta},$$

$$\frac{1}{r}\frac{\partial v_r}{\partial \theta} = b = 0 \qquad \frac{\partial v_\theta}{\partial r} = c = 0, \qquad q = \begin{vmatrix} a & b \\ c & d \end{vmatrix} = -\frac{a^2}{2} < 0$$

Consequently, as in the case analyzed in Appendix III of a Stokes flow around a sphere, this point will be a singular point of the saddle type. The separatrices in this point, as before, will pass along the Oz axis and perpendicular to the axis. The sign of v_θ in the vicinity of point A_1 will, on the basis of formula (II.17), be opposite that of dp_1/dr, thus, it will be negative. The separatrix emerging from this point satisfies the equation (II.8) [$f(r) = 1$]. Therefore, following this separatrix from A_1 towards increasing values of θ we shall get to ever increasing values of ψ_1; consequently, in this case r will always be larger than $r_0 > r_2 > 1$ and the separatrix will not cross the surface of the sphere anywhere. When

$z = -\infty$ it will pass at a finite distance $y = y_\pi$ from the motion axis. Therefore the investigated separatrix is the limiting trajectory of our problem.

By virtue of formula (II.8), the equation of the trajectory has the form

$$\psi_1 = \psi_{1,\pi} - a(1 + \cos\theta) = \frac{1}{2} y_\pi^2 (1 - g_1) - 2a\cos^2\frac{\theta}{2}. \quad \text{(II.19)}$$

Near the axis ($\theta \to 0$) the equation of the separatrix assumes by virtue of formula (II.15) the form

$$\frac{\theta^2}{2} \rho_1(r) = \frac{1}{2} y_\pi^2 (1 - g_1) - 2a\cos^2\frac{\theta}{2}. \quad \text{(II.20)}$$

Inasmuch as when $\theta = 0$ the separatrix passes through the point $r = r_0 > 1$, equation (II.14) will follow directly from formula (II.20).

From the arguments presented it follows that expression (II.14) for the capture coefficient will be valid also for laminar flow around a sphere without detachment of vortices, and in particular for a potential and axial flow around a sphere [26].

We call attention to certain limitations on the applicability of formula (II.14). It obviously will be satisfied if the distance from the vertex A_1 of the limit line to the center of large particles exceeds some of the radii of both particles ($r_0 > 1 + \sqrt{g_1}$).

In the opposite case, the small particle, the center of which moves along the separatrix BA_1, will be tangent to the large drop at some nonvanishing value $\theta = \theta_1$. From the aggregate of trajectories lying above the separatrix BA_1, there will be one tangent the sphere with radius $1 + \sqrt{g_1}$ when $\theta = \theta_0 < \theta_1$. It will represent in this case ($r_0 < 1 + \sqrt{g_1}$) the limiting trajectory and will determine the value of the capture coefficient. This circumstance can play a noticeable role for a potential stream near the large sphere. For the viscous stream of interest to us at present, flowing near the large particle, this circumstance is significant. On the basis of the equation $\alpha = F_1(r_0)$, which determines r_0 [see formula (p. 43) of Appendix III],

it is easy to show for a viscous stream that $r_0 > 1 + \sqrt{g_1}$ for any value of α, if $g_1 > 0.02$. When $g_1 > 0.02$ the relation $r_0 < 1 + \sqrt{g_1}$ is satisfied if $\alpha < 0.0025$, and consequently $E < 0.01$. Therefore, in the case of a viscous stream formula (II.14) is valid for all values of the capture coefficient $E > 0.01$ which are of practical interest.

Let us consider now the effect of induction (image) forces on the motion of a particle, the value of which forces can be appreciable as the particles come close together. As is known from electrostatics, the interaction force between two conductors* which carry charges is given by the expression

$$F_e = -\frac{1}{2}\left(\frac{ds_{11}}{dr_1}q_1^2 + 2\frac{ds_{12}}{dr_1}q_1q_2 + \frac{ds_{22}}{dr_1}q_2^2\right), \qquad \text{(II.21)}$$

where s_{ik} are the potential coefficients which determine the connection between the potentials (V_1 and V_2) and the charges of the conductors, in accordance with the equations

$$\left.\begin{aligned} V_1 &= s_{11}q_1 + s_{12}q_2 \\ V_2 &= s_{12}q_1 + s_{22}q_2 \end{aligned}\right\} \qquad \text{(II.21a)}$$

To determine the functions s_{ik} and their derivatives in the case of two charged spheres, the image method is usually employed. This method is based on the fact that a point charge q, located at distance r_1 from the center of a spherical conductor of radius R, and its "image in the sphere," i.e., the charge $q' = -Rq/r$ located at the distance R^2/r_1 from the center of the sphere (Fig. 38) produce an electric field of which the surface of the sphere is an equipotential line. Therefore, in order to obtain,

---

*We can consider cloud drops and the majority of the aerosol particles as conductors, since the have considerable conductivity. Thus, for example, in distilled water the conductivity is $\sigma \approx 2 \times 10^{-4}$ 1/ohm-meter, which corresponds to a relaxation time of the medium $\tau = \epsilon/\sigma \approx$ $\approx 3.6 \times 10^{-6}$ sec [59]. Thus, when the configuration of the drops changes, the equilibrium distribution of the charges on their surfaces is established within a time interval $\sim 10^{-5}$ second.

for example, the interaction between a point charge q and a sphere having a charge Q, two fictitious charges are located inside the sphere: q', which together with Q makes the surface of the sphere equipotential, and the charge (-q'), located at the center of the sphere, so that the total charge of the sphere is Q + q' + (-q') = Q. The force acting on the point charge q is

$$F_e = (Q - q')\frac{qr_1}{r_1^3} + \frac{qq'r_1}{r_1\left(r_1 - \frac{R^2}{r_1}\right)^2} =$$

$$= \frac{Qqr_1}{r_1^3} - \frac{q^2R^2(2r_1^2 - R^2)r_1}{r_1^4(r_1^2 - R^2)^2}. \qquad \text{(II.22)}$$

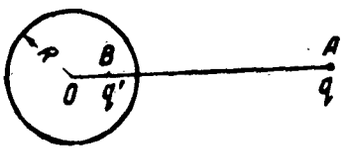

Fig. 38. "Image" of point-like charge in a sphere

$$q' = -q\frac{R}{r_1}; \quad OB = \frac{R^2}{r_1}.$$

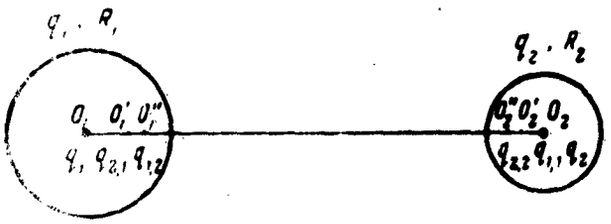

Fig. 39. System of "images" for two charged spheres.

It follows from equation (II.22) that at a large distance ($r_1 \gg R$) the charge q is acted upon by a force which is practically equal to the Coulomb force. At small distances ($\frac{r_1 - R}{R} \ll 1$), the induction term of equation

(II.22) can play an appreciable role and may even exceed in absolute magnitude the Coulomb force. Since the induction term of equation (II.22) always corresponds to a traction force, it follows from this, in particular, that at sufficiently small values of $(r_1 - R)$ the charges will attract each other even if they have the same polarities.

The interaction of two charged spheres having radii R_1 and R_2 and charges q_1 and q_2 can be obtained by considering two infinite rows of charges, consisting of charges $q_1(q_2)$ and their successive images in the spheres: $q_{1,1}(q_{2,1})$ [image of charge $q_1(q_2)$ in sphere 2(1), Fig. 39], $q_{1,2}(q_{2,2})$[image of charge $q_{1,1}(q_{2,1})$ in sphere 1(2), etc]*. The interaction forces can be represented in this case in the form of an infinite series, each term of which corresponds to charges obtained in the n-th successive image. For example, when we confine ourselves to one image (charges q_1, $q_{2,1}$, $-q_{2,1}$ on sphere 1 and charges q_2, $q_{1,1}$, $-q_{1,1}$ on sphere 2) the force F_e can be represented as follows:

$$F_{er} = \frac{q_1 q_2}{r^2} + \left\{ -\frac{q_1^2 R_2^3 (2r_1^2 - R_2^2)}{r_1^3 (r_1^2 - R_2^2)^2} - \frac{q_2^2 R_1^3 (2r_1^2 - R_1^2)}{r_1^3 (r_1^2 - R_1^2)^2} + \right.$$

$$\left. + q_1 q_2 R_1 R_2 \left[\frac{1}{r_1^2} + \frac{1}{(r_1^2 - R_1^2 - R_2^2)^2} - \frac{1}{(r_1^2 - R_2^2)^2} - \frac{1}{(r_1^2 - R_1^2)^2} \right] \right\}. \quad \text{(II.23)}$$

In equation (II.23) are represented the first two terms of the aforementioned infinite series. The first of them represents the Coulomb force, and the second (in the

---

*The system of images for two charged spheres is:

1st

$$q_1 \to q_{1,1}(O_2'); \quad -q_{1,1}(O_2); \quad q_2 \to q_{2,1}(O_1'); \quad -q_{2,1}(O_1);$$

2nd

$$q_{1,1} \to q_{1,2}(O_1'); \quad -q_{1,2}(O_1); \quad -q_{2,1} \to q'_{2,2}(O_2'); \quad -q'_{2,2}(O_2);$$

$$q_{2,1} \to q_{2,2}(O_2'); \quad -q_{2,2}(O_2); \quad -q_{2,1} \to q'_{2,2}(O_2'); \quad -q'_{2,2}(O_2).$$

In this case

$$O_1O_2 = r_1; \quad O_1O_1' = \frac{R_1^2}{r_1}; \quad O_2O_2' = \frac{R_2^2}{r_1}; \quad O_1O_1' = \frac{r_1 R_1^2}{r_1^2 - R_2^2}; \quad O_2O_2' = \frac{r_1 R_2^2}{r_1^2 - R_2^2}.$$

braces) the interaction between the fictitious charges of the first image with each other (the third term in the braces) and with charges q_1 (first term) and q_2 (second term in the braces). The term in the braces can be represented in the form of an interaction of the quasi-dipoles $q_{1.1}$; $-q_{1.1}$ and $q_{2.1}$; $-q_{2.1}$ with each other and the charges q_1 and q_2. In the next terms of this series, an interaction appears, connected with the quasi-quadrupoles $q_{2.2}$; $-q_{2.2}$, $q'_{2.2}$; $-q'_{2.2}$ and $q_{1.2}$; $-q_{1.2}$; $q'_{1.2}$; $-q'_{1.2}$ (see Fig. 39), and also with the quasi-multipoles of higher order. The infinite series which are obtained in the general case from such calculations converge well at large values of r_1 and converge poorly when $r_1 \approx R_1 + R_2$. We shall give later on the results of the calculations for some particular assumptions concerning the ratio of the charges q_1 and q_2.

Let us proceed now to a determination of the trajectories, particularly the limiting trajectory. Introducing the notation $\varkappa = -q_2/q_1$, we can represent F_e, in accordance with formula (II.21), in dimensionless coordinates

$$F_e = \frac{q_1 q_2}{l^2} f(r, \varkappa, g_1) \frac{r}{r^3}, \tag{II.24}$$

where

$$f(r, \varkappa, g_1) = 1 + l_1(r, g_1) + \varkappa l_2(r, g_1) + \\ + \frac{g_1^{3/2}}{\varkappa} l_3(r, g_1) = 1 + L(r, \varkappa, g_1). \tag{II.25}$$

Taking formula (II.23) into account, we can write for the functions l_i

$$\left.\begin{aligned} l_1(r, g_1) &= r^3 \sqrt{g_1}\left[\frac{1}{r^3} + \frac{1}{(r^3-1-g_1)^3} - \frac{1}{(r^3-1)^3} - \right. \\ &\qquad \left. - \frac{1}{(r^3-g_1)^3}\right] + \cdots \\ l_2(r, g_1) &= \frac{2r^3-1}{r(r^3-1)^3} + \cdots \\ l_3(r, g_1) &= \frac{2r^3-g_1}{r(r^3-g_1)^3} + \cdots \end{aligned}\right\} \tag{II.26}$$

In formula (II.26) are shown only the first terms corresponding to the first images of the charges and the

spheres. As $r \to \infty$, the function is

$$l_1(r) \approx \frac{6g_1^{3/2}}{r^6} + O\frac{1}{r^8},$$

and

$$l_2(r) \approx l_3(r) \approx \frac{2}{r^3} + O\left(\frac{1}{r^6}\right).$$

It is obvious that as $r \to \infty$ all the l_1, and consequently also L, tend to zero and $f(r) \to 1$. If the drops have opposite charges, then $\varkappa > 0$ and $f(r)$ has for $r \geqslant 1 + \sqrt{g_1}$* the form shown in Figure 40. In Appendix IV we analyse in detail an exact method of calculating the functions $l_1(r, g_1)$, and give a table of values of $l_1(r)$ and $l_2(r)$ for $g_1 = 0.01$ (d = 0.1D) and $g_1 = 0.04$ (d = 0.2D). It is also shown there that when the distances between the surfaces of the drops exceed the radius of the small drops we can assume accurate to 8 percent

$$f(r) = 1 + \varkappa \frac{2r^3 - 1}{r(r^3 - 1)^2}. \qquad \text{(II.25a)}$$

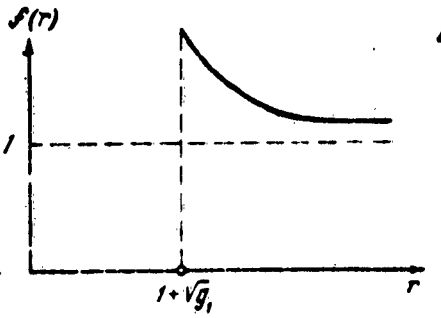

Fig. 40. Appearance of the function f(r).

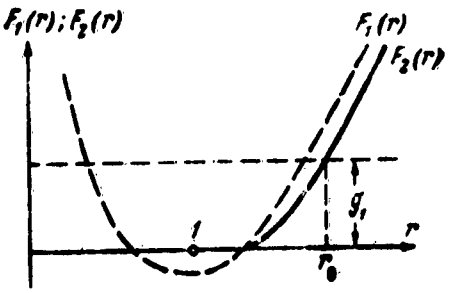

Fig. 41. Appearance of the functions $F_1(r)$ and $F_2(r)$.

Thus, in taking into account the induction forces, if it is possible to neglect the inertial forces (σ_1 is large), we obtain the equation of motion of the particles (II.4) where f(r) is specified by equation (II.25) and

---

*Obviously, the values $r < 1 + \sqrt{g_1}$ are of no physical interest, since $r = 1 + \sqrt{g_1}$ corresponds to spheres in contact.

(II.26). Consequently, in the case under consideration equation (II.8) is also valid, but it is not integrated in this case in final form (div $F_e \neq 0$). However, it is possible to obtain here, likewise, a sufficiently exact and convenient method for calculating the coefficient. For this purpose we consider first the system of the singular points of equations (II.5) with allowance for relation (II.25). As before, we can readily establish that the singular points on the Oz axis have ordinates that satisfy the following equations

$$\alpha = F_2(r) = \frac{F_1(r)}{f(r)}, \quad \text{if} \quad z > 0,$$

$$\alpha = -F_2(r) = -\frac{F_1(r)}{f(r)}, \quad \text{if} \quad z < 0.$$

Inasmuch as when $r > 1 + \sqrt{g_1}$ we have $f(r) > 1$, then $F_2(r)$ has the form shown in Figure 41. Thus, the singular point A_1, which has an ordinate $z = r_0 > 1$, has shifted to the right on the Oz axis as a result of allowing for the induction forces. Repeating the arguments made in page 110 we can show that this singular point will be of the saddle type and that the character of motion in its vicinity will be the same as in the case when the induction forces are neglected. The separatrix emerging from this point will satisfy equation (II.8), and consequently by following this separatrix from the point A_1 we shall proceed to ever increasing values of ψ_1 and r. Thus, this separatrix will be the limiting trajectory and in order to obtain the value of the capture coefficient it is sufficient to find for this separatrix the value

$$\psi_{1,\pi} = \frac{1}{2} y_z^2 (1 - g_1) = \frac{1}{2} E (1 - g_1).$$

But it follows from (II.8) and (II.25) that

$$\psi_{1,\pi} = \alpha \int_0^{\pi} f(r) \sin\theta \, d\theta = 2\alpha + \alpha \int_0^{\pi} L(r) \sin\theta \, d\theta. \qquad \text{(II.27)}$$

Integrating by parts and taking into account the fact that L(r) and its derivatives with respect to θ vanish as $r \to \infty$, we obtain the expression

$$\int_0^{\pi} L(r)\sin\theta\,d\theta = -L(r)\cos\theta\Big|_0^{\pi} + \int_0^{\pi}\frac{dL(r)}{d\theta}\cos\theta\,d\theta =$$

$$= L(r_0) + \int_0^{\pi}\frac{dL(r)}{d\theta}\,d(\sin\theta) = \ldots =$$

$$\left[L(r) - \frac{d^2L(r)}{d\theta^2} + \frac{d^{(IV)}L(r)}{d\theta^4} - \ldots\right]_{r=r_0}.$$

The series obtained converges poorly, but calculations show that in first approximation we can confine ourselves to the first term of the series, and then introduce a correction factor k_1, which obviously depends on r_0. We thus obtain (26, 28, 36]*

$$\frac{E(1-g_1)}{2} = \psi_{1,\pi} = 2\alpha\left[1 + \frac{1}{2}L(r_0)k_1(r_0)\right]. \qquad \text{(II.28)}$$

Calculations carried out for certain particular values of $\varkappa$ show that the correction factor $k_1(r_0)$ changes little with variation of r_0, and is close to unity.

Thus, formula (II.28) shows that calculations of the capture coefficient for electrically charged aerosol particles reduces in the case of large values of σ_1 to a determination of the values of r_0 from the equation $\alpha = F_2(r_0)$, the function $L(r_0)$ and the correction factor $k_1(r_0)$. In addition, it follows from formula (II.28) that an account of the induction forces leads to a larger value of E than calculation with account of the Coulomb forces only.

To obtain the capture coefficient in the case when one of the particles is not charged, it is sufficient to put in (II.28) either $q_1 = 0$ (the large particle is neutral) or $q_2 = 0$ (the small particle is neutral). We

*The fact that $\psi_{1,\pi}$ is a function of r_0 follows directly from equation (II.27), which after change of variables assumes the form

$$\psi_{1,\pi} = F_2(r_0)\int_{r_0}^{\infty} f(r)\,d[\cos\theta(r, r_0)].$$

then obtain [26, 28, 36] the expressions

$$\text{I)}\ q_1 = 0;\ E(1-g_1) = 2\beta I_2(r_0)k_2(r_0);\ \beta = \alpha x;$$

$$\sigma_2 = \frac{\beta}{k} = \frac{12q_2^2}{\pi\rho_p d^3 D u_\infty^2};\quad \beta = \frac{4q_2^2}{3\pi\eta d D^2 u_\infty}; \tag{II.29}$$

$$\text{II)}\ q_2 = 0;\ E(1-g_1) = 2\beta_1 I_3(r_0)k_3(r_0);\ \beta_1 = \frac{\alpha}{\chi}g_1^{3/2};$$

$$\sigma_3 = \frac{\beta_1}{k} = \frac{12q_1^2}{\pi\rho_p D^4 u_\infty^2};\quad \beta_1 = \frac{4q_1^2 d^2}{3\pi\eta D^3 u_\infty}, \tag{II.30}$$

where r_0 is determined from the relations

$$F_1(r_0) = \beta I_2(r_0), \tag{II.31}$$

$$F_1(r_0) = \beta_1 I_3(r_0), \tag{II.32}$$

while $k_2(r_0)$ and $k_3(r_0)$ are the corresponding correction factors.

The values of these coefficients for different values of g_1 are listed in Table 10. The values of $k_2(r_0)$ and $k_3(r_0)$ were determined by numerically integrating equation (II.8) under initial conditions $r = r_0$ with $\theta = 0$. This equation turns out to be highly convenient for the integration and made it possible to determine the limiting trajectory directly.

On the basis of Table 10 and formulas (II.29) and (II.30) we calculated the values of capture coefficient E as a function of the values of the parameters β and β_1. The results of these calculations for $g_1 = 0.01$ are shown in Figure 42.* The same Figure 42 shows by means of a

---

*We note that Table 10, and consequently also the plots of Figure 42, were calculated for values $r_0 > 1 + \sqrt{g_1}$, i.e., for cases when the coupling effect can be neglected. As shown by the plots of Figure 42, we can disregard the coupling effect even at very small values of the capture coefficient $E \approx 0.1$.

dotted line the values of

$$E(\beta) = E(\beta_1) = \left[\frac{15\pi}{4(1-g_1)}\beta\right]^{3/5},$$

calculated for the case of a homogeneous stream flowing around a large drop, and for the simplified form of the functions $l_2(r) = l_3(r) = \frac{2}{r^3}$. Such a problem was solved by Cochet [83]. It is obvious that for large values of E, corresponding to large values of r_0 (or, what is the same, β or β_1), the exact solution obtained by us in consideration of Stokes flow around the larger particle and the more exact value of the functions $l_2(r)$ and $l_3(r)$, set by means of formulas (II.26), must go over into the Cochet solution. An examination of Figure 42 shows that when $E \sim 1$ the exact solution of the problem yields a value of the capture coefficient which is approximately three times smaller than the Cochet solution. When $E \sim 0.1$, this ratio increases to six, and only when $E > 10$ does the ratio of the two solutions become smaller than 1.5.

Table 10

The Coefficients $k_2(r_0)$ and $k_3(r_0)$

r_0	$g_1 = 0{,}01$		$g_1 = 0{,}04$		$g_1 = 0{,}10$	
	k_2	k_3	k_2	k_3	k_2	k_3
1,15	—	1,67	—	—	—	—
1,20	1,23	1,58	—	—	—	—
1,30	1,20	1,46	1,32	1,59	—	—
1,40	1,18	1,38	1,25	1,44	1,60	1,76
1,60	1,14	1,29	1,20	1,32	1,36	1,41
1,80	1,13	1,24	1,17	1,26	1,21	1,30
2,00	1,12	1,21	1,15	1,23	1,17	1,25
2,50	1,10	1,16	1,12	1,17	1,13	1,19
3,00	1,09	1,13	1,10	1,14	1,12	1,18
4,00	1,07	1,10	1,08	1,10	1,08	1,12
5,00	1,06	1,08	1,07	1,08	1,07	1,09
∞	1,02	1,02	1,02	1,02	1,02	1,02

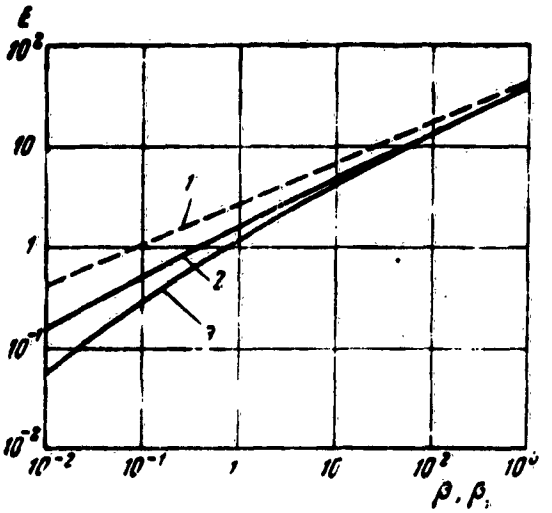

Fig. 42. Dependence of the capture coefficient E on the parameters β and β_1 for cases when one of the aerosol particles is neutral:

1 -- Cochet solution;
2 -- $E(\beta)$; 3 -- $E(\beta_1)$.

In the cases $g_1 = 0.04$ and 0.1, the plots of $E(\beta)$ and $E(\beta_1)$ practically do not differ from the plots of Fig. 42, calculated for $g_1 = 0.01$ for values $\beta > 0.1$ and $\beta_1 > 0.1$. When $\beta < 0.1$ and $\beta_1 < 0.1$ the value of E for $g_1 = 0.04$ and 0.1 is somewhat smaller than shown in Fig. 42.

When the described calculations of the capture coefficient were made and reported to the fifth Intergovernmental Conference on Problems of the Investigation of Clouds, Precipitation, and Thunderstorm Electricity, a paper appeared by Kreamer and Johnstone [101] devoted to precipitation of aerosol particles from a stream on obstacles, under the influence of electrostatic forces. Using the Illiac electronic computer, Kreamer and Johnstone calculated the trajectories of the aerosol particles using equations of motion analogous to (II.4), in which

$$l_3(r) = \frac{2}{r^3} \text{ and } l_2(r) = \frac{2r^3 - 1}{r(r^3 - 1)^2}.$$ *

*The calculations in [101] were made under initial

Comparison of the plots of Figure 42 with Figures 4 and 5 of [101] shows good agreement between the results of the calculations by both methods.

Let us consider now methods for finding the limiting trajectories taking into account the inertial term k dv/dt in equation (II.2). We note first of all that in this case the same position is retained for the singular points of the trajectory family, as considered above. Indeed, equation (II.2) can be represented in the form of a system of differential equations of first order relative to the four unknown functions z, y, v_z, and v_y:

$$\left.\begin{aligned} \frac{dz}{dt} &= v_z;\ k\frac{dv_z}{dt} = u_z - v_z + F_{ez} - g_1, \\ \frac{dy}{dt} &= v_y;\ k\frac{dv_y}{dt} = u_y - v_y + F_{ey}. \end{aligned}\right\} \qquad \text{(II.33)}$$

The aggregate of all the singular points of the system (II.33) is determined by the relations

$$\frac{dz}{dt} = \frac{dv_z}{dt} = \frac{dy}{dt} = \frac{dv_y}{dt} = 0,$$

from which follow directly the equations

$$v_z = 0;\ v_y = 0;\ u_z + F_{ez} - g_1 = 0;\ u_y + F_{ey} = 0,$$

which coincide with the conditions that determine the aggregate of the singular points of the system (II.4).

On this basis we could seek the limiting trajectory by calculating the separatrix that emerges from the point

---

conditions r = 700; $\theta = \pi$. By varying the initial conditions, a set of trajectories was obtained, from among which the computer selected the limiting one. We note here that the procedure developed in the present section, connected with a qualitative analysis of the differential equation (II.4), makes it possible to calculate directly only one limiting trajectory with the aid of equation (II.8). The latter circumstance greatly simplifies the determination of the capture coefficient.

$A_1(z = r_0, y = 0)$,* after first eliminating from the system (II.33) the time t and finding the solution in the vicinity of point A_1 by the method of indeterminate coefficients by expanding the sought functions in Taylor series.

However, specific calculations made by this method have shown that it is necessary to carry out very laborious calculations of a very large number of terms of Taylor series in order to go over into a region where it is convenient to employ ordinary difference methods of numerical integration of the equations. Therefore an estimate of the influence of the inertial term was made by a calculation on the basis of equations (II.33) of a series of trajectories, which have different values of y_π when $z = -\infty$. For large values of y_π these trajectories went to $+\infty$, while for small values of y_π they crossed the surface of the sphere. Usually, by means of a small number of trials in the choice of the value of y_π, it was possible to find two more or less nearly equal values of $y_{\pi,1}$ and $y_{\pi,2}$, of which the first determined a trajectory of the first class and the other a trajectory of the second class. It is clear that the capture coefficient is determined in this case by the value of y_π lying between $y_{\pi,1}$ and $y_{\pi,2}$.

An estimate of the influence of the inertial term of the equation (II.2) was made for several particular values of D, g_1, q_1, and q_2, neglecting induction forces. Table 11 lists the results of these calculations, while Figure 43 shows the calculated trajectories, between which lies the limiting trajectory (the dashed lines on Fig. 43 show the separatrices corresponding to the case when the inertia term is neglected). The calculations performed show that an account of the inertial term decreases the value of the capture coefficient. However, even for $\sigma_1 \approx 0.3$--0.4 this decrease in E does not exceed 10 percent, and only when $\sigma_1 \approx 0.1$ does an appreciable decrease (on the order of 35 percent) of the value of E occur.

---

*If $k < 1/4a$, where a is the derivative with respect to r of the right half of the first equation of the system (II.5) at $\theta = 0$, then the singular point A_1 remains a singular point of the saddle type (see footnote on page 85).

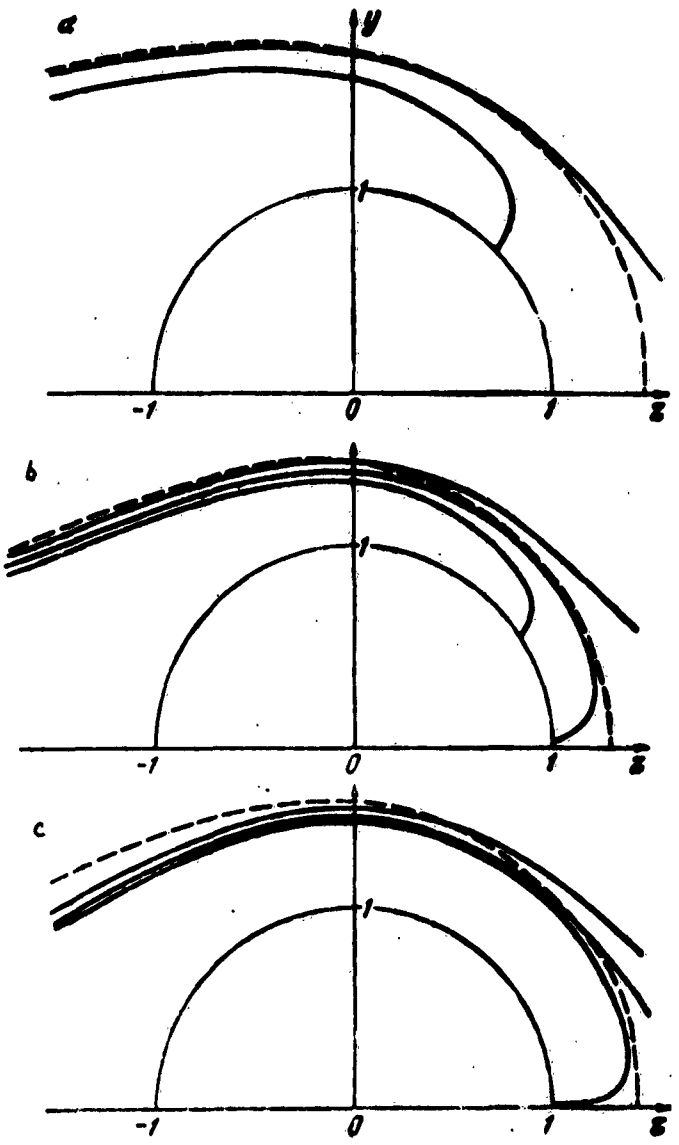

Fig. 43. Results of calculations of the limiting trajectory in the case of electrostatic coagulation of oppositely charged particles (with account of the inertial term of the equation of motion):

a — $D = 20$ μ; $d = 4$ μ; $k = 0{,}084$; $\varepsilon_1 = 3{,}81$;
b — $D = 30$ μ; $d = 6$ μ; $k = 0{,}216$; $\varepsilon_1 = 0{,}334$;
c — $D = 30$ μ; $d = 9{,}5$ μ; $k = 0{,}540$; $\varepsilon_1 = 0{,}134$.

Table 11

D, μ	g_1	k	a	a_1	E	$E = E_0$ by formula (II.14)	$\frac{E}{E_0}$
20	0,04	0,064	0,244	3,81	0,92	1,016	>0,91
30	0,04	0,216	0,0722	0,334	0,270	0,301	0,90
30	0,10	0,540	0,0722	0,134	0,209	0,321	0,65

Remark. It was assumed in the calculation that the absolute value of the charges on the drops is $|q| = 5 \times 10^{-4} d$ electrostatic units.

At small values of the Stokes number k it is possible to estimate the influence of the inertial term of equation (II.2) by the small-parameter method (see Sec. 9). We confine ourselves here to an analysis of a uniform stream around a large particle (the solution of the problem for Stokes flow of a particle leads to very cumbersome although elementary calculations). It is clear that such a formulation of the problem will reflect correctly the nature of the problem at large values of the capture coefficient E, when the limiting trajectory is located far away from the large particle. Using the same methods as in finding c_0/c_∞ in Section 9, and recognizing that for a homogeneous stream $F_1(r) = (1 - g_1)r^2$, we obtain after a series of transformations for the capture coefficient E an expression

$$E = \frac{4a}{1-g_1}\left\{1 - k\frac{0{,}8(1-g_1)^{3/2}}{\sqrt{a}} + \right.$$
$$\left. + k^2(1-g_1)^3\left(\frac{2}{a} - 1{,}084\right) + O(k^3)\right\}. \qquad \text{(II.34)}$$

Formula (II.34) shows that an account of the inertial term in accordance with the results given above of the numerical calculation leads to a certain decrease in the capture coefficient. It must be noted that at small values of a, when it is necessary to take into account the coupling effect and when one cannot make the assumptions under which formula (II.34) is derived, an account of the inertial nature of the particles should increase the capture coefficient.

12. COAGULATION OF AEROSOL PARTICLES WITH LIKE CHARGES

As was noted in Section 11, at small distances between charged particles the absolute magnitude of the induction interaction forces can exceed the Coulomb force. This means that like charged particles can attract at short distances, and consequently, under certain conditions one can expect coagulation of small particles with like charge* [26, 28].

Since the electric interaction force between particles is

$$F_{er} = \frac{q_1 q_2}{l^2 r^2}\left[1 + l_1(r, g_1) + \varkappa l_2(r, g_1) + \frac{g_1^{3/2}}{\varkappa} l_3(r, g_1)\right], \quad \text{(II.25)}$$

the attraction between particles that have like charges ($\varkappa = -q_2/q_1 < 0$) can occur at distances when the expression in the square brackets (equal to $f(r, g_1, \varkappa)$) becomes negative. This condition imposes certain limitations on the quantities $\varkappa$ and g_1. Thus, for example, if the particles are of the same dimensions ($g_1 = 1$) and the charges on them are equal, then even at very small distances between particle surfaces ($r \to 2$) there occurs no attraction force between them (when $r = 2$ a repulsion force is present, amounting to about 60 percent of the Coulomb repulsion force). At small values of g_1 ($d/D = \sqrt{g_1} < 0.2$--0.3), when the function $f(r, g_1, \varkappa)$ is well approximated by the expression

$$f(r, g_1 \varkappa) = 1 + \varkappa l_2(r) \approx 1 - \frac{q_2}{q_1} \cdot \frac{2r^2 - 1}{r(r^2 - 1)^2}, \quad \text{(II.25a)}$$

we see that the region of distances r, corresponding to attraction between particles, will be all the greater, the larger the absolute value $|\varkappa| = q_2/q_1$. Figure 44 shows the form of the function $f(r)$ corresponding to the approximation (II.25a). It is obvious that attraction between particles occurs when $r < r_8$ (we are not considering now

*Large particles of like charge will usually coagulate because for them the inertial forces predominate over the electrostatic forces (see Secs. 14 and 15).

the values $r < 1$; they will be needed later on for a qualitative investigation of the pattern of the trajectories). Table 12 lists the dependence of the coordinate r_8, which separates the regions of repulsion and attraction of the particles, on the quantity $\varkappa = -q_2/q_1$.*

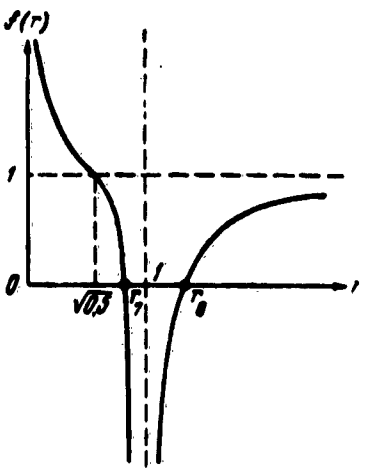

Fig. 44. Form of the function f(r) in accordance with the approximation of equation (I.25a).

Table 12

$-\varkappa = q_2/q_1$	r_8	$-\varkappa = q_2/q_1$	r_8
0,01	1,052	0,5	1,422
0,02	1,075	1	1,617
0,05	1,122	2	1,882
0,1	1,178	5	2,379
0,2	1,260	10	2,895

*The value of r_8 was calculated from the relation

$$l_2(r_8) = \frac{2r_8^2 - 1}{r_8(r_8^2 - 1)^2} = -\frac{1}{\varkappa}.$$

The data of Table 12 show that noticeable regions of attraction occur only at large values of $(-\varkappa) = 0.5$--1.0. Therefore, apparently only at appreciable values of $(-\varkappa)$ can one expect appreciable changes in the capture coefficient E for charged particles of like charges.

To simplify the problem of calculating the capture coefficient, we confine ourselves to a case when the ratio d/D is very small (for example, $g_1 < 0.01$). Then in first approximation we can assume $g_1 = 0$.* In this case the equation of motion of the particle (II.4) assumes the following form:

$$v = u + \alpha_1 [1 - \lambda l_2(r)] \frac{l}{r^2}, \qquad \text{(II.35)}$$

where

$$\lambda = -\varkappa = q_2/q_1 > 0; \quad \alpha_1 = -\alpha = \frac{4q_1q_2}{3\pi\eta dD^2 u_\infty} > 0.$$

For Stokes flow around a large particle, equation (II.35) can be written, taking into account formula (II.10), in the following form:

$$\left.\begin{aligned} v_r &= \frac{\cos\theta F_r + \alpha_1 f(r)}{r^2} \\ v_\theta &= -\frac{\sin\theta F'(r)}{2r} \end{aligned}\right\} \qquad \text{(II.36)}$$

As in Section 11, we can readily obtain the relation

$$d\psi = -\alpha_1 f(r) \sin\theta \, d\theta, \qquad \text{(II.37)}$$

which is analogous to equation (II.8) and is equivalent to equation (II.35). For the case under consideration the function f(r) is shown in Figure 44.** It is easy to see that

---

*In the case when g_1 is small but not equal to zero, the main deductions of the analysis given below should remain in force.

**If $g_1 \neq 0$, then the function f(r) as $r \to 1$ tends to some negative value of large absolute magnitude. This circumstance, however, does not change essentially the conclusions that follow.

$$f(r) \leqslant 0 \text{ FOR } r_7 \leqslant r \leqslant r_8,$$
$$f(r) \geqslant 0 \text{ FOR } r \geqslant r_8 \text{ OR } r \leqslant r_7,$$

where r_7 and r_8 are the roots of the equation

$$I_2(r) = -\frac{1}{\varkappa}. \tag{II.36}$$

Let us consider the singular points of the system (II.36). It is easy to show that they all lie on the Oz axis. The origin is a singular point of higher order. In its vicinity

$$v_r \to \frac{\cos\theta}{2r^3} + \frac{\alpha_1\lambda}{r^3}; \quad v_\theta \to \frac{\sin\theta}{4r^3}.$$

Consequently, the trajectories near the origin satisfy the equation

$$r = C\left(\sin\frac{\theta}{2}\right)^{2+4\alpha_1\lambda}\left(\cos\frac{\theta}{2}\right)^{2-4\alpha_1\lambda}.$$

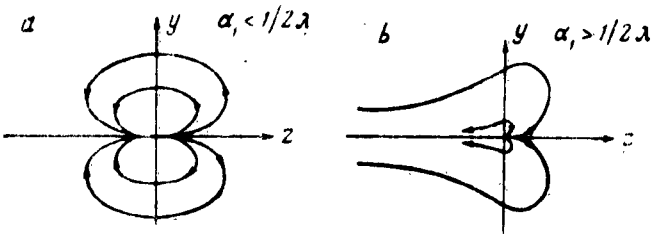

Fig. 45. Form of trajectories of equation of motion (II.36) near the origin.

When $\alpha_1 < 1/2\alpha$ (Fig. 45a), the origin is a singular point of the dipole type, and when $\alpha_1 > 1/2\alpha$ (Fig. 45b) it is an unstable node, from which all the trajectories leave only in the direction of positive z (Fig. 45).*

*In the first case the Poincare index [45] of the origin is I = + 2, while in the second case I = + 1.

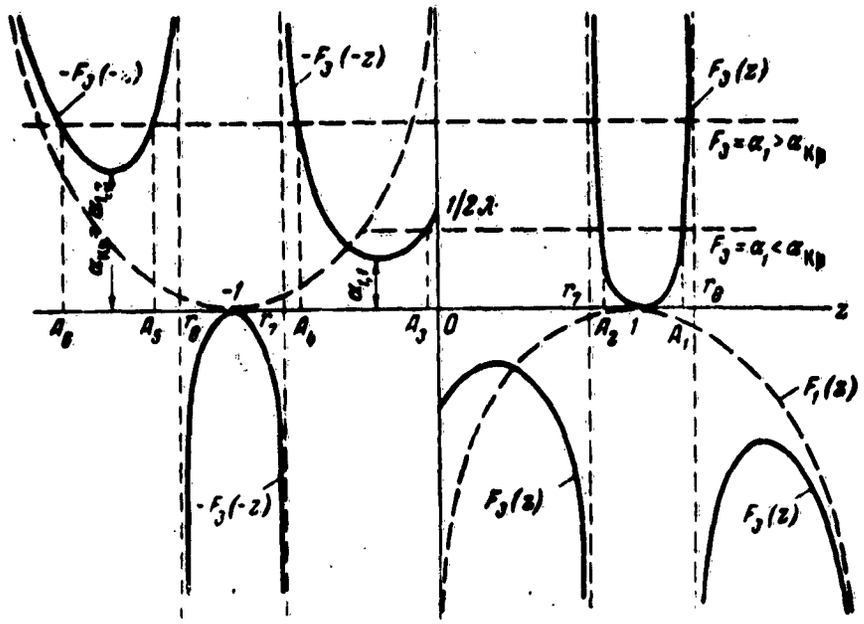

Fig. 46. Form of the function $F_3(r)$, which determines the number and location of the singular points of the equations of motion (II.36).

The remaining axial singular points are determined in accordance with the first equation of (II.36) by the relation $\alpha_1 = -\cos\theta\, F_3(r)$ or

$$\alpha_1 = F_3(r) \quad \text{when} \quad z > 0, \tag{II.38}$$

$$\alpha_1 = -F_3(r) \quad \text{when} \quad z < 0, \tag{II.39}$$

where the function $F_3(r) = -F(r)/f(r)$ has the form shown in Figure 46,* on which is presented a plot of the function

*By determining $F'_3(r)$ in the form of a rational fraction, it is easy to show, using the general rules (the Budan-Fourier theorem [17]) for the determination of the number of positive roots of the polynomial in the numerator, that the curve $F_3(r)$ has two maxima ($\alpha_{1,1}$ for $0 < r < 1$ and $\alpha_{1,2}$ for $r > 1$) and one minimum $F_3 = 0$ for $r = 1$. When $r \to 0$ the function $F_3(r) \to -1/2\lambda$.

$F_3(r)$ for $z > 0$ and of its continuation $-F_3(r)$ for $z < 0$. Figure 46 together with formula (II.38) show that at very small values of $\alpha_1 < \alpha_{1.1}$ there are two singular points A_1 and A_2.* With increasing α_1, singular points A_3 and A_4 appear, followed by A_5 and A_6. When α_1 goes through the value $1/2\lambda_0$ the singular point A_3 disappears and the character of the singularity at the origin changes.

In determining the character of all these singular points we find the values of the functions a, b, c, d [45] at these points, for which one can easily obtain the following expressions:

$$a = \frac{\partial v_r}{\partial r} = -\frac{\cos\theta F_3'(r) f(r)}{r^2}; \quad b = \frac{\partial v_r}{r\partial\theta} = 0;$$

$$c = \frac{\partial v_\theta}{\partial r} = 0; \quad d = \frac{\partial v_\theta}{r\partial\theta} = -\frac{\cos\theta F'(r)}{2r}.$$

Starting from these equations, we can construct the following table for the signs of the different functions at the investigated points**(Table 13).

Table 13

Point	$\frac{\sin\theta}{\cos\theta}$	r	$F'(r)$	$F_3'(r)$	$f(r)$	a	d	$a-d$	$p=-(a+d)$	Character of the point	$\frac{r^2\theta}{\sin\theta}$
A_1	+	$r_1<1<r<r_0$	+	+	−	+	−	−		Saddle	−
A_2	+	$r_1<r<1<r_0$	−	−	−	−	+	−		Saddle	+
A_3	−	$r<r_1<1$	−			+	−	−		Saddle	+
A_4	−	$r<r_1<1$	−	−	+	−	−	+	+	Node (stable)	+
A_5	−	$r>r_0>1$	+	+	+	+	+	+	−	Node (unstable)	−
A_6	−	$r>r_0>1$	+	−	+	−	+	−		Saddle	−

*The coordinates r_A of the singular points are obtained, in accordance with equation (II.38), as the coordinates of the points of intersection of the curve $F_3(z)$; $-F_3(-z)$ with the line $F_3(z) = \alpha_1$. Calculations show that $\alpha_{1.1} < \alpha_{1.2}$.

**To set up the table it must be noted that

Qualitative patterns of the trajectories in the case under consideration are shown in Figure 47. It is seen from Figure 47 that when $\alpha_1 < \alpha_{1,2} = \alpha_{cr}$ there exists a limiting trajectory, which represents a separatrix arriving from $z = -\infty$ at the point A. Consequently, when $\alpha_1 < \alpha_{cr}$ there exists a non-zero value of the capture coefficient E. When $\alpha > \alpha_{cr}$, we have $E = 0$.

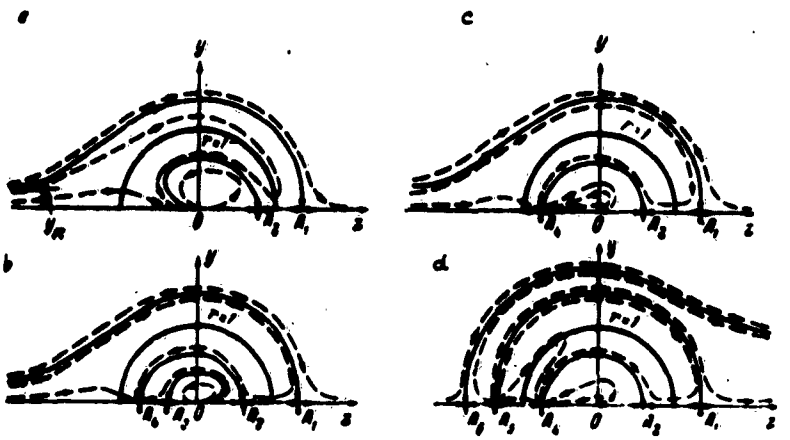

Fig. 47. Qualitative pattern of the trajectories of the equations of motion (II.36), which determine the electrostatic coagulation of aerosol particles of like charges:

$$a - \alpha_1 < \alpha_{1,1};\quad b - \alpha_{1,1} < \alpha_1 < \frac{1}{2\lambda};$$

$$c - \frac{1}{2\lambda} < \alpha_1 < \alpha_{cr};\quad d - \alpha_1 > \alpha_{cr}.$$

Thus, in accordance with the statements made at the beginning of the present section, there exist such relations between the parameters of motion of two particles of like charge ($\alpha_1 < \alpha_{cr}$), for which the drops can coagulate [26,

---

$F'(r) > 0$ for $r > 1$ and $F'(r) < 0$ for $r < 1$; the sign of $v_\theta/\sin\theta$ is opposite the sign for $F'(r)$ while quantity $q = ad - bc < 0$ for points of the saddle type and $q > 0$ for nodes and foci [45]. However, by virtue of the axial symmetry of the problem the points A_4 and A_5 are nodes and not foci.

28, 36].

Table 14 gives the values of α_{cr} as a function of the quantity $\lambda = q_2/q_1$.

Table 14

λ	α_{cr}	α_{cr}/λ
10	15	1,50
5	8,5	1,70
2	3,8	1,90
1,0	1,97	1,97
0,5	0,98	1,96
0,2	0,392	1,96
0,1	0,189	1,89

It follows from Table 14 that the charge of a large particle can increase to a critical value q_{1cr} for which

$$\frac{\alpha_1}{\lambda} = \frac{24q_{1cr}^2}{\pi\rho_p g d D^4} \approx 1{,}5 \div 2{,}0. \qquad \text{(II.40)}$$

If we measure q_1 in terms of elementary charges [e], while D and d are measured in microns, then the relation assumes the form

$$q_{1cr}[e] \approx 3D^3_{\mu}\sqrt{d_{\mu}}. \qquad \text{(II.41)}$$

This means, for example, that

for $D = 10$ μ, $d = 1$ μ: $q_{1cr} \approx 300$ e;

for $D = 20$ μ, $d = 2$ μ: $q_{1cr} \approx 1700$ e;

for $D = 40$ μ, $d = 4$ μ: $q_{1cr} \approx 10\,000$ e;

etc.

Consequently, with such a mechanism of charge accumulation, considerable charges can arise on the particles. Of course, since the capture coefficients for particles of like charge are small for small values of λ, the probability of appearance of such limiting charges is small. How-

ever, for particles with charges of the same order of magnitude, ($\lambda \approx 1$) the value of the capture coefficient E is sufficiently large. This can be seen from Table 15, in which are represented the values of the capture coefficient E for like charge particles and different values of the parameters α_1 and λ. The values of Table 15 were obtained by numerically integrating (II.37), making it possible to determine directly the limiting trajectory after determining the coordinate r_0 of the singular point A_1 from equation (II.38).

Table 15

Capture Coefficients for Aerosol Particles of Like Charges

α_1	$\lambda = 1$	$\lambda = 2$	$\lambda = 5$
0,1	0,32	0,53	0,96
0,333	0,31	0,68	1,42
1	0,10	0,55	1,65

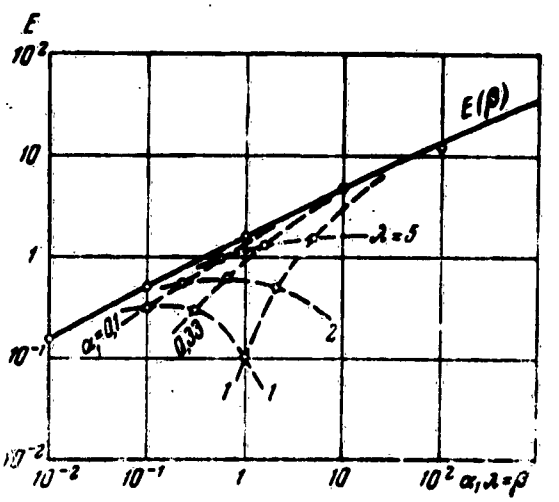

Fig. 48. Dependence of the capture coefficient E for electrostatic coagulation of aerosol particles of like charge on the parameters α_1 and λ.

The data of Table 15 are shown in Figure 48, where the abscissa represents $\beta = \alpha\varkappa = \alpha_1\lambda$. The same figure shows a plot of $E(\beta)$ -- the dependence of the capture coefficient E on the parameter β in the case when the large particle is neutral ($\lambda = q_2/q_1 = \infty$). Obviously, at large values of λ the plots of $E(\alpha_1, \lambda)$ should approach the plot of $E(\beta)$.*

An examination of Table 15 and Figure 48 allows us to advance the hypothesis that coagulation of drops of like charge can play a noticeable role in the process of coagulation of cloud drops (see Sec. 14).

13. INFLUENCE OF EXTERNAL ELECTRIC FIELD ON THE COAGULATION OF AEROSOL PARTICLES

Let us consider the influence of a vertical electric field on gravitational coagulation of particles of coarsely dispersed aerosol. The solution of such a problem can be of interest, in particular, for an estimate of the rate of coagulation of cloud drops in an atmospheric-electricity field.

If the external field E_0 is directed vertically downward (usual direction of atmospheric-electric field), then it polarizes the aerosol particles, producing on them dipoles with moments** $m_1 = D^3E_0/8$ (large particle) and $m_2 = d^3E_0/8$ (small particle), as shown in Figure 49. The electric force of interaction between the aerosol particles can be represented in first approximation as a sum of forces:

---

*It is seen from Figure 48 that when $\alpha_1 = 0.1$ the value of $E(\alpha_1, \lambda)$ is smaller than $E(\beta)$ by 1.5 times even when $\lambda = 1$, and for $\alpha_1 = 1/3$ this takes place at $\lambda = 5$.

**We assume the aerosol particles to be conductors (see footnote on page 114) and we therefore assume that the factor $\frac{\varepsilon - 1}{\varepsilon + 2}$ (where ε is the dielectric constant of the material of the particles), standing in the expression for the moments m_1 and m_2, to be equal to unity.

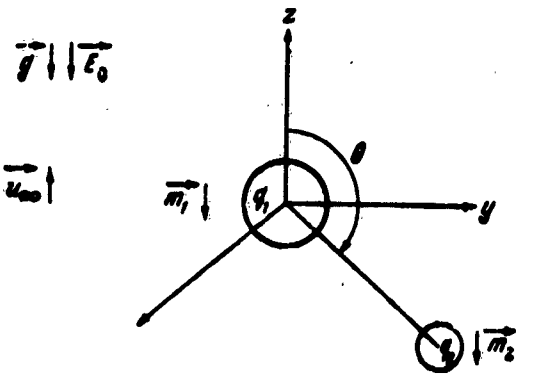

Fig. 49. Coordinate system.

a) Force of interaction of the charges q_1 and q_2 on the particles (see Sec. 11)

$$F_1 = \frac{q_1 q_2}{r_1^3} f(r, \varkappa, g_1) r_1;$$

b) Force of interaction of the charge q_2 with the dipole m_1, the field of which is $E_{m_1} = -\operatorname{grad}\left(\frac{m_1 r_1}{r_1^3}\right)$ [59, page 161]

$$F_2 = \frac{D^3 E_0 q_2}{8} \operatorname{grad}\left(\frac{\cos\theta}{r_1^2}\right);$$

c) Force of interaction of the charge q_1 with the dipole m_2

$$F_3 = -\frac{1}{8} d^3 E_0 q_1 \operatorname{grad}\left(\frac{\cos\theta}{r_1^2}\right);$$

d) Force of interaction of the dipoles m_1 and m_2 [59, page 161]

$$F_4 = \operatorname{grad}(m_2 E_{m_1}) = \frac{1}{64} d^3 D^3 E_0^2 \operatorname{grad}\left(\frac{3\cos^2\theta - 1}{r_1^3}\right).$$

In addition, the small particle will be acted upon by a force $F_5 = q_2 E_0$.

Taking into account the influence of all these electrostatic forces, the gravity forces, and the aerodynamic force, the equation of motion of the small particle in the coordinate system connected with the large particle (Fig. 49) will have the following form (in dimensionless quantities):

$$k\frac{dv}{dt} + v = u - \alpha f(r, \varkappa, g_1)\frac{r}{r^3} + (\delta_1 - \delta_2)\operatorname{grad}\left(\frac{\cos\theta}{r^2}\right) + \\ + \frac{\gamma}{3}\operatorname{grad}\left(\frac{3\cos^2\theta - 1}{r^3}\right) + (\delta_1 + g_1)G_1. \qquad \text{(II.42)}$$

where

$$\alpha = -\frac{4q_1q_2}{3\pi\eta d D^2 u_\infty};\quad \delta_1 = \frac{E_0 q_2}{3\pi\eta d u_\infty};\quad \delta_2 = -\frac{\delta_1 g_1^{3/2}}{\varkappa} = \frac{E_0 q_1 d^2}{3\pi\eta D^3 u_\infty};$$

$$\gamma = \frac{E_0^2 d^3}{4\pi\eta D u_\infty} = \frac{3\delta_1^2 g_1^{3/2}}{\alpha\varkappa};\quad u_\infty = \frac{\rho_\rho D^2 g}{18\eta} + \frac{E_0 q_1}{3\pi\eta D}. \qquad \text{(II.43)}$$

In the case when the Stokes number is small compared with the coefficients α, δ_1, δ_2, and γ, equation (II.42) can, as was done in Section 11, be reduced to a form convenient for integration

$$d\left[\psi - \frac{\delta_1 - \delta_2}{r}\sin^2\theta - \frac{\gamma\sin^2\theta\cos\theta}{r^2} - (\delta_1 + g_1)\frac{r^2\sin^2\theta}{2}\right] = \\ = \alpha f(r, \varkappa, g_1)\sin\theta d\theta. \qquad \text{(II.44)}$$

If we can neglect here the induction forces and put $f(r, \varkappa, g_1) = 1$, then equation (II.44) is integrated in final form and has a solution

$$\psi + \alpha\cos\theta - \frac{\delta_1 - \delta_2}{r}\sin^2\theta - \frac{\gamma\sin^2\theta\cos\theta}{r^2} - \\ - (\delta_1 + g_1)\frac{r^2\sin^2\theta}{2} = \text{const} = \frac{1}{2}v_\infty^2(1 - g_1 - \delta_1) - \alpha. \qquad \text{(II.45)}$$

A determination of the limiting trajectories and of the capture coefficient for the general case described by equations (II.42), (II.44), and (II.45) is made difficult by the numerous combinations of signs and values of the coefficients α, δ_1, δ_2, and γ. We therefore confine ourselves to an examination of some particular cases.

If the charges on the particles are large, and the field E_0 is small, the coefficients δ_1, δ_2, and γ will be

small relative to α and we can neglect the terms of the equation containing these coefficients. In this case the problem reduced to the cases of coagulation of charged particles in the absence of an external field, already considered in Sections 11 and 12. Expressions (II.43) make it possible to estimate the relations

$$\omega_1 = \frac{\delta_1}{\alpha}; \quad \omega_2 = \frac{\delta_2}{\alpha} = -\frac{\omega_1 g_1^{1/3}}{\varkappa}; \quad \omega_3 = \frac{\gamma}{\alpha} = \frac{3\omega_1^2 g_1^{1/3}}{\varkappa}. \qquad \text{(II.46)}$$

A. If the large particle has a very small charge and the induction forces due to the charge of the small particle can be neglected, then the coefficients α, δ_2, and γ will be very small. Then the trajectories of the small particle, in accordance with formula (II.45), will have the form*

$$\frac{\sin^2\theta}{2}\left[F_1(r) - \delta_1\frac{2+r^3}{r}\right] = \text{const.} \qquad \text{(II.47)}$$

It follows from (II.47) that the trajectories of the particles are symmetrical relative to the plane $\theta = \pi/2$. In particular, it follows from this that for the trajectories $\psi_{1,\pi} = \psi_{1,0}$ ($\theta = 0$). At first glance this means that no matter how close to the Oz axis the trajectory may lie at $\theta = \pi$ ($\psi_{1,\pi}$ small), it will be located at $\theta = 0$, that is, after moving past the large particle, at the same distance from the Oz axis. This should denote that the small particles will not be captured by the larger one and the capture coefficient will be equal to zero. However, a more detailed investigation of the trajectory pattern shows that this is not the case.

The trajectory patterns described by equation (II.47) will differ in character, depending on the values of the parameter δ_1.

A qualitative analysis of the differential equations

---

*Neglecting the inertial term corresponds here to the condition

$$\varepsilon_5 = \frac{\delta_1}{k} = \frac{3E_0 q_2 D}{\pi\rho_p d^3 v_\infty} \ll 1.$$

of motion leads to the following results (see Appendix V.A).

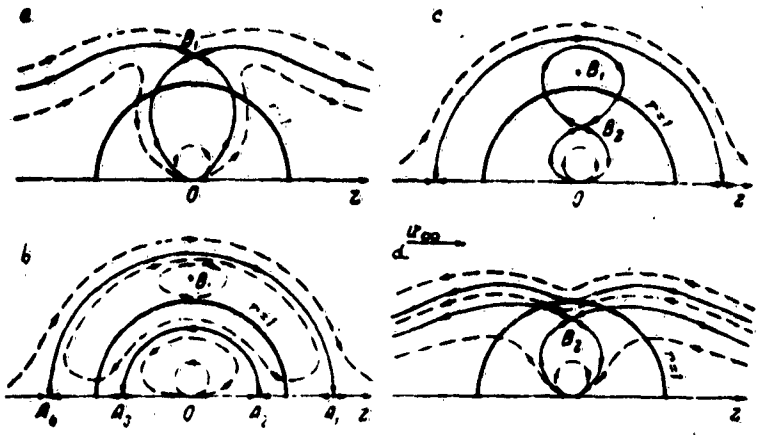

Fig. 50. Qualitative picture of the trajectories in case of electrostatic coagulation, due to the interaction between the charge of the small particle of the aerosol with the dipole induced by the external field on the large particle:

$$a-\delta_1<\delta_{cr};\quad b-\delta_{cr}<\delta_1<\frac{1}{4};$$

$$c-\frac{1}{4}<\delta_1<1-g_1;\quad d-\delta_1>1-g_1.$$

1) If

$$\delta_1<\delta_{cr}=\left(\frac{rF_1(r)}{2+r^3}\right)_{min}=F_4(r_m)^*,$$

then the system of singular points consists of a dipole at the origin and two saddles in the plane $\theta=\pi/2$. The limiting trajectory passes through the saddle B_1 (Fig. 50a). From equation (II.47) we obtain for it the equation (from the condition $r=r_{B_1}$ for $\theta=\pi/2$)

*Here r_m is the value at which the function $F_4(r)=\frac{rF_1(r)}{2+r^3}$ reaches a minimum (see Appendix V.A).

$$F_1(r_{B_1}) = \delta_1 \frac{2 + r_{B_1}^3}{r_{B_1}} \quad y_\kappa^2 (1 - \delta_1 - g_1).$$

Consequently, in this case the capture coefficient is

$$E = y_\kappa^2 \frac{2 + r_{B_1}}{(1 - \delta_1 - g_1) r_{B_1}} |F_4(r_{B_1}) - \delta_1|. \qquad \text{(II.48)}$$

Expansion of the function $F_4(r)$ in a Taylor series near the point $r = 1$ shows that $F'_4(r) = 0$ when $r_m = 1 + \frac{2}{3} g_1 + \frac{2}{9} g_1^2 + \ldots$, and $\delta_{cr} = F_4(r_m) = -\frac{g_1}{3}\left(1 + \frac{2}{3} g_1 + \frac{4}{27} g_1^2 \ldots\right)$. Thus, $\delta_{cr} \approx -\frac{1}{3} g_1$ and is usually small in absolute magnitude. Since in the case under consideration $1 < r_{B_1} < r_m$, the value of $F_4(r_m)$ lies between $F_4(1) = -\frac{1}{3} g_1$ and $F_4(r_m) \approx \approx -\frac{1}{3} g_1\left(1 + \frac{2}{3} g_1\right)$ and it can be assumed equal to $-\frac{1}{3} g_1$. The fraction $\frac{2 + r_{B_1}^3}{r_{B_1}}$ can be assumed equal to 3 with accuracy to 1 percent. Therefore expression (II.48) can be rewritten in the form

$$E = \frac{-3\delta_1 - g_1}{1 - g_1 - \delta_1}. \qquad \text{(II.48a)}$$

2) When $\delta_{cr} < \delta_1 < 1/4$, the system of singular points consists of a dipole at the origin, four saddles on the axis of motion at the points A_1, A_2, A_3, and A_4, and two centers B_1 in the plane $\theta = \pi/2$, having ordinates $r_{2(3)} < r_{B_1} < r_{1(4)}$ (see Fig. 50b). The capture coefficient is in this case equal to zero.

3) When $1/4 < \delta_1 < 1 - g_1$, the system of singular points consists of a dipole at the origin and two saddles on the axis of motion at the points A_1 and A_4. In the plane $\theta = \pi/2$ there are two centers B_1 and two saddles

B_2 ($r_{B_2} < 1 < r_{B_1} < r_{A_1(4)}$; see Fig. 50c). In this case the capture coefficient is also equal to zero.

4) When $\delta_1 > 1 - g_1$, the system of singular points consists of a dipole at the origin and two saddles B_2 in the plane $\theta = \pi/2$ ($r_{B_2} < 1$; see Fig. 50d). We call attention to the fact that the general direction of motion along the trajectories away from the particle is opposite the direction of the vector u_∞. This means that the dimensionless rate of falling of the small particle, due to the field E_0 and the force of gravity $-(\delta_1 + g_1)$ is larger than the rate of falling of the large particle (equal to unity). In this case the smaller particles overtake the larger one. The trajectory passing through the saddle B_2 does not encompass all the trajectories that terminate on the sphere, since $r_{B_2} < 1$. The boundary trajectory will be determined from the condition of tangency of the small particle to the large one at $r = 1 + \sqrt{g_1}$, $\theta = \pi/2$. We then obtain from (II.47)

$$E = y_\infty^2 = \frac{1}{1 - g_1 - \delta_1}\left[F_1(1 + \sqrt{g_1}) - \delta_1 \frac{2 + (1 + \sqrt{g_1})^3}{1 + \sqrt{g_1}}\right]. \quad \text{(II.49)}$$

At small values of g_1 we have

$$F_1(1 + \sqrt{g_1}) \approx \frac{g_1}{2}(1 - 5\sqrt{g_1} - g_1 \ldots).$$

$$E = \frac{-3\delta_1 + \frac{1}{2} g_1}{1 - \delta_1 - g_1}. \quad \text{(II.49a)}$$

At values $\delta_1 \approx 1$ the capture coefficient becomes very large. This circumstance is the consequence of the fact that in this case the rate of falling of the large and small particles become almost equal, and then even small attraction forces will cause the large particle to capture the small particles from a larger volume (for more details see Sec. 14).

B. We now consider a case when both drops are very weakly charged and they can be regarded as neutral (in this case the coefficients α, δ_1, and δ_2 are very small

compared with the parameter γ). Then equation (II.42) assumes the form

$$\left.\begin{aligned} k\frac{dv_r}{dt}+v_r &= u_r+k\sigma_4\frac{1-3\cos^2\theta}{r^4}-g_1\cos\theta,\\ k\frac{dv_\theta}{dt}+v_\theta &= u_\theta-k\sigma_4\frac{\sin 2\theta}{r^4}+g_1\sin\theta, \end{aligned}\right\} \qquad \text{(II.50)}$$

where

$$\sigma_4=\frac{9E_0^2}{4\pi\rho_p u_\infty^3}, \quad k\sigma_4=\gamma=\frac{9g_1E_0^2}{2\pi\rho_p gD}, \qquad \text{(II.51)}$$

since

$$u_\infty=\frac{\rho_p D^2 g}{18\eta}.$$

For water drops (ρ_p = 1) we have

$$\sigma_4=0{,}717\frac{E_0^2}{u_\infty^2}=0{,}812\frac{E_{0v}^2}{D_\mu^4}; \quad \gamma=1{,}624\cdot10^{-4}\frac{E_{0v}^2g_1}{D_\mu}, \qquad \text{(II.52)}$$

where D_μ is the diameter of the large drop in microns; E_{0v} is the electric field in volts per centimeter.

If $\sigma_4 \gg 1$, the inertial term k dv/dt in the equations can be neglected and equation (II.42) will have a solution in the form (II.45)

$$\psi_1-\frac{\gamma\sin^2\theta\cos\theta}{r^2}=\text{const}=\psi_{1,\pi}=\frac{1}{2}y_\pi^2(1-g_1). \qquad \text{(II.53)}$$

We note that it follows from equation (II.53) that $\psi_{1,\pi}=\psi_{1,0}(\theta=0)$. Here, as in the preceding case, to separate a definite trajectory from the family (II.53) it is necessary to investigate qualitatively the pattern of the trajectories, and the investigation yields the following results (see Appendix V.B).

The character of the pattern of the trajectories depends on the ratio of the quantity γ to the extrema of the function $F_1(r)=\frac{r^2}{2}F_1(r)$. We denote by γ_{cr} the absolute

value of the minimum of $F_6(r)$ and by γ_1 the value of the maximum of $F_6(r)$.* In accordance with the combination of relationships of γ, γ_1, and γ_{cr}, Figure 51 shows four different trajectory patterns. An examination of Figure 51 shows that when $\gamma < \gamma_{cr}$, the capture coefficient is $E = 0$.

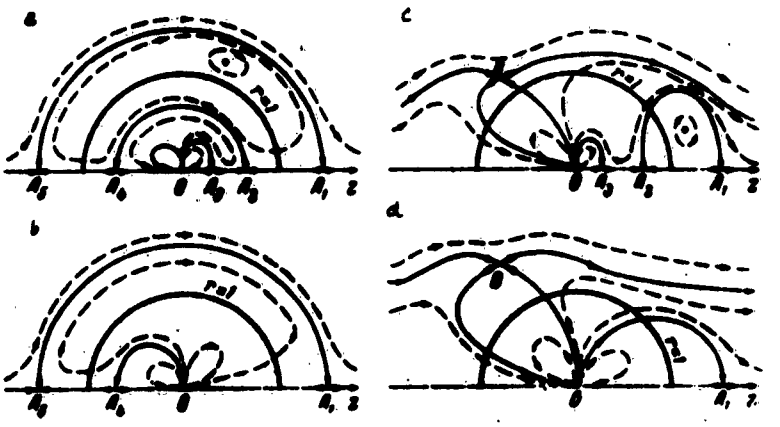

Fig. 51. Qualitative pattern of the trajectories in the case of electrostatic coagulation of two neutral drops moving in an external vertical electrostatic field:

a — γ small ($\gamma < \gamma_{cr}$; $\gamma < \gamma_1$);

b — $\gamma_1 < \gamma < \gamma_{cr}$;

c — $\gamma_{cr} < \gamma < \gamma_1$;

d — γ large ($\gamma > \gamma_{cr}$; $\gamma > \gamma_1$).

When $\gamma > \gamma_{cr}$, the value of the capture coefficient is determined by the limiting trajectory, which represents a separatrix passing through the saddle B which is not on the axis. The value of γ_π for this separatrix can be readily obtained from equation (II.53), by putting in it $r = r_B$ for $\theta = \theta_B$ (r_B and θ_B are the coordinates of the saddle B).

---

*The form of the function $F_6(r)$ is shown in Fig. 88. The values of γ_{cr} and γ_1 as functions of the parameter g_1 are listed in Table a.III (see Appendix V.B).

We then readily obtain the expression

$$\psi_{1,2} = \frac{1}{2} y_\infty^2 (1 - g_1) = \psi_1(B) - \frac{\gamma \cos\theta_B \sin^2\theta_B}{r_B^2} =$$

$$= r_B^2 \sin^2\theta_B [N_2(r_B) - g_1],$$

where

$$N_2(r) = 1 - \frac{9}{8r} + \frac{1}{8r^3}. \qquad \text{(II.54)}$$

It follows therefore that [28]

$$E = y_\infty^2 = \frac{2y_B^2 [N_2(r_B) - g_1]}{1 - g_1}. \qquad \text{(II.55)}$$

Table 16

Capture Coefficient E for Neutral Aerosol Particles in an External Electric Field.

$D = 20\ \mu$		$D = 10\ \mu$		$D = 5\ \mu$						
E_0 [v/cm]	σ_4	E_0 [v/cm]	σ_4	E_0 [v/cm]	σ_4	E	r_B	$-\cos\theta_B$	γ	g_1
1375	9,6	972	77	690	620	0,100	1,10	0,574	0,154	0,01
2260	26	1600	210	1130	1660	0,252	1,20	0,552	0,413	0,01
2690	37	1900	290	1345	2350	0,341	1,25	0,546	0,587	0,01
1025	5,3	724	43	510	340	0,189	1,20	0,578	0,342	0,04
1460	10,8	1032	86	730	690	0,370	1,30	0,554	0,693	0,04
1910	18,6	1360	148	960	1190	0,580	1,40	0,540	1,190	0,04
705	3,1	500	25	360	200	0,220	1,30	0,603	0,496	0,1
920	4,3	650	35	460	280	0,314	1,35	0,583	0,691	0,1
1210	7,4	860	59	600	480	0,530	1,45	0,560	1,190	0,1

Table 16 lists the results of calculation by means

of formula (II.55) for large values of σ_4.* The data of Table 16 show that for neutral aerosol particles and for the presence of an external electric field, the capture coefficient can reach noticeable values for large fields on the order of several volts per centimeter.

In the atmosphere fields like these arise only under conditions of developed cumulus and thunderstorm clouds. Under these conditions, however, the considered form of electrostatic coagulation can hardly play an important role in the process of development of the cloud, for in this case there exist in the cloud many large drops, which guarantee sufficiently rapid gravitational coagulation resulting from inertial settling.

In aerosol technology such large electric fields are encountered in electric filters, for which the role of the coagulation mechanism, described in the present section for the aerosol particles, calls for a special analysis.

It must be noted, as was already indicated above in other cases, that for particles of comparable dimensions the value of the capture coefficient can be appreciably larger than calculated in Table 16, owing to the decrease in the denominator $1 - g_1$ in formula (II.55) with increasing g_1.

This position is all the more probable since the data of Table 16 (where the influence of the parameter g_1 on the capture coefficient due to the change in the denominator $1 - g_1$ in formula (II.55) is still insignificant) show an appreciable increase in E with increasing g_1 at constant fields E_0. The physical meaning of this circumstance can be readily understood if it is recalled that the dipole moments induced by the external field in the aerosol particles are proportional to the cube of the particle diameters, and the force of interaction between the dipoles is proportional to the product of their moments.

*The calculations were carried out in the following manner. Values of g_1 and r_B were assigned, and then by formulas (a.71) and (a.73) (see Appendix V.B) were used to determine γ and $\cos \Theta_B$, and finally formula (a.76) was used to determine E. The value of γ determined, on the basis of formula (a.51), the value of E_0^2/D, and consequently the value of E_0 for each value of D.

14. ROLE OF ELECTROSTATIC COAGULATION OF CLOUD DROPS IN THE PROCESS OF CLOUD DEVELOPMENT

After analyzing methods for determining the value of the capture coefficient, due to the electrostatic forces of different types, we can now proceed to an estimate of the influence of the electrostatic coagulation on the process of enlargement of cloud drops. For this purpose it is necessary to turn first of all to experimental and theoretical material and charges of cloud drops.

As was already indicated above, measurements of electric charges of drops in clouds and fogs were carried out by a small number of authors and the results obtained are still contradictory in character. The first such experiments were set up by Wiegand [132] in 1925. Wiegand measured in the cloud the average charge of one polarity $-q_a$ per drop. He showed that the drops of fog have charges of both sides, and the average values (obtained from a series of experiments) are $q_a = 250--350$ e (e is the elementary charge). The average diameter of fog drops was in these experiments 20--28 microns. In individual experiments the values of q_a reached 1,000--22,000 e. Wiegand's experiments were repeated by Aderkas in 1940 [1], with analogous results.

Gunn [93] in 1951, and Gunn and Webb [130] in 1954 measured the total charge of drops in clouds and high-mountain fogs. They showed that the average total charge (summed over the charges of both signs) per drop, $-q_s$, reaches in clouds values of ~ 30 e for drops with diameters of about 10 microns [93] and values ~ 1 e in fogs [130].

This circumstance is evidence that either the charges of the investigated drops are small, or that the charge distribution is almost symmetrical with respect to sign. A comparison with data obtained by others gives preference to the second assumption.

Recently the results of measurements of a few others were published. Solov'yev and Makhotkin [58], [42] and Twomey [127] were the first to describe measurements of charges of individual drops, carried out by the method of Fuks and Petryanov [62]. Because of the features of the method employed by them, the number of drops on which the charge was measured was small. In the case of Solov'yev

and Makhotkin, for example, the measurements were carried out on approximately 500 drops, of which approximately 25 percent were charged.

Solov'yev and Makhotkin, who carried out measurements in fogs, have found that for drops with average diameter $d \approx 8$ microns one gets $\bar{q}_a \sim 80$ e. In some drops of this size they observed charges on the order of 400 e.

Twomey observed in warm clouds a very large (~ 80 percent) number of charged drops. He gives the relation

$$q[e] \approx 1{,}95 d_{\mu}^{3{,}06},$$

connecting the charge with the drop dimensions.

The most significant results on the measurement of charges of individual cloud drops were obtained by Sergiyeva [53, 54]. She noticeably improved the method of Gillespie and Langstroth [88] as applied to cloud measurements and measured the charges on several thousand cloud drops. Her measurements were made on a high-mountain station (3000 meters above sea level) of the Elbruss expedition of the Institute of Applied Geophysics of the Academy of Sciences USSR in stratus and stratocumulus clouds. In 1957 she carried out twenty-seven series of measurements in fifteen clouds. Her results, which are of importance to the problem considered here, can be summarized briefly as follows. In the investigated clouds there was always a considerable number of charged drops (about 30--50 percent of all the drops). Both in warm and in supercooled clouds, there were always drops having charges of both signs. The asymmetry of the distribution function of the drops relative to charges of both signs was usually low, so that there was always a large number of equally charged drops. The distribution function by charges is unimodal and is similar to a Gaussian distribution, although the latter circumstance could not be proved conclusively. The instrument measured directly the ratio of the charge of the drop to its diameter, q/d, with subsequent determination by means of microphotography of the dimension and then of the charge of the drop. The range of measured values of q/d lies within the limits $q[e]/d_{\mu} = 4.5$--8. Considering drops whose diameters lie in this interval, Sergiyeva found that $\bar{q}_a[e]/d_{\mu} \approx 6$--$8$. At the same time, for certain measurements in the clouds, there was a small percentage of drops having a ratio $q[e]/d_{\mu} = 80$

and dimensions d_μ = 4--22.

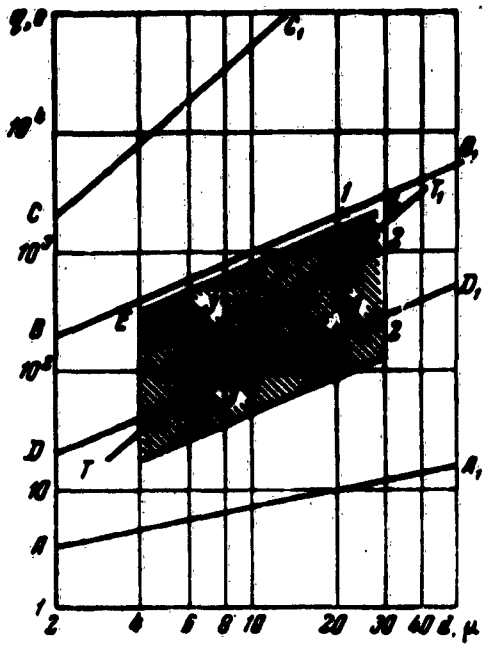

Fig. 52. Results of the measurements of electric charges of cloud drops.

Figure 52 shows the results of the described experiments. The abscissas show the value of the diameters of the drops in microns, and the ordinates the value of the charges of the drops in elementary units [e].* The same Figure 52 shows some theoretical distributions of particle charges. The line AA_1 corresponds to the Fuks theory [64] of charging of drops by ionic diffusing, which leads to a

*The shaded region in Figure 52 corresponds to the range of values measured on the instrument of Sergiyeva. The number 3 denotes the results of Solov'yev and Makhotkin, while the numbers 1 and 2 denote the results of Wiegand. The crosses correspond to the maximum values of $\bar{q}_a$, and the circles to the average values of $\bar{q}_a$. The data of Twomey are represented by the straight line TT_1.

relation $\bar{q}_a[e] = 2.3\sqrt{d_\mu}$.* The line BB corresponds to the absorption theory of drop charging (Frankel [61]) for the value of the electrokinetic potential 0.3 volt, leading to a relation $q[e] = -100\, d_\mu$. The line CC_1 corresponds to maximum charge on the drops, at which the electric field at the surface of the drop is equal to the breakdown voltage of 30 kv/cm. Here $q[e] = 500\, d_\mu^2$.

Recently several papers devoted to measurements of electrical charges in clouds have been published. Chao Po-ling using the apparatus of Sergiyeva carried out measurements on a free balloon in stratus clouds [13]. Petrov, using a procedure that he developed for the observation of tracks of drops in a stationary electric field of a capacitor, measured charges of drops during an airplane flight through cumulus and stratocumulus coulds [47, 13]. The results of the measurements of Chao Po-ling and Petrov turn out in the mean to be close to each other, and in Figure 52 they are described by a straight line DD_1, corresponding to the relation $\bar{q}_a[e] = 10\, d_\mu$. The measurements oh Phillips, Kinzer, and Allee [78] [113], carried out on mountains in newly-formed stratocumulus warm and supercooled clouds, gave for the drop charges values close to the straight line AA_1 in Figure 52.**

An examination of Figure 52 shows that the measured average absolute values of the drop charges in clouds and fogs as obtained by different authors differ appreciably from one another. This circumstance, in addition to the difference in the measurement procedure, can also be due to differences in the physical nature of the investigated clouds and fogs.

One can tentatively assume the line DD_1 in Figure 52

---

*The Fuks theory received good confirmation in the experiments of Lissowski on artificial aerosols [104]. In 1955 Gunn published a theoretical paper [94] which essentially repeats the results of Fuks. However, in calculating the quantity q_a, Gunn exaggerated its value by a factor of $\pi/2$.

**It should be noted that in thunderstorm clouds, Phillips and Kinzer found very large drop charges (approximately three times larger on the average than the charges measured by Petrov and Chao Po-ling).

to be some average of all the measured values of $\bar{q}_e$ and to give the connection between $\bar{q}_e$ and d in the form

$$\bar{q}_e [e] = 10 d_\mu . \qquad \text{(II.56)}$$

The maximum measured values of the charges, which group around the line EE_1 are:

$$\bar{q}_e [e] \approx 80 d_\mu . \qquad \text{(II.57)}$$

Let us estimate now the expected values of the capture coefficients for drops of different dimensions, with charges corresponding to formulas (II.56) and (II.57).

According to relation (II.56), the parameters of the electrostatic coagulation can be expressed directly in terms of the drop diameters. It is necessary to take into account here the fact that for drops with diameter less than 30 microns one can assume a rate of fall determined from the Stokes law and equal to $u_\infty = 0.31 \times 10^{-2} D_\mu^2$ ($\eta = 1.8 \times 10^{-4}$ poise). Then

$$\left.\begin{aligned}
&k = 2.10^{-4} g_1 D_\mu^2 ; \quad x = -q_2/q_1 = d/D = \sqrt{g_1} \\
&\alpha = -\frac{4 q_1 q_2}{3\pi\eta\, d D^2 u_\infty} = \frac{20}{D_\mu^2} ; \quad \sigma_1 = \frac{\alpha}{k} = \frac{10^6}{g_1 D_\mu^4} \\
&\beta = \alpha x = \frac{20\sqrt{g_1}}{D_\mu^2} ; \quad \sigma_2 = \frac{\beta}{k} = \frac{10^6}{\sqrt{g_1} D_\mu^4} \\
&\beta_1 = \frac{\alpha g_1^{1/2}}{x} = \frac{20 g_1}{D_\mu^2} ; \quad \sigma_3 = \frac{\beta_1}{k} = \frac{10^6}{D_\mu^4} \\
&\delta_1 = \frac{E_0 q_2}{3\pi\eta\, d u_\infty} = \frac{0{,}032 E_{0v}}{D_\mu^2} ; \quad \sigma_4 = \frac{\delta_1}{k} = \frac{160 E_{0v}}{g_1 D_\mu^4}
\end{aligned}\right\} \qquad \text{(II.58)}$$

Using relation (II.58) we can obtain the values of D_μ and E_{0v} (the value of the electric field in volts per centimeter) at which the capture coefficient will still have a noticeable value, for example exceeding 0.3. For this purpose it is necessary to recognize that at small values of α and δ_1 the values of the capture coefficients will be equal to $E \approx 5\alpha$* and $E \approx 3\delta_1$ respectively. We

*The coefficient 5 in lieu of 4 in formula (II.14)

then obtain from Figure 42 that E = 0.3 for $\beta = 0.04$ and $\beta_1 = 0.1$. The results obtained in this manner are summarized in Table 17.

Table 17

Values of D_μ for which E > 0.3

Coagulation mechanism	Defining parameter	D_μ	Value of σ for $D_{\mu,max}$
Drops charged differently	σ	< 7	$\frac{0,9}{g_1}$
Small drop neutral	β_1	< 2,7 ($g_1 = 0,1$) < 1,8 ($g_1 = 0,01$)	$\frac{2,5}{g_1^2}$
Large drop neutral	β	< 5,5 ($g_1 = 0,1$) < 3,7 ($g_1 = 0,01$)	$\frac{0,4}{g_1^{2/3}}$
External electric field (large drop neutral)	δ_1	< 0,6 ($E_{0v} = 1$) < 7 ($E_{0v} = 100$)	$\frac{480}{g_1 D_\mu^3}$

Inasmuch as charges on the order of the mean values described by relation (II.56) are encountered sufficiently frequently, almost each combination of the encountered drops with dimensions indicated in Table 17 can lead to an effective coming closer of their coagulation. Thus, the mean values of the charges, described by equation (II.56), can cause appreciable values of the capture coefficient and lead to electric coagulation of cloud drops with diameters smaller than 7 microns.

The electrostatic coagulation due to an external atmospheric-electric field E_0 and described by a parameter σ_1 can arise, as can be seen from Table 17, only for a field on the order of hundreds of volts per centimeter. By adding the results obtained in Section 13D, we can state

---

of Section 11 is obtained here because of the factor 1 + + 0.5L(r_0) in formula (II.28) of the same section. For the numerical calculations of E see [23, 26, 28].

that the influence of the atmospheric-electric field on the coagulation of the cloud drops can be noticeable only at field intensities of several hundred volts per centimeter.

The question of the influence of the electric coagulation on the growth of cloud drops with a diameter larger than 7 microns at the present-day status of the experimental investigation of the charge distribution function of cloud drops has not yet been solved. In favor of the possibility of such an influence we can advance the following arguments:

1. The distribution of the values of the charges has a statistical character, and a sufficiently large number of drops have charges appreciably larger than the mean value $\bar{q}_e$, defined by relation (II.56). This means that drops with much larger values of the charges than $\bar{q}_e$ can come close together. The frequency of such encounters depends on the form of the charge distribution function, which so far has not yet been sufficiently investigated. In particular, at the present time measurements of the charges were carried out only in fogs and only in several types of clouds. Many types of clouds and particularly clouds which produce precipitation, remain so far uninvestigated.

2. During precipitation formation, an increase takes place not in all the cloud drops, but only in an insignificant part of them. Usually in a rain the number of drops per unit volume is approximately 10^6 times smaller than in the clouds. The number of drops precipitated in the form of drizzle ($d \approx 100$ microns) is 3--4 orders of magnitude smaller than the total number of drops. This means that the process of enlargement of the cloud drops which leads to precipitation can be the result of the enlargement of an insignificant part of the initial number of drops. In the investigation of coagulation it is necessary to regard the collisions as a statistical process, as was done (under many simplifications) by Telford [126]. The role of large charges, even those rarely encountered, can turn out to be appreciable here for the coagulation of drops.

3. What attracts attention is the growth in the capture coefficient E for given charges (for given α, β, β_1, and δ_1) with decreasing difference in the drop dimensions (as $\varepsilon_1 \to 1$). Indeed, in all the formulas of Secs.

11--13 the capture coefficient increases in inverse proportion to the difference $1 - g_1$. This circumstance is connected with the decrease in the difference in the rate of fall of the drops and the corresponding increase in the momentum of the electrostatic forces of attraction between drops. Roughly speaking, in the limit, when the rates of fall of the drops are equal ($g_1 = 1$), the drops interact for an infinitely long time (in the presence of attraction forces the distance between drops can only decrease). They can therefore be attracted to one another for any initial distance between them. Of course, the realization of such a process occurs after an infinite time and along an infinite path of falling drops. Obviously, the turbulence of the atmosphere complicates this process appreciably. It is nevertheless clear that at small values of the difference $1 - g_1$, values of the capture coefficients due to the electrostatic attraction forces can be large. Analogous results for the capture coefficients caused by hydrodynamic interaction between drops were obtained by Pearcey and Hill [111], who, considering the hydrodynamic interaction of the drops in accordance with the Oseen scheme, have reached a conclusion that for drops close in dimensions, the capture coefficients will be very large (on the order of 10^3--10^4) for $d > 20$ microns.*

4. The data shown in Figure 52 show that the mean values of the charges $\bar{q}_a$ measured in the clouds are one order of magnitude higher than the value $\bar{q}_a[e] = 2.3\sqrt{d_\mu}$, predicted by the Fuks theory of ionic diffusion. This circumstance, as it seems to us, offers indirect evidence of the presence of drop coagulation which leads to an increase in the average charge. In particular, the coagulation may be due here to the interaction between drops of like charges (Sec. 12).

All the foregoing considerations enable us to assume that the influence of electrostatic coagulation on the

*Pearcey and Hill have found that the coefficient of gravitational coagulation is equal to zero when $d < 20$ microns. This means that an account of the hydrodynamic interaction decreases the critical value of the Stokes parameter, obtained by Langmuir (according to the value $k_{cr} = 1.214$, Langmuir arrived at the conclusion that $E = 0$ when $d < 28$ microns).

growth of cloud drops with diameter less than 20--30 microns is appreciable to the extent that it can lift the hindrance against coagulation, predicted by the theories of gravitational coagulation of Langmuir and of Pearcey and Hill. Of course, for a rigorous solution of this problem it would be necessary to consider the kinetics of the enlargement of the drops at this initial stage of the development of the cloud. It would be necessary to consider also the coagulation of drops of comparable dimensions, due to hydrodynamic and electrostatic interactions.

At the present time, however, the experimental material on the distribution of charges of cloud drops is insufficient to be able to consider it advantageous to carry out these complicated theoretical investigations.

It follows from all the foregoing that as the diameter D of the larger drop increases, the capture coefficient, due to the electrostatic forces, decreases sharply. This fact has a simple explanation: with increasing diameter D the time of passage of the small drop past the larger one decreases and at the same time the momentum of the electric forces decreases. It is easy to show that for very large drops (drizzle, rain) the electric forces should not influence the coagulation. Let us consider, for example, the coagulation of unlike charged drops of this range of dimensions ($D > 1$ mm, $d > 100$ microns) in the case when their charges are so large that an electric field is produced at the surface of the drops, equal to half the breakdown voltage, that is, 15,000 v/cm. Then $q[e] = (1/8)d_{mm}^2$.* For the rate of drop of the drops of drizzle and rain, one can assume a simpler approximation formula (from the results of [91]): $u_\infty [cm/sec] = 400 d_{mm}$ (it is very well satisfied for $0.1 \text{ mm} < d < 1$ mm; when $1 \text{ mm} < d < 3$ mm it exaggerates the rate of drop by not more than 1.5 times). Then the ratio of the electrostatic forces to the inertial forces is

$$\sigma_1 = \frac{12 q_1 q_2}{\pi \rho_p D d^2 u_\infty^2} \approx \frac{0{,}004}{D_{MM} d_{MM}}.$$

Therefore if $D > 1$ mm and $d > 100$ microns, then $\sigma_1 < 0.04$; if $D > 2$ mm and $d > 0.5$ mm, then $\sigma_1 < 0.004$ etc.

---

*Here d_{mm} is the diameter of the drop in millimeters.

It is obvious that under these conditions it is difficult to expect a noticeable influence of the electrostatic forces on the coagulation of such drops.

This circumstance explains also for example the results of the experiments by Gunn and Hitchfield [92]. In these laboratory experiments, an investigation was made of the calculation of large drops (D = 3.2 mm) with small cloud drops by measuring the increase in the weight of the large drops as they fall through a volume of cloud drops, the height of which was on the order of 2 meters. In many of these experiments the large drops were charged (their charge reached 0.2 electrostatic units). However, no influence of the charge on the coagulation was observed. It is easy to see that this influence should not be expected, since under the experimental conditions the value of σ_1 did not exceed 10^{-3}, even if we assume the charges of the cloud drops to be $q[e] = 80\, d_\mu$.

Our estimate of the charges for rain and drizzle drops is, of course, greatly exaggerated. If we assume that the charges of the cloud drops ($d < 100$ microns) are determined by the upper limit of the observations described above, so that $q[e] = 100\, d_\mu$, then the parameter α will in this case be equal to $2000\, D_\mu^{-6}$ and for $D > 50$ microns the expected value of α will be less than 0.015, and the corresponding capture coefficient, due to the electrostatic forces, is smaller than 0.075. Thus, when the large drops have diameters $D > 50$ microns the electrostatic coagulation becomes negligibly small. Its influence can be neglected all the more since at such drop dimensions the capture coefficients of the gravitational coagulation become already large [103]. This circumstance was not taken into account by Gunn in his theory of random electrification of large drops [96]. In the next section we shall present a critique of this theory.

In concluding this section let us consider the experiments with coarsely dispersed aerosols, in which the effect of electrostatic coagulation was observed. In 1938 Vager, by causing small drops of water charged in an electric field to fall through a chemical fog, observed rapid scattering of the latter [7]. Analogous experiments were made by Pauthenier in 1948 on an artificial water cloud in a chamber [110]. A characteristic of the rate of scattering of the fog in both cases was the rate of change of its

transparency. In Figure 53 the thick line represents plots of the variation of the visibility of clouds with time in the experiments of Vager and Pauthenier. For comparison, the thin lines show the variation of the visibility without artificial action (injection of drops in the chamber). In Figure 53b* (experiments by Pauthenier), the dashed curve corresponds to an experiment in which uncharged water drops were injected in the fog (with the same quantity of water as in the case of injection of charged drops). An examination of Figure 53 shows a clear-cut influence of the electrostatic coagulation under the experimental conditions.

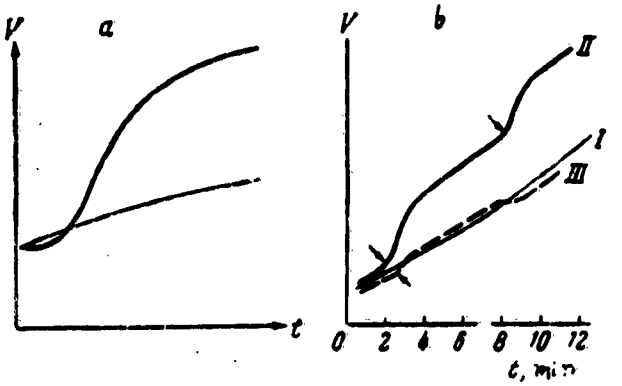

Fig. 53. Effect of electrostatic coagulation in the experiments of Vager (a) and Pauthenier (b).

I -- naturally scattered fog; II -- scattering due to injection of charged drops; III -- scattering upon injection of neutral drops. The arrows indicate the instants of injection of the drops.

In the experiments of Telford, Thorndike, and Bowen [125] an appreciable influence of the electrostatic forces on the coagulation of the drops was observed. In these experiments the authors produced artificial bipolar charging of drops of nearly equal dimension ($d \simeq 130$ microns) with large charges on the order of $(2\text{--}9) \times 10^{-4}$ electrostatic units. The rates of drop of the drops did not differ from each other by more than 10 cm/sec. Under these conditions,

*The arrows in Fig. 53b indicate the instants of injection of the drops in the chamber.

the authors observed an increase in the rate of coagulation by a factor of several times compared with the coagulation of similar uncharged drops. Since in the latter case the authors observed in such drops of comparable dimensions very large capture coefficients, $E \approx 12$, in the case of electrically charged drops ($q \approx 9 \times 10^{-4}$ electrostatic units) the capture coefficient should be of the order of 100. The presence of such large capture coefficients do not contradict the considerations developed in the present section, namely that the charges of the drops are very large [$q[e] = (3{,}000\text{--}14{,}000)d_\mu$]. At these charges and for $u_\infty \approx 10$ cm/sec, the parameter is $\alpha = 4.3$ for $q = 2 \times 10^{-4}$ electrostatic units and $\alpha = 86$ for $q = 9 \times 10^{-4}$ electrostatic units.

15. RANDOM ELECTRIFICATION OF CLOUD AND RAIN DROPS

In the present section we consider the problem of random electrification of cloud and rain drops, closely connected with the question of electrostatic coagulation.

As was already mentioned above, the theory of random electrification of very small cloud drops due to diffusion of light ions was developed by Fuks [64] and was essentially repeated by Gunn [94].

In 1955 Gunn published two papers [95, 96], in which he assumes that the function of the distribution of charges on large cloud and rain drops is determined by the random electrification which occurs during the process of the orthokinetic coagulation of the large drops with charged small drops.

In the first of these investigations [95] Gunn considered the falling of large cloud drops in a cloud with drops having diameters $4\ \mu < d < 40\ \mu$, while in the second paper [96] he considered the falling of drizzle and rain drops in a cloud with drops having $d > 40\ \mu$ in diameter.

In both these articles the distribution function of the charges on the large drops is calculated in analogous fashion. The author considered the process of electrification of large drops of radius r_2, falling in a medium containing smaller drops of radius r_1 with relative velocity u_R. It is assumed that half of the smaller drops has a charge $+q$ and the other half a negative charge $-q$. The

influence of the electrostatic forces on the orthokinetic coagulation of the drops is reduced by Gunn to a systematic shift s of the almost-vertical trajectory of the smaller drop relative to the larger one in a direction perpendicular to the force of gravity. The number of smaller drops captured by the larger one per unit time is then equal to

$$\pi (r_2 + r_1 + s)^2 u_R n(r_1),$$

where $n(r_1)$ is the counted concentration of the smaller drops. The capture coefficient of the smaller drops by the larger one will therefore be determined by the formula

$$E = \left(1 + \frac{s}{r_1 + r_2}\right)^2, \qquad \text{(II.59)}$$

where $s > 0$ for drops of unlike charge and $s < 0$ for drops of like charges. The calculation of the shift s is carried out in simplified fashion both in the formulation of the problem and in the procedure for its solution. Thus, for example, in Gunn's first paper the air stream around the drop is assumed to be homogeneous (at very small distances of the limiting trajectory from the large drop!), while in the second paper the influence of the air on the motion of the drops is not taken into account at all. These assumptions lead in both cases to the equality $E = 1$ in the absence of charges on the drops ($s = 0$). The latter is in principle unacceptable for the first paper, where cloud drops are considered with diameters lying in the range where gravitational coagulation is forbidden.

Further, Gunn assumes that as a result of the large number of collisions with the charged smaller drops a stationary normal distribution of charge is established on the large drops. The unknown parameters (the variance σ and the mode) of this distribution are determined from a comparison of the two expressions for the ratio F_{z+1}/F_z -- the number of large drops having respectively charges $Q = (z + 1)q$ and $Q = qz$. This expression is obtained in the first time starting from the normal distribution with unknown parameters. The second method of calculating this ratio is based on the statistical principle of detailed balance. Essential use is made here of the dependence (II.59) of the capture coefficient on s and of the dependence of s on the charges, dimensions, and velocities of the drops. In both cases the ratio F_{z+1}/F_z is in the form of a

series. Two unknown parameters of the sought normal distribution are obtained from a comparison of the first two terms of these series.* In [95] q_a is assumed to be the mean absolute value of the charge q_a formed on the smaller drops as the result of ionic diffusion (here and throughout q_a is defined as the mathematical expectation $|q - \bar{q}|$, where $\bar{q}$ is the mode of the distribution). In [96] the value of q is assumed to be the mean absolute value of the charge, calculated from the distribution obtained in the article [95].**

It seems to us that the results obtained by Gunn in [95, 96] are in error for the following reasons.

In [96] there is considered the coagulation of drizzle and rain drops ($d > 40$ microns) with cloud drops. The results obtained in that work are determined by the presence of electrostatic coagulation for drops of the indicated range of dimensions. However, as was already mentioned in the preceding section, the influence of the electrostatic forces on the coagulation is negligible for these drops and therefore cannot be important for any physical processes. This can be seen from the same paper by Gunn. Actually, in Figure 2 of this paper [96] Gunn, in confirmation of his theoretical calculations, gives the experimentally obtained distribution of the electric charges on the rain drops falling in the cloud. The average dimensions of the rain drops are $\bar{r}_2 = 500$ microns, and that of the cloud drops $\bar{r}_1 = 50$ microns. The same Figure 2 shows the theoretical distribution calculated from formula (15) of the same paper [96] for the indicated values of r_1 and r_2. If we assume the charges on the drops to be $q = 10^{-5}$ and $q = 10^{-3}$ electrostatic units (these data are taken from the curve of Figure 1 of Gunn's paper [96]),

*We note that in comparing the next terms of the series, different results are obtained for the sought parameters of the distribution.

**It should be noted that in [95, 96], as well as [94], Gunn overestimates the value of q_a by a factor $\pi/2$, since he assumes that for a symmetrical Gaussian distribution $\bar{q}_a = \sqrt{\pi/2}\,\sigma$ (σ is the standard of the normal distribution). Actually, however, $\bar{q}_a = \sigma\sqrt{2/\pi}$.

then we obtain for the value of s, from formula (8) of that paper, a value

$$\left(u_R = 376\,\frac{см}{сек}\right)$$

$$\frac{s}{r_1+r_2} = \frac{qQ}{(r_1+r_2)\,u_R^2}\left(\frac{1}{m_1}+\frac{1}{m_2}\right) =$$

$$= \frac{10^{-3}\cdot 10^{-6}}{0{,}055\cdot 376^2}\left[\frac{1}{0{,}524\cdot 10^{-6}}+\frac{1}{0{,}524\cdot 10^{-3}}\right] \approx 2{,}5\cdot 10^{-3}.$$

This calculation, carried out on the basis of Gunn's data, confirms once more that for drops of the dimensions under consideration the influence of the electric forces on the value of the capture coefficient, and consequently on the coagulation rate, is negligible. The coagulation rate on the other hand enters in a decisive fasion into the equation of detailed balance, therefore the parameters of the stationary distribution of the charges, sought by Gunn, are sensitive to the influence of the electric charges on the capture coefficient (when $s \to 0$ the stationary distribution obtained by Gunn acquires an unlimited variance). It is impossible to agree with the fact that a phenomenon which is actually of no significance in this case (the influence of the charges on E) would determine in essential fashion the course of the process of random electrification of large drops.

It seems to us that the solution of this problem should be sought not in a determination of the stationary distribution, but in an investigation of the stochastic process of charging of large drops, analogous to the random walk problem (see, for example, [71]). In this case the problem considered by Gunn in [96] reduces directly to the simplest variant of random walks; a large drop, falling among the smaller ones (which have with equal probability charges +q and -q), obtains a charge increment +q or -q, with probability 1/2, upon each collision with the smaller drop. The binomial distribution of charges which is established in this case on the large drops is well approximated, even for a small number of collisions N, by the normal distribution [71]*:

*From Table 1 (page 11) of the monograph by Chandrasekhar [71] we see that already when $N > 10$ formula (II.60) describes sufficiently well the sought distribution.

$$F(z) = \frac{1}{\sqrt{2\pi N}} e^{-\frac{z^2}{2N}}. \qquad \text{(II.60)}$$

where F(z) is the number of large drops with charge zq.

The problem formulated by Gunn [96] (the smaller drops have charges $\pm$ q with equal probability) can be generalized to include the case when the distribution function of the charge on the smaller drops f(q) is in practice arbitrary. If we assume that in the entire volume of the cloud the function f(q) remains constant, then the solution of such a problem reduces to the general case of random walk, in which the distribution function of the displacement after the i-th movement does not depend on the number i.* Using formula (103) from the book of Chandrasekhar [71] we readily obtain for the distribution density of the charges Q on the large drops the expression

$$F(Q, t) = \frac{1}{\sqrt{2\pi N \sigma_q^2}} \exp\left[-\frac{(q - N\bar{q})^2}{2N\sigma_q^2}\right], \qquad \text{(II.61)}$$

where N is as before the number of collisions between the large drops with the smaller ones during the time t; $\bar{q}$ and σ_q^2 are the mathematical expectation and variance of the charge on the smaller drops.

In equation (II.60) and (II.62) the number of collisions can be related with the altitude H through which the large drop falls

$$N = \pi (r_1 + r_2)^2 E n(r_2) H. \qquad \text{(II.62)}$$

From (II.61) and (II.62) we see that the variance σ_Q and the mode $\bar{Q}$ of the distribution (II.61) are

---

*We note that in such a formulation of the problem an essential factor is the independence of the capture coefficient E of the charges on the drops. This signifies that the probability of collision between the large drop and the smaller one does not depend on the charges on the drops, that is, on i.

$$\sigma_Q^2 = N\sigma_q^2 \sim H\sigma_q^2, \tag{II.63}$$

$$\bar{Q} = N\bar{q} \sim H\bar{q}. \tag{II.64}$$

Although the formulation of the problems whose solutions are equations (II.60) and (II.61) is simplified [f(q) does not depend on the height, the capture coefficient is the same for all drops*] it seems to us that the main character of relations (II.63) and (II.64), that is, the increase in the mode and variance of the distribution, and consequently in the mean absolute value of the charge of the large drops

$$\bar{Q}_a = \overline{|Q - \bar{Q}|} = \int_{-\infty}^{\infty} |Q - \bar{Q}| F(Q)\, dQ = \sqrt{\frac{2}{\pi}}\,\sigma_Q$$

with increasing distance H through which they fall would be advantageously subjected to an experimental verification. Apparently, an account of the dependence of f(q) on the altitude will not introduce any principal difficulties in the solution of the problem.

In the paper by Gunn [95], in which the electrification of cloud drops with $r_2 < 20$ microns is considered, the formulation of the problem has been intolerably simplified. The point is that Gunn assumed in this paper, in the calculation of the trajectory of the small drops relative to the large one, that the air flowing around the latter is uniform. Actually, the uneven character of the flow around the large drop leads to the existence of a minimum dimension of the drops that can be captured by the larger one and to forbiddenness of gravitational coagulation (E = 0) when $r_2 < 10$--15 microns. The presence of electric charges on such drops can lead to the apparence of large values for E, and consequently, to the lifting of the forbiddenness of the gravitational coagulation (see Sec. 14), that is, to an essential change in the coagulation process. Inasmuch as expression (II.59) is not applicable to this region,** the results obtained by Gunn in [95] are incorrect.

---

*The latter limitation is not very essential, since for rain and drizzle drops the capture coefficient approaches unity [103].

**According to formula (10) of [95] we have $s_x = -\frac{qQ}{6\pi\eta u_R r_1 r_2} = \alpha r_2$, where α is the parameter for the coagulation

Because of the fact that in the considered region of drop dimensions ($r_2 < 20$ microns) the capture coefficient E depends essentially on the charges of the drops, the theory of random walk can no longer be employed here directly. In this range of dimensions the problem of random electrification calls for a special analysis, in which it is necessary to take into account the dependence of the probability of collision of large drops with the smaller ones on the magnitude of their charge.

After the results considered in the present section were published [25], a new paper by Gunn appeared [97], devoted to "Nonequilibrium Electrification of Rain Drops." In this paper Gunn, using the method of the theory of random walk, considered the electrification of rain drops falling among cloud drops carrying charges +q (with probability p) and -q (with probability $\nu = 1 - p$). However, even in this paper Gunn does not forego his erroneous notion of the stationary distribution of the rain-drop charges.

16. ELECTROSTATIC PRECIPITATION OF AEROSOL PARTICLES FROM A STREAM ON LARGE BODIES

In the present section we confine ourselves to an examination of electrostatic precipitation of charged aerosol particles on a large obstacle (collector) with charge Q that is opposite in sign to the particle charge q. Usually it is possible to neglect here the induction forces* and the cohesion effect. Such a neglect greatly simplifies the determination of the capture coefficient and yields for E a formula which is valid essentially for a body of arbitrary form and for an incompressible stream

---

of drops of like charges [see formula (II.5), Sec. 11]. Therefore the capture coefficient according to Gunn will in this range of dimensions be, according to equation (II.59)

$$E = \left(1 + \frac{\varepsilon}{1 + \sqrt{\varepsilon_1}}\right)^2$$

whereas actually $E = \frac{4\varepsilon}{1 - \varepsilon_1}$ [see formula (II.14), Sec. 11].

*The influence of the induction forces can be appreciable at small values of the capture coefficient, when a considerable segment of the limiting trajectory passes near the collector surface.

of arbitrary type, if the inertial forces acting on the particle are small compared with the electrostatic forces [34].

When neglecting the inertial term of equation (II.2), we obtain for the velocity of motion of the aerosol particles v the following equation

$$v = u - \frac{\alpha r}{Q} E_e(r). \qquad \text{(II.65)}$$

where

$$\alpha = -\frac{qQ}{3\pi\eta l^2 u_\infty}; \qquad \text{(II.66)}$$

u_∞ -- velocity of the air stream incident on the collector at infinity;
l -- characteristic dimension of the collector;
$E_e(r)$ -- electrostatic field of the charged collector.

To calculate the capture coefficient of the aerosol particles by the collector we use a procedure proposed by Dukhin and Deryagin [8] and determine the flux of particles that settle on the surface of the collector:

$$I = \iint n(r) u_\infty v_n(r) d\sigma_1. \qquad \text{(II.67)}$$

In this formula v_n is the component of the dimensionless velocity v along the outward normal to the collector surface, and n(r) is the counted concentration of the aerosol particles at its surface. The integration in (II.67) is carried out over that part of the surface, where the particles settle. In the general case the determination of the region of integration is connected with an investigation of the limiting trajectories (see, for example, Sec. 13) and of the functions n(r). In the case considered here, however, the problem simplifies for the following reasons.

Since div u = 0 (the stream is incompressible) and the electrostatic field of the collector is solenoidal (div E_e = 0), the counted concentration of the particles along all the current lines of the particles, starting with infinity ($z = -\infty$), remains constant and $n(r) = n_\infty$ (see Sec. 3).

Further, in our case $v_n > 0$ over the entire surface of the collector, since $u_n = 0$ for any air stream and

$\left(-\frac{eR}{Q}E_{en}\right)>0$ (the collector and the aerosol particles are charged oppositely; there is no external electrostatic field). This means that the aerosol particles settle over the entire surface S_1 of the collector, and the limiting trajectory is located outside S_1 and does not cross it. Therefore the integration in (II.67) must be carried out over the entire surface of the collector. Then

$$I = n_\infty u_\infty \oint_{S_1} v_n(r)\,dS_1 = -n_\infty u_\infty \frac{eR}{Q}\oint_{S_1} E_{en}(r)\,dS_1. \qquad \text{(II.68)}$$

The integral in the right half of (II.68) represents the flux of the vector E_e inside the closed surface of the collector. By virtue of the known theorem of electrostatics, its value is $-4\pi Q$ and consequently

$$I = 4\pi n_\infty u_\infty R^2\alpha = -\frac{4n_\infty eQ}{\delta\eta}. \qquad \text{(II.69)}$$

As shown by formula (II.69), the particle flux to the collector does not depend on the velocity u_∞ of the air stream and on the dimensions, shape, and orientation of the collector [34].

Let us calculate now the collector capture coefficient, equal to the ratio of the flux I to the flux of particles "moving past the collector": $n_\infty u_\infty S_M$, where S_M is the mid-section of the collector (the projection of the collector surface on a plane perpendicular to u_∞):

$$E = \frac{I}{n_\infty u_\infty S_M} = \alpha\frac{4\pi R^2}{S_M} = -\frac{4eQ}{\delta\eta dS_M u_\infty}. \qquad \text{(II.70)}$$

Formulas (II.69) and (II.70) are characterized by great generality -- they have been derived for a body of arbitrary form; the only assumption made with respect to the air stream was that it is incompressible and stationary [34].

From the general formula (II.70) we can derive several particular formulas.

Assuming for a spherical collector by way of the characteristic length l the radius of the sphere R, we obtain from (II.70) an expression already known from Sec.

11 ($S_M = \pi R^2$):

$$E = 4a. \tag{II.71}$$

For a cylindrical collector with round cross section of radius $R = l$ we obtain from equation (II.70) an expression first derived by Natanson [43]:

$$E = \frac{4\pi R^2}{2R \cdot 1\,[L]}\, a = -\frac{2q\,Q_1}{3\eta\, dR u_\infty} = 2\pi a_c, \tag{II.72}$$

where Q_1 is the charge of the cylinder per unit length, and

$$a_c = \frac{al}{1\,[L]} = -\frac{qQ_1}{3\pi\eta\, d l u_\infty} \tag{II.73}$$

is the parameter of electrostatic settling for cylindrical bodies.* For an elliptical cylinder with large semiaxis a and eccentricity e, the midsection is

$$S_M = 2a\sqrt{1 - e^2\cos^2\varphi},$$

where φ is the angle of inclination of the major axis of the ellipse to the vector u_∞.

Consequently, the capture coefficients will be determined in this case by the expression ($l = a$):

$$E = -\frac{2qQ_1}{3\eta\, da u_\infty \sqrt{1 - e^2\cos^2\varphi}} = \frac{2\pi a_c}{\sqrt{1 - e^2\cos^2\varphi}}. \tag{II.74}$$

---

*We note here that, as shown by Natanson [43], expression (II.72) is valid also for a homogeneous flow around a cylinder (where the method which we are employing is not suitable, since $u_n \neq 0$). Therefore expression (II.72) is also suitable for the determination of the rate of settling of particles with allowance for the force of gravity.

In the more general case equation (II.70) is valid also when taking into account the influence of the force of gravity on the motion of the aerosol particles, provided only $(qE_{en} + mgG_{1n}) > 0$ over the entire surface of the collector, where G_1 is the unit vector of the force of gravity. In this case we must take u_∞ in formulas (II.72) and (II.70) to mean the modulus of the sum of the vectors u_∞ and the velocity of sedimentation v_s.

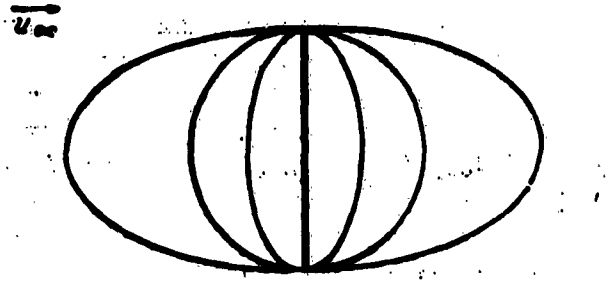

Fig. 54. Cross sections of various cylinders with identical capture coefficients for electrostatic precipitation.

When e = 0 (the ellipse becomes a circle) formula (II.74) goes over into (II.72).

For a plate (e = 1)

$$E = -\frac{2qQ_1}{3\eta d a u_\infty \sin\varphi} = \frac{2na_c}{\sin\varphi}. \qquad \text{(II.75)}$$

It is easy to see, for example, that a plate, a round cylinder, and all elliptical cylinders shown in Figure 54 have identical capture coefficients, provided the values of Q_1 on them are the same.

We recall that all the results obtained in the present section are valid when the inertial forces are much smaller than the electrostatic forces, that is, when the parameters

$$\sigma = -\frac{6qQ}{\pi\rho_p d^3 l u_\infty^2}, \qquad \text{(II.76)}$$

or

$$\sigma_c = -\frac{6qQ_1}{\pi\rho_p d^2 u_\infty^2} \qquad \text{(II.77)}$$

are large.

To the contrary, if the parameter σ (σ_c) is very small, then electrostatic precipitation can be neglected compared with inertial precipitation. Thus, for example,

calculation of E and σ by means of equations (II.70) and (II.76) shows that electrostatic precipitation of cloud and rain drops on the surface of an airplane is negligible. To demonstrate this, we replace the fuselage of the airplane by an elongated ellipsoid of revolution with major axis parallel to the velocity of the airplane. The greatest electric charge density on such an ellipsoid will occur on the ends, where it is equal to $\omega = Q/\pi b^2$ [59] (Q is the ellipsoid charge and b its minor semiaxis). Taking as the characteristic length l the minor semiaxis b and recognising that the electrostatic field at the surface of a conductor is $4\pi\omega$, we obtain for E, in accordance with formula (II.70), the following expression ($Q = l^2 E_{0,\max}$; $S_M = \pi l^2$):

$$E = \frac{4qQ}{3\pi\mu d u_\infty S_M} = \frac{4q E_{0,\max}}{3\pi\mu d u_\infty}. \qquad \text{(II.78)}$$

Assuming $E_{0,\max} < 15$ kV/cm, $u_\infty = 70$ meters/sec and $q[e] < 100\ d_\mu$ (maximum charges of the cloud drops; see Sec. 14), we obtain on the basis of (II.78)

$$E < \frac{4(100\, d_\mu \cdot 4{,}8\cdot 10^{-10})\cdot 50}{3\pi\cdot 1{,}8\cdot 10^{-4}(d_\mu\cdot 10^{-4})\cdot 7\cdot 10^{3}} < 0{,}01. \qquad \text{(II.79)}$$

From inequality (II.79) it follows that the settling of charged cloud and rain drops on the surface of an airplane is determined by the inertial mechanism. Analogous deductions are obtained also for airplane and land-base traps for cloud drops (provided the stream velocity in the latter is $u_\infty \approx 10$ meters/sec.

CHAPTER III

SOME RESULTS OF EXPERIMENTAL INVESTIGATIONS

17. AEROSOL TRAPS USED IN THE OPERATIONS OF THE ELBRUSS EXPEDITION

In the high-mountain all-inclusive Elbruss expedition of the Institute of Applied Geophysics of the Academy of Sciences USSR, many investigations have been in progress since 1950 on various problems of the physics of clouds.

The principal base of the expedition is located on the bottom of the valley of the River Azau at the foothills of Elbruss. In addition to this base, the expedition has a few other high-mountain stations, located on the slopes of the mountains forming the valley. This location of the stations and of the base of the expedition makes it possible to investigate thoroughly the meteorological conditions and the microstructural characteristics at various points of local clouds which are formed in the valley, for in this case many of the observation points, located on the mountain slopes, are situated in the cloud. A tied balloon which is secured in the region of the main base (in the middle of the valley) permits measurement of many physical characteristics at points of different altitudes in the same cloud.

It is quite natural that under such conditions of cloud observation it became necessary to create land-based and balloon-borne traps for cloud drops, making it possible to determine the microstructural characteristics of various parts of the investigated local cloud.

The main method chosen for the investigation of the

microstructure of the clouds and the fogs was that of inertial settling of cloud drops from the stream onto an obstacle [3, 22]. To prevent the settling drops from evaporating, the obstacle is covered with a thin layer of a mixture of transformer oil and chemically pure vaseline [63, 3]. Subsequent processing of the gathered sample of cloud drops reduces to taking a microphotograph of the sample and subsequent determination of the distribution functions of the photographed drops by dimensions.

The construction of the traps was based on the following considerations.

1. The form of the received obstacle, on which the drops settle, should be simple, so that it becomes possible to determine the air stream near it by methods of theoretical aerodynamics. This requirement was dictated by the need for theoretically determining the capture coefficient of the receiver, since an experimental determination of the capture coefficient turned out to be quite difficult, owing to the difficulty of obtaining a stream of iso-dispersed aerosol in the investigated particle-dimension range.

2. The receiving surface should desirably be that of a transparent plate (in view of the subsequent microphotography).

3. Inasmuch as the capture coefficient of the aerosol particles depends on the velocity of the airstream incident on the receiver, it is necessary to produce in the traps a stationary air stream, the velocity of which can be measured in a simple manner. It should be noted that in the previously employed land-based traps, the air stream was not stationary.

4. In order to make the minimum dimensions (d_{min}) of the drops settling on the receiver not too large, the working velocity of the stream in the trap should be sufficiently large, and the dimensions of the receiver sufficiently small (see Sec. 6).

5. Since the formation of a stationary stream in land-based traps always entails the aspiration of the air through the instrument, in order that the distribution functions of the drop dimensions not be appreciably distorted in this case, it is necessary to produce considerable volume flows of the air through the trap. In addition, the

velocity of the stream in the trap should exceed by several times the wind velocity at which the microstructure of the clouds are usually measured (see Sec. 9).

6. To determine the counted concentration, the water content, and the specific cross section of the drops it is necessary to expose the receiving part of the glass in the stream for a definite time. The time of exposition of the receiver, in view of the need for working in clouds of different density, should be readily adjustable.

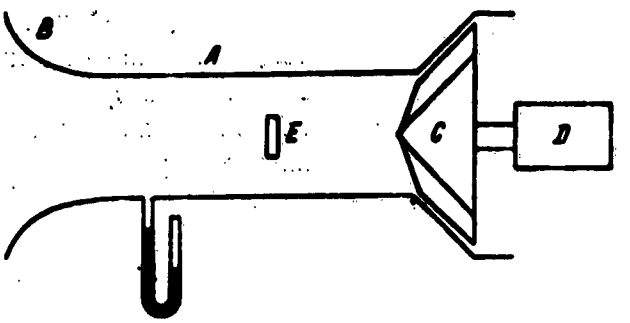

Fig. 55. Diagram of "flow-through" land-based trap for cloud drops.

7. For operation under field conditions it is desirable to construct a trap of small weight, consuming relatively little electricity.

Starting from the foregoing requirements, there was constructed in 1951 the so-called "flow-through" trap for cloud drops, the principal diagram of which is shown in Figure 55. The trap consists of a tube A with a confusor B (in order to produce a uniform stream), into which a fan C, rotated by an electric motor D, produces a stationary homogeneous air stream drawn in from the cloud. A shaft of rectangular cross section, inside of which a long glass plate E can move and serve as a receiver for the cloud drops, passes through tube A. In the center of the tube, on the shaft, is located a shutter, with the aid of which part of the glass plate E becomes uncovered for a definite time. The shutter is opened remotely by means of an electromagnet with the aid of a control panel, on which it is possible to adjust the exposure time of the receiver

during each sampling of the drops* (the control panels and individual units of the traps are described in [27]). Along with the opening of the shutter, the glass plate is displaced in the shaft a distance somewhat larger than the length of the exposure window. This makes it possible to take very rapidly several samples in sequence (18 samples in 20--30 seconds). The velocity of the stream in the trap is measured by means of a U-shaped manometer, one end of which is connected to the atmosphere and the other to the static-pressure receiver located on the wall of tube A in front of the receiving glass plate (at a distance of 1.5--2 calibers of the tube). Since the losses of the total pressure in this part of the tube can be neglected, the difference in pressures measured by the binometer is equal to the velocity head of the stream in the tube.**

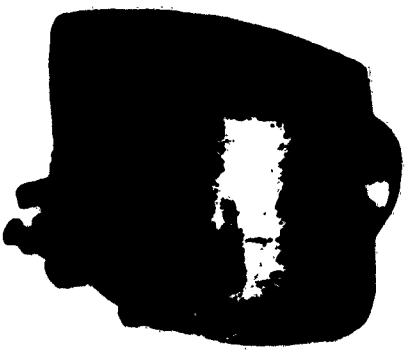

Fig. 56. Overall view of the flow-through trap for the cloud drops.

---

* On a balloon-borne trap (secured to the cable of the tied balloon), the shutter is turned on by means of a clockwork mechanism. In this case two samples are taken successively with different exposures, in order to be able to choose the better exposure from among them.

**The stream in the working part of the trap is the initial portion of the turbulent flow in a tube with rounded entrance (see [60], pages 57--60). In this case at a distance of 2--2.5 calibers from the inlet, the stream is sufficiently homogeneous over its cross section, and the pressure loss is equal, with accuracy to within 4 percent, to the velocity head.

The main parameters of the traps, in accordance with the foregoing, were chosen as follows. Tube diameter D = = 32 mm. Stream velocity in the tube u_∞ = 15 meters/sec (depending on the density of the cloud, work was carried out sometimes at values u_∞ = 20 and 10 meters/sec). The volume flow of air through the tube was Q = 12,000 cm^3/sec. The width of the receiving plate was $2l$ = 4 mm.

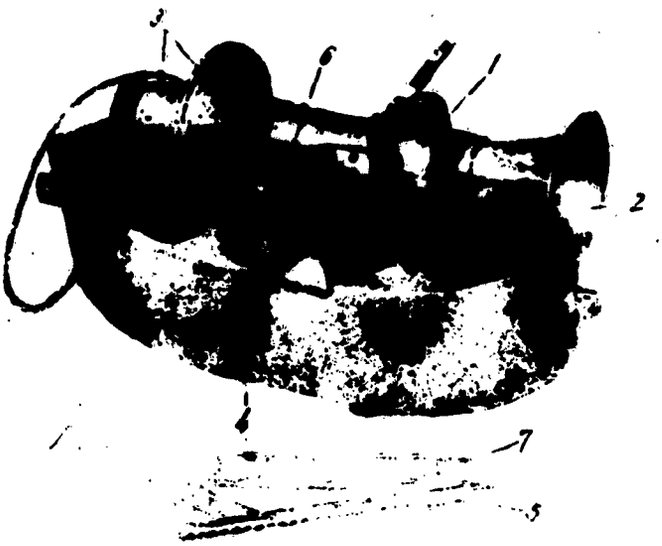

Fig. 57. Flow-through trap for cloud drops with cover removed:

1 -- Tube; 2 -- Confusor; 3 -- Fan and electric motor; 4 -- Shaft; 5 -- Comb with glass; 6 -- Electromagnet displacing the comb with the glass in the shaft; 7 -- Cuvette for storage of the glass with the samples.

These parameters ensure absence of appreciable distortion in the average flow concentration of drops with diameter d < 30 microns at a wind velocity u_w = 2--3 meters/sec [see (I.130), Sec. 9]. The minimum diameter of the drops settling on the receiving glass is $d_{min} \approx 4$ microns [see (I.69), sec. 6]. A description of the computation procedure and the results of the calculations of the

capture coefficients of the traps are given in Secs. 7--8. An overall view of the described traps is shown in Figures 56 and 57. The trap weighs 1.3 kg. The trap motors are fed with storage batteries NKN-10 at 24--30 volts. The battery current is 0.3--4 amp. The battery weighs 20 kg for the land-based model and 7 kg for the balloon model.

The main experimental investigations of the microstructure of the clouds were carried out with traps of the type described above. Recently, however, there have been developed by the expedition traps of several other types, a brief description of which is given below.

The so-called "flow-through trap with drum shutter" is used to trap cloud drops both for land-based conditions and on an attached balloon. The main difference between it and the previously described traps is that the shaft with the receiving glass is replaced by a drum located outside the tube. The axis of the drum is perpendicular to the axis of the tube. Inside the drum there are twenty through openings, in which rods are located, on the end of which are fastened receiving glass plates measuring 3.5 by 15 mm. In the tube there is an opening whose diameter is somewhat larger than the diameter of the rods. After a stationary air stream is established in the tube, an electromagnet pushes out, for a definite time, one of the rods of the drum into the tube. After the rod returns inside the drum, the latter turns through 18°, to permit the next rod to be advanced by the electromagnet into the tube. After one complete rotation of the drum the control of the trap is blocked, so that it is impossible to take a second sample on one and the same glass (rod). Slots 1 mm width are cut through the rods under the glasses (where they have a semicircular cross section), making it possible to illuminate the sample from below when the rod is placed on the stage of a microscope. In the land-based variant, the trap is controlled remotely from a control panel, while in the case of a balloon-borne trap it is controlled by clockwork mechanism. This construction has many advantages. The drops cannot be drawn onto the sample (in the preceding construction the drops could be drawn partially through the shaft of the trap). The trap operates reliably without heating regardless of whether the cloud temperature is above or below zero (in traps with shafts, the shutter has to be electrically heated when working with supercooled clouds). An overall view of the trap with drum shutter is shown in Figures 58 and 59.

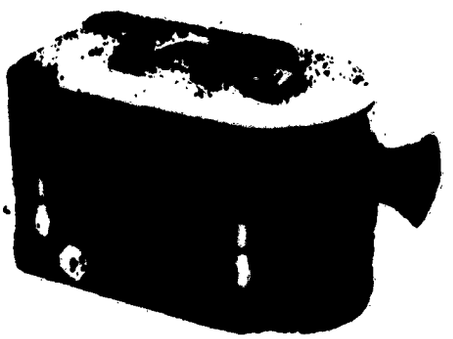

Fig. 58. Overall view of flow-through trap for cloud drops with drum shutter.

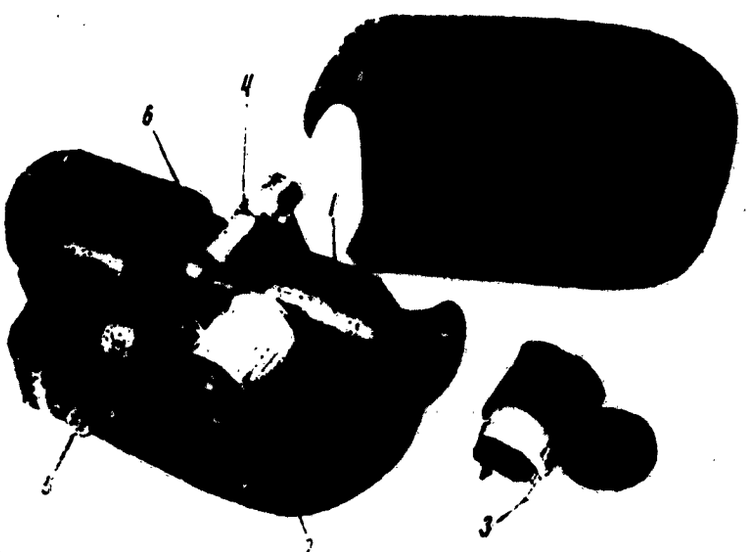

Fig. 59. Flow-through trap for cloud drops with drum shutter, with cover removed:

1 -- Tube; 2 -- Drum; 3 -- Rods with glasses; 4 -- Electromagnet to move the rods; 5 -- Electromagnet to rotate the drum; 6 -- Fan with electromagnet.

Fig. 60. Cassette of jettisoned trap for cloud drops.

To gather samples of cloud drops in clouds, A. V. Chudaykin advanced the idea and constructed a jettisoned trap for cloud drops [73] (Fig. 60).* It represents a closed metallic chamber with a sharp end piece, on the end of which is cut a slot. Inside the cassette are located two coil-cassettes, on which an acetate (non-inflammable) motion picture film, coated with a layer of lampblack (base) and magnesium oxide is wound. When the trap drops through the air, a small windmill rotates the coil, so that the ribbon is rewound from one coil to the other. The ribbon then passes alongside the slot and replicas of the cloud drops that fall on the magnesium layer are produced on it.

The jettisoned trap is first raised by a pilot balloon to the required altitude. At a definite adjustable altitude, a system of pressure chambers connects a pocket dry cell to a wire, which burns out the nylon thread with which the trap is fastened to the pilot balloon. The trap

*Ye. A. Kuz'min and A. A. Ordzhonikidze participated in the further development of the procedure and in perfecting the trap.

begins to drop and at the same time begins to gather samples of the cloud drops. After the trap has dropped to a definite and specified altitude (below the cloud), the system of pressure chambers releases, with the aid of a different heater wire, a parachute fastened to the tail end of the trap. To prevent the trap against striking the earth, a wire-wound shock absorber is used. When the parachute is released, a signal rocket is ignited making it possible to determine the position where the trap will fall.* Figure 61 shows an overall view of the trap with shock absorber and stabilizer.

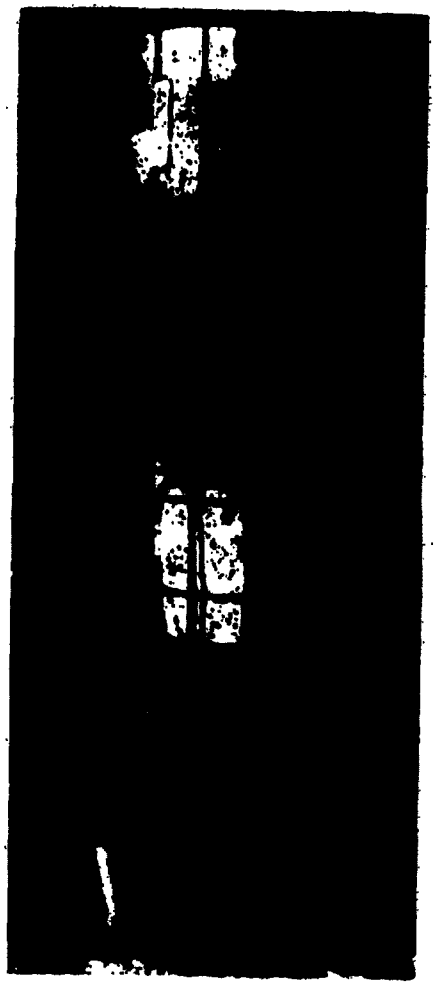

Fig. 61. Overall view of jettisoned trap for cloud drops.

The jettisoned trap makes it possible to gather samples of cloud drops in clouds where airplane flights are dangerous. In addition, it can produce directly, within a short time, a vertical profile of the microstructural characteristics of the cloud. At the present time it is possible to gather with the aid of a jettisoned trap only semi-quantitative information concerning the microstructure of the cloud, since the capture coefficient of the trap and the transfer ratio from the diameter of the replica on the magnesium coating to the diameter of the drop forming the

*A procedure of dropping the trap from an airplane has by now been developed.

replica are not yet known.

It is appropriate to note here that the development of a procedure for obtaining drop replicas on magnesium coating calls for considerable efforts. In many papers by British investigators [106, 107, 122] it was indicated that it is possible to obtain replicas on a simple layer of magnesium oxide, produced by inserting a cold surface in the smoke from burning magnesium. Numerous experiments, carried out in the expedition, have led A. V. Chudaykin to the idea of using a very thin magnesium oxide layer, deposited on a layer of lampblack, in order to obtain the replicas. In one of the latest communications by Squires [123] it is mentioned that Australian researchers have also given up the magnesium coating since 1954 and have resorted to obtaining replicas on a layer of lampblack.

Let us dwell briefly on the description of two other types of traps. The first is intended for capturing cloud drops from an airplane. The airplane trap for cloud drops, constructed by the Central Astronomical Observatory, has along with several positive properties one major shortcoming in that it does not permit the gathering of many samples from a single cumulus cloud, since a considerable time is necessary to reload the trap. Therefore the Elbruss expedition and the Institute of Applied Geophysics have developed for several years various versions of airplane traps, making it possible to gather a relatively large number of samples of cloud drops within a short time. The last variant of the trap, tests of which have already shown favorable results, is shown in Figures 62 and 63. The receiver for the cloud drops is an acetate motion picture film covered with a layer of lampblack and of magnesium oxide and passing next to the slot. Motion of the tape, the speed of which can be regulated in accordance with the operator's wishes, is by means of an electric motor which rewinds the tape from one cassette to another. The slot is located on the front part of the loop-like part of the trap, which imitates quite well a flat plate. The latter circumstance facilitates the theoretical determination of the capture coefficient of the trap (see Sec. 8).

The narrow part of the trap is placed in a special opening, in the front part of the airplane fuselage, so that the receiving part (the slot) is located at a distance of 40 cm from the shell of the fuselage. Such a distance makes certain that the receiving part of the trap is outside the aerodynamic shadow for the drops forming when the

aerosol flows around the obstacle (fuselage). A special device on the trap permits lines to be drawn on the tape from time to time and markers to be produced simultaneously on a loop oscillograph, which records other characteristics of the cloud. This makes it possible to correlate the microstructure of the cloud with different characteristics (temperature, humidity, etc.).

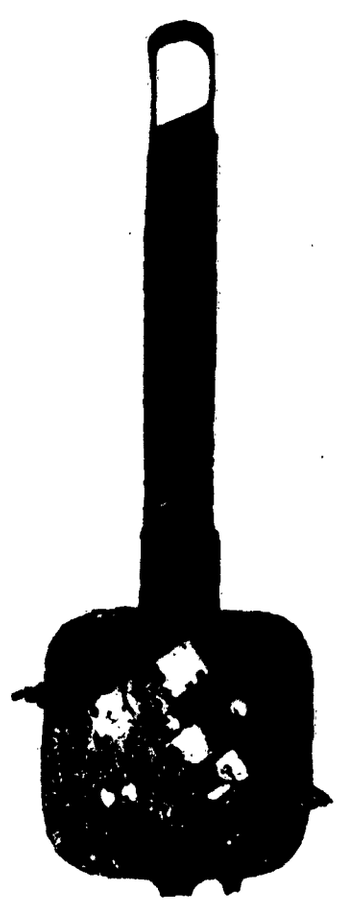

Fig. 62. Overall view of airplane trap of cloud drops.

Fig. 63. Airplane trap of cloud drops with cover removed.

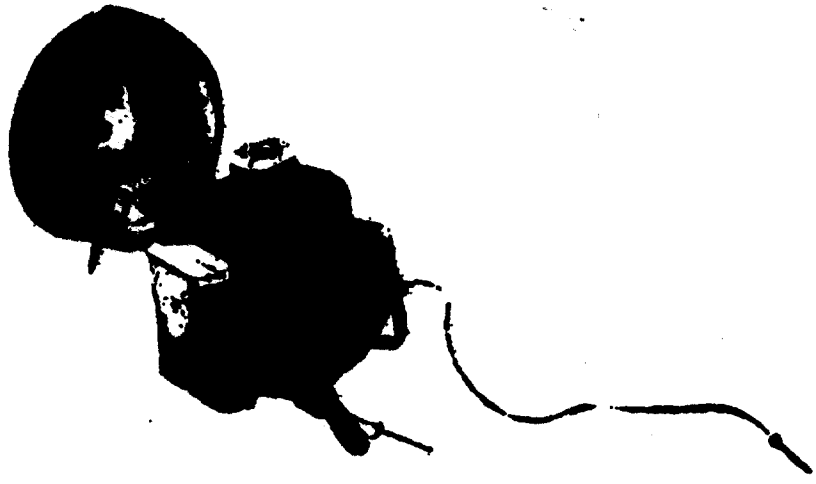

Fig. 64. Automatic impactor for the investigation of solid aerosols.

The latest type of trap used in the Elbruss expedition is an automatic impactor for the investigation of solid aerosols in the free atmosphere. It is used essentially for simultaneous gathering of samples of dust particles at different altitudes (for which purpose the traps are suspended from different parts of the cable of a bound balloon). This trap represents a slot-type impactor (slot 100 microns wide and 1 mm long), in which the dust is drawn through the slot into a balloon with a capacitance of about 300 cm^3, first evacuated to a pressure of approximately 10 mm Hg. The aperture leading to the slot is covered with a rubber cap, which is uncovered at the required instant of time by a spring released by the clockwork mechanism of an alarm clock. Under the slot (at a distance of about 100 microns) is located the receiving glass, covered with a layer of cedar oil. So long as the pressure in the balloon p_b does not exceed half the outside atmospheric pressure p_a, the airflow through the slot has a velocity equal to the local velocity of sound (about 300 meters/sec). The capture coefficient for aerosol particles with diameter greater than 0.5 microns is in this case practically equal to unity, inasmuch as for a slot impactor $E \approx 1$ for $k > 0.32$ [115]. In order not to

deal with variable stream velocity through the slot, when the ratio p_b/p_a becomes larger than 0.5, a system of barometric chambers opens a large aperture in the balloon at the instant when $p_b/p_a = 0.5$. Thus, the dust falls on the receiving glass only when the velocity of the stream through the slot is stationary (equal to the velocity of sound).

An overall view of the trap for solid aerosols is shown in Figure 64. The trap weighs 470 grams (without the clockwork mechanism).

The following methodological investigations were carried out with flow-through traps.

Up to eighteen samples of cloud drops were gathered on the glass of the flow-through traps in succession during the course of a rather long time (sometimes the duration of the gathering of eighteen samples reaches one hour). To protect the gathered samples against evaporation, the shafts with the glass are closed on both ends with covers, and gauze moistened with water is located inside the shaft. The non-hermetic covering of the shaft has made it necessary to check the rate of evaporation of the gathered drops. The check is carried out in the following manner. The glass with the taken sample was microphotographed, and then again inserted into the shaft. After an hour the glass was again photographed. A comparison of the obtained microphotographs of one and the same sample has shown that when the sample is situated in the shaft (when the trap is in the cloud) a certain evaporation of the drops does take place. The average reduction in the calculated water content (during one hour) amounts to about 9 percent.

It must be noted that photography of the gathered eighteen samples of the cloud drops lasts for about one hour. Therefore to protect the drops against evaporation, the glass with the samples is placed between the time that it is removed from the shaft and the end of the photography in a transparent plexiglass cassette, containing moistened gauze. A check, analogous to that described above, has shown that the reduction in the calculated characteristics of the sample, due to the evaporation of the drops during the time that the sample stayed in the cassette, amounting to four hours, is 5.6 percent for the water content, 4 percent for the counted concentration, and 3 percent for

the average diameter. In similar experiments carried out with a protective cassette, the reduction in the calculated characteristics during one hour amounted to 19.3 percent for the water content, 6 percent for the counted concentration, and 5 percent for the average diameter.

Inasmuch as the glass is placed in a vertical position in the shaft of the trap, special experiments were set up in order to determine the character of the runoff of the oil and of the sample of the cloud drops from the glass when the latter is located for a long time in the shaft. In photographing the sample of the cloud drops immediately after their sampling and after definite time intervals, when the drops were located in the shaft in a vertical position, no appreciable displacement of the individual drops relative to reference marks placed directly on the glass was observed. During one hour of being located in the shaft, the displacement of the drops on the sample did not exceed 10 microns.

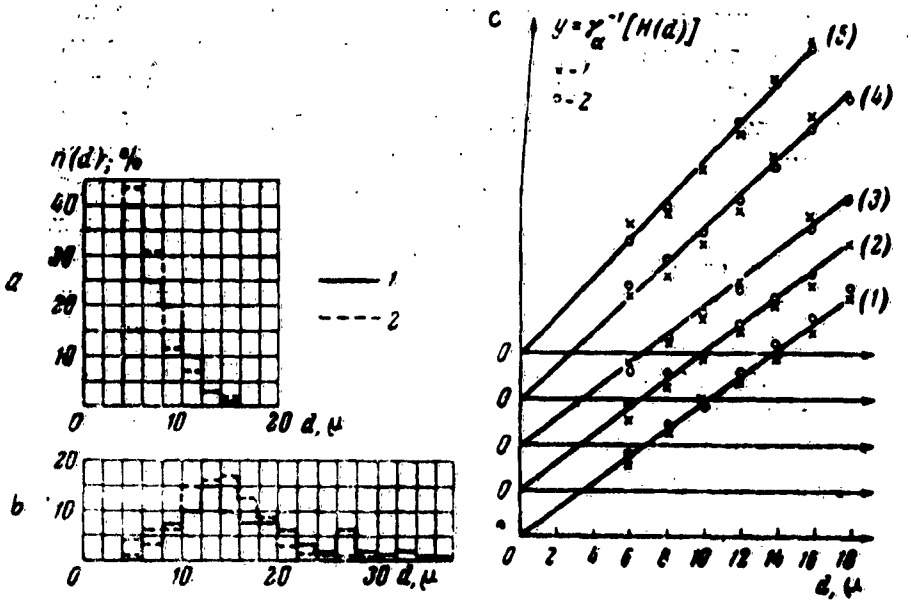

Fig. 65. Comparison of the results of measurements of the microstructure of clouds and fogs, carried out with the aid of the Laktionov instrument and the "flow-through trap": a--Measurements in artificial fog; b--Measurements in natural fog (1--measurements in traps, 2--measurement with the Laktionov instrument); c--Results of comparative measurements in artificial fogs, carried out in 1957 (1--Laktionov instrument, 2--trap).

A check on whether the results of the measurement of the microstructure characteristics by means of traps are representative could not be made by any absolute methods, in view of the fact that there is at present no other sufficiently well developed procedure for measuring the microstructure of coarsely-dispersed aqueous aerosols. Such a check was therefore carried out with the aid of different indirect methods. In 1951 the cross sections of drops, measured with the traps, were correlated with the visibility in clouds [22] and with the measurements of the attenuation of the electromagnetic radiation (in the visible and infrared regions) in clouds and in artificial fogs [4, 5, 6]. In the same year, a comparison was made between the water content measured with the traps and measured by the filtration method [2]. All these measurements have shown that on the average the compared results agree accurate to 20--40 percent. In 1952--1954 a methodical investigation was made to compare the microstructural characteristics obtained on different traps when samples of cloud drops are gathered on them simultaneously. It was established there that all the flow-through traps of the expedition give identical results in measurements of water content, counted concentration, and specific cross section of the drops, with an accuracy of 10 percent (mean-square measurement error), provided one gathers with each trap four samples in succession (with intervals on the order of one second) and the values obtained from these four samples are averaged. The values of the average diameters of the cloud drops are then measured with a great accuracy (3--4 percent). A considerable spread was observed in these experiments in the values of the counted concentration, water content, and specific cross section of the drops, calculated on the basis of processing of individual samples of cloud drops, gathered in succession at short time intervals. An analysis of this circumstance is given in Section 20.

Finally, in 1955 and 1957, a comparison was made between the results of measurements of the microstructure characteristics of clouds and artificial fogs by means of flow-through traps and by means of an instrument developed by A. G. Laktionov [18]. This instrument represents a flow-through automatic installation which makes it possible to determine, by means of the intensity of the light scattered by individual drops, the distribution function of the cloud-drop dimensions and the counted concentration of the drops N. Figure 65 shows the results of these measurements. In Figs. 65a and b the continuous lines represent the results of the measurements with traps, while the

dashed line represents the results obtained with the Laktionov instrument. Figure 65a corresponds to measurements in an artificial fog, and Fig. 65b in natural fog (on a high-mountain station; altitude 2,200 meters above sea level). The results of the comparative measurements carried out in 1957 with artificial fogs are shown in Fig. 65c in the form of rectified distribution diagrams (the rectification is by means of the method described in Sec. 18). The counted drop concentrations N, measured in the described experiments, are listed in Table 18.

Table 18

Number	Figure	$N\ [cm^{-3}]\ (d \geq 4\ \mu)$	
		Trap	Laktionov instrument
1	65,*a*	970	800
2	65,*b*	60	45
3	65,*c 1*	240	297
4	65,*c 2*	214	174
5	65,*c 3*	167	125
6	65,*c 4*	88	66
7	65,*c 5*	78	63

The table shows that the difference between the counted concentrations N, measured by the instruments of both types, did not exceed 25--30 percent. The agreement between the distribution functions of the drop dimensions, obtained in these measurements, can be regarded as good.

In conclusion let us describe briefly the procedure used in the expedition to process the samples gathered by the traps.

To measure the distribution of the photographed drops* by dimensions, the microphotographs were projected by means of a diascope on a ground-glass screen in such a way that the linear magnification of the drops (due to

*The sample of the drops, gathered by the trap, are photographed (on 35-mm film) on five frames from locations located on the axis of the sample (axis of the plate, see Sec. 7). To determine the magnification, the reticle of the object micrometer is photographed on a separate frame.

photography and projection on the screen) was equal to 2,000.* The range of measured drop diameters from 0 to 60 microns was broken up into equal intervals of 2 microns each. The number of drops in each interval was counted on the sample with the aid of a special rule, analogous to that described by V. P. D'yachenko [9]. The rule is broken up into equal intervals of 4 mm each (2 microns times 2,000). At the end of each interval there is a metallic contact, connected to its own counter. In the measurements the rule is so placed against the screen, that its zero division coincides with the edge of the diameter of the image of some drop. By means of a sharply-pointed rod one closes the contact for the interval in which the second end of the diameter is located. This causes operation of the counter of the given interval. The rule with the system of counters are shown in Figure 66.

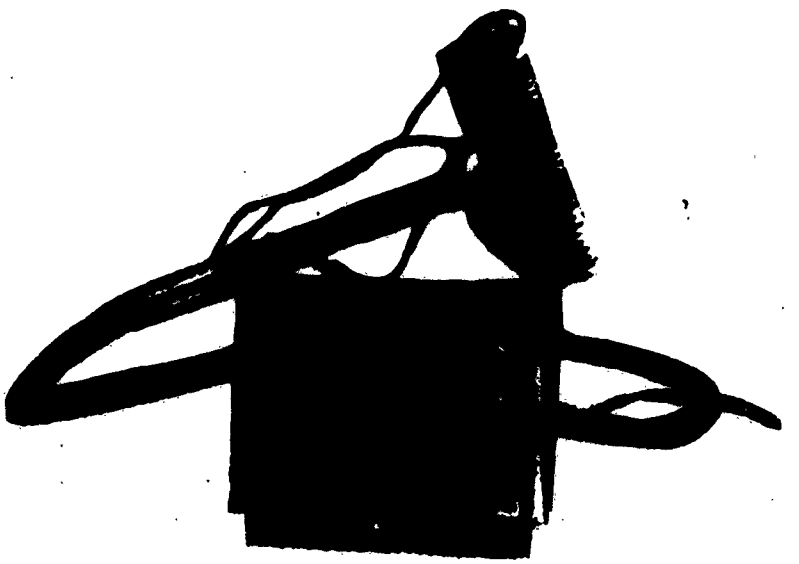

Fig. 66. Overall view of special rule with system of counters.

To simplify the recording of the measurement results, the computation, and the plotting of the corresponding figures, special computation forms were developed.

---

*The linear magnification of the drops during the microphotography was usually approximately 80.

After counting the number of drops in the given i-th interval of dimensions on the microphotograph, $\nu_f(d_i)$, one determines the distribution of the drops by dimensions in the sample, $\nu(d_i)$, by multiplying $\nu_f(d_i)$ by the quantity $1/E(d_i)$, where $E(d_i)$ is the average value of the capture coefficient of the trap for the i-th interval of diameters.

After finding $\nu(d_i)$ one determines the main microstructural characteristics of the cloud by means of the following formulas.

1. Counted concentration of the drops in the given i-th interval

$$n(d_i) = \frac{\nu(d_i)}{w} \ [см^{-3}]. \qquad \text{(III.1)}$$

2. Counted concentration of the drops

$$N = \sum_i n(d_i) = \frac{1}{w} \sum_i \nu(d_i) \ [см^{-3}]. \qquad \text{(III.2)}$$

3. Water content of the drop

$$q = \frac{\pi}{6} \sum_i d_i^3 n(d_i) = \frac{0{,}524}{w} \sum_i \nu(d_i) d_{i\mu} \cdot 10^{-6} \ [г/м^3]. \qquad \text{(III.3)}$$

4. Specific (geometric) cross section of the cloud drops (the geometric cross section of the drops per unit volume)

$$S_g = \frac{\pi}{4} \sum_i d_i^2 n(d_i) = \frac{0{,}785}{w} \sum_i \nu(d_i) d_{i\mu}^2 \cdot 10^{-3} \ [км^{-1}]. \qquad \text{(III.4)}$$

5. Mean-cubic diameter of the drops

$$d_3 = \sqrt[3]{\frac{\sum_i \nu(d_i) d_{i\mu}^3}{\sum_i \nu(d_i)}} \ [\mu]. \qquad \text{(III.5)}$$

6. Mean-square diameter of the drops

$$d_s = \sqrt{\frac{\sum_i \nu(d_i) d_{i\mu}^2}{\sum_i \nu(d_i)}} \quad [\mu]. \qquad \text{(III.6)}$$

In these formulas

$$w = S_{fr} n_{fr} u_{\infty} T \quad [cm^3]. \qquad \text{(III.7)}$$

where S_{fr} -- is the area of the photographed field on one frame, in square millimeters;
n_{fr} -- number of frames taken from the sample;
$S_{fr}n_{fr}$ -- area of the photographed part of the sample;
u_{∞} -- velocity of the stream in the trap in meters per second;
T -- time of opening of the shutter ("exposure of the drops") in seconds;
$d_{i\mu}$ -- average diameter of drops of the i-th interval, in microns.

Since the end of 1957 this arithmetic procedure for processing the samples was replaced by a simplified graphic procedure, a description of which is given in Section 18.

18. ON THE DISTRIBUTION FUNCTION OF CLOUD DROPS BY DIMENSIONS

The physical properties of aerosols depend in essential fashion on the degree of their dispersion. Since the aerosols with which one usually deals are polydispersed, to investigate and analyze the physical processes in them it is necessary to know the function of the distribution of the particles of the aerosol under consideration by dimensions. Thus, for example, information of the dimension distribution functions of cloud drops (or, as they are called in the specialized literature, the spectra of the drops), enter in essential fashion in the theory of various phenomena in clouds: the theory of the growth of cloud drops and precipitation formation, the theory of attenuation of electromagnetic radiation in clouds (visibility), theory of airplane icing, etc.

Of course, it is not convenient to employ the experimentally obtained aerosol-particle distribution functions

when solving theoretical and applied aerosol problems. Therefore, in the investigation of aerosols (clouds) the tendency is always to obtain for the distribution function an analytic expression which approximates in one degree or another the experimental dimension distribution curves of the particles. Of course, the value of the proposed analytic expression will be the greater, the larger the class of experimental curves to which it is applicable. This means that the analytic expression for the distribution function should contain a sufficient number of parameters, variation of which should enclose a great variety of experimental cases. However, the number of distribution parameters should not be likewise very large. Although in the case of a large number of parameters it is possible to obtain an approximation of a very large class of experimental distribution curves, nevertheless an increase in the number of parameters always complicates the determination of the numerical values of the parameters under which the proposed analytic expression characterizes the experimental curve. At the same time, the number of distribution parameters must not be very small, usually two parameters are necessary in order to be able to vary separately the average dimension of the particle and the variance of the distribution.

The complexity and the insufficient knowledge of the physical processes of formation and development of aerosols (clouds) make it difficult to determine theoretically the distribution functions. There are only two known theoretical schemes. In one of them, M. Smoluchowski [57], in an analysis of the coagulation of particles of a highly-dispersed aerosol (initially isodispersed) and assuming that the coagulation constant is the same for all the particles, has derived for the distribution density function an asymptotic formula (for large duration of the coagulation process)*

$$n(d) = Ad^2 e^{-bd^3}. \qquad \text{(III.8)}$$

*We call attention to the fact that formula (III.8) contains only one parameter b, characterizing the distribution (the parameter A characterizes the counted concentration of the particles). It is interesting to note that Smoluchowski's theoretical scheme relates the average aerosol particle dimension with the variance of the distribution function.

Later on this scheme for obtaining the distribution function was applied without sufficient physical justification by Schumann to processes occurring in clouds [120]. The second theoretical distribution is connected with the work of A. N. Kolmogorov [14], who showed that under sufficiently general assumptions concerning the random process of fractionalisation of the particles, the distribution density of the particles by dimensions tends asymptotically to a logarithmic normal distribution

$$n(d) = \frac{1}{\sqrt{2\pi}\,\sigma_l d} \exp\left[-\frac{1}{2\sigma_l^2}\left(\ln\frac{d}{d_0}\right)^2\right], \qquad \text{(III.9)}$$

where σ_l is the dispersion of the logarithm of the particle diameter d; d_0 is the median of the distribution.

Very many empirical formulas have been proposed for the distribution functions of aerosol particles and for cloud and rain drops. A review of these functions for aerosols is given in the book by N. A. Fuks [66, page 18]. For distributions of cloud drops by dimensions, the following functions were proposed (in addition to formula (III.8), [120, 76]). In 1950--1952 Best proposed for the distribution density of cloud and rain drops the expression [81, 82]

$$n(d) = Ad^{n-1}\exp\left[-\left(\frac{d}{a}\right)^n\right]. \qquad \text{(III.10)}$$

On the basis of a processing of the experimental material obtained by A. M. Borovnikov [3], A. Kh. Khrgian and I. P. Mazin proposed in 1952 the following simple and convenient formula [68, 70]

$$n(d) = Ad^2 e^{-bd}. \qquad \text{(III.11)}$$

A similar formula (III.11) was proposed for the distribution density function of rain drops by Ye. A. Polyakova and K. S. Shifrin, on the basis of the processing of obtained or experimental material [48]. Later on the applicability of formula (III.11) to rain drops was confirmed by means of a large amount of experimental material by I. V. Litvinov [39].

In 1952--1953 the Elbruss expedition has gathered with the aid of flow-through traps for cloud particles (see Sec. 17) a large amount of experimental material, which made it possible to analyze in detail the question

of the distribution function of cloud drops by dimensions. Because of the fact that the traps of the expedition made it possible to gather many samples in succession at the same point of the cloud, the material obtained has good statistical certainty, since it was possible to gather as many as 20 thousand drops within a short time interval (15--20 seconds).

An analysis of the applicability of formula (III.11) to the obtained material has shown that this equation is applicable over a large portion of the spectrum of the drops ($d \approx$ 10--30 microns). For small drops, however, ($d \approx$ 4--10 microns), noticeable deviations from formula (III.11) were noticed in many cases. This circumstance has made it necessary to seek a distribution function capable of better approximating the experimental material. Such a distribution was the logarithmic normal law (III.9) [24].

To verify the applicability of the logarithmic normal law to the experimentally obtained sampling of the investigated experiment, there exists a simple procedure (see, for example [67, Chapter VII]). One plots along the abscissa axis the logarithm of the drop diameter, and along the ordinate axis

$$y = \Phi^{-1}[H(d)],$$

where H(d) is the distribution function of the sampling (the drops in the sample), that is, the relative number of drops in the sample with diameter $\leq d$, while Φ^{-1} is a function that is the reciprocal of the normalized normal-distribution function

$$\Phi(x) = \frac{1}{\sqrt{2\pi}} \int_{-\infty}^{x} e^{-t^2/2} dt \text{ *.}$$

---

*If we plot against each value

$$y = \Phi^{-1}[H(d)]$$

on the ordinate axis the corresponding value of H(d), we obtain a so-called probability-logarithmic grid, which is very convenient for the plotting of distribution functions [67, p 115.]

In these coordinates the logarithmically-normal distribution is represented by a straight line. The point where this straight line crosses the abscissa axis gives the value of in d_0, while the slope of the line is equal to σ_l.

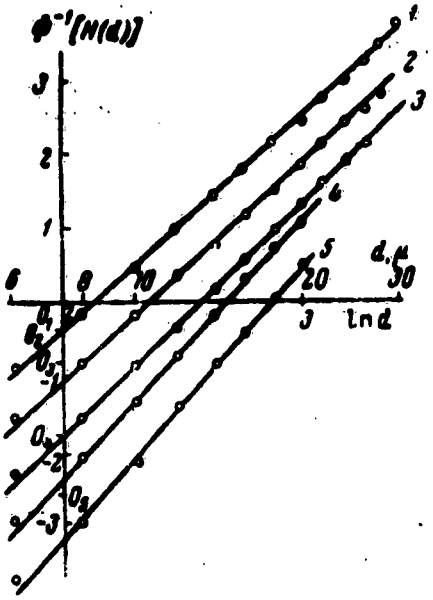

Fig. 67. Rectified accumulated cloud-drop dimension distribution diagrams (probability-logarithmic grid). The number of each curve corresponds to shifted origins in the vertical direction.

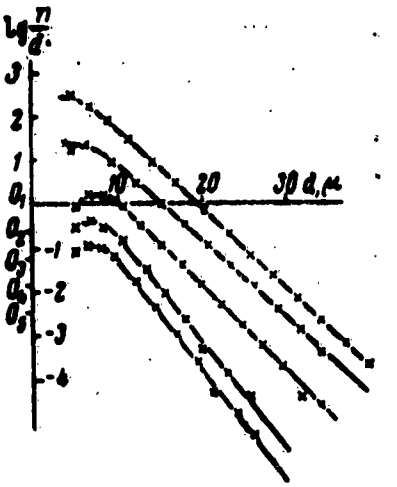

Fig. 68. Diagrams of cloud-drop dimension distribution densities in coordinates d -- lg(nd^{-2}). The curves correspond successively to vertically-displaced origins.

Figure 67 shows the so rectified cloud-drop distribution diagrams, for drops obtained from individual clouds (previously, in view of the small number of drops gathered in individual samples, the various distribution functions were verified for the summary spectra of drops gathered in a series of clouds of the same type -- see, for example, [68]). Figure 67 shows that the obtained experimental data for clouds are well described by a logarithmic normal distribution. Later on the applicability of the logarithmically normal distribution to cloud

drops was confirmed in work at the Central Astronomical Observatory [70].

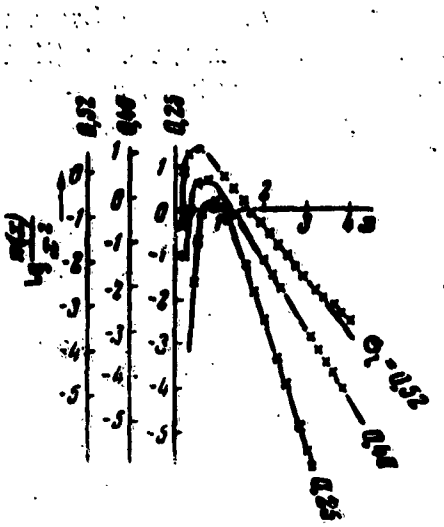

Fig. 69. Diagram of logarithmic normal distributions n(x) in coordinates x; lg (nx^{-2}).

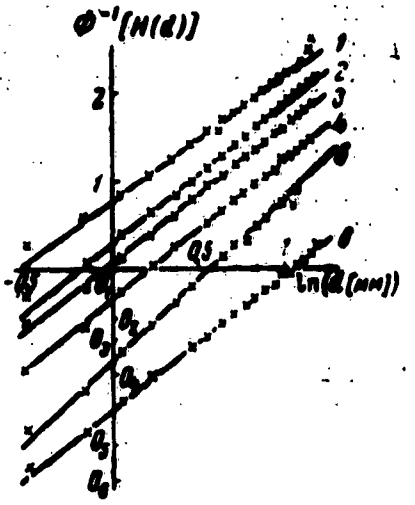

Fig. 70. Rectified (in the probability-logarithmic grid) accumulated diagrams of distribution of the raindrops by dimensions.

To compare the applicability of formulas (III.11) and (III.9), Figure 68 shows diagrams for the same experimental data as in Fig. 67, in coordinates (d, lg$[n(d)d^{-2}]$), where n(d) is the distribution density of the sampling by dimensions. In these coordinates the function (III.11) should be represented by a straight line. Fig. 68 confirms the good applicability of function (III.11), indicated above, for drops with d > 10 microns. For drops with diameter d < 10 microns, Fig. 68 shows a noticeable deviation from the function (III.11). It seems to us that the distribution of A. Kh. Khrgian and I. P. Mazin is a satisfactory approximation of the logarithmic normal law over a large range of drop dimensions. This can be seen from Fig. 69, which shows plots of lg$[n(x)x^{-2}]$, where n(x) is given by formula (III.9).* The plots on Figure 69 show that for

*The unit scale on the abscissa axis of Figure 69 is taken to be the median of the distribution x_0.

the range σ_1 = 0.25--0.52, that is, the range which covers in practice the value of σ_1 encountered in the investigated clouds, the relationship (III.9) is sufficiently well satisfied for $x > x_1 = (0.5--1)x_0$. When $x < x_1$ one observes the characteristic bending of the curve $\lg[n(x)x^{-2}]$, which is noted on almost all the experimental $\lg[n(d)d^{-2}]$ curves (see Fig. 68) corresponding to the distribution shown in Figure 67.

It must also be noted here that the plots of Fig. 68 show that the distribution (III.8) of Smoluchowski-Schumann is not applicable to the obtained experimental material. This follows from the fact that in the coordinates of Fig. 68 the distribution (III.8) should be represented by a cubic parabola $y = - bd^3$. As can be seen from Fig. 68, the latter circumstance does not take place.

An investigation of the materials of the Elbruss expedition on the spectra of the rain drops has shown that for rain drops the logarithmic normal distribution is likewise applicable. This is seen from Figure 70, which shows the rectified diagrams of the summary spectra of several rains of equal intensity I.

Thus, the logarithmic-normal distribution of particles by dimensions is observed in many types of clouds. It is usable for rain drops. A similar distribution is obtained in many other aerosols [66, page 21]. At the same time, the analytic expression of the logarithmic-normal law is rather complicated, and its use is not always convenient in many theoretical papers.

Many empirical distributions of cloud and rain drops, proposed by Khrgian and Mazin [68], Polyakova and Shifrin [48], Marshall and Palmer [105] and others have, in view of their analytic simplicity, certain advantages over the logarithmic-normal law. However, these distributions do not always describe sufficiently well the experimental data over the entire investigated range of dimensions (see, for example, Fig. 68).

One can point out a whole class of functions which have sufficient analytic simplicity and with the aid of which, as shown by an analysis of the experimental materials of the Elbruss expedition, it is possible to approximate well the distributions of cloud drops [30]. Such a class of functions are the gamma distributions, the density of which

is expressed by the formula

$$n_{\alpha,\beta}(d) = \begin{cases} \frac{1}{\Gamma(\alpha+1)\beta^{\alpha+1}} d^{\alpha} \exp\left(-\frac{d}{\beta}\right) & \text{for } d > 0 \\ 0 & \text{for } d \leqslant 0, \end{cases} \qquad \text{(III.12)}$$

where the parameters $\alpha > -1$, $\beta > 0$, and $\Gamma(\alpha+1)$ is the gamma function (equal to $\alpha!$ for integer α). The distribution function corresponding to the density (III.12) (the "accumulated (buildup) function") is

$$P_{\alpha,\beta}(d) = \int_0^d n_{\alpha,\beta}(d)\,Dd = \gamma_{\alpha}\left(\frac{d}{\beta}\right), \qquad \text{(III.13)}$$

where

$$\gamma_{\alpha}(z) = \int_0^z \frac{t^{\alpha}}{\Gamma(\alpha+1)} e^{-t}\,dt \qquad \text{(III.14)}$$

is the incomplete gamma function of index α.*

The main characteristics of the gamma distributions (III.12) are listed in Table 19. This table shows that many of the principal characteristics of the distribution, namely d_2 (which determines the specific geometric cross section of the cloud), d_3 (which determines the water content of the cloud), σ (which determines the width of the spectrum), d_{mn}, d_{mS}, and d_{mq} are proportional to the parameter β. This circumstance will be used later on for a rapid determination of these characteristics. We note also that the normalized distribution function of the geometrical cross section and the volume (water content) of the particles by dimensions are also gamma distributions with indices $\alpha + 2$ and $\alpha + 3$ respectively.

---

*We note that the Khrgian-Mazin distribution for cloud drops and the Polyakove-Shifrin distribution for rain drops represent a particular case of formula (III.12), corresponding to the index value $\alpha = 2$. On the other hand the formula $n(d) = Ae^{-bd}$ of Marshall and Palmer [105] for rain drops corresponds to $\alpha = 0$.

Table 19

Main Characteristics of Gamma Distributions

1. Characteristic function $f(t) = \mathbf{M}(e^{itd})$*	$(1 - i\beta t)^{-(\alpha+1)}$
2. Mode d_m	$\beta\alpha$
3. Diameter of drops giving maximum contribution to the geometrical cross section, d_{mS}	$\beta(\alpha + 2)$
4. Diameter of drops giving maximum contribution to the water content, d_{mq}	$\beta(\alpha + 3)$
5. p–th initial moment $M_p = \mathbf{M}(d^p)$	$\beta^p \frac{\Gamma(\alpha + p + 1)}{\Gamma(\alpha + 1)}$
6. Mean diameter $d_1 = M_1$	$\beta(\alpha + 1)$
7. Mean square diameter $d_2 = \sqrt{M_2}$	$\beta\sqrt{(\alpha + 1)(\alpha + 2)}$
8. Mean–cubic diameter $d_3 = \sqrt[3]{M_3}$	$\beta\sqrt[3]{(\alpha + 1)(\alpha + 2)(\alpha + 3)}$
9. Variance of the distribution $D = \sigma^2 = M_2 - M_1^2$	$\beta^2(\alpha + 1)$
10. Asymmetry coefficient	$2(\alpha + 1)^{-1/2}$
11. Excess coefficient	$6(\alpha + 1)^{-1}$

A comparison of the gamma distribution with the logarithmic-normal distributions shows that the gamma distributions approximate well the logarithmic normal law over a sufficiently large range of dimensions.** Figure 71 shows the "rectified" diagrams of gamma distributions with different indices α in a probability-logarithmic scale. Fig. 71 shows that normal-logarithmic distribution is approximated all the better by the gamma distribution, the higher the index α of the latter, for in this case its plot is closer to a straight line. At the same time, the gamma distribution with higher index α corresponds to smaller values of the variance of the logarithm of the dimension σ_l of the corresponding logarithmic-normal law. This circumstance is also

* The symbol M denotes mathematical expectation.

**This approximation for the values of the index $\alpha = 2$ and $\alpha = 0$ was indicated already in [24] (see Fig. 69).

illustrated in Table 20, which shows the values of $\sigma_l = (tg\varphi)^{-1}$, where φ is the mean angle of inclination of the plots on Fig. 71 for the range of values of the functions $\gamma_\alpha = 0.1$--0.99.

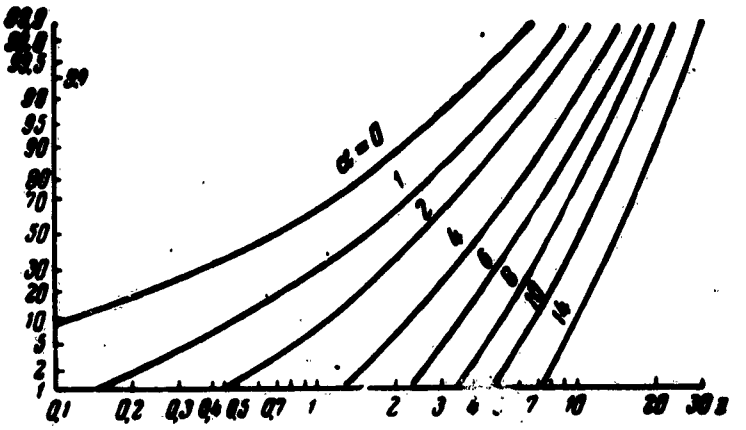

Fig. 71. Diagrams of gamma distributions with different indices α, "rectified" with the aid of the probability-logarithmic grid.

Table 20

α	0	1	2	3	4	6	8	10	14
σ_l	0,92	0,63	0,52	0,45	0,41	0,35	0,30	0,28	0,24

It follows from Figures 67 and 70 that in cloud drops $\sigma_l = 0.27$--0.36, while in rain drops $\sigma_l = 0.45$--0.60. A comparison of these quantities with the data of Table 20 enables us to advance the hypothesis that the distribution of the cloud drops will be approximated by a gamma distribution with index $\alpha = 6$--10, while the distribution of cloud drops will correspond to an index $\alpha = 1$--3.

To verify this hypothesis it would be necessary to analyze the experimental material gathered by the expedition. Such a verification has made it necessary to create a convenient procedure for determining the agreement between the

experimental data and the gamma distributions. Of course, such a verification could be made by constructing rectified graphs of the density of the experimental distribution n(d), for which purpose it would be necessary to plot n(d) in coordinates $(d, \lg[n(d) \cdot d^{-\alpha}])$.* It is faster and more convenient, however, to carry out this verification by rectifying the accumulated experimental distribution diagram. For this purpose one plots along the abscissa axis the diameter of the particles, and along the ordinate axis $y = \gamma_\alpha^{-1}[H(d)]$, where H(d) is the relative number in the sample of drops with diameter $\leq d$ and χ_α^{-1} is a function that is the reciprocal of the incomplete gamma function with index α. If H(d) is in this case close to the distribution $P_{\alpha,\beta}(d) = \gamma_\alpha(d/\beta)$ [see formula (III.13)], then one obtains in these coordinates a straight line $y = d/\beta$ passing through the origin.

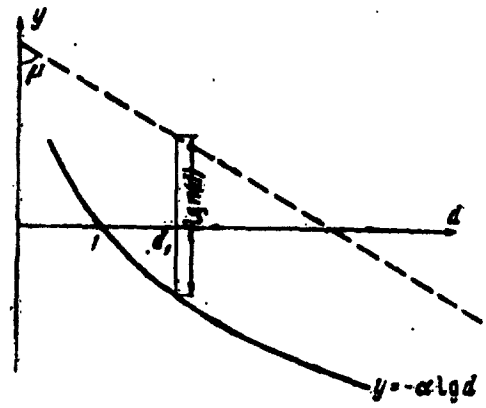

Fig. 72. Method of rectifying the plot of the density of the gamma distributions in coordinates d; lg n. Here the parameter is $\beta = \operatorname{tg} \mu$.

*To simplify these operations it is necessary to plot in Cartesian coordinates (d, y) the curve $y = -\alpha \lg d$, and from it to measure, with the aid of a rule having a logarithmic scale, segments parallel to the y axis and equal to lg n(d) (Fig. 72).

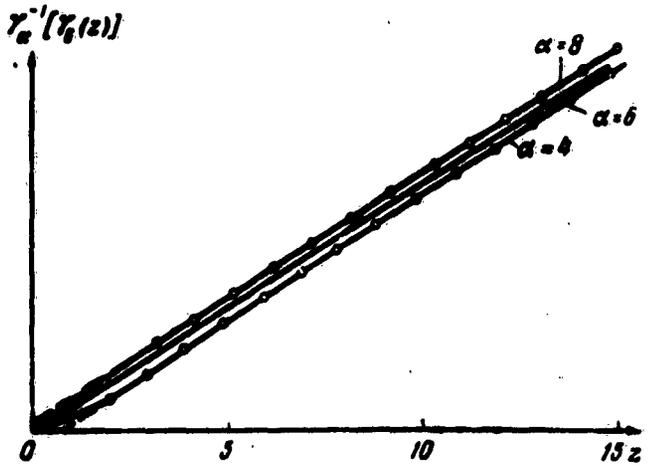

Fig. 73. Location of rectified accumulated gamma-distribution diagrams in the case of incorrect choice of the index α.

Such a construction can be easily realized with the aid of a special rule, on which the value $y = \gamma_\alpha^{-1}[H(d)]$ is laid off in suitable scale (analog of a probability grid for the rectification of the normal or logarithmic-normal distribution). For convenience in use of such a rule, one marks on it not the value of the function y, but the corresponding value H(d). If a set of such rules is available for different indices α, it is easy to choose a value of α such as to yield the best approximation of the experimental curves to a straight line passing through the origin. The choice of α can be simplified by noting that in plotting by the indicated method the gamma distribution with index α_1 with the aid of a scale corresponding to the index $\alpha_2 < \alpha_1$ one obtains a plot consisting of a large almost linear section, the continuation of which does not pass through the origin, but crosses the abscissa axis to the right of the origin. On the other hand, if $\alpha_2 > \alpha_1$, then the continuation of the obtained segment of the line crosses the ordinate axis above the origin. This means that by first choosing the rule in arbitrary fashion, it is possible to judge from the intersection between the continuation of the obtained linear segment of the plot and the abscissa axis

to determine whether the true value of the index α will be larger or smaller than that initially chosen. The foregoing is illustrated in Figure 73, which shows plots of the incomplete gamma function $\gamma_6(z)$, rectified with the aid of scales with indices $\alpha_2 = 6.4$ and 8.

By drawing in the above manner the line that passes in the best fashion through the experimental points, we can determine the distribution parameter β as being the abscissa of that point of the line, at which the ordinate $y = 1$ (Fig. 74). Since such characteristics of the gamma distribution as d_1, d_2, d_3, d_{mn}, d_{ms}, d_{mq}, and σ are proportional to β, we can readily obtain from the same plot the values of these characteristics, provided we mark on the above-mentioned rules segments equal to the corresponding proportionality coefficients. Thus, for example, the mean-square diameter for the gamma distribution is $d_2 = \beta\sqrt{(\alpha+1)(\alpha+2)}$. On the obtained plot, the diameter d_2 will correspond to that point of the line, having the ordinate

$$y = \sqrt{(\alpha+1)(\alpha+2)}.$$

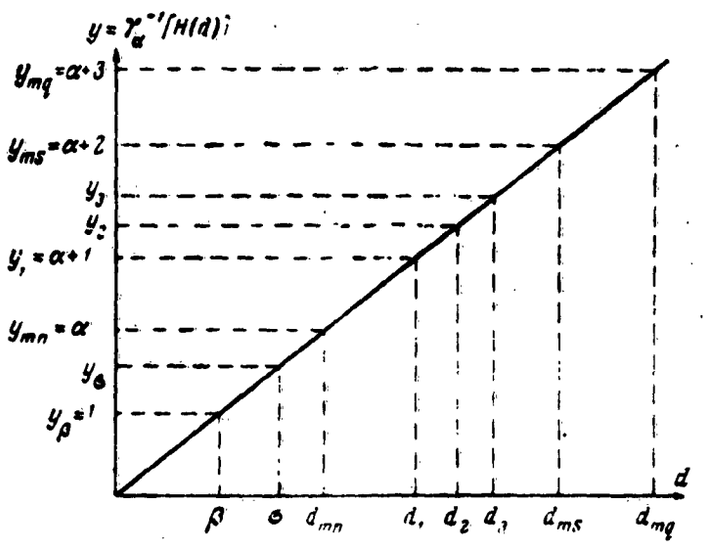

Fig. 74. Diagram for determining the main characteristics of the distribution using the rectified accumulated diagram.

Table 21

Values of the Function $y = \gamma_\alpha^{-1}[H(d)]$

$H(d)$	γ_0^{-1}	γ_1^{-1}	γ_2^{-1}	γ_3^{-1}	γ_4^{-1}	γ_5^{-1}	γ_6^{-1}	γ_7^{-1}	γ_8^{-1}	γ_9^{-1}	γ_{10}^{-1}
0,002	—	—	0,233	0,292	0,862	1,257	1,696	2,183	2,716	3,241	3,891
0,005	—	0,102	0,333	0,656	1,077	1,526	2,023	2,763	3,116	3,697	4,488
0,01	0,011	0,141	0,432	0,828	1,277	1,775	2,319	2,896	3,495	4,127	4,756
0,02	0,022	0,213	0,564	1,014	1,528	2,078	2,679	3,297	3,948	4,604	5,300
0,05	0,051	0,353	0,817	1,364	1,968	2,606	3,278	3,978	4,698	5,420	6,159
0,1	0,106	0,531	1,102	1,742	2,432	3,150	3,891	4,651	5,431	6,144	7,018
0,15	0,164	0,683	1,330	2,038	2,785	3,533	4,345	5,152	5,972	6,790	7,636
0,20	0,224	0,824	1,535	2,295	3,089	3,903	4,736	5,573	6,426	7,269	8,152
0,25	0,288	0,261	1,727	2,534	3,368	4,218	5,081	5,956	6,836	7,725	8,620
0,30	0,358	1,098	1,914	2,763	3,633	4,517	5,410	6,311	7,220	8,133	9,048
0,35	0,432	1,235	2,098	2,988	3,892	4,806	5,727	6,654	7,586	8,522	9,482
0,40	0,511	1,376	2,285	3,211	4,148	5,091	6,039	6,991	7,947	8,905	9,884
0,45	0,598	1,527	2,476	3,439	4,406	5,379	6,352	7,328	8,306	9,294	10,285
0,50	0,693	1,678	2,674	3,673	4,671	5,671	6,670	7,670	8,670	9,730	10,670
0,55	0,799	1,844	2,883	3,918	4,946	5,974	7,000	8,023	9,043	10,062	11,084
0,60	0,917	2,023	3,106	4,176	5,238	6,293	7,344	8,392	9,436	10,477	11,515
0,65	1,051	2,219	3,348	4,456	5,550	6,633	7,712	8,782	9,851	10,916	11,976
0,70	1,204	2,440	3,616	4,763	5,893	7,008	8,113	9,212	10,303	11,387	12,474
0,75	1,387	2,693	3,921	5,111	6,275	7,424	8,561	9,687	10,302	11,919	13,021

Table 21 (continued)

$H(d)$	γ_0^{-1}	γ_1^{-1}	γ_2^{-1}	γ_3^{-1}	γ_4^{-1}	γ_5^{-1}	γ_6^{-1}	γ_7^{-1}	γ_8^{-1}	γ_9^{-1}	γ_{10}^{-1}
0,80	1,610	2,995	4,280	5,516	6,722	7,908	9,078	10,233	11,380	12,523	13,666
0,85	1,896	3,373	4,724	6,014	7,269	8,497	9,706	10,900	12,089	13,280	14,464
0,88	2,121	3,660	5,057	6,386	7,675	8,933	10,169	11,389	12,602	13,797	14,971
0,90	2,303	3,890	5,324	6,684	7,995	9,276	10,533	11,773	12,998	14,208	15,412
0,92	2,527	4,169	5,644	7,036	8,380	9,688	10,970	12,230	13,474	14,708	15,928
0,93	2,681	4,334	5,832	7,244	8,604	9,928	11,224	12,498	13,755	15,002	16,228
0,94	2,814	4,523	6,045	7,482	8,860	10,201	11,512	12,801	14,071	15,331	16,570
0,95	2,986	4,744	6,297	7,756	9,156	10,513	11,846	13,152	14,438	15,710	16,964
0,96	3,220	5,016	6,599	8,099	9,513	10,886	12,248	13,588	14,877	16,159	17,430
0,97	3,507	5,355	6,988	8,509	9,966	11,373	12,747	14,097	15,428	16,735	18,032
0,98	3,910	5,835	7,521	9,086	10,587	12,028	13,438	14,822	16,175	17,516	18,852
0,985	4,200	6,171	7,899	9,491	11,018	12,492	13,917	15,320	16,698	18,059	19,399
0,99	4,600	6,637	8,413	10,043	11,601	13,119	14,599	16,068	17,499	18,907	20,445
0,992	4,825	6,901	8,692	10,350	11,926	13,455	14,929	16,388	17,782	19,185	20,568
0,995	5,330	7,435	9,279	10,975	12,606	14,153	15,676	17,128	18,570	20,001	21,415
0,997	5,840	8,014	9,916	11,650	13,327	14,993	16,457	17,900	19,491	20,870	22,268
g_2	1,414	2,449	3,464	4,472	5,477	6,481	7,483	8,485	9,487	10,488	11,489
g_3	1,817	2,884	3,915	4,932	5,944	6,952	7,958	8,963	9,967	10,970	11,972
g_6	1,000	1,414	1,732	2,000	2,236	2,449	2,646	2,828	3,000	3,162	3,317

This ordinate must be marked on the scale in order to facilitate the determination of the mean-square diameter of the obtained distribution (Fig. 74).

Table 20 lists the values of

$$y = \gamma_0^{-1}[H(d)]$$

and of the coefficients

$$y_2 = \sqrt{(\alpha+1)(\alpha+2)},$$

$$y_3 = \sqrt[3]{(\alpha+1)(\alpha+2)(\alpha+3)},$$

$$y_0 = \sqrt{\alpha+1},$$

which relate the diameters d_2 and d_3 as well as the mean-square deviation of the distribution σ, with the parameter β ($d_2 = y_2\beta$; $d_3 = y_3\beta$; $\sigma = y\beta$). From the data of Table 21 we can readily construct the aforementioned rule.

In Appendix VI is given an example of the described graphic processing of the experimental material.

We now proceed to describe the results of an analysis of the experimental material, obtained in the expedition. Approximately five hundred samples of drops, gathered in natural clouds and in artificial fogs produced in a large chamber of the Elbruss expedition (with volume 500 cu m) were subjected to analysis. The investigations in the clouds were carried out in stratocumulus cloudiness of local origin on the Terskol peak (3,000 meters above sea level). The fogs were produced in the chamber by admitting into it saturated steam from a boiler in which the pressure was 2--3 atm. During the analysis, the graphic treatment described above was applied to previously calculated samples, for which the values of d_2, d_3, the water content q, and the specific cross section S_g were found by the usual arithmetic method (see Sec. 17). Such a processing was carried out in order to establish how well the experimental data were approximated by the gamma distributions and how accurately the above method yielded the values of d_2 and d_3 or, more accurately, the values of q and S_g determined from these values of d_3 and d_2. For the sake of simplicity the processing was carried out with the aid of rules with

indices $\alpha = 0, 2, 4, 6,$ and 8.*

The processing of 497 samples (188 in the chamber and 309 in the clouds) has shown that all satisfied sufficiently well the gamma distribution with one of the indices indicated above. The frequency of occurrence f of different indices α is shown in Table 22.

Table 22

α	0	2	4	6	8
f [%], Chamber	0	3,2	15,4	17,4	64,0
f [%], Clouds	1,0	2,6	12,5	12,5	71,4

It is seen from Table 22 that distributions with indices 0 and 2 are encountered both in clouds and in the investigated fogs very rarely (approximately 4 percent). The most frequently encountered (about 65 percent) are distributions with index $\alpha = 8$. This confirms the considerations advanced above.

Table 23

Relative error, %	$\delta(S_g)$		$\delta(q)$	
	Chamber	Clouds	Chamber	Clouds
$\delta > 10$	1,6	1,3	1,6	3,2
$10 \geq \delta > 5$	6,4	5,5	5,8	11,6
$\delta < 5$	92,0	93,2	92,6	85,2

The accuracy of calculation of the water content q and of the specific cross section S_g by the indicated mtthod can be characterized by means of Table 23, which

*Table 20 shows that the value of σ_f varies very little when α increases from 8 to 14. We therefore confined ourselves to rules with values $\alpha \leq 8$. During the course of the processing it became necessary sometimes to use a rule with $\alpha > 8$. However, the use of a rule with $\alpha = 8$ did not introduce appreciable errors in the determination of d_2 and d_3.

represents the statistics of the errors of the graphical method for all the processed samples. In this table $\delta(S_g)$ and $\delta(q)$ are the relative errors of the graphic method of calculation of S_g and q as compared with the ordinary arithmetic method.*

Table 23 shows that errors larger than 10 percent are encountered rarely (2--3 percent of the cases), and the overwhelming majority of errors (about 90 percent of the cases) do not exceed 5 percent. Therefore it seems that the method described for the processing of the experimental material can be recommended as being sufficiently accurate and less laborious than the ordinary arithmetic method. Since 1957 the processing of the experimental data is carried out in the expedition by the graphic method, and the time consumed in the processing of a single sample has been reduced on the average by a factor 2--3.

An analysis of the experimental material on rain drops has shown that for them there are applicable gamma distributions with the distribution index α for rain lying in the narrow limits $\alpha = 1\text{--}3$, and usually having a value of 2. Thus, for rain drops the distribution (III.11), proposed by Polyakova and Shifrin, can be regarded as fully satisfactory. It is interesting to note that the preliminary results of experiments by I. V. Litvinov on the distribution of the spectra of solid precipitation [40] have shown that in this case the gamma distribution is applicable. It must be noted that for those aerosols, in which a logarithmic-normal distribution of particles by dimensions is sufficiently well realized, it is necessary to expect the gamma distributions to approximate satisfactorily the experimental data.

Summarizing we can state that gamma distributions are one class of distributions which describe well the experimental material for a broad class of aerosols and

---

*Here

$$\delta(S_j) = |1 - (d_{gj}/d_{aj})^6|,$$

and

$$\delta(q) = |1 - (d_{3g}/d_{3a})^3|,$$

where the index "g" pertains to the graphic method and "a" to the arithmetic method.

hydrometeors. Were it possible to establish their applicability to elements of heavy cumulus and thunderstorm clouds, this would facilitate the solution of the difficult experimental problem of investigating the microstructure of these clouds. Indeed, in this case it would be sufficient to determine two distribution parameters α and β, and the counted concentration of the cloud drops. It is possible that this problem could also be solved with the aid of radars with greatly different wavelengths. In this case there would arise a highly operative possibility of investigating the microstructure of clouds in those places, where the introduction of any instruments entails great technical difficulties and is frequently connected with great danger to the lives of the experimenters.

19. CALCULATION OF THE OPTICAL DENSITY OF CLOUDS

As was already noted in the preceding section, the gamma distributions have a sufficient analytic simplicity, making it possible to apply them relatively simply to various theoretical problems. Let us illustrate this circumstance using the calculation of the optical density of clouds [30, 33].

The optical density of a cloud V_{opt} is defined by the equation

$$\frac{I}{I_0} = 10^{-V_{opt} \cdot l}, \qquad \text{(III.15)}$$

where I is the intensity of light passing a distance l in the medium (cloud);
I_0 intensity of light at the beginning of this segment.

The value of the optical density in clouds (characterizing the attenuation of the radiation) for the visible part of the spectrum, where there is no absorption of the radiation by the water, is determined by the scattering of the light by the individual drops. In this case the scattering cross section S_{opt} for radiation with wavelength λ by a drop of diameter d is determined by the formula

$$S_{opt} = \frac{\pi d^2}{4} K(\rho), \qquad \text{(III.16)}$$

where the dimensionless parameter is

$$\rho = \frac{\pi d}{\lambda}. \qquad \text{(III.17)}$$

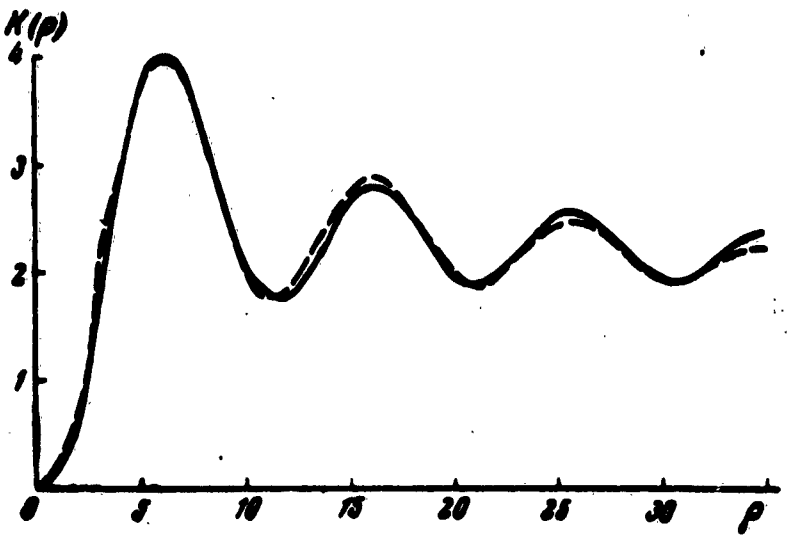

Fig. 75. The function K(ρ) after Penndorf (continuous line) and its approximation by means of formula (III.19) (dashed line).

For water drops the function K(ρ) was calculated by Haoughton and Chalker [98] under the assumption that the refractive index of water is n = 1.333. Figure 75 shows (solid line) a plot of the function K(ρ) from the data of the calculation of Penndorf ([112]; n = 1.33). We note that for large values of the parameter ρ, according to the scattering of radiation by spherical particles, the function K(ρ) → 2 [75].

The optical cross section of cloud particles per unit volume is made up of the optical cross sections of the individual particles, and can be represented on the basis of (III.16) in the form

$$S_{opt} = \lg e \cdot V_{opt} = \int_0^\infty \frac{\pi d^2}{4} K(\rho) Nn(d) Dd, \qquad \text{(III.18)}$$

where N is the counted concentration of the cloud particles.

Taking into account the character of the analytical expression of the distribution n(d) of the cloud particles by dimensions (III.12), the following approximation function $K(\rho)$ was chosen:

$$\left.\begin{aligned} K(\rho) = K_1(\rho) &= +e^{-0.09\rho}\left[1{,}313 + 2{,}012\sin\left(\frac{\pi\rho}{4{,}9} - \frac{5\pi}{6}\right)\right] \quad \text{for } \rho > \pi \\ K(\rho) = K_1(\rho) &= 2{,}307 + 1{,}108\rho - 0{,}2295\rho^2 + 0{,}0346\rho^3 \quad \text{for } \rho \leqslant \pi \end{aligned}\right\} \tag{III.19}$$

The function (III.19) is shown dashed in Figure 75. This figure shows that the function (III.19) approximates the curve $K(\rho)$ sufficiently well. At the same time, substitution of the formula (III.19) in formula (III.18) in lieu of $K(\rho)$ makes it possible to determine readily the integral contained in it. Indeed, substituting formulas (III.12) and (III.19) into the expression (III.18) and introducing the dimensionless quantities

$$\delta = d/\beta \quad \text{and} \quad \Lambda = \lambda/\beta, \tag{III.20}$$

we can readily obtain after simple integration the ratio of the optical cross section of the cloud S_{opt} to its geometrical cross section S_g:

$$\frac{S_{опт}}{S_g} = 2 + 1{,}313\,a^{-(\alpha+3)} + \\ + 2{,}012\,(a^2 + l^2)^{-0.5(\alpha+3)}\sin\left[(\alpha+3)\operatorname{arc\,tg}\frac{l}{a} - \frac{5\pi}{6}\right] - I_4, \tag{III.21}$$

where

$$I_4 = 2{,}307\,\gamma_{\alpha+3}(\Lambda) - 3{,}482\,(\alpha+3)\,\Lambda^{-1}\gamma_{\alpha+3}(\Lambda) + \\ + 2{,}265\,(\alpha+3)(\alpha+4)\,\Lambda^{-2}\gamma_{\alpha+3}(\Lambda) - \\ - 1{,}072\,(\alpha+3)(\alpha+4)(\alpha+5)\,\Lambda^{-3}\gamma_{\alpha+3}(\Lambda), \tag{III.22}$$

$$a = 1 + \frac{0{,}08\,\pi}{\Lambda};\ l = \frac{2{,}015}{\Lambda};\ S_g = \int_0^\infty \frac{\pi d^2}{4} Nn(d)\,Dd = N\frac{\pi d_2^2}{4}. \tag{III.23}$$

We note that in accordance with formula (III.21) the ratio of the optical cross section to the geometric cross section for a given value of the index of the gamma distribution α is a function of only one dimensionless variable Λ. This variable represents a combination of the wavelength λ and the distribution parameter β (or the mean-square diameter $d_2 = \beta\sqrt{(\alpha+1)(\alpha+2)}$).

On the basis of formulas (III.20)--(III.23) we calculated the function $s_\alpha = S_{opt}/S_g$ for the gamma-distribution index values $\alpha = 2, 4, 6, 8$, and 10. The results of these calculations are listed in Table 24. The plots of some of these functions are shown in Figure 76, where the abscissas represent the dimensionless variable $R = \pi d_2/\lambda$, connected with Λ by the relation

$$R = \frac{\pi d_2}{\lambda} = \frac{\pi\sqrt{(\alpha+1)(\alpha+2)}}{\Lambda}. \qquad \text{(III.24)}$$

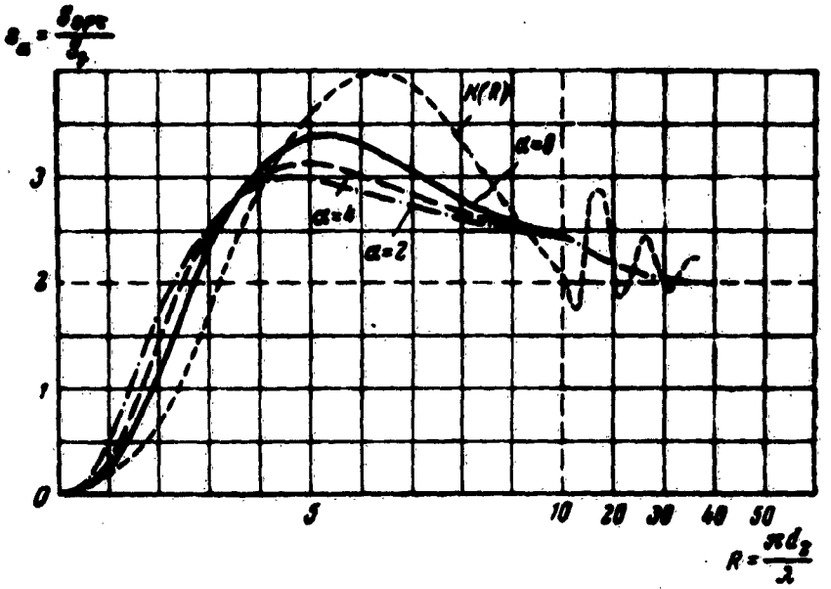

Fig. 76. Plot of the functions $s_\alpha(R)$ for $\alpha = 2, 4, 8$.

With such a choice of the variable, plotted along the abscissa axis, one can see clearly the influence of the index α of the distribution on the value of s_α, for a fixed value of the mean-square diameter d_2. To disclose the

Table 24

Values of the Functions $s_0(\Lambda)$

Λ	α				
	10	8	6	4	2
0,2	2,00	2,00	2,00	2,00	2,02
0,3	2,00	2,00	2,00	2,02	2,06
0,4	2,00	2,01	2,01	2,04	2,10
0,5	2,01	2,02	2,04	2,08	2,17
0,6	2,01	2,03	2,06	2,11	2,23
0,7	2,02	2,04	2,08	2,15	2,28
0,8	2,04	2,06	2,11	2,19	2,32
0,9	2,05	2,09	2,14	2,23	2,37
1,0	2,07	2,11	2,18	2,26	2,43
1,1	2,08	2,13	2,20	2,28	2,50
1,2	2,11	2,16	2,24	2,34	2,56
1,3	2,13	2,19	2,26	2,37	2,60
1,4	2,16	2,22	2,29	2,40	2,63
1,5	2,18	2,24	2,32	2,44	2,71
1,6	2,20	2,26	2,34	2,50	2,75
1,7	2,22	2,29	2,36	2,52	2,77
1,8	2,25	2,31	2,38	2,54	2,81
1,9	2,27	2,33	2,39	2,59	2,89
2,0	2,29	2,34	2,46	2,64	2,91
2,5	2,36	2,40	2,57	2,89	2,96
3,0	2,38	2,49	2,75	3,08	2,74
3,5	2,44	2,67	2,88	3,12	2,57
4,0	2,56	2,89	3,14	3,08	2,31
4,5	2,80	3,13	3,24	2,96	2,05
5,0	3,06	3,20	3,23	2,75	1,88
5,5	3,25	3,38	3,12	2,55	1,66
6,0	3,38	3,35	2,99	2,40	1,43
6,5	3,45	3,31	2,83	2,19	1,22
7,0	3,45	3,21	2,64	1,80	1,07
7,5	3,41	3,06	2,42	1,73	0,95
8,0	3,33	2,91	2,22	1,57	0,93
8,5	3,21	2,74	2,03	1,47	0,81
9,0	3,10	2,59	1,85	1,25	0,66
10	2,84	2,26	1,56	1,03	0,53
11	2,57	1,95	1,14	0,82	0,41
12	2,31	1,68	1,11	0,65	0,31
13	2,05	1,47	0,84	0,52	0,23
14	1,85	1,30	0,79	0,49	0,21
15	1,56	1,09	0,67	0,43	0,18

influence of the polydispersed nature of the cloud on its optical cross section, the same Figure 76 shows dashed the function K(R), calculated from equation (III.19).*

As shown by the plots of Figure 76, when $R > 10$ the influence of the index α on the value of $s_\alpha(R)$ is practically nil.

It is seen further from this same figure that the function s_α has only one maximum. The maximum of the function s_α increases with the index α and ranges between 3.0 and 3.5. The value of R in the external point lies within the limits 4.5--5.5. It increases with increasing α, remaining for all the calculated values of α less than the value $R = 6.4$ which determines the maximum of the function K(R). At small values of R the value of $s_\alpha(R)$ increases with decreasing α. In this range of the parameter R the function $s_\alpha(R) > K(R)$. All these features of mutual location of the curves $s_\alpha(R)$ and K(R) can be simply explained if notice is taken of the following:

a) For a given value of the mean square diameter d_2 (or R) the variance of the gamma distribution $\sigma^2 = d_2^2/(\alpha + 2)$ decreasing with increasing index α;

b) With increasing α, the mode of the gamma distribution d_{mn} approaches the value of the mean square diameter d_2, so that

$$d_{mn}/d_2 = \frac{\alpha}{\sqrt{(\alpha+1)(\alpha+2)}};$$

c) According to Table 21, the geometric cross section of the drops with diameter $d > d_2$** is 2--3 times

* The dashed curve on Figure 76 shows the value of the optical cross section of a monodispersed cloud with the same counted concentration as the considered polydispersed cloud, and for which the diameter of all the drops is $d = d_2$.

**We recall that for the gamma distribution of the number of particles with index α, the distribution of the geometric cross section represents a gamma distribution of index $(\alpha + 2)$ with the same parameter β.

larger than the cross section of drops with $d < d_2$.*

On the basis of the calculated functions $s_\alpha(\Lambda)$, Table 25 was compiled, in which the heavy rectangle contains the ratio S_{opt}/S_g for values of the index $\alpha = 4$ and 8, the mean-square diameter $d_2 = 15$, 10, 7.5, and 5 microns for the wavelength $\lambda = 0.4$, 0.7, and 1.0 micron.** We note here that within the indicated intervals of d_2, α, and λ we can neglect in expression (III.21) the third and fourth terms and assume that

$$s_\alpha = \frac{S_{opt}}{S_g} = 2 + 1{,}313\left[\frac{d_2}{0{,}08\pi\lambda\sqrt{(\alpha+1)(\alpha+2)}}\right]^{\alpha+3} \qquad \text{(III.25)}$$

Table 25

Ratio of Optical and Geometrical Cross Sections of the Drops, s_α.

d_2 [μ]	15	10	7.5	5		1		0.63	
α / λ [μ]	8	8	8	8	4	8	4	8	4
0,4	2,00	2,01	2,02	2,08	2,06	2,90	2,75	3,37	3,15
0,7	2,01	2,04	2,08	2,20	2,18	3,28	3,15	2,06	2,30
1,0	2,04	2,10	2,17	2,32	2,31	2,40	2,55	1,10	1,35
1,24	2,06	2,15	2,25	2,39	2,40	1,75	2,00	0,65	0,87
1,70	2,12	2,26	2,36	2,65	2,62	0,99	1,20	0,30	0,43
3,7	2,40	2,75	3,20	3,18	3,10	0,13	0,24	0,03	0,05
10	3,32	2,40	1,55	0,62	0,85	—	—	—	—

* The property c) of the gamma distributions explains the behavior of the curves $s_\alpha(R)$ for small and large values of R, while the properties a) and b) explain the behavior of the curves $s_\alpha(R)$ in the vicinity of the extremal points.

**That is, in the region of wavelengths where we can put with sufficient approximation $n = 1.33$ and where consequently the calculations of Penndorf for the function $K(\rho)$ [112] are applicable.

An examination of Table 25 shows that in the entire indicated range of variation of the parameters of the phenomenon (d_2, λ, α), the ratio S_{opt}/S_g increases with decreasing mean-square diameter d_2 and is practically independent of α.* The ratio s_α differs very little in this case from the limiting ratio (for large d_2) $s_\alpha = 2$. Only for the extreme values $d_2 = 5$ microns and $\lambda = 1.0$ micron does this ratio exceed $s_\alpha = 2$ by merely 15 percent. Further, in the entire considered range of parameters, the calculations predict an insignificant anomalous dispersion in the optical density (cross section) of the cloud -- for the long-wave radiation the density (cross section) is larger than for the short-wave radiation.** This dispersion is quite negligible for $d_2 = 15$ and 10 microns, and only for $d_2 = 5$ microns does it reach in the visible region ($\lambda = 0.4$--0.7 microns) the value 7 percent, while in the range of wavelengths $\lambda = 0.4$--1.0 microns it reaches a value of 16 percent. Since in clouds the mean-square diameter of the drops usually exceeds 5--6 microns, the data of Table 25 show that in clouds there should be no noticeable dispersion of the optical density (cross section) in the considered range of wavelengths, that is, that the attenuation of the visible and near-infrared part of the spectrum (up to $\lambda = 1$ micron) of the electromagnetic radiation in the clouds should be neutral. This conclusion agrees with the fact already noted in [98], that clouds and fogs do not have any color, and also the results of many measurements of the attenuation in clouds and fogs [4, 5, 6]. In particular, Bricard et al [80] observed in stable fogs either neutral (Fig. 77a) or slightly anomalous-dispersed (Fig. 77b) attenuation of radiation at a wavelength 0.35--3.7 microns. Only in haze (visibility of approximately 1 km, Fig. 77d) and in very rarely encountered small-drop fogs (the authors observed them only in the vicinity of Paris, with visibility of approximately 250 meters, Fig. 77c), they observed a sharply pronounced normal dispersion.

---

*Even at $d_2 = 5$ microns the variation of α from 4 to 8 practically doesn't change the value of s_α. At $d_2 > 5$ the influence of α on the ratio of s_α is even smaller.

**Under the normal dispersion of optical section, it is usually understood that dispersion of the Rayleigh type for which the optical section is inversely proportional to the fourth degree of the wavelength.

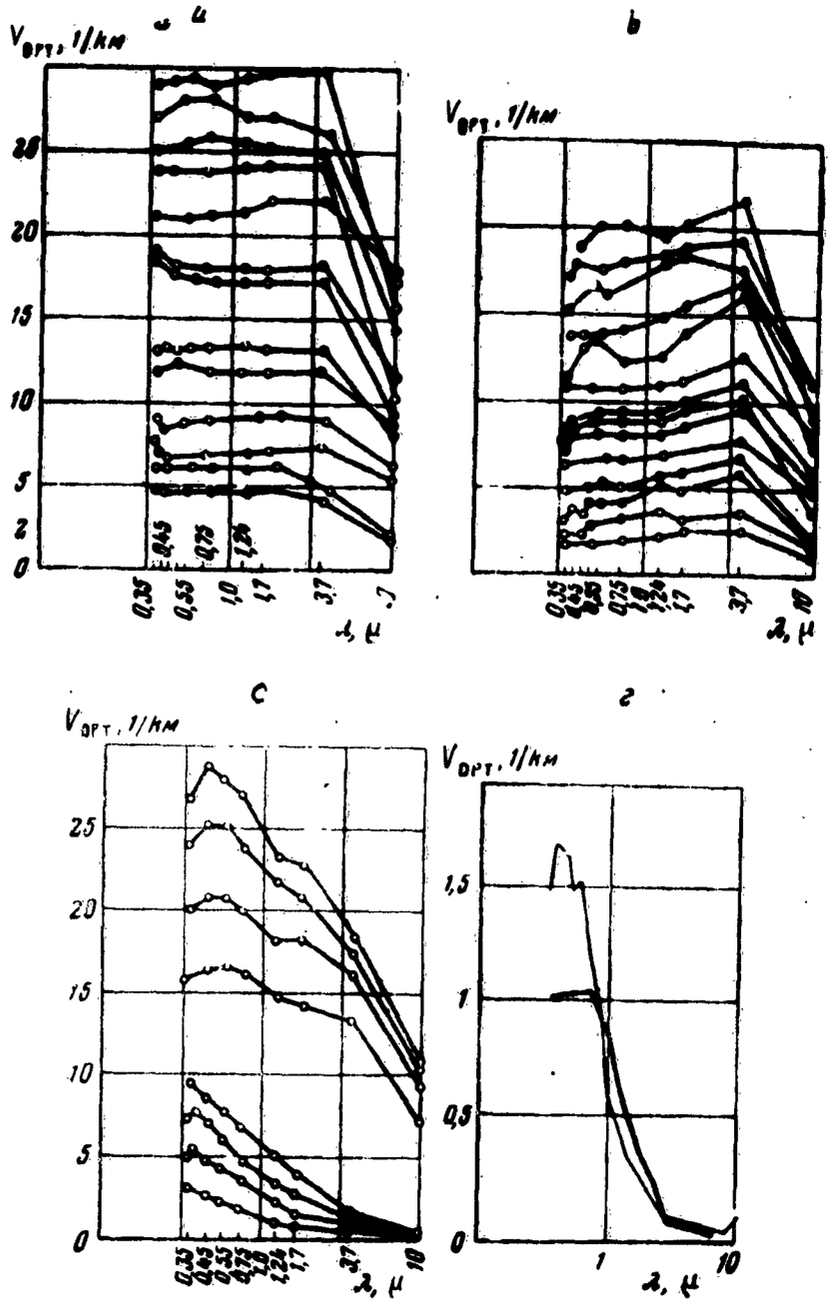

Fig. 77. Attenuation of light in clouds and fogs, according to the data of the experiments of Bricard et al [80].

We note that an appreciable dispersion of optical density can, in accordance with the calculations by formula (III.21), occur only when the indicated range of wavelengths λ and of the mean-square diameters d_2 is extended so as to increase λ or to decrease d_2. In Table 25, outside the outlined rectangle, are shown the values of s_α, calculated additionally for wavelengths λ = 1.24, 1.70, 3.7, and 10 microns* and diameter d_2 = 15, 10, 7.5, 5, and 0.63 microns. Of course, extrapolation of the calculations of the function $K(\rho)$ [112] to the infrared region and the existence of fogs with such small values of d_2 = 1 and 0.63 microns, and also the applicability of the gamma distributions to them call for a special experimental and theoretical analysis. However, it is interesting to a certain degree to estimate in this manner at least the character of variation of the ratio s_α in this expanded region of values d_2 and λ. An examination of the complete Table 25** shows that for large-drop fogs and clouds (d_2 = 10 microns and above) it is possible to expect within the wavelength range λ = 0.4--10 microns an anomalous dispersion in the attenuation of the radiation, and the ratio of the optical densities on the ends of this range should not exceed 1.7. When d_2 = 0.63 microns*** (it is possible that such a value of mean-square diameter is encountered in haze) one can expect normal dispersion of the optical density over the entire range of wavelengths λ = 0.4--10 microns. Here even in the visible region (λ = 0.4--0.7 micron) the ratio of the optical density on the ends of the range can reach

---

*These wavelengths correspond to the well known "transmission windows" of water in the infrared region. Measurements of the optical density in clouds and fogs were carried out in [80] for the same values of λ.

**We note that the difference in the values of s_α, calculated for α = 8 and 4 and for d_2 = 5, 1, and 0.63 microns is very small. When $d_2 > 5$ microns the difference is practically nil.

***For d_2 = 0.63 microns, the value of the parameter R = 5 for λ = 0.4 microns. Corresponding to this value of the parameter R is a maximum of the curve s_α (α = 8) on Fig. 76. Therefore when $d_2 < 0.63$ microns the dispersion of the optical density will be normal over the entire range of wavelengths $\lambda > 0.4$ micron.

values 1.6 and higher. For intermediate values of d_2 ($0.63\ \mu < d_2 < 10\ \mu$) the optical density can have a maximum in the wavelength range $\lambda = 0.4$--10 microns. When $d_2 = 5$ and 7.5 microns, this maximum lies in the region $\lambda \approx 3.7$ microns, and for $d_2 = 1$ micron it lies at $\lambda = 0.7$ microns.

It appears that the result of the experiments of Bricard et al [80], shown in Figure 77, confirm to some degree the foregoing estimate of the dispersion of the optical density (cross section). In these measurements, as was already noted above, in stable clouds there was observed a neutral or anomalous-dispersed attenuation of the radiation up to wavelengths $\lambda = 3.7$ microns, which corresponds to the data of Table 25 for values of the parameter $d_2 = 15$--5 microns (that is, the values of the parameter d_2, usually encountered in fogs). The normal dispersion of the optical density which they obtained for haze offers evidence, apparently, that in the investigated hazes the values of the mean-square diameter d_2 was approximately 1 micron.

In conclusion it must be noted that the procedure developed for determining the optical density of the clouds and fogs can turn out to be useful in the calculation of the attenuation of radiation in regions where the refractive index of water differs greatly from the value $n = 1.33$ assumed in [112], if the corresponding functions $K(\rho)$ are calculated; some calculations of such functions are given, for example, in [100]. If such work were to be carefully done, it could help solve the inverse problem -- the determination of the microstructure of clouds and fogs from the attenuation of radiation of waves of different wavelengths in them.

20. FLUCTUATION OF MICROSTRUCTURAL CHARACTERISTICS OF CLOUDS

As was already mentioned in Section 17, numerous investigations of the microstructure of clouds in the Elbruss expedition have shown that samples of drops, gathered from a cloud by means of several traps simultaneously in one place (the traps were placed at a distance 0.5--1 meter from one another) or by one trap in succession (with intervals of about one second between samples) greatly differ in such microstructural characteristics as the counted concentration, the water content, and the specific cross section of the drops.

Table 26

Coefficients of Variability of Microstructure Characteristics

n	$\bar{N}$	$\delta(N)$	$\bar{q}$	$\delta(q)$	$\bar{S}_\sigma$	$\delta(S_\sigma)$	$\bar{d}_0$	$\delta(d_3)$	$\delta(d_2)$	Date	Time	h
15	190	8	0,23	19	23	17	13,4	6	6	16/VIII 1965	13—60	2
16	160	15	0,37	18	31	18	16,4	6	4	16/VIII 1965	14—65	27
16	320	14	0,48	20	49	16	13,8	5	5	16/VIII 1965	17—65	2
16	350	8	0,17	17	24	13	10,0	6	6	20/VIII 1965	16—67	27
16	190	17	0,11	25	13	21	10,8	4	4	20/VIII 1965	20—60	27
16	720	20	0,14	23	27	19	7,1	4	4	27/VIII 1965	17—60	2
16	1050	16	0,25	22	46	19	7,7	6	7	27/VIII 1965	17—60	27
16	720	19	0,19	14	34	15	7,9	4	4	28/VIII 1965	16—65	2
16	940	20	0,20	28	50	25	8,5	5	5	28/VIII 1965	16—65	27
14	210	13	0,46	18	38	12	16,2	9	8	28/VIII 1965	19—60	27
16	480	15	0,23	27	33	23	10,1	7	7	29/VIII 1965	20—65	2
16	350	15	0,49	7	58	8	11,8	4	4	29/VIII 1965	20—65	27
17	310	26	0,29	44	25	24	10,6	7	5	29/VIII 1965	20—60	2
17	600	11	0,39	15	52	13	10,4	3	7	29/VIII 1965	22—60	27
16	220	23	0,21	28	26	27	11,4	2	3	31/VIII 1965	20—60	2
16	240	26	0,18	36	23	33	11,4	5	6	31/VIII 1965	20—60	27
17	190	16	0,15	26	18	22	11,4	3	5	12/IX 1965	19—60	2
16	170	27	0,15	30	18	33	11,7	7	7	12/IX 1965	19—60	27
Average		17,3	—	23,7	—	20,6	—	5,2	5,4	—	—	—

Remark: Here N — counted concentration of the drops [cm^{-3}]; d_3 and d_2 [microns]; S_σ — specific cross section of the drops [km^{-1}]; q — water content of the cloud [g/m^3]; h — height of top above the earth's surface [meters]; n — number of gathered samples in a given series of observations (the bar above the quantity denotes averaging over all samples of the given series); δ (N), δ (q), δ (S_σ), δ (d_3), and δ (d_2) are the coefficients of variability of N, q, S_σ, d_3, and d_2 (in percent), calculated for a given series of samples. The coefficient of variability is $\delta = \sigma/\mu$, where μ is the mathematical expectation of the quantity and σ is the mean square deviation from μ [67, page 97].

In order to clarify the reasons for this spread, detailed investigations of this phenomenon were undertaken [31]. For this purpose several series of land-based measurements were undertaken in 1955, in clouds, for which 15--18 samples of cloud drops were gathered on one flow-through trap during 30--40 seconds. The results of the statistical processing of the attained samples of drops are represented (essentially) in Table 26.

An examination of Table 26 shows that in the samples of cloud drops obtained in succession within a short time interval, and gathered in one place, the main microstructural characteristics N, q, and S_g, have a considerable spread (the coefficient of variability in the mean for N, q, and S_g is approximately 20 percent).*

To calculate the reasons for this scattering in the results of the measurement, let us estimate the fluctuations of the values of N, q, and S_g, due to the limited volume from which drops are gathered for a single sample. The size of this volume is

$$w = u_\infty S_s T,$$

where S_s -- area of that part of the sample with which the microphotography of the drops is carried out.
T -- time of opening of the shutter of the trap.

In the discussed experiments u_∞ = 15 m/sec, T = = 0.2--0.3 sec, S_s = 0.8--1 mm^2, and consequently w $\approx$3--4 cm^3. This volume contained in the mean N_w = 400--4000 drops. One can therefore expect that the counted concentration of the drops, for example due to the limitation on

*We note that the large value of the coefficient of variability of q, N, and S_g (which is approximately equal to 20 percent), obtained on traps, does not make it possible to obtain a representative value of these quantities according to the data of one sample. It is easy to see that to determine the values of q, N, and S_g with a mean squared error on the order of 10 percent it is necessary to average the results of the measurements over four samples.

the sampling, would have a variability coefficient [71, page 80]*

$$\delta(N) = \frac{1}{\sqrt{Nv}} = 5 \div 1{,}5\%. \qquad \text{(III.26)}$$

However, the estimate of formula (III.26) must be made more precise, taking into account the specific nature of the processing procedure used in the calculation of the value of N, consisting in introducing a correction by taking into account the coefficient E for capture of cloud drops by the receiving unit of the trap (see Sec. 17). Indeed, let the distribution of the drop dimensions in the cloud, normalized to unity, have a density $n(d)\left(\int_0^\infty n(d)\,Dd = 1\right)$. Then in a volume w there is on the average $wNn(d_i)\Delta d$ drops whose diameters lie in the interval $d_i - d_i + \Delta d$.** On the photographed area S_0 of the sample there are on the average $\nu_i = wNE(d_i)n(d_i)\Delta d$ drops, whose dimensions are in the mentioned interval. The actual number of these drops, N_i, on the separately taken sample, obeys the Poisson distribution [71, page 80]:

$$p(N_i) = \nu_i^{Ni}\frac{e^{-\nu_i}}{N_i!}. \qquad \text{(III.27)}$$

This distribution has a mathematical expectation

$$\mu_i = \nu_i, \qquad \text{(III.28)}$$

and a variance

$$\sigma_i^2 = \nu_i = wNE(d_i)n(d_i)\Delta d \qquad \text{(III.29)}$$

---

*In a limited sampling the number of particles obeys a Poisson distribution, for which the variability coefficient is $\delta = 1/\sqrt{\nu}$, where ν is the average number of particles in the sample.

**We recall that in the procedure used by the expedition to process the samples the diameters of the drops were subdivided into intervals of width $\Delta d = 2$ microns.

and a variability coefficient

$$\delta_i = \frac{\sigma_i}{\mu_i} = \frac{1}{\sqrt{\nu_i}} = \frac{1}{\sqrt{E(d_i)}} \cdot \frac{1}{\sqrt{wNn(d_i)\Delta d}}. \qquad \text{(III.30)}$$

Relation (III.30) shows that the variability coefficient of the number of drops of a given interval of dimensions, gathered on the photographed part of the sample, increases with decreasing $E(d_i)$, w, N, $n(d_i)$, and Δd. It can become very large in that part of the spectrum where $n(d_i)$ is small (that is, for large drops), and where $E \to 0$, that is, when d_i approaches the minimum diameter (d_{min}) of the drops still captured by the trap (see Sec. 17). Consequently, relation (III.30) shows that on the ends of the spectrum of the gathered drops the representation of the measurement always becomes very small.

Let us estimate now the coefficient of variability of the quantities N, q, and S_g, defined by the formulas

$$N = \frac{1}{w} \sum_i \frac{N_i}{E(d_i)}, \qquad \text{(III.31)}$$

$$q = \frac{1}{w} \sum_i \frac{\pi d_i^3}{6} \frac{N_i}{E(d_i)}, \qquad \text{(III.32)}$$

$$S_g = \frac{1}{w} \sum_i \frac{\pi d_i^2}{4} \cdot \frac{N_i}{E(d_i)}. \qquad \text{(III.33)}$$

Formula (III.31) shows that the counted concentration N can be regarded as a random quantity, equal to the sum of the independent random quantities $N_i/wE(d_i)$.* Inasmuch as

*Although the mean values of the quantities $N_i/wE(d_i)$, which are equal to $\nu_i/wE(d_i) = Nn(d_i)\Delta d$, are interrelated by a functional dependence, the quantities $N_i/wE(d_i)$ themselves can be regarded as random independent quantities, since in a given sample the deviation of N_i from its mean value ν_i for different values of d_i (different intervals) are independent of each other.

the mathematical expectation and the variance of a sum of independent random quantities is equal to the sum and mathematical expectations and variances, respectively, of the components [67, page 105], we have

$$\mu(N) = \sum_i \mu\left(\frac{N_i}{wE(d_i)}\right) = \sum_i \frac{\nu_i}{wE(d_i)} = N\sum_i n(d_i)\,\Delta d \quad \text{(III.34)}$$

and

$$\sigma^2(N) = \sum_i \sigma^2\left(\frac{N_i}{wE(d_i)}\right) = \sum_i \frac{\nu_i}{w^2E^2(d_i)} = \frac{N}{w}\sum_i \frac{n(d_i)\,\Delta d}{E(d_i)}. \quad \text{(III.35)}$$

It follows from formulas (III.34) and (III.35) that the coefficient of variability of the countel concentration N of the cloud drops, due to the limited sampling of the drops in the sample and the processing procedure of the gathered material, is

$$\delta(N) = \frac{A}{\sqrt{N\bar{w}}}, \quad \text{(III.36)}$$

where

$$A = \frac{\sqrt{\sum_i \frac{n(d_i)\,\Delta d}{E(d_i)}}}{\sum_i n(d_i)\,\Delta d}. \quad \text{(III.37)}$$

Analogously from formulas (III.32) and (III.33) we obtain expressions for the variability coefficients of the water content q and the specific cross section S_g, due to the same causes

$$\delta(q) = \frac{B}{\sqrt{N\bar{w}}}; \quad \delta(S_g) = \frac{C}{\sqrt{N\bar{w}}}, \quad \text{(III.38)}$$

where

$$B = \frac{\sqrt{\sum_i \frac{d_i^6\, n(d_i)\,\Delta d}{E(d_i)}}}{\sum_i d_i^6\, n(d_i)\,\Delta d}; \quad C = \frac{\sqrt{\sum_i \frac{d_i^6\, n(d_i)\,\Delta d}{E(d_i)}}}{\sum_i d_i^6\, n(d_i)\,\Delta d}. \quad \text{(III.39)}$$

An estimate of the coefficients A, B, and C can be made by replacing in formulas (III.37) and (III.39) summation by integration with respect to d within the limits from d_{min} to ∞, and approximating the distribution $n(d_i)$ by a gamma distribution (see Sec. 19). Calculations by means of formulas (III.37) and (III.39) can be readily carried out by taking it into account that in the experiments under consideration the capture coefficient E is well approximated by the expression

$$\frac{1}{E} = 1 + \frac{70}{d^2 \mu}. \qquad \text{(III.40)}$$

The results of such calculations are represented in Table 27.

Table 27

d_0 [μ]	8		16	
c	4	8	4	8
A	2,5	2,5	1,6	1,4
B	1,4	1,2	1,4	1,2
C	1,8	1,5	1,8	1,5

Simultaneous examination of Tables 26 and 27 shows that in accordance with formulas (III.36) and (III.38) the coefficients of variability $\delta(N)$, $\delta(q)$, and $\delta(S_g)$ should not exceed 6--8 percent, if their values are determined by the limitation on the sampling of the drops in the tests. Actually, the values of $\delta(N)$, $\delta(q)$, and $\delta(S_g)$ are two or three times larger than this quantity. An analysis of the remaining errors, due to the different operations during the process of determination of N, q, and S_g shows that they cannot lead to such large coefficients of variability in the results of the measurement of these microstructural characteristics of the cloud (see, for example [3]). It is therefore natural to suggest that the described fluctuations of these characteristics are inherent in the cloud itself and are not connected with the measurement procedure. The latter conclusion cannot be something unexpected to anyone who has been inside a cloud and observed it with an illuminated projector. We can always see here inside the

cloud puffs of different optical density, moving in space. It therefore appears that the measured time variations of N, q, and S_g are connected with the spatial fluctuations of these quantities in the cloud with relatively small scale (on the order of 1 meter).* Finally, the fact that the coefficient of variability of the diameters d_2 and d_3 is three or four times smaller than $\delta(N)$, $\delta(q)$, and $\delta(S_g)$ enables us to advance the hypothesis that the disperse nature of the aforementioned puffs of cloud is not very variable. This can denote that the greater variability of $\delta(q)$ and $\delta(S_g)$ is connected with the variability of the counted concentration N, and not with the variability of the distribution function of the drops.**

The presence in the cloud of considerable fluctuations of the specific cross section of the drops S_g can be experimentally verified by drawing in from the cloud air with drops into the working volume of a Topler instrument, in which there is located a photoelectric multiplier behind a Foucault edge. Such an instrument is a good indicator of the appearance of scattering particles in its working volume. Roughly speaking, the readings of the photomultiplier should be proportional to the optical cross section of the scattering particles. Therefore, by recording the photomultiplier readings obtained by aspiration of the air through the instrument, we should observe in the case of fluctuations of the value of S_g, and consequently of the optical cross section, also fluctuations in the readings of the photomultiplier. Preliminary experiments with such an instrument, made in the expedition by V. Avzyanov, have shown that there exist in the clouds appreciable fluctuations of the optical cross section.

It appears that systematic measurements of the described fluctuations of the microstructural characteristics of the cloud can help relate the microstructure of the clouds with the macrostructure of small scale and can be useful in the study of turbulence in clouds.

---

*Equal to the product of the time interval between the samples ($\sim$1 sec) by the average wind velocity ($\sim$0.5--1 m/sec).

**We note here that when the drop distributions in the samples are gathered in succession are approximated by means of gamma distributions, the index α usually remains constant within the given series of samples.

APPENDICES

I. FIELD OF AIR VELOCITIES NEAR THE SYMMETRY LINE AND THE CRITICAL POINT OF THE STREAM

Let us consider two-dimensional symmetrical incompressible stream of air, flowing around a certain obstacle (see Fig. 13). In such a stream the stream function $\psi(x,y)$ is antisymmetrical with respect to y: $\psi(x,y) = -\psi(x,-y)$. Near the symmetry line (small y) the stream function can be expanded in powers of y. From symmetry conditions, this series will contain only odd powers of y and consequently will have the form

$$\psi(x,y) = a_1(x)\,y + a_3(x)\,y^3 + a_5(x)\,y^5 + \ldots \qquad (a.1)$$

It follows therefore that in the vicinity of the symmetry line the velocity components $u_x(x,y)$ and $u_y(x,y)$ have the form

$$\left.\begin{aligned} u_x &= \frac{\partial\psi}{\partial y} = a_1(x) + 3a_3(x)\,y^2 + 5a_5(x)\,y^4 + \ldots \\ u_y &= -\frac{\partial\psi}{\partial x} = -a_1'(x)\,y - a_3'(x)\,y^3 - a_5'(x)\,y^5 - \ldots \end{aligned}\right\} \qquad (a.2)$$

and with accuracy to second-order terms in y they can be represented by

$$u_x = a(x) + 0(y^2);\quad u_y = -y\,[a'(x) + 0(y^2)]. \qquad (a.3)$$

If the stream under consideration is in addition potential, then by virtue of the equality rot u = 0, the equations (a.2) assume the form

$$\left.\begin{aligned} u_x(x, y) &= \varphi(x) - \frac{1}{2!}\varphi''(x)y^2 + \frac{1}{4!}\varphi^{IV}(x)y^4 \dots \\ u_y(x, y) &= -\varphi'(x)y + \frac{1}{3!}\varphi'''(x)y^3 - \frac{1}{5!}\varphi^{V}(x)y^5 \dots \end{aligned}\right\} \qquad (a.4)$$

Near the critical point (origin) of the potential stream under consideration the stream function can be expanded in homogeneous polynomials, which are solutions of the harmonic equation which the function satisfies. By virtue of the aforementioned condition, this expansion will contain only those harmonic polynomials, which contain y to an odd degree. Recognizing that at the origin the velocity components u_x and u_y are equal to zero, we obtain for ψ, u_x, and u_y the expressions

$$\left.\begin{aligned} \psi(x, y) &= a_2xy + a_3(3x^2y - y^3) + a_4(x^3y - xy^3) + \\ &+ a_5(5x^4y - 10x^2y^3 + y^5) + \dots \\ u_x &= a_2x + 3a_3(x^2 - y^2) + a_4(x^3 - 3xy^2) + \\ &+ 5a_5(x^4 - 6x^2y^2 + y^4) + \dots \\ u_y &= -a_2y - 6a_3xy - a_4(3x^2y - y^3) - \\ &- 20a_5(x^3y - xy^3) - \dots \end{aligned}\right\} \qquad (a.5)$$

Let us consider various cases corresponding to equations (a.5).

a) $a_2 \neq 0$. Since the stream flows from the left and $u_x > 0$, we have $a_2 < 0$. Near the origin $\psi \approx a_2xy$ and the stream lines are approximated by hyperbolas $xy = \text{const}$, that is, near the critical point this stream is hyperbolic. Further, equating the stream function to zero. we obtain the two equations:

$$y = 0,$$

$$F(x, y) = a_2x + a_3(3x^2 - y^2) + a_4(x^3 - xy^2) + \dots = 0.$$

The first of these corresponds to current lines along the symmetry line, the second represents the equation of the wall of the obstacle near the critical point. If the wall is convex, then at the point $x = y = 0$ the second

derivative $d^2x/dy^2 > 0$ for the equation $F(x,y) = 0$. But at the origin

$$\frac{d^2x}{dy^2} = -\frac{2F_yF_xF_{xy} - F_x^2F_{yy} - F_y^2F_x}{F_x^3}\Bigg|_{\substack{x=0\\y=0}} = \frac{2a_2}{a_1}.$$

Inasmuch as $a_2 < 0$, the condition $d^2x/dy^2 > 0$ leads to the inequality $a_3 < 0$. This means that $\frac{\partial^2 u_x}{\partial x^2}\Big|_{\substack{x=0\\y=0}} = 6a_3 < 0$. Thus, for a convex wall of the obstacle the first and second derivatives of the component u_x with respect to x are negative at the origin.

b) $a_2 = 0$; $a_3 \neq 0$. Since $u_x > 0$ when $x < 0$, we get $a_3 > 0$. Equating the stream function to zero, we obtain the equation of the wall

$$F(x, y) = a_3(3x^2 - y^2) + a_4(x^3 - xy^2) + \ldots = 0,$$

which can be approximated by

$$F(x, y) \approx a_3(3x^2 - y^2) = a_3(x\sqrt{3} + y)(x\sqrt{3} - y).$$

In this case the origin is a double point for the contour of the wall (an example of such a stream is given below). If not only a_2 but also a_3 vanishes, then we obtain quite analogously that the origin will be a triple point of the contour, etc. Perfectly analogous relations are obtained also for an axially-symmetrical stream. For such a stream equations (a.2) and (a.5) assume the form

$$\left.\begin{aligned} u_z(z, \rho) &= \varphi(z) - \frac{1}{4}\varphi''(z)\rho^2 + \frac{1}{64}\varphi^{IV}(z)\rho^4 - \frac{1}{2304}\varphi^{VI}(z)\rho^6 \ldots \\ u_\rho(z, \rho) &= -\frac{1}{2}\varphi'(z)\rho + \frac{1}{16}\varphi'''(z)\rho^3 - \\ &\quad - \frac{1}{384}\varphi^{V}(z)\rho^5 + \frac{1}{6048}\varphi^{VII}(z)\rho^7 \ldots \end{aligned}\right\} \quad (a.6)$$

and

$$\left.\begin{aligned}\varphi(z,\rho)&=\frac{A}{2}z\rho^2+\frac{B}{4}(4z^2\rho^2-\rho^4)+C(4z^2\rho^2-3z\rho^4)\dots\\ u_z(z,\rho)&=-Az+B(-2z^2+\rho^2)+4C(-2z^3+3z\rho^2)\dots\\ u_\rho(z,\rho)&=\frac{A}{2}\rho+2Bz\rho+3C(4z^2\rho-\rho^3)\dots\end{aligned}\right\}\quad(a.7)$$

All the conclusions with respect to the form of the wall and its connection with the values of the derivatives $\partial u_z/\partial z$ and $\partial^2 u_z/\partial z^2$ for an axially-symmetrical stream are the same as given above for a plane symmetrical stream.

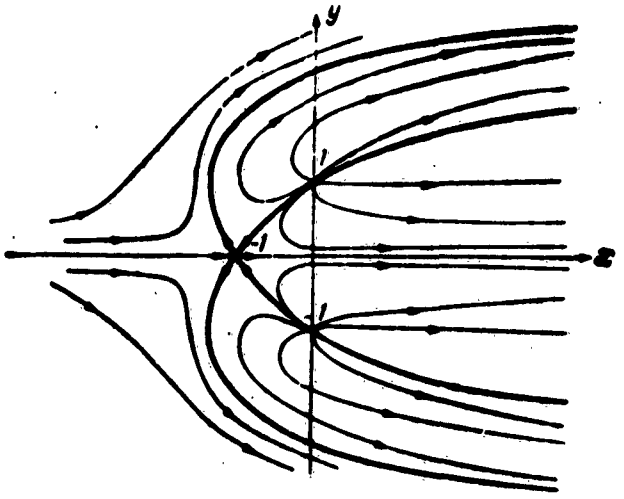

Fig. 78. Potential stream having at the critical point values $\frac{\partial u_x}{\partial x}=\frac{\partial u_x}{\partial y}=0$.

Let us consider in conclusion an example of a plane potential stream, in which at the critical point $\partial u_x/\partial x = \partial u_y/\partial y = 0$. Such a stream can be readily constructed by adding a homogeneous stream with unity velocity to two sources of identical strength (equal to 2π), located at the points $(0, \pm 1)$. Such a summary stream will have a complex potential (if $z = x + iy$)

$$w(z)=z+\ln(z-i)+\ln(z+i)$$

and a stream function

$$\psi = y + \operatorname{arctg} \frac{2xy}{x^2 - y^2 + 1}.$$

From this we can obtain the equation of the wall and expressions for the stream velocity. Figure 78 shows a qualitative picture of the stream lines of the stream under consideration. The critical point has coordinates (-1, 0). At this point $\frac{\partial u_x}{\partial x} = 0$ and $\frac{\partial^2 u_x}{\partial x^2} = +1$. The function $u_x(x, 0) = \varphi(x)$ is plotted in Figure 79. It has a point of inflection at $x = -\sqrt{3}$ and is similar to the functions $u_x(x, 0)$ which are characteristic of a viscous stream. By adding at the point (0,0) a very weak source, we shift somewhat to the left the critical point. Then at this point the value of $\partial u_x/\partial x$ will be negative (very small in absolute value) and $\partial^2 u_x/\partial x^2 \approx +1$. Such a stream will be similar to stream No. 8 of Table 4 (see Sec. 6).

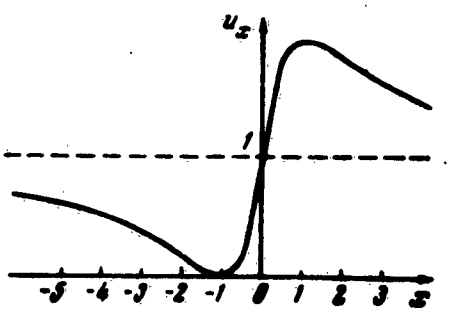

Fig. 79. The function $u_x(x,0)$ for the stream shown in Fig. 78.

II. CALCULATION OF THE FIELD OF THE AIR VELOCITIES NEAR A SYMMETRY LINE AND THE CRITICAL POINT FOR VARIOUS OBSTACLES

A. Triaxial ellipsoid. Let us consider the flow around a triaxial ellipsoid

$$\frac{x^2}{a^2}+\frac{y^2}{b^2}+\frac{z^2}{c^2}=1 \qquad (a.8)$$

by a translational stream of incompressible liquid, the velocity of which at infinity is directed along the O axis and is equal to unity. The potential of the velocity field of such a stream has the form [15, page 355]:

$$\varphi(x, y, z)=x+\frac{xA(x, y, z)}{2-A_0}, \qquad (a.9)$$

where

$$A(x, y, z)=abc\int_{\lambda}^{\infty}\frac{du}{(a^2+u)\sqrt{(a^2+u)(b^2+u)(c^2+u)}}, \qquad (a.10)$$

and $\lambda(x,y,z)$ is the positive root of the equation

$$F(x, y, z)=\frac{x^2}{a^2+\lambda}+\frac{y^2}{b^2+\lambda}+\frac{z^2}{c^2+\lambda}-1=0. \qquad (a.11)$$

On the surface of the ellipsoid $\lambda = 0$, and $A(x,y,z) = A_0$, where

$$A_0=abc\int_{0}^{\infty}\frac{du}{(a^2+u)\sqrt{(a^2+u)(b^2+u)(c^2+u)}}. \qquad (a.12)$$

On the axis $Ox(y = z = 0)$ the function $\lambda = x^2 - a^2$ and the component of the velocity u_x on this axis assumes the form

$$u_x(x)=1+\frac{1}{2-A_0}\left[A(x)+x\frac{dA(x)}{dx}\right], \qquad (a.13)$$

where

$$A(x) = abc \int_{x^2-a^2}^{\infty} \frac{du}{(a^2+u)\sqrt{(a^2+u)(b^2+u)(c^2+u)}}. \qquad \text{(a.14)}$$

The derivative $\partial u_x/\partial x$ necessary for the calculation of the critical Stokes number will in this case be determined by the formula

$$\frac{\partial u_x}{\partial x} = \frac{1}{2-A_0}\left[2\frac{dA(x)}{dx} + x\frac{d^2A(x)}{dx^2}\right].$$

Differentiating (a.14) twice with respect to the coordinate x we readily obtain the value of $\partial u_x/\partial x$ at the critical point (-a,0):

$$\frac{\partial u_x}{\partial x} = -\frac{2a}{2-A_0}\left(\frac{1}{b^2}+\frac{1}{c^2}\right). \qquad \text{(a.15)}$$

Choosing for unity the semiaxis of the ellipsoid, located on the axis Ox(l = a), we obtain the value of the critical Stokes number for the considered triaxial ellipsoid:

$$k_{cr} = \frac{(2-A_0)b^2c^2}{8(b^2+c^2)}. \qquad \text{(a.16)}$$

The value of the coefficient A_0 can be calculated from the following formulas:

a) $$A_0 = \frac{2abc}{(a^2-b^2)\sqrt{a^2-c^2}}\left\{F\left(\arcsin\sqrt{1-\frac{c^2}{a^2}};\sqrt{\frac{a^2-b^2}{a^2-c^2}}\right)-\right.$$

$$\left.-E\left(\arcsin\sqrt{1-\frac{c^2}{a^2}};\sqrt{\frac{a^2-b^2}{a^2-c^2}}\right)\right\}, \qquad \text{if } a^2>b^2>c^2;$$

b) $$A_0 = -\frac{2c^2}{a^2-c^2} + \frac{2abc}{(b^2-a^2)\sqrt{b^2-c^2}} \times$$

$$\times\left\{\frac{b^2-c^2}{a^2-c^2}E\left(\arcsin\sqrt{1-\frac{c^2}{b^2}};\sqrt{\frac{b^2-a^2}{b^2-c^2}}\right)-\right.$$

$$\left.-F\left(\arcsin\sqrt{1-\frac{c^2}{b^2}};\sqrt{\frac{b^2-a^2}{b^2-c^2}}\right)\right\}, \qquad \text{if } b^2>a^2>c^2;$$

c) $$A_0 = \frac{2c^2}{c^2-a^2} - \frac{2abc}{(b^2-a^2)\sqrt{b^2-c^2}} \times$$

$$\times E\left(\arcsin\sqrt{1-\frac{a^2}{c^2}}; \sqrt{\frac{b^2-c^2}{b^2-a^2}}\right), \qquad \text{if } b^2 > c^2 > a^2,$$

where F and E are elliptic integrals of the first and second kind, respectively. Putting in formula (a.12) the axis $b = \infty$, we can readily obtain the value $A_0 = 2c/(a + c)$ for an elliptical cylinder. Choosing as the unit length the semiaxis c, transverse to the direction of the stream ($\ell = c$), we obtain for the critical Stokes number the expression

$$k_{cr} = \frac{1}{4(1+A)}, \qquad (a.17)$$

where $A = a/c$ is the ratio of the longitudinal axis of the elliptical cylinder (relative to the stream) to the transverse axis.

When $A = 1$ we obtain a value $k_{cr} = 1/8$ for transverse flow around a circular cylinder. Putting in (a.17) the axis $a = 0$ ($A = 0$) we obtain a value $k_{cr} = 1/4$ for a non-detached potential stream flowing around an infinite plate (at infinity the stream is perpendicular to the plane of the plate).

Assuming in (a.12) that two of the semiaxes are equal, we obtain after elementary transformations formulas for k_{cr} of the ellipsoids of revolution Nos. 2 and 3 in Table 2. Putting in these formulas $e = 0$, we obtain the value of $k_{cr} = 1/12$ for a sphere; putting on the other hand in formula (2b) for the eccentricity $e = 1$, we obtain $k_{cr} = \pi/16$ for a round disc.

B. Flow around a plate situated in a tube (two dimensional flow with detachment of the jets). N. Ye. Zhukovskiy developed a general method for investigating the motion of a liquid with detachment of the jets [10]. This method, unlike those previously published, makes it possible to obtain solutions for cases with arbitrary number of special points and jets. By the same token, the method of N. Ye. Zhukovskiy makes it possible to find solutions of many problems. Referring the reader to the original article for details we point out only that by specifying a complex

potential w and the variable introduced by Zhukovskiy $\ln(\omega/\zeta)$ (where ω is the velocity on the boundary of the jet and $\zeta = dw/dz$ is the complex velocity) in the form of a function of an auxiliary complex variable t

$$w = \chi(t), \tag{a.18}$$

$$\ln \frac{\omega}{\zeta} = \Phi(t) \tag{a.19}$$

and determining from the character of the problem the singular points of the functions χ and Φ, Zhukovskiy readily constructed a great variety of streams of the indicated type. Among them he solved the problem of flow around a plate in a tube (see Fig. 23).

In this case [10, page 571]

$$\Phi(t) = \frac{i}{2}\arcsin\left[\frac{c^2-e^2}{c(t-e)} - \frac{e}{c}\right] + \frac{i}{2}\arcsin\left[\frac{c^2-e^2}{c(t+e)} + \frac{e}{c}\right] \tag{a.20}$$

and

$$\chi(t) = \alpha \ln \frac{t}{c}, \tag{a.21}$$

where c and e characterize the locations of the singular points of the functions Φ and χ.

To determine from this the connection between the complex coordinate $z = x + iy$ and the complex velocity $\zeta = u_x - iu_y$, we note that

$$e^{\Phi(t)} = \frac{\omega}{\zeta} = \omega \frac{dz}{dw} \tag{a.22}$$

and consequently

$$dz = \frac{1}{\omega} e^{\Phi(t)}\, dw = \frac{1}{\omega} e^{\Phi(t)} \chi'(t)\, dt. \tag{a.23}$$

Integrating the formula (a.23), we obtain $z = z(t)$. Eliminating t from the relation $z = z(t)$ and

$$\zeta = \frac{dw}{dz} = \omega e^{-\Phi(t)}, \tag{a.24}$$

we obtain a connection between ζ and z.

To find in our case, from equation (a.20) the functions $e^{\Phi(t)}$ we proceed in the following fashion.

We introduce the notation

$$\frac{e}{c} = \sin 2\mu, \quad \frac{t}{c} = t_1,$$

$$\lambda_1 = \frac{1 - \frac{e^2}{c^2}}{\frac{t}{c} - \frac{e}{c}} - \frac{e}{c} = \frac{1 - t_1 \sin 2\mu}{t_1 - \sin 2\mu},$$

$$\lambda_2 = \frac{1 - \frac{e^2}{c^2}}{\frac{t}{c} + \frac{e}{c}} + \frac{e}{c} = \frac{1 + t_1 \sin 2\mu}{t_1 + \sin 2\mu}.$$

Then

$$e^{2\Phi(t)} = e^{i \arcsin \lambda_1} e^{i \arcsin \lambda_2} = |\sqrt{1 - \lambda_1^2} + i\lambda_1| \, |\sqrt{1 - \lambda_2^2} + i\lambda_2| =$$

$$= \left| \frac{\cos 2\mu \sqrt{t_1^2 - 1}}{t_1 - \sin 2\mu} + i \frac{1 - t_1 \sin 2\mu}{t_1 - \sin 2\mu} \right| \times$$

$$\times \left| \frac{\cos 2\mu \sqrt{t_1^2 - 1}}{t_1 + \sin 2\mu} + i \frac{1 + t_1 \sin 2\mu}{t_1 + \sin 2\mu} \right| =$$

$$= \frac{t_1^2 - 1 - \cos^2 2\mu + 2i \cos 2\mu \sqrt{t_1^2 - 1}}{t_1^2 - \sin^2 2\mu} = \frac{(\sqrt{t_1^2 - 1} + i \cos 2\mu)^2}{t_1^2 - \sin^2 2\mu}.$$

Consequently

$$e^{\Phi(t)} = \frac{\sqrt{t_1^2 - \sin^2 2\mu}}{\sqrt{t_1^2 - 1} - i \cos 2\mu} \qquad (a.25)$$

and

$$\zeta = \frac{dw}{dz} = \omega e^{-\Phi(t)} = \omega \frac{\sqrt{t_1^2 - 1} - i \cos 2\mu}{\sqrt{t_1^2 - \sin^2 2\mu}}. \qquad (a.26)$$

Further

$$dz = \frac{e^{\Phi(t)}}{\omega} \chi'(t)\, dt = \frac{a}{\omega} \frac{\sqrt{t_1^2 - 1} + i \cos 2\mu}{\sqrt{t_1^2 - \sin^2 2\mu}} \cdot \frac{dt_1}{t_1}. \qquad (a.27)$$

Integrating (a.27) we obtain

$$\frac{\omega'}{a} = \frac{1}{2}\ln\frac{1+\sigma}{1-\sigma} - \frac{1}{2\sin 2\mu}\ln\frac{1+\sigma\sin 2\mu}{1-\sigma\sin 2\mu} + \\ + \frac{\operatorname{ctg} 2\mu}{2}\ln\frac{\sqrt{t_1^2-\sin^2 2\mu} - i\sin 2\mu}{\sqrt{t_1^2-\sin^2 2\mu} + i\sin 2\mu} + C, \qquad (a.28)$$

where

$$\sigma = \sqrt{\frac{t_1^2-1}{t_1^2-\sin^2 2\mu}}.$$

Using the relations (a.26) in the form

$$\zeta_1 = \frac{\zeta}{\omega} = \frac{\sqrt{t_1^2-1} - i\cos 2\mu}{\sqrt{t_1^2-\sin^2 2\mu}} = \sqrt{\frac{\sqrt{t_1^2-1} - i\cos 2\mu}{\sqrt{t_1^2-1} + i\cos 2\mu}},$$

we obtain

$$\sqrt{t_1^2-1} = \frac{i\cos 2\mu\,(1+\zeta_1^2)}{1-\zeta_1^2} \quad \text{и} \quad t_1^2-\sin^2 2\mu = -\frac{4\zeta_1^2\cos^2 2\mu}{(1-\zeta_1^2)^2}$$

and then we readily eliminate t_1 from (a.28):

$$\frac{\omega z}{a} = \ln\frac{1+\zeta_1}{1-\zeta_1} - \frac{1}{2\sin 2\mu}\ln\frac{2\zeta_1 + (1+\zeta_1^2)\sin 2\mu}{2\zeta_1 - (1+\zeta_1^2)\sin 2\mu} + \\ + \frac{\operatorname{ctg} 2\mu}{2}\ln\frac{2\zeta_1\cos 2\mu - (1-\zeta_1^2)\sin 2\mu}{2\zeta_1\cos 2\mu + (1-\zeta_1^2)\sin 2\mu} + C. \qquad (a.29)$$

The integration constant is obtained from the condition

$$\zeta_1 = 0 \text{ for } z = 0.$$

From this we get

$$C = i\frac{\pi}{2}\operatorname{tg}\mu.$$

Further we find from formulas (100) and (102) on pages 570 and 571 of the paper [10] by N. Ye. Zhukovskiy

$$\frac{u_\infty}{\omega} = \operatorname{tg}\mu \quad \text{or} \quad \zeta_1 = \zeta \operatorname{tg}\mu, \tag{a.30}$$

$$\frac{L-l}{L} = \operatorname{tg}\mu\left(1 + \frac{2}{\pi} \cdot \frac{2\mu}{\operatorname{tg} 2\mu}\right), \tag{a.31}$$

$$\frac{\omega}{\alpha} = \frac{\pi}{2L \operatorname{tg}\mu}. \tag{a.32}$$

Substituting the values of ω, u_∞, and α from equations (a.30) -- (a.32) into (a.29), we obtain ultimately

$$\frac{\pi z}{2L \operatorname{tg}\mu} = \ln \frac{1+\zeta \operatorname{tg}\mu}{1-\zeta \operatorname{tg}\mu} - \frac{\operatorname{ctg}\mu}{2} \ln \frac{1+\zeta}{1-\zeta} - \frac{\operatorname{tg}\mu}{2} \ln \frac{1+\zeta \operatorname{tg}^2\mu}{1-\zeta \operatorname{tg}^2\mu}, \tag{a.33}$$

where μ is determined from (a.31).

In the vicinity of the critical point z and ζ are small, and from (a.33) we get

$$\frac{\pi z}{2L \operatorname{tg}\mu} = -(4 \operatorname{tg}\mu \operatorname{ctg}^2 2\mu)\zeta,$$

that is,

$$\zeta = -\frac{\pi}{8L} \frac{\operatorname{tg}^2 2\mu}{\operatorname{tg}^2 \mu}.$$

Consequently for a plate in a tube we have

$$k_{cr} = \frac{2L \operatorname{tg}^2 \mu}{\pi \operatorname{tg}^2 2\mu}. \tag{a.34}$$

C. <u>Impact of a jet leaving a nozzle against an infinite plane</u>. Such a flow occurs in so-called slot impactors, a diagram of which is shown in Figure 80. From a nozzle of width $2l$ there flows out a jet striking a plane located at a distance h from the end of the nozzle. To construct the velocity field in such a stream we use the aforementioned work of N. Ye. Zhukovskiy [10]. In this case*

*In the formula for χ [10, page 534] we assume $\gamma = 0$, since we are considering the impact of a jet against an infinite plane [10, page 595, formula (135)]. In the case under consideration $\theta_1 = 0$ and $\gamma = l = 0$.

$$\Phi(t) = \frac{i}{2} \arcsin\left[\frac{2c_1^2c^2}{c_1^2 - c^2} \cdot \frac{1}{t^2} - \frac{c_1^2 + c^2}{c_1^2 - c^2} + i\frac{\pi}{4}\right], \qquad (a.35)$$

$$\chi(t) = -\alpha \ln \frac{t^2 - c^2}{\pi^2/16} + 2\pi i \qquad (a.36)$$

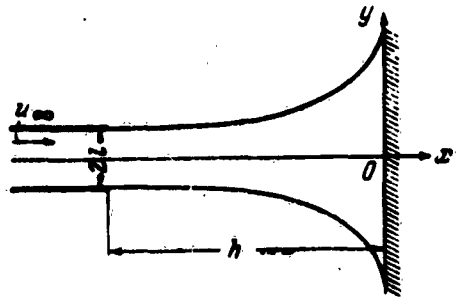

Fig. 80. Diagram of the jet leaving the nozzle and flowing over the infinite plane (diagram of the stream in the slot impactors).

and in addition [10, page 298, formulas (133) and (140)]:

$$\frac{h}{l} = \operatorname{tg}\frac{\nu}{2}\left[1 - \frac{2}{\pi \sin\nu} \ln \operatorname{tg}\left(\frac{\pi}{4} - \frac{\nu}{2}\right)\right] \qquad (a.37)$$

and

$$\omega = u_\infty \operatorname{ctg}\frac{\nu}{2} = \operatorname{ctg}\frac{\nu}{2}, \qquad (a.38)$$

where

$$\cos\nu = c/c_1.$$

In analogy with the preceding case, after elementary but laborious transformations we obtain

$$iz\frac{\pi}{l}\cos^2\frac{\nu}{2} = \operatorname{arc\,tg}\frac{2\zeta_1}{i\sin\nu(1+\zeta_1^2)} +$$

$$+\cos\nu \cdot \operatorname{arc\,tg}\frac{2\zeta_1\cos\nu}{i\sin\nu(1-\zeta_1^2)} - 2i\cdot\sin\nu \operatorname{arc\,tg}\zeta_1. \qquad (a.39)$$

where

$$\zeta_1 = \zeta/a.$$

In particular, as $h \to \infty$, the quantity $\nu \to \pi/2$, and in this case

$$s = -\frac{2l}{\pi}\left[\ln\frac{1-\zeta_1}{1+\zeta_1} - 2\operatorname{arctg}\zeta_1\right]. \qquad (a.40)$$

From (a.39) we obtain

$$\left(\frac{ds}{d\zeta}\right)_{s\to 0} = -\frac{2l}{\pi}\cos^{-4}\frac{\nu}{2}$$

and

$$k_{cr} = \frac{1}{2\pi}\cos^{-4}\frac{\nu}{2}. \qquad (a.41)$$

In the particular case when $h = \infty$ ($\nu = \pi/2$) we have:

$$k_{cr} = \frac{2}{\pi}.$$

Table a.1

h/l	k_{cr}	h/l	k_{cr}
0	0,159	1,885	0,465
0,165	0,162	2,385	0,555
0,522	0,191	3,014	0,610
0,991	0,268	∞	0,636
1,330	0,343		

In Table a.1 is tabulated the dependence of the critical Stokes number on the distance h from the fitting, from which the jet of air emerges, to the plane. Usually this distance in slot-type impactors is on the order of the width of the slot ($h/l \approx 2$). As shown by the data of Table a.1, a change in the ratio h/l within the limits 1.8--3 changes k_{cr} insignificantly (by 30 percent) and d_{min} insignificantly (by 15 percent).

III. QUALITATIVE ANALYSIS OF THE TRAJECTORIES FOR THE CASE OF TWO DROPS OF LIKE CHARGES

To construct a general pattern of the trajectories described by equation (II.12) and to separate from them the limiting trajectories, let us investigate the singular points of the system (II.5), confining ourselves to the case $\alpha > 0$ (drops with like charges). In the case under consideration [$f(r) = 1$, stream function determined by equation (II.10)], equation (II.5) assumes the form

$$\left.\begin{aligned} v_r &= \frac{\cos\theta \cdot F_1(r) - \alpha}{r^2} \\ v_\theta &= -\frac{\sin\theta F_1'(r)}{2r}. \end{aligned}\right\} \qquad (a.42)$$

The singular points of the system (a.42) will be the points at which the ratio v_r/v_θ is indeterminate, which will occur in three cases:

$$\text{I) } \sin\theta = 0;\ r \neq 0;\ \alpha = \cos\theta F_1(r);\ \text{II) } r = 0;$$

$$\text{III) } \sin\theta \neq 0;\ F_1'(r) = 0;\ \alpha = \cos\theta F_1(r).$$

Let us consider them in succession.

I) In this case the singular points lie on the Oz axis:

$$\left.\begin{aligned} \alpha &= F_1(r), \quad \text{if} \quad z > 0 \quad (z = r) \\ \alpha &= -F_1(r), \quad \text{if} \quad z < 0 \quad (z = -r) \end{aligned}\right\} \qquad (a.43)$$

Figure 81 shows dashed the form of the functions

$$F(z) = \frac{(z-1)^2(2z+1)}{2z} \quad \text{FOR } z > 0.$$

The continuous line on the same figure represents the form of the function $F_1(z)$ for $z > 0$ and its continuation $-F_1(-z)$ for $z < 0$, that is, the function corresponding to equation (a.43). The ordinates of the singular points,

lying on the Oz axis, are determined by finding the points of intersection of the curve $F_1(z)$; $-F_1(-z)$ and the line $F_1 = \alpha$. For small values of α, as can be seen from Fig. 81, there will be four such points: A_1, A_2, A_3, A_4.

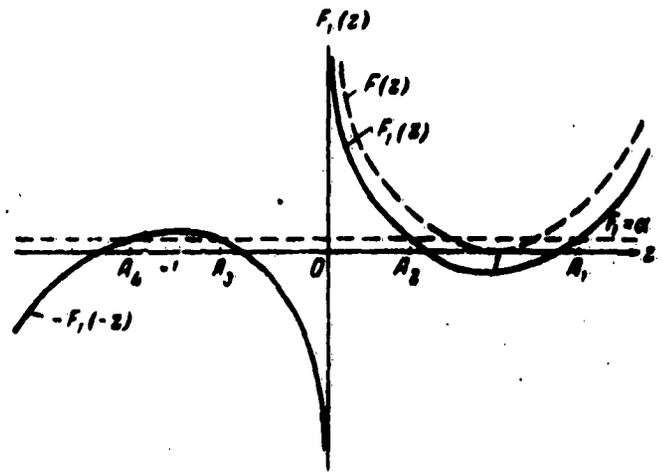

Fig. 81. Form of the functions $F(z)$, $F_1(z)$, and $-F_1(z)$.

With increasing value of α, the point A_1 goes away to the right along the Oz axis, the point A_2 approaches the origin, and the points A_3 and A_4 come together and at values of α exceeding the maximum of the curve $F_1(z)$; $-F_1(-z)$ they vanish from the Oz axis. The extrema of the curve $F_1(z)$; $-F_1(-z)$ are located at the points $z = \pm r_0$, where r_0 is the root of the equation

$$\text{or} \qquad F_1'(r) = 2r\left[1 - \frac{3}{4r} - \frac{1}{4r^3} - g_1\right] = 0, \tag{a.44}$$

where the function

$$N(r_0) = g_1, \tag{a.45}$$

$$N(r) = 1 - \frac{3}{4r} - \frac{1}{4r^3}$$

has the form shown in Figure 82. It is easy to see that $r_c > 1$ (since $g_1 > 0$), and the maximum value of the function $-F_1(-z)$ is equal to $3(r_c^2 - 1)4r_c$.

To determine the character of the obtained four singular points, located on the Oz axis, let us find the values at these points of the following functions [45]:

$$a = \frac{\partial v_r}{\partial r}; \quad b = \frac{1}{r} \cdot \frac{\partial v_r}{\partial \theta}; \quad c = \frac{\partial v_\theta}{\partial r}; \quad d = \frac{1}{r} \cdot \frac{\partial v_\theta}{\partial \theta}.$$

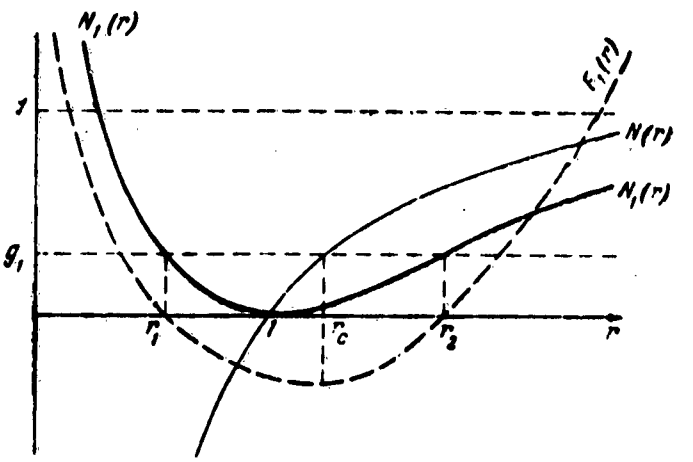

Fig. 82. Form of the functions $N(r)$ and $N_1(r)$.

Elementary calculations show that at these points

$$a = \frac{\cos\theta F_1'(r)}{r^3} = -2d; \; b = c = 0.$$

Since in this case we have

$$q = \begin{vmatrix} a & b \\ c & d \end{vmatrix} = -\frac{a^2}{2} < 0,$$

consequently all the four determined points represent singular points of the saddle type [45].

By virtue of the axial symmetry of the problem, the separatrices at these points are directed along the Oz axis or perpendicular to the Oz axis. To determine the direction of motion along the separatrices in the vicinity of the

singular points, let us consider the sign of $v_\theta/\sin\theta$ near them. Obviously, $v_\theta/\sin\theta$ will have a sign opposite that of $F'_1(r)$ [see formula (a.42)] and in the vicinity of A_1, A_4 the ratio $v_\theta/\sin\theta < 0$ (since $F'_1(r) > 0$), while in the vicinity of A_2 and A_3 the ratio $v_\theta/\sin\theta > 0$ ($F'_1(r) < 0$).

II) The origin represents a singular point of higher order. In this vicinity

$$v_r = \cos\theta\left(1 - \frac{3}{2r} + \frac{1}{2r^3}\right) - \frac{a}{r^3} - g_1\cos\theta \to \frac{\cos\theta}{2r^3},$$

$$v_\theta = -\sin\theta\left(1 - \frac{3}{4r} - \frac{1}{4r^3}\right) + g_1\sin\theta \to \frac{\sin\theta}{4r^3}.$$

Consequently, the equation of the trajectories in the vicinity of the origin assumes the form

$$\frac{1}{r}\cdot\frac{dr}{d\theta} = \frac{v_r}{v_\theta} = \frac{2\cos\theta}{\sin\theta}.$$

Its solution will be a family of closed curves $r = c\sin^2\theta$. We see therefore readily that the origin is a singular point of dipole type and in the vicinity of this point the pattern of the trajectories has the form shown in Figure 83, which shows also the behavior of the trajectories near the points A_1, A_2, A_3, and A_4.

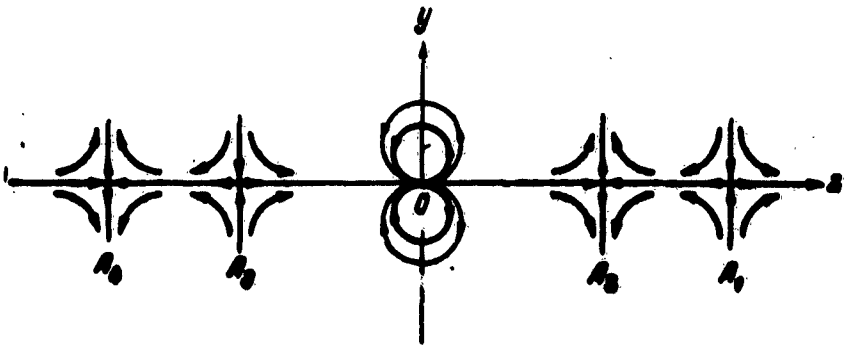

Fig. 83. Behavior of the trajectories of the equations of motion (a.42) near the axial singular points.

III) Inasmuch as in this case $F'_1(r) = 0$, the sought

singular point should lie on the circle $r = r_c$ [see formula (a.44)]. Then $\cos\theta = \frac{a}{F_1(r_c)} < 0$, since $F_1(r_c) < 0$. Thus, the case under consideration corresponds to two singular points A_5 and A_6 away from the axis, symmetrically located relative to the Oz axis in the region of negative values of z. With increasing α the value of $|\cos\theta|$ and consequently of $|z_A|$ increases. It reaches the value $|z_A| = r_c$ when $\alpha = -F_1(r_c) = \frac{3}{4}\cdot\frac{r_c^2-1}{r_c}$. For the same value of α, as we have seen above, there occurs a merging of the points A_3 and A_4 on the Oz axis at the point $z = -r_c$.

Thus, when $\alpha = 0$ the points A_5 and A_6 lie on the Oy axis ($y = r_c$). With increasing α they shift along the circle $r = r_c$ toward negative values of z when $\alpha = \frac{3}{4}\cdot\frac{r_c^2-1}{r_c}$ they merge with the singular points A_3 and A_4 which approach the point $(-r_c, 0)$. When $\alpha > \frac{3}{4}\cdot\frac{r_c^2-1}{r_c}$ all four points A_3, A_4, A_5, and A_6 vanish.

Calculating at the points A_5 and A_6 the values of a, b, c, and d we obtain the following formulas:

$$a = d = 0;\quad b = -\frac{\sin\theta F_1(r_c)}{r_c^2};\quad c = -\frac{\sin\theta F_1'(r_c)}{2r_c},$$

consequently

$$q = \begin{vmatrix} a & b \\ c & d \end{vmatrix} = \frac{\sin^2\theta F_1(r_c) F_1'(r_c)}{2r_c^4} > 0,$$

since $F_1(r_c) < 0$ and $F''_1(r) > 0$ for all values of r. The quantity $p = -(a + d) = 0$. Therefore the points A_5 and A_6 are singular points of the type of center or focus [45].

Before we proceed to construct the qualitative picture of the trajectories of our problem let us consider the limiting case $\alpha = 0$, corresponding to the absence of

charges on the particles. It is easy to see that in this case all the singular points listed above remain the same, as does their character. The function $F_1(z)$; $-F_1(-z)$ crosses the axis $y = 0$ ($\alpha = 0$) at four points: $z = \pm r_1$; $z = \pm r_2$, where r_1 and r_2 are the roots of the equation

$$F_1(r) = r^3 |N_1(r) - g_1| = 0,$$

where

$$N_1(r) = 1 - \frac{3}{2r} + \frac{1}{2r^3}. \qquad \text{(a.46)}$$

A plot of $N_1(r)$ is shown in Figure 82.

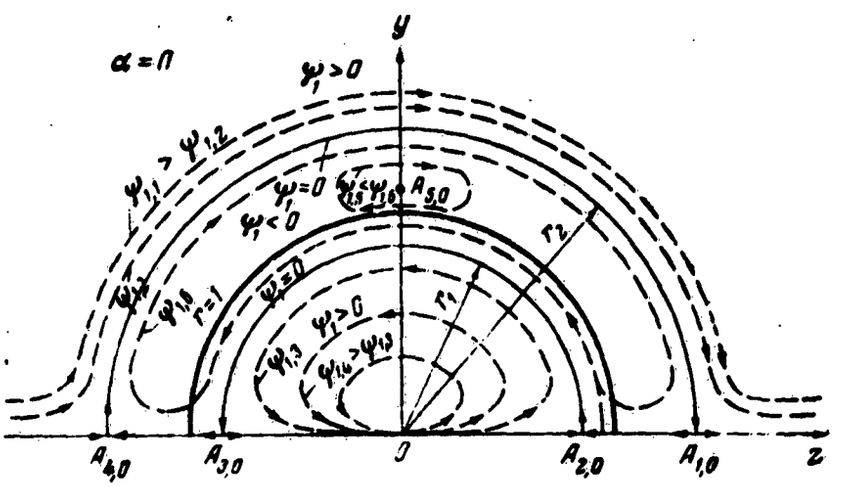

Fig. 84. Qualitative picture of the trajectories of the equations of motion (a.42) in the case $\alpha = 0$.

In this case the trajectories are determined by the equation $\psi_1(r,\theta) = \text{const}$. By virtue of the symmetry of the function ψ_1 relative to the Oy axis, the points A_5 and A_6, which lie for $\alpha = 0$ on the Oy axis, are singular points of the type of a center. Starting from these remarks, we can readily construct a qualitative picture of the trajectories for the case $\alpha = 0$. It is shown in Figure 84. The continuous lines in Fig. 84 are the separatrices, and the thick continuous line is the surface of a sphere. The same figure shows the variation of the function ψ_1 on the plane Oyz.

Taking into account equation (II.8) [f(r) = 1] and the character of variation of ψ_1, we can plot on the Oyz plane qualitative patterns of the trajectories for the case $\alpha > 0$. For this purpose we first determine the qualitative character of the transformation of the separatrices as α varies from zero to a certain small positive value. The separatrices A_1A_4 and A_2A_3 assume for $\alpha > 0$ the form shown in Figure 85, for if we follow them from the points A_1 and A_2 (with increasing value of ϑ), the value of ψ_1 will increase in accordance with formula (II.8) (the dashed lines in Figure 85 show the separatrices $A_{10}A_{40}$ and $A_{20}A_{30}$ for the case $\alpha = 0$). On the other hand, if we proceed along these separatrices from the points A_3 and A_4 (with decreasing value of ϑ), the value of ψ_1 will decrease. Furthermore, from the fact that at the point A_1 we have $r > 1$, it follows that the separatrix A_1B, in view of the increase in the value of ψ_1 along it, never crosses the surface of the drop ($r = 1$) and will be the sought limiting trajectory.

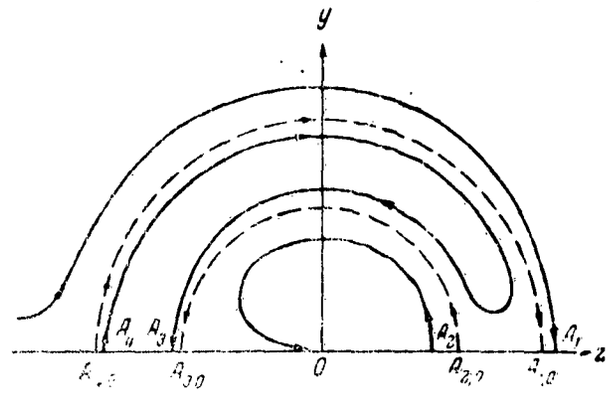

Fig. 85. Character of transformation of the separatrices of the trajectories of the equations of motion (a.42) with variation of α.

If we take into consideration these factors, we can readily construct a general qualitative pattern of the trajectories, as shown in Fig. 36.*

*Fig. 36a shows a pattern of the trajectories under the assumption that the points A_5 and A_6 are of the center

We note that the principally essential factor for us is the behavior of the separatrix that emerges from the point A_1, since this is the separatrix that separates the trajectories coming from $z = -\infty$ into two classes: those entering the sphere $r = 1$ and those going to infinity ($z = +\infty$). Thus, the separatrix emerging from the point A_1 is the limiting trajectory, and the value of y_∞^2 for this separatrix is equal to the capture coefficient E.

IV. INTERACTION BETWEEN TWO CHARGED CONDUCTING SPHERES

Let us examine in somewhat greater detail, than in Sec. 11, the method of calculating the force of interaction between two charged conducting spheres.

To find this force it is customary to determine first the so-called capacitive coefficient c_{ik}, which relate the charges q_i on the spheres with their potentials D_i, by means of the formulas:

$$\left.\begin{aligned} q_1 &= c_{11}V_1 + c_{12}V_2 \\ q_2 &= c_{12}V_1 + c_{22}V_2 \end{aligned}\right\} \qquad (a.47)$$

Comparing formulas (a.47) with equation (II.21a), we find that the potential coefficients s_{ik} necessary for the calculation of the interaction force F_e [see equation (II.21)] are connected with the capacitive coefficients c_{ik} by the following relations:

$$s_{11} = \frac{c_{22}}{\Delta};\quad s_{22} = \frac{c_{11}}{\Delta};\quad s_{12} = -\frac{c_{12}}{\Delta};\quad \Delta = \begin{vmatrix} c_{11} & c_{12} \\ c_{12} & c_{22} \end{vmatrix}. \qquad (a.48)$$

---

type. We can analogously plot patterns of trajectories under the assumption that A_5 and A_6 are singular points of the type of focus. However, such a concretization of the form of the points A_5 and A_6 is of no principal significance for our problem.

For the capacitive coefficient c_{ik} we obtain by the method of successive approximation, described in Sec. 11, the following series [56, 87]:

$$\left.\begin{aligned} c_{11} &= R_1 \operatorname{sh}\mu \sum_{s=0}^{\infty} \frac{1}{\operatorname{sh}(s\lambda+\mu)} \\ c_{12} &= -\frac{R_1R_2}{r} \operatorname{sh}\lambda \sum_{s=1}^{\infty} \frac{1}{\operatorname{sh}(s\lambda)} \\ c_{22} &= R_2 \operatorname{sh}\mu_1 \sum_{s=0}^{\infty} \frac{1}{\operatorname{sh}(s\lambda+\mu_1)} \end{aligned}\right\}, \qquad (a.49)$$

where R_1 and R_2 -- radii of the spheres (we assume that $R_1 > R_2$);

r -- distance between their centers;

λ, μ, and μ_1 -- functions of r, determined from the relations:

$$\operatorname{ch}\lambda = \frac{r^2 - R_1^2 - R_2^2}{2R_1R_2}; \quad \operatorname{ch}\mu = \frac{r^2 + R_1^2 - R_2^2}{2rR_1}; \quad \operatorname{ch}\mu_1 = \frac{r^2 - R_1^2 + R_2^2}{2rR_2}. \qquad (a.50)$$

The series (a.49) converge rather slowly, particularly at small distances between the spheres. Kirchhoff has proposed a method of transforming equations (a.49) which leads to rapidly converging series. If we introduce the notation

$$u = e^{-\lambda}; \; v = e^{-\mu}; \; v_1 = e^{-\mu_1}, \qquad (a.51)$$

then the series (a.49) can be readily changed into

$$\left.\begin{aligned} c_{11} &= R_1(1-v^2) \sum_{s=0}^{\infty} \frac{u^s}{1-v^2u^{2s}}, \\ c_{12} &= -\frac{R_1R_2}{r}(1-u^2) \sum_{s=0}^{\infty} \frac{u^s}{1-u^{2s+2}} \\ c_{22} &= R_2(1-v_1^2) \sum_{s=0}^{\infty} \frac{u^s}{1-v_1^2u^{2s}}. \end{aligned}\right\} \qquad (a.52)$$

In formulas (a.52) the series have the form

$$\sum_{s=0}^{\infty} \frac{\gamma^s}{1-\delta\gamma^{2s}}, \qquad (a.53)$$

where $\gamma = u$ and δ is equal to either v, v_1, or u.

Kirchhoff obtained the following transformation of expressions (a.53), which improves the convergence of the series [87]:

$$\sum_{s=1}^{\infty} \frac{\gamma^s}{1-\delta\gamma^{2s}} = \sum_{s=0}^{\infty} (\delta^s\gamma^{s+1})^s \frac{1-\delta\gamma^{s+s}}{(1-\delta^2\gamma^{2s})(1-\gamma^{2s+1})}. \qquad (a.54)$$

Using expression (a.54), we obtain for the capacitive coefficient c_{ik} from (a.52) the following series:

$$\left.\begin{aligned}
c_{11} &= R_1 \frac{1-v^2u}{1-u}\left\{1+\frac{v^2u^2(1-v^2)(1-u)(1-v^2u^2)}{(1-v^2u^2)(1-v^2u)(1-u^2)}+\right.\\
&\left.+\frac{v^4u^{10}(1-v^2u^2)(1-v^2)(1-u)}{(1-v^2u)(1-v^2u^4)(1-u^2)}+\dots\right\}\\
c_{12} &= -\frac{R_1R_2}{r}(1+u+u^2)\left\{1+\frac{u^2(1-u^7)(1-u^2)(1-u)}{(1-u^4)(1-u^2)^2}+\right.\\
&\left.+\frac{u^{14}(1-u^{11})(1-u^2)(1-u)}{(1-u^6)(1-u^4)(1-u^2)}+\dots\right\}\\
c_{22} &= R_2\frac{1-v_1^2u}{1-u}\left\{1+\frac{v_1^2u^2(1-v_1^2)(1-u)(1-v_1^2u^2)}{(1-v_1^2u^2)(1-v_1^2u)(1-u^2)}+\right.\\
&\left.+\frac{v_1^4u^{10}(1-v_1^2u^2)(1-v_1^2)(1-u)}{(1-v_1^2u)(1-v_1^2u^4)(1-u^2)}+\dots\right\}
\end{aligned}\right| \qquad (a.55)$$

If we recognize that u(r) decreases like $\sqrt{g_1}/r^2$,* v(r) decreases as 1/r, and $v_1(r)$ decreases as $\sqrt{g_1}/r$, we can see from (a.55) that the second term in the square brackets

*Here r is the dimensionless distance between the centers of the sphere, referred to the radius of the largest sphere, and $\sqrt{g_1} = R_2/R_1$.

will be of order $g_1^{5/2}r^{-10}$ (or $g_1^{5/2}r^{-8}$, or $g_1^{3/2}r^{-8}$), the third term will be of order $g_1^7r^{-28}$ (or $g_1^5r^{-24}$ or $g_1^7r^{-24}$) etc. Thus, the series in (a.55) converge very rapidly, and expressions (a.55) are convenient for the calculation of the capacitive coefficients c_{ik}.

After finding the capacitive coefficients c_{ik} we can use formulas (a.48) to determine the potential coefficients s_{ik} and the functions $l_1(r, g_1)$, $l_2(r, g_1)$, and $l_3(r, g_1)$ which, in accordance with formula (II.21), are connected with the derivatives ds_{ik}/dr in the following manner:

$$l_1(r, g_1) = -r^3\frac{ds_{12}}{dr} - 1;\ l_2(r, g_1) = \frac{r^3}{2}\cdot\frac{ds_{22}}{dr};$$

$$l_3(r, g_1) = \frac{r^3}{2}\cdot\frac{ds_{11}}{dr}. \qquad (a.56)$$

The scheme described above was used by us to calculate the functions l_1 and l_2 for the cases $g_1 = 0.01$, $g_1 = 0.04$, and $g_1 = 1$.*

In Table a.II are shown the calculated values of the functions $1 + l_1(r)$ and $l_2(r)$. For comparison we show here also the approximate values of the function $l_2(r) \approx$ $\approx \frac{2r^3-1}{r(r^3-1)^3}$. An examination of the table shows that for small values $\sqrt{g_1} = \frac{d}{D} = \frac{R_2}{R_1}$ even at relatively short distance between the spheres (the distance δ between the surface of the sphere does not exceed the radius of the small sphere) the function $1 + l_1(r, g_1)$ does not exceed unity by more than 0.08, and the function $l_2(r, g_1)$ differs from its approximate

*The function $l_3(r)$ for the cases $g_1 = 0.01$ and 0.04 could not be calculated with sufficient accuracy, for at the calculation accuracy employed by us (s_{ik} was calculated with five significant figures) the derivatives ds_{11} were too small to be determined. For $g_1 = 1$, the function $l_3(r) = l_2(r)$. The results obtained for $g_1 = 1$ agree well with the results of the calculations of Kelvin [99].

value by not more than 8 percent (these relations occur for $g_1 = 0.04$, when $r \geqslant 1.4$, and for $g_1 = 0.01$ when $r > 1.2$). For equal spheres, similar relations occur when $\delta = 0.6$ ($r = 2.6$).

We can thus state that with sufficient accuracy for practice, in cases when the charge ratio $\varkappa = -q_2/q_1$ is not very small in absolute magnitude (the charge on the small sphere is not very small), the function f(r) can be approximated by the expression

$$f(r) \approx 1 + \varkappa l_2(r) \approx 1 + \varkappa \frac{2r^2 - 1}{r(r^2-1)^2}. \qquad (a.57)$$

Expression (a.57) leads, of course, to a somewhat underestimated value of f(r), if the spheres are charged oppositely, and somewhat overestimated value if the charges are of like polarity. In the former case this corresponds to an underestimate of the force of attraction between the spheres, and in the latter to an overestimate of the repulsion between the spheres. Either circumstance leads in the calculation of the capture coefficient (Secs. 11 and 12) to a somewhat reduced calculated value of E.

Table a.II

$g_1 = 0{,}01; \frac{d}{D} = 0{,}1$

r	$1+l_1(r)$	$l_2(r)$	$l_2(r)_{\text{APPROX.}}$	$\frac{l_2(r)}{l_2(r)_{\text{APPROX.}}}$
1,11	2,10	53,9	24,5	2,20
1,12	1,88	34,0	20,8	1,63
1,13	1,59	25,4	17,9	1,42
1,14	1,30	20,45	15,63	1,31
1,15	1,22	16,85	13,75	1,22
1,16	1,16	14,36	12,21	1,18
1,18	1,11	10,83	9,82	1,10
1,20	1,08	8,73	8,09	1,08
1,22	1,06	7,14	6,79	1,05
1,24	1,04	6,05	5,79	1,04
1,26	1,03	5,18	5,00	1,03
1,28	1,03	4,47	4,36	1,02
1,30	1,02	3,91	3,85	1,02

$g_1=0{,}04$; $d/D=0{,}2$

r	$1+I_1(r)$	$I_2(r)$	$I_2(r)_{\text{approx.}}$	$\frac{I_2(r)}{I_2(r)_{\text{approx.}}}$
1,23	1,88	11,77	6,26	1,88
1,24	1,66	9,75	5,79	1,69
1,25	1,52	8,25	5,37	1,54
1,26	1,41	7,13	5,00	1,43
1,28	1,30	5,64	4,36	1,29
1,30	1,22	4,67	3,85	1,21
1,32	1,17	3,98	3,42	1,16
1,34	1,14	3,45	3,06	1,13
1,36	1,12	3,03	2,75	1,10
1,38	1,09	2,71	2,49	1,08
1,40	1,06	2,41	2,26	1,07
1,45	1,05	1,91	1,82	1,05
1,50	1,04	1,54	1,49	1,03
1,55	1,03	1,28	1,25	1,03
1,60	1,02	1,08	1,06	1,02

$g_1=1$; $d=D$

r	$1+I_1(r)$	$I_2(r)$	$I_2(r)_{\text{approx.}}$	$\frac{I_2(r)}{I_2(r)_{\text{approx.}}}$
2,02	5,11	2,132	0,374	5,70
2,03	3,90	1,684	0,366	4,60
2,04	3,31	1,348	0,359	3,74
2,06	2,63	1,002	0,345	2,90
2,08	2,25	0,797	0,332	2,46
2,10	2,00	0,667	0,320	2,12
2,12	1,83	0,591	0,309	1,92
2,14	1,71	0,527	0,298	1,77
2,16	1,62	0,476	0,287	1,66
2,18	1,54	0,435	0,277	1,57
2,20	1,47	0,404	0,268	1,51
2,25	1,36	0,339	0,246	1,38
2,30	1,29	0,288	0,226	1,27
2,35	1,23	0,257	0,209	1,23
2,40	1,19	0,227	0,194	1,17
2,45	1,16	0,204	0,180	1,14
2,50	1,13	0,187	0,167	1,12
2,55	1,11	0,170	0,156	1,08
2,60	1,09	0,155	0,145	1,07

V. TRAJECTORIES OF PARTICLES IN THE PRESENCE OF AN EXTERNAL ELECTRIC FIELD

A. Let us consider the trajectories of a charged small particle relative to an almost neutral large particle in the presence of an external electrostatic field E_0. In this case the coefficients δ_2, γ, and α can be assumed equal to zero (we neglect the mirror-image forces). If in addition we can also neglect the inertial term, then equations (II.42) and (II.45) assume the form

$$v_r = \frac{rF_1(r) - \delta_1(2 + r^3)}{r^3} \cos\theta, \tag{a.58}$$

$$v_\theta = -\frac{r^3F_1'(r) + 2\delta_1(1 - r^3)}{2r^3} \sin\theta, \tag{a.59}$$

$$\frac{\sin^2\theta}{2}\left[F_1(r) - \frac{2\delta_1}{r} - \delta_1 r^2\right] = \text{const}. \tag{a.60}$$

We note first of all that in accordance with the formula (a.60) the trajectories of the particles will in this case be symmetrical relative to the plane $\theta = \pi/2$, since $\sin\theta_1 = \sin(\pi - \theta_1)$. To construct the qualitative picture of the trajectory of the system (a.58) and (a.59), let us find its singular points.

To find the singular points lying on the axis of motion ($\sin\theta = 0$), we obtain from formula (a.58) the equation

$$\delta_1 = \frac{rF_1(r)}{2 + r^3} = F_4(r). \tag{a.61}$$

The function $F_4(r)$ is shown in Figure 86. We denote the minimum value of $F_4(r)$, which it assumes at the point $r = r_m$, by δ_{cr}. Then when $\delta_1 < \delta_{cr}$ and $\delta_1 > 1 - g_1$ there are no axial singular points. When $\delta_{cr} < \delta_1 < 1/4$, there exist four axial singular points A_1, A_4 and A_2, A_3 whose coordinates are, in accordance with formula (a.61) obtained on Fig. 86 as the coordinates of the points of

intersection of the curve $F_4(r)$ and the line $F_4 = \delta_1$. When $1/4 < \delta_1 < 1 - g_1$ there exist two axial singular points A_1 and A_4.

Noting that $rF_1(r) = (2 + r^3)F_4(r)$, we readily obtain for v_θ the expression

$$v_\theta = -\sin\theta\left[\frac{2+r^3}{2r^3}F_4'(r) + \frac{r^3-1}{r^3}(F_4(r) - \delta_1)\right]. \qquad (a.62)$$

On the basis of formulas (a.58) and (a.62) we obtain by differentiation that in the axial singular points, where equation (a.61) is satisfied, the following relations hold true

$$a = \frac{\partial v_r}{\partial r} = \cos\theta\left(1 + \frac{2}{r^3}\right)F_4'(r); \quad b = \frac{1}{r}\cdot\frac{\partial v_r}{\partial\theta} = 0;$$

$$c = \frac{\partial v_\theta}{\partial r} = 0; \quad d = \frac{1}{r}\cdot\frac{\partial v_\theta}{\partial\theta} = -\frac{\cos\theta}{2}\left(1 + \frac{2}{r^3}\right)F_4'(r) = -\frac{a}{2}.$$

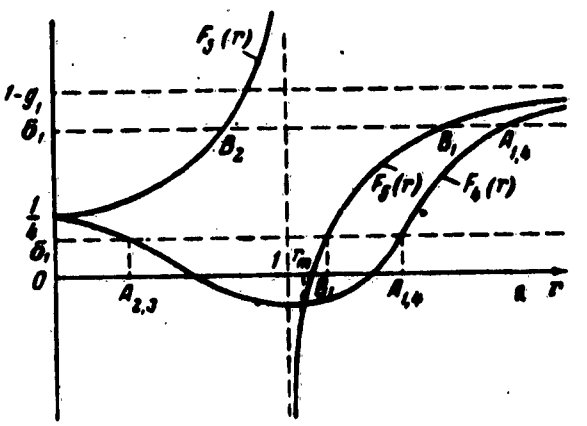

Fig. 86. Form of the functions $F_4(r)$ and $F_3(r)$.

Consequently, for axial points the determinant

$q = \begin{vmatrix} a & b \\ c & d \end{vmatrix} = -\frac{a^2}{2} < 0$, and all represent singular points of the saddle type. It is easy to conclude from (a.62) that in the vicinity of axial singular points the sign of $v_\theta/\sin\theta$ coincides with the sign of $[-F'_4(r)]$ and consequently in

the vicinity of A_1 and A_4 the components $v_\theta < 0$, and in the vicinity of A_2 and A_3 the components $v_\theta > 0$.

The origin represents a singular point of higher order. In its vicinity for $\delta_1 \neq 1/4$ we have $v_r \to$ $\to \frac{\cos\theta(1-4\delta_1)}{2r^2}$, and $v_\theta \to \frac{\sin\theta(1-4\delta_1)}{4r^2}$. Consequently, in the vicinity of the origin the equation of the trajectories will have the form

$$\frac{dr}{r\,d\theta} = \frac{v_r}{v_\theta} = \frac{2\cos\theta}{\sin\theta}$$

or

$$r = C\sin^2\theta.$$

Thus, the origin will represent a singular point of the dipole type with Poincare index I = + 2. The trajectories near the origin will have the form shown in Figure 87, where one can also see the behavior of the trajectories near the points A_1, A_2, A_3, and A_4.

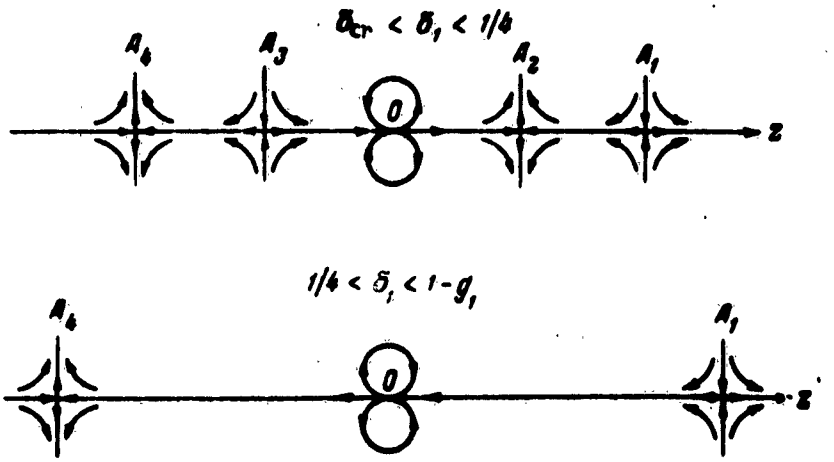

Fig. 87. Behavior of the trajectories of the equations of motion (a.58) and (a.59) near axial singular points.

The singular points away from the axis ($\sin\theta \neq 0$) cannot be located outside the plane $\theta = \pi/2$, for in the

opposite case ($\cos\theta \neq 0$) it would follow from (a.58) that $\delta_1 = F_4(r)$, and it would follow from the formula (a.62) that at these singular points $F'_4(r) = 0$. With the exception of the bifurcation values of the parameter $\delta_1 = \delta_{cr}$ and $\delta_1 = 1/4$, such a situation is impossible (it is seen from Fig. 86 that when $\delta_1 \neq \delta_{cr}$ and $\delta_1 \neq 1/4$ the derivative $F'_4(r) \neq 0$). Therefore singular points outside the axis lie in the plane $\theta = \pi/2$.

The coordinate of the point r_B outside the axis is determined from the equation $v_\theta/\sin\theta = 0$ or

$$\delta_1 = \frac{r^3 F'_1(r)}{2(r^3-1)} = F_5(r). \qquad \text{(a.63)}$$

The function $F_5(r)$ is represented on the same Fig. 86,* from which it is seen that when $\delta_1 < 1/4$ there is only one point outside the axis ($r = r_{B_1} > 1$; $\theta = \pi/2$) and when $1/4 < \delta_1 < 1 - g_1$ there are two points outside the axis ($r = r_{B_1} > 1$; $\theta = \pi/2$ and $r = r_{B_2} < 1$; $\theta = \pi/2$) and, finally, for $\delta_1 > 1 - g_1$ there is one point away from the axis ($r = r_{B_2} < 1$; $\theta = \pi/2$).

Differentiating (a.58) and (a.59) we obtain for the points away from the axis ($\theta = \pi/2$; $r = r_{B_1}$ or $r = r_{B_2}$) the following equations:

$$a = \frac{\partial v_r}{\partial r} = 0;\ b = \frac{1}{r}\cdot\frac{\partial v_r}{\partial \theta} = -\sin\theta\,\frac{2+r^3}{r^4}\,[F_4(r_B) - \delta_1];$$

$$c = \frac{\partial v_\theta}{\partial r} = -\sin\theta\,\frac{3(r-1)^2(r+2)+12g_1 r}{4r^3(r^3-1)};\ d = \frac{1}{r}\cdot\frac{\partial v_\theta}{\partial \theta} = 0.$$

---

*Differentiating equation (a.61), we can readily show that

$$F'_4(r) = \frac{2(r^3-1)}{r(2+r^3)}\,[F_5(r) - F_4(r)].$$

from which it follows that the curves $F_4(r)$ and $F_5(r)$ cross at the point where $F'_4(r) = 0$, that is, at the point $r = r_m$. Since to the right of r_m the derivative $F'_4(r) > 0$ and $r_m > 1$, we have $F_5(r) > F_4(r)$ for $r > r_m$.

Consequently, for the points away from the axis the determinant is

$$q = \begin{vmatrix} a & b \\ c & d \end{vmatrix} = -bc.$$

The sign of b coincides with the sign of $\delta_1 - F_4(r_B)$. The sign of c coincides with the sign of $1 - r^3$. Therefore the following holds true.

1) If $\delta_1 < \delta_{cr}$, then $q_{B_1} < 0$ (since $r_{B_1} > 1$ and $\delta_1 < F_4(r_{B_1})$). The point B_1 is of the saddle type.

2) If $\delta_1 > \delta_{cr}$, then $q_{B_1} > 0$ (since $r_{B_1} > 1$ and $\delta_1 > F_4(r_{B_1})$). Since, in addition, we also have $a + d = 0$, the point B_1 is a center.*

3) If $\delta_1 > 1/4$, then $q_{B_2} < 0$ [since $r_{B_2} < 1$ and $\delta_1 > F_4(r_{B_2})$]. The point B_2 is of the saddle type.

We can now readily construct the trajectory patterns for different values of the parameter δ_1.

1) $\delta_1 < \delta_{cr}$ (Fig. 50a). Singular points: dipole at the origin ($I = + 2$) and two saddles B_1 in the plane $\theta = \pi/2$ ($I = - 1$). The limiting trajectory passes through the saddle B_1.

2) $\delta_{cr} < \delta_1 < 1/4$ (Fig. 50b). Singular points: dipole at the origin ($I = + 2$), four saddles on the axis at the points A_1, A_4, and A_2, A_3 ($I = - 1$), two centers B_1 in the plane $\theta = \pi/2$ ($I = + 1$). The coordinate $r_{A_{2,3}} < r_{B_1} < r_{A_{1,4}}$. The trajectory pattern is similar to that shown in Fig. 84 in the case of the absence of electrostatic forces. The capture coefficient is $E = 0$.

---

*When $q > 0$ and $a + d = 0$ the point can also be a focus [45]. But in our case the symmetry of the trajectories with respect to the plane $\theta = \pi/2$ leaves only one variant -- a point of the type of center.

3) $1/4 < o_1 < 1 - g_1$ (Fig. 50c). Singular points: dipole at the origin (I = + 2), two saddles on the axis at the points A_1 and A_4 (I = - 1). In the plane $\theta = \pi/2$ -- two centers B_1 (I = + 1) and two saddles B_2 (I = - 1). The coordinate $r_{B_2} < 1 < r_{B_1} < r_{A_{1,4}}$. The capture coefficient is E = 0.

4) $\delta_1 > 1 - g_1$ (Fig. 50d). Singular points: dipole at the origin (I = + 2), two saddles B_2 in the plane $\theta = \pi/2$. General direction of the trajectories away from the sphere is opposite the direction of the vector u_∞.

B. Let us consider now the pattern of the trajectories in the case of two neutral particles moving in an external vertical electrostatic field E_0. If we can neglect here the inertial term, the equations of motion will have the form [see equations II.42)]:

$$v_r = \frac{\cos\theta F_1(r)}{r^3} + \gamma\frac{1-3\cos^2\theta}{r^4}, \qquad (a.64)$$

$$v_\theta = -\frac{\sin\theta F_1'(r)}{2r} - \gamma\frac{\sin 2\theta}{r^4}. \qquad (a.65)$$

The ordinates of the axial singular points ($\sin\theta = 0$) satisfy the following equations:

$$\gamma = \frac{r^3}{2}F_1(r) = F_6(r) = F_6(z) \quad (z > 0),$$

$$\gamma = -\frac{r^3}{2}F_1(r) = -F_6(r) = -F_6(-z) \quad (z < 0). \qquad (a.66)$$

Figure 88 shows with a dashed curve the function $F_6(z) = \frac{1}{4}z(z-1)^2(2z+1)$ for $z > 0$ and $g_1 = 0$. The solid line on the same figure shows the form of the function $F_6(z)$ for $z > 0$ ($g_1 \neq 0$), and its continuation $-F_6(-z)$ for $z < 0$. The coordinates of the axial points are obtained on Fig. 88 as the coordinates of the points of intersection of the curve $F_6(z)$; $-F_6(-z)$ with the line $F_6 = \gamma$. As can be seen from Fig. 88, for small values of γ on the Oz axis there are, in addition to the origin, five singular points A_1, A_2, A_3, A_4, and A_5. With increasing γ

the points A_2 and A_3, and also A_4 and A_5 come together pairwise and, starting with certain values of γ (equal to the maximum ordinates of the curve $F_6(z)$; $-F_6(-z)$, respectively) they vanish from the Oz axis, leaving then one singular axial point A_1. The maximum ordinates correspond to values $z = r_3$ and $z = -r_4$, where r_3 and r_4 are the roots of the equation $F'_6(r) = 0$ or

$$N_2(r) = 1 - \frac{\theta}{g_r} + \frac{1}{g_{rr}} = g_1. \qquad (a.67)$$

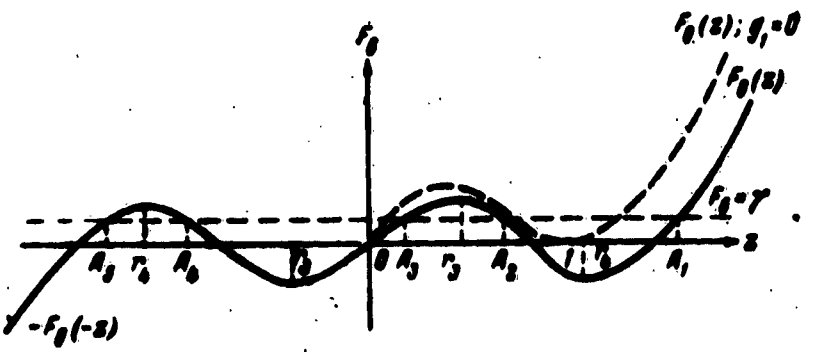

Fig. 88. Form of the functions $F_6(z)$ and $-F_6(-z)$.

The function $N_2(r)$ is shown in Figure 89.

The calculations of the functions a, b, c, and d in the axial singular points yield for them the following values:

$$a = \frac{2\cos\theta F'_6(r)}{r^4} = -2d; \quad b = c = 0.$$

Since in this case $q = -a^2/2 < 0$, it follows therefore that all five obtained points are singular points of the saddle type. From (a.65) it is easy to conclude that in the vicinity of the axial singular points $\frac{v_\theta}{\sin\theta} = -\frac{F'_6(r)}{r^4}$ and consequently in the vicinity A_1, A_3, A_5 the component $v_\theta < 0$, and in the vicinity A_2 and A_4 we have $v_\theta > 0$.

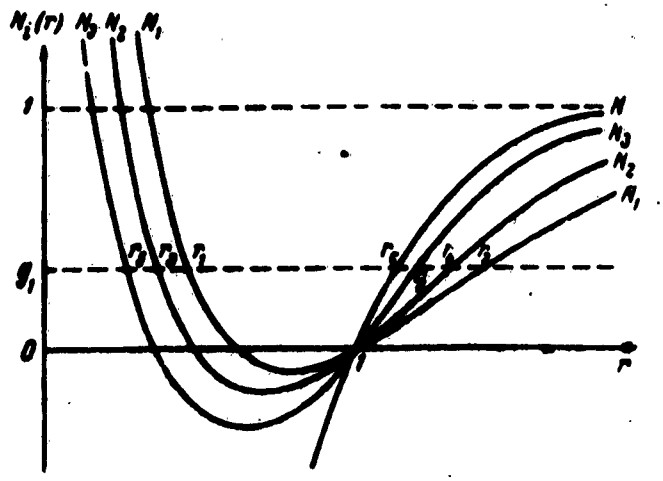

Fig. 89. Form and neutral placement of the functions $N(r)$, $N_1(r)$, $N_2(r)$, and $N_3(r)$.

The origin represents a singular point of higher order. In its vicinity we have $v_r \to \gamma \frac{1-3\cos^2\theta}{r^4}$; $v_\theta \to -\gamma \frac{\sin 2\theta}{r^4}$. From this we obtain for the trajectories near the origin the equation $r^2 = c \sin 2\theta \sin \theta$. The trajectories near the origin are shown in Figure 90, where one can also see the behavior of the trajectories near the points A_1, A_2, A_3, A_4, and A_5.

Let us consider now the singular points away from the axis ($\sin \theta \neq 0$). Their coordinates satisfy the two equations:

$$\cos\theta r^3 F_1(r) + \gamma(1-3\cos^2\theta) = 0,$$
$$r^3 F_1'(r) + 4\gamma\cos\theta = 0. \qquad \text{(a.68)}$$

It follows therefore that in the singular point away from the axis we have

$$\cos\theta = -\frac{r^3 F_1'(r)}{4\gamma},$$

$$\gamma^2 = \frac{r^3 F_1'(r)\,|4F_1(r) + rF_1'(r)|}{16}. \qquad \text{(a.69)}$$

Taking into consideration the formula (a.68), we can show that in these points $a = \frac{2\cos\theta P_2'(r)}{r^3} = -d$. Consequently, $p = a + d = 0$, and the points away from the axis will be of the saddle, center, or focus type.

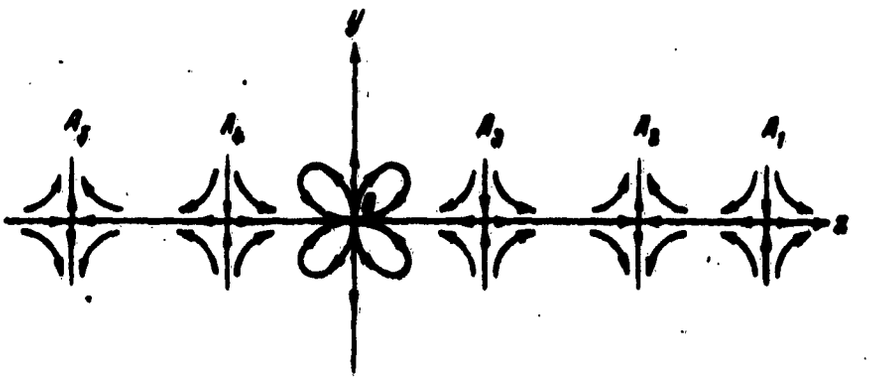

Fig. 90. Behavior of the trajectories of the equations of motion (a.64) and (a.65) near the axial singular points.

According to formulas (II.10) and (a.45), equations (a.69) can be represented by

$$\cos\theta = -\frac{(N-g_1)r^4}{2\gamma}, \tag{a.70}$$

$$\gamma = \frac{\sqrt{5}}{2} r^4 \sqrt{(N-g_1)(N_3-g_1)}, \tag{a.71}$$

where

$$N_3(r) = 1 - \frac{21}{20r} + \frac{1}{20r^3}. \tag{a.72}$$

Formula (a.71) shows that in the singular points away from the axis the functions $N - g_1$ and $N_3 - g_1$ have identical signs and consequently

$$\cos\theta = -\operatorname{sign}(N-g_1)\sqrt{\frac{N-g_1}{5(N_3-g_1)}}. \tag{a.73}$$

Inasmuch as $|\cos\theta| \leq 1$, we can readily obtain from (a.73) the conditions satisfied in these singular points:

$$\left.\begin{array}{ll} N_3 - g_1 \geqslant 0 & \text{for } N_3 - g_1 > 0 \\ N_3 - g_1 \leqslant 0 & \text{for } N_3 - g_1 < 0 \end{array}\right\} \qquad (a.74)$$

Let us consider now the conclusions that follow from relations (a.73) and (a.74). For this purpose it is necessary to take into account the mutual placement of the plots of the functions N, N_1, N_2, and N_3, shown in Fig. 89.*

Let us trace the solutions of the system (a.68) lying to the left ($\cos\theta < 0$) and to the right ($\cos\theta > 0$) of the Oy axis. In the first case $N - g_1 \geqslant 0$ and the difference $N_3 - g_1$ is positive. This is possible if in the sought point $r > r_6$ (see Fig. 89). However $|\cos\theta|$ becomes smaller than unity in this case if $r \geqslant r_4$ (see (a.74)), and when $r = r_4$ we have $\cos\theta = -1$. We note further that since when $r \geqslant r_4$ in the right half of (a.71) is a monotonically increasing function of r, equation (a.71) has one and only one root $r \geqslant r_4$. It follows therefore that so long as γ is very small and equation (a.71) is satisfied by values of r lying in the interval $r_6 < r < r_4$, there exist no solutions of the system (a.68), since it leads to the relation $|\cos\theta| > 1$. Such a solution appears when γ increases to such an extent that equation (a.71) acquires a root $r \geqslant r_4$.

We note that for γ corresponding to a solution of (a.71) $r = r_4$ there occurs also the merging of two singular points on the Oz axis -- the points A_4 and A_5. Actually, $r = r_4$ is the root of the equation $N_2(r) = g_1$. Substituting in (a.66) and (a.71) in place of g_1 its value at the point $r = r_4$, equal to $N_2(r_4)$, we obtain that γ in both cases will be equal to $\frac{3\,r_4}{16}(r_4^2 - 1)$. This means that when the singular points A_4 and A_5 on the Oz axis merge and disappear with increasing γ, then on the left of the Oy axis there will arise two singular non-axial points, corresponding to equations (a.68). Inasmuch as for this value $\gamma = \frac{3\,r_4}{16}(r_4^2 - 1)$

---

*The correctness of the mutual placement of these plots on Fig. 89 can be readily verified by setting up the differences $N - N_3$, $N_3 - N_2$, and $N_2 - N_1$, each of which has the form $\lambda(r^2 - 1)$, where $\lambda > 0$.

there occurs no change whatever in either the number or the character of the other singular points, except those mentioned above, and since the sum of the Poincare indices of all the singular points on going through this value of γ should not change, it is obvious that the singular points that arise anew outside the axis (in place of A_4 and A_5) will also be of the saddle type (a Poincare index equal to -1 is conserved).

Let us consider now the solution of the system (a.68) lying to the right of the Oy axis ($\cos\theta > 0$). In this case $N - g_1 \leq 0$ and the difference $N_3 - g_1$ is negative. According to formula (a.74) the difference $N_2 - g_1$ is then also negative. From Fig. 89 we readily see that the sought solution has a value of r lying in the interval $r_3 \leq r < r_0$, with $r = r_0$ when $\gamma = 0$. In this last case $\cos\theta = 0$ and we have the pattern of the trajectories shown in Fig. 84. With increasing γ, the value of r corresponding to equation (a.71) decreases from r_0 to r_3, and value of $\cos\theta$ increases from zero to unity, and furthermore if $r = r_3$ then $\cos\theta = +1$ and $\gamma = \frac{3 r_3}{16}(r_3^2 - 1)$.

We note that for this same value $\gamma = \frac{3 r_3}{16}(r_3^2 - 1)$ the two saddles A_3 and A_2 merge on the Oz axis. Since further increase in γ there disappear on the Oz axis the two singular points (the saddles A_2 and A_3), and two singular points located to the right of the Oy axis disappear away from the axis, too [the value of $\cos\theta$ calculated from the system (a.68) becomes larger than unity], at a time when no changes occur in the number and character of the other singular points, then by virtue of the constancy of the summary Poincare index we can conclude that the singular points away from the axis, lying to the right of the Oy axis ($\cos\theta > 0$) have Poincare indices +1. This means that these points are either centers or foci.

If we now summarize the changes in the number and character of the singular points of equations (a.64) and (a.65), we can state the following.

1. When $\gamma = 0$ there are on the Oz axis four saddles (their total Poincare index is $I_\Sigma = -4$) and a dipole at

the origin (I = + 2). Outside the Oz axis there are two centers -- on the Oy axis (I_Σ = + 2) (see Fig. 84).

2. At very small values of γ the dipole at the origin breaks up into a quadrupole (I = + 3) located at the origin and a saddle A_3(I = - 1). The two centers located at γ = 0 on the Oy axis shift toward positive values of z(cos $\theta > 0$). It is possible that they are transformed into foci. The saddles A_2, A_3, and A_4, A_5 approach pairwise with increasing γ.

3. With further increase in γ, if g_1 is small, the saddles A_4 and A_5 first merge, with subsequent transition to a non-axial position (cos $\theta < 0$), and then with further increase in γ, the saddles A_2 and A_3 merge with two non-axial centers (or foci; cos $\theta > 0$), which arrive (for one and the same value of γ) simultaneously with the saddles at the Oz axis at the merging points of A_2 and A_3. With further increase in γ all these four points vanish. If g_1 is large, then at first (with increasing γ) there occurs a merging and vanishing of the four points (A_2, A_3, and the non-axial centers), and then a transition of the points A_4 and A_5 to a non-axial position. In all cases, upon vanishing of the points A_4 and A_5, two non-axial saddles B appear.

4. When γ is larger than both maximal values of the function $F_6(z)$; $-F_6(-z)$, the system of singular points consists of a quadrupole at the origin (I = + 3), a saddle A_1(I = - 1) on the Oz axis, and two non-axial saddles B (cos $\theta < 0$; I_Σ = - 2). Figure 51 shows qualitative trajectory patterns for all the cases under consideration. Fig. 51a shows the case of a small value of γ, smaller than the value of both maxima of the curve $F_6(z)$; $-F_6(-z)$. Fig. 51b and c show cases when the quantity γ lies between the two values of the maxima of the curve $F_6(z)$; $-F_6(-z)$. Fig. 51b corresponds to the case $|F_6(r_4)| > F_6(r_3)$, and Fig. 51c to the case $|F_6(r_4)| < F_6(r_3)$. Fig. 51d shows the case when the parameter γ is larger than both maxima of the curve $F_6(z)$; $-F_6(-z)$. Qualitative patterns of the trajectories shown in Fig. 51 show that in the case $\gamma < \gamma_{cr} = - F_6(r_4)$, the capture coefficient is equal to zero. To calculate the value of the capture coefficient for $\gamma > \gamma_{cr}$ it is necessary to find the value of y_π for the separatrix passing

through the non-axial saddle B. The value of y_{π} for this separatrix can be readily obtained from equation (II.53), if one knows the coordinates (r_B, θ_B) of the non-axial saddle B. Indeed, from equations (II.53) and (a.70) it follows that

$$\psi_{1,*} = \frac{1}{2} y_*^2 (1 - g_1) = \psi_1 (B) - \frac{\gamma \cos\theta_B \sin^2\theta_B}{r_B} = \\ = \frac{1}{2} r_B^2 \sin^2\theta_B [N_1(r_B) + N(r_B) - 2g_1] \tag{a.75}$$

and consequently

$$E = y_*^2 = \frac{2y_B^2 [N_1(r_B) - g_1]}{1 - g_1}. \tag{a.76}$$

The values of γ_{cr} can be readily obtained by expanding the functions $N_2(r)$ and $F_6(r)$ in a Taylor series in powers of $(r - 1)$. We thus obtain for small values of the parameter g_1:

$$\left.\begin{aligned} r_4 &= 1 + \frac{4}{3} g_1 + \frac{8}{9} g_1^2 + \ldots \\ \gamma_{cr} &= -F_6(r_4) = \frac{g_1}{2} \left(1 + \frac{8}{3} g_1 + \frac{224}{27} g_1^2 + \ldots\right) \end{aligned}\right\} \tag{a.77}$$

Table a.III shows the values of r_3, r_4, $\gamma_1 = F_6(r_3)$ and $\gamma_{cr} = -F_6(r_4)$ for several values of $g_1 = d^2/D^2$.

Table a.III

d/D	g_1	r_3	r_4	$\gamma_1 = F_6(r_3)$	$\gamma_{cr} = -F_6(r_4)$
0	0	0,422	1,000	0,0650	0
0,1	0,01	0,420	1,013	0,0648	0,0051
0,2	0,04	0,415	1,054	0,0643	0,0224
0,32	0,1	0,406	1,142	0,0636	0,0675

VI. EXAMPLE OF CONSTRUCTION OF THE GAMMA DISTRIBUTION FROM EXPERIMENTAL DATA

We present an example of processing of the result of an experimental measurement of cloud drops by dimensions.

In Table a.IV we list the distribution of the drops by dimensions obtained with the aid of a flow-through trap in an artificial fog (chamber).

Table a.IV

Diameter interval (μ)	Number of drops*	$H(d)$ [%]	Diameter interval (μ)	Number of drops*	$H(d)$ [%]
4—6	94	9,1	14—16	102	93,1
6—8	155	24,1	16—18	41	97,0
8—10	222	45,5	18—20	22,3	99,2
10—12	234	68,1	20—22	7,3	99,9
12—14	156	83,2	22—24	1,2	100,0

$\Sigma = 1035$

*The non-integer number of drops in this column is the result of an account of the capture coefficient.

Figure 91 shows the rectified accumulated distribution diagram H(d) of Table a.IV (see Sec. 18). To the left of the ordinate axis is shown a ruler with a scale corresponding to the value of the index $\alpha = 8$. As can be seen from Fig. 91, the experimental points fitted sufficiently well the straight line passing through the origin.

The dashed curve beginning at the point ($d = 4$ microns, $y = 0$) and going over into the straight line represents the portion of the actually obtained truncated distribution. We recall that the experimental distributions obtained with a flow-through trap, owing to the existence of a minimum drop diameter d_{min} of the drops caught by the receiver, are truncated distributions [67, page 127]. For the traps of the expedition $d_{min} = 4$ microns, and the

distributions of the drops are measured for diameters $d \geq 4$ microns. If we assume that the complete distribution (including the interval d = 0--4 microns) is a gamma distribution with index $\alpha = 8$, a plot of which is shown in Fig. 91 by a straight line, then the degree of truncation of the actually obtained distribution turns out to be very small. As shown by the plot (Fig. 91), there will be here approximately 1 percent of drops with diameter $d < 4$ microns.

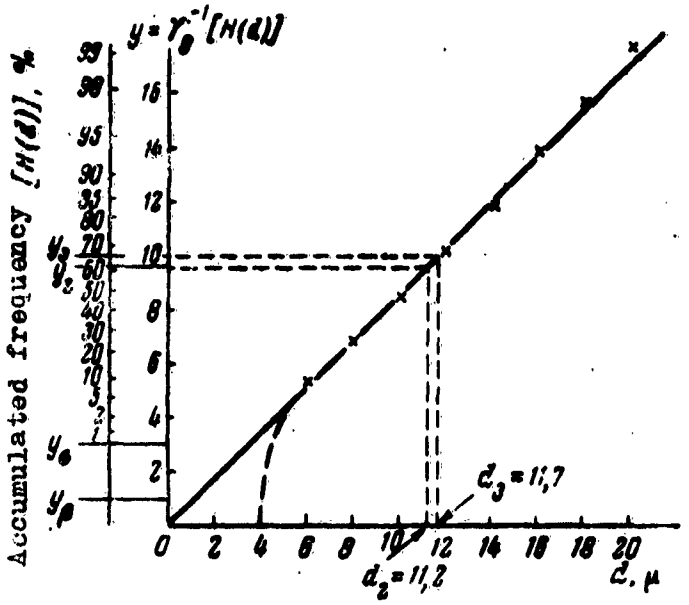

Fig. 91. Example of construction of the rectified accumulated diagram for the dimension distribution of cloud drops ($\alpha = 8$).

The determination of the value of $d_{2g} = 11.2$ microns and $d_{3g} = 11.7$ microns with the aid of the plot of Fig. 91 coincides with the values $d_{2a} = 11.2$ microns and $d_{3a} = 11.7$ microns, arithmetically calculated with the aid of Table 4. The values of the parameter β are thus calculated from the relations $\beta = d_3/y_3$ or $\beta = d_2/y_2$, than to plot them from the graph ($\beta = d$ for $y = 1$), for in the former case one obtains a larger accuracy in the determination of the value of β.

BIBLIOGRAPHY

1. Aderkas, O. Yu., "Determination of the Average Charge of Fog Drops." Tr. NIU GUGMS (Works, Scientific Institute for Fertilizers, Main Administration of the Hydrometeorological Service USSR), series 1, No. 1, 76, 1941.
2. Balabanova, V. N. "Determination of the Water Content of Clouds by the Method of Filtering." Tr. El'brusk Ekspeditsii IPG AN SSSR, (Works, Elbrus Expedition, Institute of Applied Geophysics, Academy of Sciences USSR) No. 2 (5) (in press).
3. Borovikov, A. M. "Some Results of a Study of Cloud Elements." Tr. TSAO (Works, Central Astronomical Observatory), No. 3, 1948.
4. Bocharov, Ye. I. "Some Problems in the Spectral Transparency of Clouds and Fogs." Diss. Geofiz. IN-T AN SSSR (Dissertation. Geophysical Institute, Academy of Sciences USSR), Moscow, 1955.
5. Bocharov, Ye. I. "Spectral Transparency of Clouds." Izv. AN SSSR, ser. geofiz. (News of the Academy of Sciences USSR, Geophysics Series), No. 5, 678, 1958.
6. Bocharov, Ye. I. "Attenuation of Infrared Radiation by Water Fog." Ibid, No. 6, 791, 1958.
7. Vager, N. A. "Laboratory Experiments in the Precipitation of Fog by Means of Dispersed Electrified Water." Tr. NIU, GUGMS, series 1, No 1, 174, 1941.
8. Dukhin, S. S., Deryagin, B. V. "On the Procedure for Calculating the Settling of Dispersed Particles from a Stream on Obstacles." Kolloid. zh. (Colloidal Journal), Vol. 20, No 3, 326, 1958.
9. D'yachenko, P. V. "Experience in Applying the Methods of Mathematical Statistics in the Study of the Structure of Natural Fogs and Clouds,"

Diss. LGU (Dissertation, Leningrad State University), Leningrad, 1950.

10. Zhukovskiy, N. Ye. "Modification of the Kirchhoff Method for the Determination of Motion in Two Dimensions at a Constant Velocity, Given on an Unknown Stream Line." Sobr. Soch. (Collected Works), Vol. 2, 489, Moscow, 1949.
11. Kazanskiy, A. B., Levin, L. M. "Change in Local Capture Coefficient Transverse to a Plate." Tr. El'bruss ekspeditsii IPG AN SSSR, No 2 (5) (in press).
12. Kamke, E. Handbook of Ordinary Differential Equations. Izd-vo inostr. lit. (Publishing House of Foreign Literature), Moscow, 1951, p. 228.
13. Katsyka (Sergiyeva), A. P., Makhotkin, L. G., Petrov, G. D., Chao Po-ling. "Electric Charges of Drops of Clouds and Fogs." Izv. AN SSSR, ser. geofiz., No. 1, 1961.
14. Kholmogorov, A. N. "Logorathmically-normal Law of Distribution of Particle Dimensions During Atomization," Dokl. AN SSSR (Reports of the Academy of Sciences USSR), Vol. 31, No 2, 1941.
15. Kochin, N. Ye., Kibel', I. A., Roze, N. V. Theoretical Hydromechanics, Vol. 1, Gostekhizdat, Leningrad-Moscow, 1948.
16. Kochin, N. Ye. Vector Analysis and Introduction to Tensor Analysis, Izd-vo AN SSSR (Publishing House of the Academy of Sciences USSR), Moscow, 1951.
17. Kurosh, A. G. Course of Higher Algebra, Sec. 47, Gostekhizdat, Moscow, 1955.
18. Laktionov, A. G. "Instrument for Continuous Automatic Determination of the Particle Concentrations and Measurement of the Dimensions of Solid and Liquid Aerosol Particles." Sb. Issledovaniye oblakov, osadkov i grozovogo elektrichestva (Collection: Investigation of Clouds, Precipitation, and Thunderstorm Electricity), p. 200, Gidrometeoizdat, Leningrad, 1957.
19. Lamb, H. Hydrodynamics [Russian translation], Sec. 66 and 74, Gostekhizdat, Moscow-Leningrad, 1947.
20. Lebedev, N. N. Special Functions and Their Applications, Gostekhizdat, Moscow, 1953.
21. Levin, L. M. "Settling of Particles from a Stream of Aerosol on Obstacles." Dokl. AN SSSR, Vol. 91, No 6, 1953.
22. Levin, L. M., Starostina, R. F. "Some Results of Investigations of the Structure of Clouds." Dokl. AN SSSR, Vol. 93, No 2, 1953.

23. Levin, L. M. "On the Coagulation of Charged Cloud Drops." Ibid., Vol. 94, No 3, 1954.
24. Levin, L. M. "On the Distribution Function of Cloud and Rain Drops by Dimensions." Ibid., Vol. 94, No 6, 1954.
25. Levin, L. M. "Considering Random Electrification of Cloud and Rain Drops." Izv. AN SSSR, ser. geofiz., No 11, 1358, 1956.
26. Levin, L. M. "Electric Coagulation of Cloud Drops." Collection: Investigation of Clouds, Precipitation and Thunderstorm Electricity, Gidrometeoizdat, Leningrad, 1957, p 200.
27. Levin, L. M., Starostina, R. F., Chudaykin, A. V. "Aerosol Traps Employed by the Elbruss Expedition," Ibid., p 192.
28. Levin, L. M. "Electrostatic Coagulation of Drops in Clouds." Paper presented at the Eleventh General Assembly of the International Geophysical and Geodetic Union, Toronto, September, 1957.
29. Levin, L. M. "On the Gathering of Aerosol Samples." Izv. AN SSSR, ser. geofiz., No 7, 914, 1957.
30. Levin, L. M. "On the Distribution Functions of Cloud Drops by Dimensions. Optical Density of a Cloud." Ibid., No 10, 1211, 1958.
31. Levin, L. M. "Fluctuations of the Microstructure Characteristics of a Cloud." Ibid., No 12, 1510, 1958.
32. Levin, L. M. "On the Critical Settling of Aerosol Particles from a Viscous Flow on Obstacles," ibid., No 3, 422, 1959.
33. Levin, L. M. "Attenuation of Light by a Cloud." Sb. Issledovaniya po eksperimental'noy i teoreticheskoy fizike. Pamyati G. S. Landsberg (Collection: Investigations on Experimental and Theoretical Physics. In Memory of G. S. Landsberg.) Publishing House of the Academy of Sciences, Moscow, 1959.
34. Levin, L. M. "Electrostatic Settling of Aerosol Particles from a Stream on Large Bodies." Izv. AN SSSR, ser. geofiz., No 7, 1073, 1959.
35. Levin, L. M. "Theory of Aerosol Traps." Tr. El'brusak Ekspeditsii IPG AN SSSR, No 2 (5) (in press).
36. Levin, L. M. "Electric Coagulation of Cloud Drops." Ibid, No 2 (5) (in press).
37. Levich, V. G. "Theory of Coagulation of Colloids in a Turbulent Stream of Liquid." Dokl. AN SSSR, Vol 99, No 6, 1954.

38. Levich, V. G. "Theory of Coagulation and Settling of Aerosol Particles in Turbulent Stream of Gas. On the Coefficient of Trapping Aerosol Particles." Dokl. AN SSSR, Vol 99, No 6, 1954.
39. Litvinov, I. V. "On the Distribution of Function of Particles of Liquid Precipitation." Izv. AN SSSR, ser. geofiz., No 6, 838, 1957.
40. Litvinov, I. V. "Experience in the Study of the Distribution of Snowfall Particles by Size." Ibid, No 10, 1473, 1959.
41. Mazin, I. P. "Calculation of the Settling of Drops on Round Cylindrical Surfaces." Tr. TsAO, No 7, 39, 1952.
42. Makhotkin, L. G., Solov'yev, V. A. "On the Role of Electric Charges in the Coagulation of Fog Drops." Tr. GGO (Works of the Main Geophysical Observatory), No 73, 116, 1958.
43. Natanson, G. L. "Settling of Aerosol Particles from a Stream Flowing Around a Cylinder under the Action of Electrostatic Attraction." Dokl. AN SSSR, Vol 112, No 4, 1957.
44. Natanson, G. L. "Critical Conditions for Inertial Settling of Aerosols in the Case of Viscous Flow Around a Cylinder and Sphere." Ibid., Vol 116, No 1, 1957.
45. Nemytskiy, V. V., Stepanov, V. V. Qualitative Theory of Differential Equations, Chapter II, Gostekhizdat, Moscow-Leningrad, 1949.
46. Novikov, Ye. A. "Settling of Aerosol Particles from the Stream on an Obstacle." Izv. AN SSSR, ser. geofiz., No 8, 1034, 1957.
47. Petrov, G. D. "Procedure of Measuring Charges and Dimensions of Aerosol Particles from an Airplane." Ibid., No 11, 1665, 1959.
48. Polyakova, Ye. A., Shifrin, K. S. "Microstructure and Transparency of Rain." Tr. GGO, No 42 (104), 84, 1953.
49. Pshenay-Severin, S. V. "Influence of Hydrodynamic Interaction of Small Cloud Drops on the Rate of Their Falling." Izv. AN SSSR, ser. geofiz. No 8, 1045, 1957.
50. Pshenay-Severin, S. V. "On the Hydrodynamic Interaction Between Cloud Drops at Small Distances." Ibid., No 10, 1254, 1958.
51. Pshenay-Severin, S. V. "Possible Influence of Hydrodynamic Interaction on the Coagulation of Cloud Drops." Tr. El'brussk Ekspeditsii IPG AN SSSR, No 3 (5) (in press).

52. Sansone, J. Ordinary Differential Equations (Russian translation), Vol. II, p 353--363. Publishing House of Foreign Literature, Moscow, 1954.
53. Sergiyeva, A. P. "On Electric Charges of Cloud Particles." Izv. AN SSSR, ser. geofiz., No 3, 347, 1958.
54. Sergiyeva, A. P. "On Electric Charges of Cloud Particles." Ibid., No 7, 1018, 1959.
55. Slezkin, N. A. Dynamics of Viscous Incompressible Liquid, p. 247, Equation (5.27), Gostekhizdat, Moscow, 1955.
56. Smythe, W., Static and Dynamic Electricity (Russian translation), Gostekhizdat, 1954.
57. Smoluchowski, M., "Experience in the Mathematical Theory of the Kinetics of Coagulation of Colloidal Solutions." Sb. Koagulyatsiya Kolloidov (Coagulation of Colloids), p 20, ONTI, Moscow-Leningrad, 1936.
58. Solov'yev, V. A. "Concerning One Method of Measuring Charges and Dimensions of Fog Drops." Trudy GGO, No 58 (120), 1956. Sb. Issledovaniye oblakov, osadkov i grozovogo elektrichestva, p 170. Gidrometeoizdat, 1957.
59. Stratton, J. A., Electromagnetic Theory (Russian translation), Gostekhizdat, Moscow-Leningrad, 1948.
60. Tietjens, O. Hydro- and Aeromechanics (after lectures by L. Prandtl), Vol. II, ONTI, Moscow-Leningrad, 1935.
61. Frenkel', Ya. I. Theory of Phenomena of Atmospheric Electricity. Gostekhizdat, Moscow-Leningrad, 1949.
62. Fuks, N. A., Petryanov, I. V. "Determination of Dimension and Charge of Fog Particles." Zh. fiz. khim. (Journal of Physcial Chemistry), Vol. 4, No 5, 1933.
63. Fuks, N. A. "Determination of the Dimension of Drops in Water Fogs." Zh. eksperim. i teor. fiz. (Journal of Experimental and Theoretical Physics), Vol 7, No 4, 563, 1937.
64. Fuks. N. A. "On the Sizes of Charges on Particles of Atmospheric Aerocolloids." Izv. AN SSSR, ser. geograf. i geofiz. (News of the Academy of Sciences USSR, Geography and Geophysics Series), No 4, 341, 1947.
65. Fuks, N. A. "Contribution of the Theory of Rain from 'Warm' Clouds." Dokl. AN SSSR, Vol 81, No 6, 1951.

66. Fuks, N. A. Mechanics of Aerosols, Publishing House of the Academy of Sciences USSR, Moscow, 1955.
67. Hald, A. Mathematical Statistics with Engineering Applications (Russian translation), Publishing House of Foreign Literature, Moscow, 1956.
68. Khrgiyan, A. Kh., Mazin, I. P. "On the Distribution of Drops by Dimensions in Clouds." Tr. TsAO, No 7, 56, 1952.
69. Khrgiyan, A. Kh., Mazin, I. P. "Calculation of Errors of an Airborne Drop Collector." Ibid., No 12, 3, 1953.
70. Khrgiyan, A. Kh., Mazin, I. P. "Analysis of Methods for Describing the Spectra of the Distribution of Cloud Drops," ibid., No 17, 1956.
71. Chandrasekhar, S. Stochastic Problems in Physics and Astronomy (Russian translation), Publishing House of Foreign Literature, Moscow, 1947.
72. Chaplygin, S. A. "New Method of Approximate Integration of Differential Equations." Sobr. Soch. (Collected Works), Vol 1, 349, 1948.
73. Chudaykin, A. V. "Jettisoned Trap for Cloud Drops." Tr. El'brusk Ekspeditsii IPG AN SSSR, No 2 (5) (in press).
74. Chudaykin, A. V. "Automatic Impactor for the Investigation of Solid Aerosols in the Free Atmosphere." Ibid, No 2 (5) (in press).
75. Shifrin, K. S. Scattering of Light in a Turbid Medium, Gostekhizdat, Moscow-Leningrad, 1951.
76. Shishkin, N. S. Clouds, Precipitation and Thunderstorm Electricity. Gostekhizdat, Moscow-Leningrad, 1954.
77. Schlichting, H. Boundary Layer Theory (Russian translation), p 78--82, Publishing House of Foreign Literature, Moscow, 1956.
78. Allee, P. A., Phillips, B. B. "Measurement of Cloud Droplet Charge, Electric Field and Polar Conductivities in Supercooled Clouds," J. Meteorol., 16, N 4, 405, 1959.
79. Albrecht, F. "Theoretische Untersuchungen ueber die Ablagerung von Staub aus Stroemender Luft und ihre Anwendung auf die Theorie der Staubfilter. Phys. Zs. 32, N 1, 48, 1931.
80. Arnulf A., Bricard, T., Cure E., Veret, C. "Transmission by Haze and Fog in the Spectral Region 0.35 to 10 microns." J. Opt. Soc. Amer., 47, N 6, 491, 1957.
81. Best, A. C. "The Size Distribution of Rain Drops." Quart. J. Roy. Meteorol. Soc. 76, N 327, 16, 1950.

82. Best, A. C. "Drop-Size Distribution in Cloud and Fog." Quart. J. Roy. Meteorol. Soc., 77, N 333, 418, 1951.
83. Cochet, R. "Evolution d'une gouttelette d'eau chargee dans un nuage a temperature positive.," Ann. geophys., 8, N 1, 33, 1952.
84. Davies, C. N. "The Sedimentation of Small Suspended Particles." "Symposium on Particle Size Analysis." Suppl. Trans. Inst. Chem. Eng., 25, 25, 1947.
85. Davies, C. N., Pietz, C. V. "Impingement of Particles on a Transverse Cylinder." Proc. Roy. Soc., Ser. A, 234, N 1197, 269, 1956.
86. East, T. W. A., Marschall, I. S. "Turbulence in Clouds as a Factor in Precipitation." Quart. J. Roy. Meteorol. Soc., 80, N 343, 26, 1954.
87. Geiger, H., Scheel, K. Handbuch der Physik. Bd. XII, Berlin, 1927.
88. Gillespie, T., Langstroth, G. O. "An Instrument for Determining the Electric Charge Distribution in Aerosols." Canad. J. of Chemistry, 30, 10[illegible], 1953.
89. Glauert, M. "A Method of Constructing the Path of Raindrops of Different Diameters Moving in the Neighbourhood of (I) a Circular Cylinder, (2) an Aerofoil, Placed in a Uniform Stream of Air, and Determination of the Deposit of the Drops on the Surface and the Percentage of Drops Couth" Brit. Aeronautical Research Committee, Rep. a. Memor., N. 2025, 1940.
90. Griffiths, I. H., Jones, T. D. "The Determination of Dust Concentrations in Mine Atmospher." Trans. Inst. Min. Eng., 98--99, 150, 1939--1940.
91. Gunn R., Kinzer, G. D. "The Terminal Velocity of Fall for Water Droplets in Stagnant Air." J. Meteorol., 6, N 4, 243, 1949.
92. Gunn, R., Hitschfeld, W. "A Laboratory Investigation of the Coalescence Between Large and Small Water Drops." J. Meteorol., 8, N 1, 7, 1951.
93. Gunn, R. "The Electrification of Cloud Droplets in Non-Precipitating Cumuli." J. Meteorol., 10, N 6, 397, 1952.
94. Gunn, R. "The Statistical Electrification of Aerosols by Ionic Diffusion." J. Colloid Sci., 10, 107, 1955.
95. Gunn, R. "Droplet-Electrification Processes and Coagulation in Stable and Unstable Clouds." J. Meteorol., 12, N 6, 511, 1955.

96. Gunn, R. "Raindrop Electrification by the Association of Randomly Charged Cloud Droplets," J. Meteorol., 12, N 6, 562, 1955.
97. Gunn, R. "The Non-Equilibrium Electrification of Raindrops by the Association of Charged Cloud Droplets." J. Meteorol., 14, N 4, 326, 1957.
98. Houghton, H. G., Chalker, W. R. "The Scattering Cross Section of Water Drops in Air for Visible Light." J. Opt. Soc. Amer., 39, N 11, 955, 1949.
99. Jeans, J. H. The Mathematical Theory of Electricity and Magnetism. Cambridge, 1925.
100. Johnson, C., Terrel, J. R. "Transmission Cross Section for Water Spheres Illuminated by Infrared Radiation." J. Opt. Soc. Amer., 45, N 6, 451, 1955.
101. Kreamer, H. F., Johnstone, H. F. "Collection of Aerosol Particles in Presence of Electrostatic Fields." Ind. A. Eng. Chem., 47, N 12, 2426, 1955.
102. Langmuir, I., Blodgett, K. B. "A Mathematical Investigation of Water Droplet Trajectories." USA Air Force, Techn. Rep., N 5418, 1946.
103. Langmuir, I., "The Production of Rain by a Chain Reaction in Cumulus Clouds of Temperature Above Freezing." J. Meteorol., 5, N 5, 175, 1948.
104. Lissowski, P. "Das Laden von Aerosolteilchen in einer bipolaren Ionenatmosphaere." Acta Physicochimica URSS, 13, N 2, 157, 1940.
105. Marshall, J. S., Palmer, W. "The Distribution of Raindrops with Size." J. Meteorol., 5, N 4, 165, 1948.
106. May, K. R. "The Cascad-Impactor: an Instrument for Sampling Coarse Aerosols." J. Sci. Instr., 22, 187, 1945.
107. May, K. R. "Measurement of Airborne Droplets by the Magnesium Oxide Method." J. Sci. Instr., 27, 5, 1950.
108. May, K., Druett, H. "The Pre-Impinger, a Selective Aerosol Sampler." Brit. J. Ind. Medicine, 10, 142, 1953.
109. Mueller, H. Mathematische Stroemungslehre. 140. Berlin, 1928.
110. Pauthenier, M. "Sur la coalescence electrique des brouillards et eventuellement des nuages a temperature quelconque au sein d'aerosols electrises." Comp. rendu, 226, N 7, 587, 1948.
111. Peaceck, R., Hill, G. W. "A Theoretical Estimate of Collection Efficiencies of Small Droplets." Quart. J. Roy. Meteorol. Soc., 83, N 355, 77, 1957.

112. Penndorf, R. "Mie Scattering Coefficient for Water Droplets in Air." J. Meteorol., 13, N 2, 219, 1956.
113. Phillips, B. B. Kinzer, G. D. "Measurement of the Size and Electrification of Droplets in Cumuliform Clouds." J. Meteorol., 15, N 4, 369, 1958.
114. Ranz, W. E., Wong, J. B. "Jet Impactors for Determining the Particle -- Size Distributions of Aerosols." Arch Ind. Hygiene a. Occupational Medicine, 5, N 5, 464, 1952.
115. Ranz, W. E., Wong, J. B. "Impaction of Dust and Smoke Particles on Surface and Body Collectors." Ind. a. Eng. Chem., 44, N 6, 1371, 1952.
116. Robinson A. "On the Motion of Small Particles in a Potential Field of Flow." Communications on Pure and Applied Mathematics., 9, N 1, 69, 1956.
117. Sartor, D. "A Laboratory Investigation of Collision Efficiencies, Coalescence and Electrical Charging of Simulated Cloud Drops." J. Meteorol., 11, N 2, 91, 1954.
118. Schotland, R. M. "The Collision Efficiency of Cloud Droplets." Symposium "Artificial Stimulation of Rain," 170, London, N. Y., Paris, Pergammon Press, 1957.
119. Schotland, R. M. "The Collision Efficiency of Cloud Drops of Equal Size." J. Meteorol., 14, N 5, 381, 1957.
120. Schumann, T. E. W. "Theoretical Aspects of the Size Distribution of Fog Particles." Quart. J. Roy. Meteorol. Soc., 66, N 283, 195, 1940.
121. Sell W. "Staubausscheidung an einfachen Koerpern und in Luftfiltern." VDI-Forschungsheft 347, 1931.
122. Squires, P., Gillespie, C. A. "A Cloud-Droplet Sampler for Use on Aircraft." Quart. J. Roy. Meteorol. Soc., 78, N 337, 387, 1952.
123. Squires, P. "The Microstructure and Colloidal Stability of Warm Clouds, Part I, The Relation Between Structure and Stability." Tellus, 10, N 2, 256, 1958.
124. Taylor, G. I. "Notes on Possible Equipment and Technique for Experiments on Icing on Aircraft." Brit. Aeronaut. Res. Committee, Rep. a. Memor. N 2024, 1940.
125. Telford, T. W., Thorndike, N. S., Bowen, E. G. "The Coalescence Between Small Water Drops." Quart. J. Roy. Meteorol. Soc., 81, N 348, 241, 1955.

126. Telford, T. W. "A New Aspect of Coalescence Theory." J. Meteorol., 12, N 5, 436, 1955.
127. Twomey, S. "The Electrification of Individual Cloud Droplets." Tellus, 8, N 4, 445, 1956.
128. Walton, W. H. Discussion in "Simposium on Particle Size Analysis," p 137, 1947.
129. Watson, H. H. "Errors Due to Anisokinetic Sampling of Aerosols." Amer. Ind. Hygiene Assoc. Quart., 15, N 1, 21, 1954.
130. Webb, W. L., Gunn, R. "The Net Electrification of Natural Cloud Droplets at the Earth's Surface." J. Meteorol., 12, N 3, 211, 1955.
131. Webb, W. L. "Particulate Counts in Natural Clouds and Fogs." J. Meteorol., 13, N 2, 203, 1956.
132. Wiegand, A. "Ladungsmessungen an natuerlichem Nebel." Phys. Zs., 27, N 23, 803, 1926.